1-1-2020

Cyanines, Squaraines, And Xanthene Based Nir Emissive Materials For Biological Imaging

Jacqueline N. Gayton

Follow this and additional works at: https://egrove.olemiss.edu/etd

CYANINES, SQUARAINES, AND XANTHENE BASED NIR EMISSIVE MATERIALS

FOR BIOLOGICAL IMAGING

A Dissertation

presented in partial fulfillment of requirements

for the degree of Doctor of Philosophy

in the Department of Chemistry and Biochemistry

The University of Mississippi

By

JACQUELINE GAYTON

MAY 2020

ABSTRACT

The need for NIR fluorescent dyes is widely accepted for imaging and communications applications. Cyanines are a commonly used family of dyes for biological imaging due to their tunability, often rapid synthesis, ease of bioconjugation, intense molar absorptivities and strong NIR emissions. Since the invention of indocyanine green (ICG), many efforts have been made to improve on the design achieving farther red-shifted dyes with larger quantum yields and enhanced Stokes shifts. A series of squaraine, cyanine, and xanthene based dyes using the indolizine heterocycle as a donor in place of the commonly used indoline donor are discussed. The indolizine donor allows for red-shifts farther into the NIR region due to the indolizine being fully conjugated. Additionally, an enhanced Stokes shift is observed to enable high resolution imaging. These series of dyes are discussed with a focus on structure-property relationships concerning the effects on the photophysical properties.

DEDICATION

This dissertation is dedicated to everyone who helped me towards the goal of achieving my

doctorate. I want to especially thank my mom and stepfather, Sonja and Kim Slater, as well as

my fiancé CJ Cooper.

ACKNOWLEDGEMENTS

TABLE OF CONTENTS

LIST OF FIGURES

ix

xv

LIST OF TABLES

LIST OF SCHEMES

CHAPTER 1

INTRODUCTION

1.1 INTRODUCTION TO NIR EMISSIVE MATERIALS FOR BIOLOGICAL IMAGING

Near infrared (NIR) emissive materials are in high demand. These materials absorb and emit

light in the NIR region (600-1400 nm). There are a variety of applications for these materials

including dye-sensitized solar cells, night vision googles, NIR organic light emitting diodes

(OLEDs), and biological imaging agents. NIR emissive materials are attractive as biological

imaging agents due to their lower energy absorption which allows photons to penetrate deeper

into the skin. The most well known and commercially available dye is a cyanine derivative

known as indocyanine green (ICG). However other classes of NIR emissive dyes such as

squaraines and xanthene based dyes have also made great progress in the field. The work

presented here has focused on three main classes of NIR emissive dyes for biological imaging:

cyanines, squaraines, and xanthene based dyes (**Figure 1**). Each series of dyes employs the same

indolizine donor with variation of the R-groups attached to the aryl ring. The indolizine donor

was chosen due to its fully planar geometry, fully conjugated π-system involving the nitrogen

loan-pair and reduced resonance stabilization energy of the aromatic indolizine. These properties

are all attractive when selecting a donor for NIR imaging materials, which rely on strong

intramolecular charge transfer events.
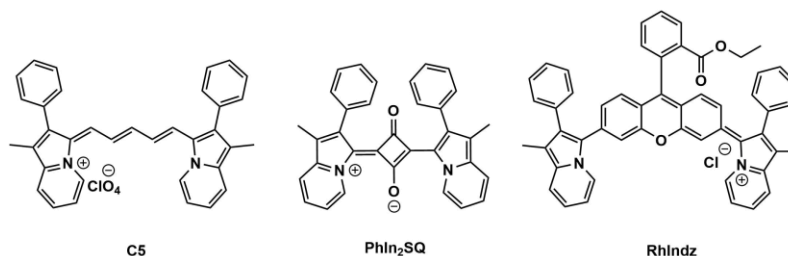
Figure 1. Representative dye structures presented in this work.

Absorption and emission in the NIR region are paramount for a biological imaging dye but are not the only requirements. A biological imaging dye should have a high molar absorptivity (ε), high quantum yield (ϕ), high molecular brightness ($\varepsilon \times \phi$), large Stokes shift, and water solubility. A high molar absorptivity and a high quantum yield (ratio of photons absorbed and emitted) allow a biological imaging dye to be used in minimal amounts. The molecular brightness is the molar absorptivity multiplied by the quantum yield and balances the two terms. A Stokes shift is the difference between the absorption and emission maximums. A small Stokes shift yields lower resolution images. A large Stokes shift can be achieved by increasing the reorganization energy of the dye. However achieving a large Stokes shift is a double edged sword. The Energy Gap Law dictates that the quantum yield will be lower at lower energy wavelengths due to energy loss in thermal relaxations. A large Stokes shift will provide higher resolution images but will deplete the quantum yield making the dye less desirable for imaging applications. Therefore consideration of both properties is vital to the design of a biological imaging dye and some middle ground must be found.

In this work three classes of dyes are presented. Each one absorbs well into the NIR region as well as has high molar absorptivities (**Figure 2**). Variability of photophysical properties is noted with each.
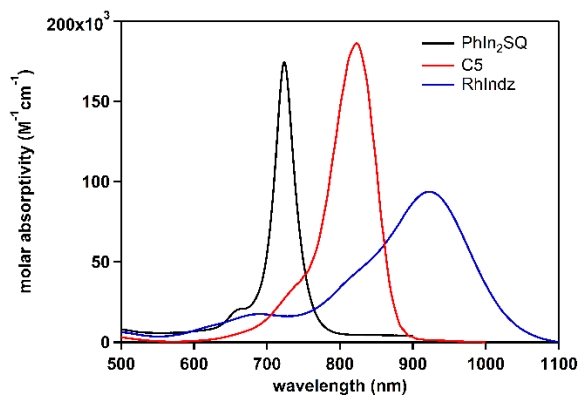
Figure 2. Molar absorptivity curves for the representative dye structures presented in this work.

Overall, each series of dyes outperforms the commercially available ICG in one or more aspects. Absorption maxima range from 600 to 900 nm with molar absorptivity remaining high at up to 260,000 $M^{-1}cm^{-1}$. Stokes shifts range from 20 to 194 nm with quantum yields of up to 3.5 %. Conjugation as well as electronic effects on photophysical properties are probed along with steric interactions and effect of counter anion variability.

3

CHAPTER 2

2.1 INDOLIZINE-CYANINE DYES: NEAR INFRARED EMISSIVE CYANINE DYES WITH INCREASED STOKES SHIFTS

Adapted with the permission from **Jacqueline Gayton**, Shane A. Autry, William Meador, Sean R. Parkin, Glake Alton Hill, Jr., Nathan I. Hammer, and Jared H. Delcamp.; *J. Org. Chem.* **2019**, *84*, 687-697. Copyright (2019) American Chemical Society.

This project is a collaborative project between Dr. Delcamp's group and Dr. Hammer's group, where Shane Autry contributed to the work by measuring the emission and quantum yield of the organic dyes. William Meador contributed to the project by synthesizing two of the cyanine dyes. Dr. Glake Alton Hill, Jr. contributed by performing all computational studies presented. Dr. Sean R. Parkin analyzed and solved the crystal structures. Jacqueline Gayton synthesized the indolizine-cyanine dyes as well as carried out characterizations.

ABSTRACT

Molecular engineering strategies designed to red-shift cyanine dye absorptions and emissions further into the near-infrared (NIR) spectral region are explored. Through the use of a novel donor group, indolizine, with varying cyanine bridge lengths, dye absorptions and emissions, were shifted deeper into the NIR region than common indoline-cyanines. Stokes shifts resulting from

intramolecular steric interactions of up to ~60 nm in many cases were observed and explained computationally. Molecular brightnesses of up to 5800 deep into the NIR region were observed. Structure−property relationships are explored for the six indolizinecyanine dyes with varying cyanine bridge length and indolizine substituents showing broad absorption and emission tunability. The dyes are characterized by crystallography, and the photophysical properties are probed by varying solvent for absorption and emission studies. Computational data show involvement of the entire indolizine π-system during light absorption, which suggests these systems can be tunable even further into the NIR region through select derivatizations.

INTRODUCTION

Near infrared (NIR) emissive materials are a widely researched class of compounds with applications in an array of areas[1] including biological imaging, communications, and secure displays.[2-7] Dye designs based on cyanine structures are ubiquitous because of the intense molar absorptivity of these structures in the NIR region.[1] Additionally, the cyanine dye absorption wavelength is highly tunable based on methine chain length selection.[8] The tunability, rapid synthesis, facile bioconjugation, intense molar absorptivities (ε), strong NIR emissions, and high molecular brightness (MB) values make this class of dyes attractive for further exploration as NIR emissive materials.[8-9] In addition to deeper NIR absorption and emission, dyes with large Stokes shifts and high quantum yields are in high demand.[9-12] For many applications, longer wavelength absorptions allow for access to differential dye properties relative to currently available dyes, and a larger Stokes shift provides dramatically higher resolution images in biological applications by reducing background signals.[5, 13-14] Importantly, a significant MB is needed to give high resolution images with smaller amounts of emissive material.[15] A balance between long wavelength use,

Stokes shifts, and quantum yield must be struck for many functional materials in the NIR region, since the energy gap rule dictates diminished quantum yields as wavelengths increase.[16-19] Stokes shifts, which arise from molecular reorganizations, also tend to diminish quantum yields as the Stokes shift increases in magnitude. Introduction of molecular design elements which can increase Stokes shifts and wavelength of both absorption and emission, while retaining a reasonable molecular brightness, can addresses a fundamental need in NIR emissive dye design.[20] Both the Stokes shift and lower energy absorption/emission challenges can be addressed by replacing the indoline donor of typical indoline cyanine dyes (such as FDA approved, commercially available, and widely used indocyanine green **ICG**) with a fully conjugated indolizine donor to delocalize the frontier molecular orbitals further (**Figure 3**). **ICG** serves as a good benchmarking cyanine dye since it is one of the most widely used cyanines over the last 6 decades with multiple reviews concerning the utility of this compound.[21-22] In the specific case of our study, the single nitrogen heteroatom donor groups of indoline-cyanines can be directly compared to the single nitrogen heteroatom donor groups of novel indolizine-cyanine dyes since the donor heteroatom remains constant and a similar number of π-bonds are present in both donor groups. Additionally, the polycyclic indolizine donor provides a steric presence near the cyanine bridge, which requires either a deviation from planarity of the π-system or non-ideal bond angles. Strain such as this in the ground state often affects excited state geometries differently, leading to increased reorganizations upon photoexcitation and thus enhanced Stokes shifts [23-24]

prior work

- small reorganization energy
- planar π-system
- HOMO/LUMO localized to cyanine

indocyanine green (**ICG**)

this work

- increased reorganization energy
- steric strain on π-system
- extended HOMO/LUMO heavily delocalization to indolizine

indolizine cyanine

steric induced dihedral
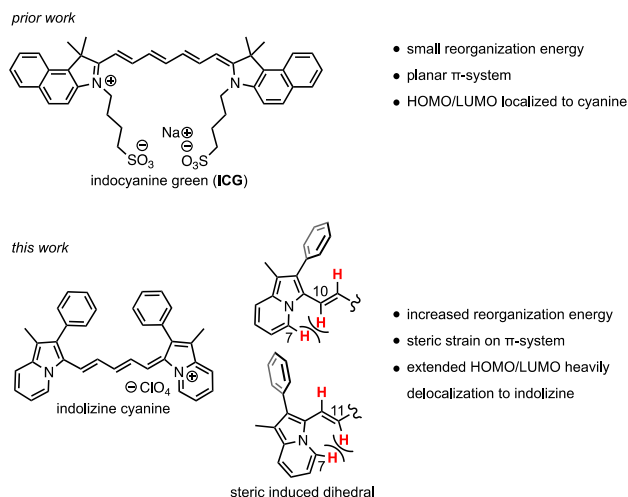
Figure 3. Comparison of an indoline cyanine dye and an indolizine cyanine dye. Hydrogens are drawn in for a portion of the indolizine cyanine on the right to show steric interactions. The indolizines are drawn in a *cis* conformation with a C7-C10 closest interaction as observed by crystallography for this specific compound. A second conformation exists for a C7-C11 close interaction which is also observed via crystallography in an example.

Recently, our group published a series of squaraine dyes using an indolizine heterocycle as a donor in place of an indoline donor.[25] The indolizine donor allows for red shifts farther into the NIR region due to the proaromatic nature of the indolizine, which generates an aromatic stabilized pyridinium ring after electron donation.[26] Additionally, an increased Stokes shift was observed, due in part to the planarization of aryl substituents on the indolizine ring in the excited state. This is significant as indoline-squaraine dyes are known for very narrow energy gaps between the absorption and emission spectrum. Importantly, the molar absorptivities and quantum yields (and by default the MB, where MB = ε × Φ) remained high despite these changes. We reasoned that a similar strategy could be employed with cyanine bridges in place of the squaraine bridge. The

cyanine-bridged dyes are attractive targets due to the simplistic tunability of the absorption wavelength by methine-bridge length selection. This type of straightforward absorption spectrum tuning is attractive, but is challenging to achieve with squaraine bridges. In this work, a series of dyes utilizing a constant indolizine donor structure with cyanine bridges between the donors of varying lengths with one, three, and five carbons (**C1**, **C3**, and **C5**) were prepared to probe the effects of methine bridge length on optical properties (**Figure 4**). Additionally, the electronic activity of positions on the indolizine donors are evaluated ranging from electron donating to electron withdrawing (**PhOMeIndz-C5**, **PhCNIndz-C5**, and **PhIndzOMe-C5**) in order to probe structure-property relationships on the dye optical properties.
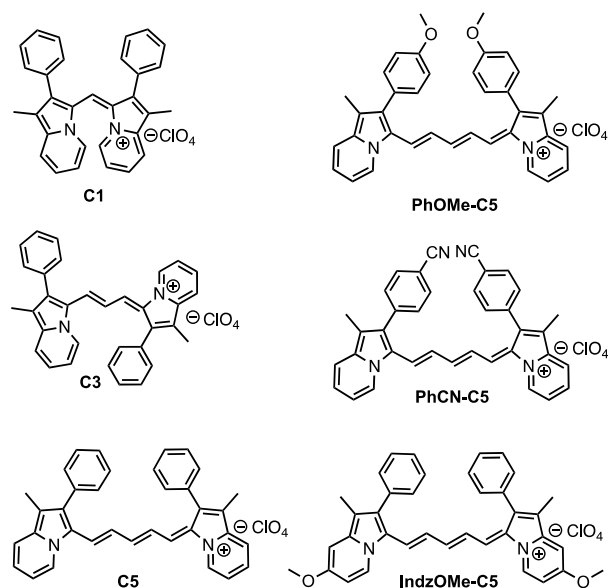
Figure 4. Target indolizine cyanine dyes.

Results and Discussion: Target dyes **C1**, **C3**, and **C5** were synthesized from a known phenyl indolizine (**PhIndz**), which is available in two steps from commercially available 2-

ethylpyridine (**1** when R' = H) and 2-bromoacetophenone (**2** when R = H) via an *N*-alkylation reaction followed by a base catalyzed condensation reaction sequence (**Figure 5**).[23] **PhIndz** was then reacted with methine bridge precursors **4**, **5** and **6** in the presence of perchloric acid to give **C1**, **C3**, and **C5**, respectively, in moderate to high yield (38-85%). **PhOMe-C5** and **PhCN-C5** follow the same synthetic route as **C5** beginning with known indolizine building blocks **PhOMeIndz** (**3** when R = Ome and R' = H) and **PhCNIndz** (**3** when R = CN and R' = H), respectively. The synthesis of **IndzOMe-C5** began with the alkylation of commercially available 2-ethyl-4-methoxypyridine (**1** when R' = Ome) with 2-bromoacetophenone, followed by cyclization to give **PhIndzOMe**. Reaction of **PhIndzOMe** with iminium salt **6** afforded **IndzOMe-C5** in low isolated yield, presumably due to the low stability of the indolizine precursor in the reaction mixture as the starting indolizine was consumed during the reaction. In general, the starting indolizines were handled with care due to limited stability as they were found to decompose in solution under air and on silica gel; however, once the indolizine was incorporated into a cyanine dye the motif became stable to prolonged ambient exposure.
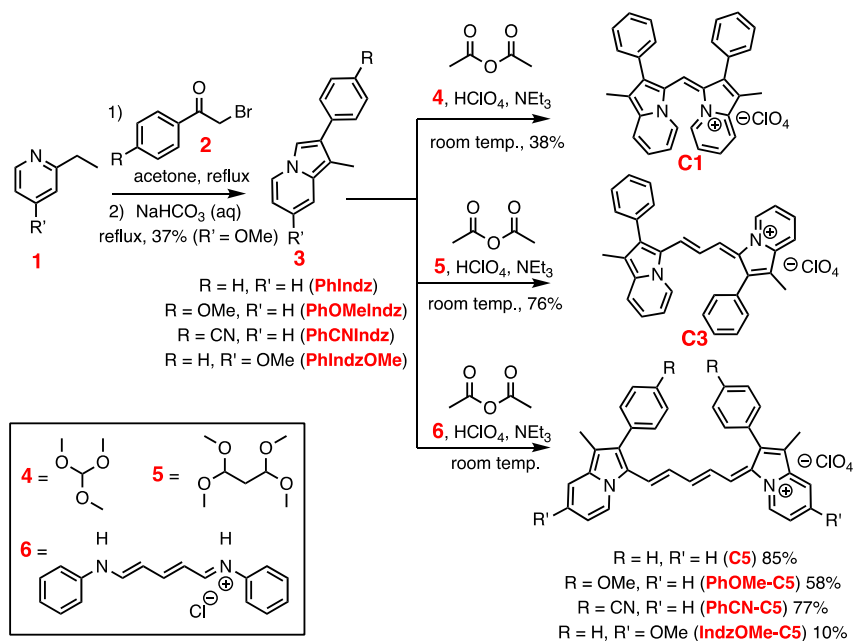
Figure 5. Synthetic route to the target indolizine cyanine dyes. The product conformations are drawn to match those obtained by crystal structure analysis of **C1**, **C3**, and **C5** (see below).

With the target dyes in hand, single-crystal X-ray diffraction studies were undertaken to probe planarity of the dye π-system and to analyze the cyanine bridge bond lengths. We hypothesized: (1) **C1** potentially cannot adopt a conformation with both indolizine heterocycles co-planar due to steric interactions between the indolizine groups with the short single carbon bridge, and (2) both **C3** and **C5** require some deviation from ideal bond angles or π-system planarity due to steric interactions between the indolizine and cyanine bridge. To probe these predictions, crystals suitable for crystallographic studies were grown by slow evaporation of MeCN from **C1**, or via vapor diffusion techniques in the cases of **C3** and **C5**. The crystals grew as thin needles or granules with a metallic like orange luster, as is common for very high molar

10

absorptivity organic materials. The resolved structures are shown below (**Figure 6**) with select properties reported in **Table 1**.
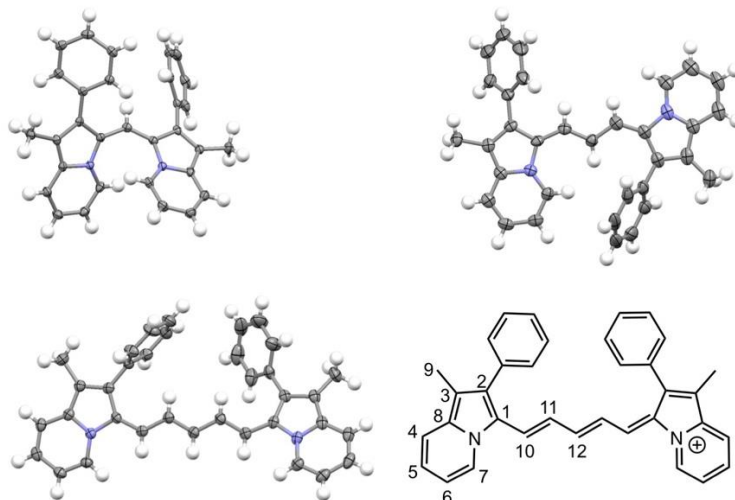
Figure 6. Crystal structures of **C1, C3,** and **C5** with co-crystallized solvents and counter ions omitted. Hydrogens are included in order to emphasize potential steric interactions.

First, the planarity of each derivative was analyzed. As expected, the indolizine groups of **C1** are not co-planar and have π-systems perturbed by a 43° dihedral angle (**Table 1**). As a result, **C1** adopts a propeller type molecular shape, which significantly affects the molar absorptivity of this derivative. **C3** and **C5** have lengthened methine chains that can allow for more co-planar conformations. The indolizine groups can adopt two different *cis* conformations or a *trans* type conformation with the phenyl groups either on the same side of the methine bridge or on opposite sides, respectively (see appendix **Table 17**). The *trans* conformer is the observed conformation of **C3** in the crystal structure, with a 175° dihedral angle (5° from co-planarity). Upon extending the methine chain to a five-carbon segment, the *cis* conformer was observed via crystallography, with a deviation of indolizine-indolizine π-faces from planarity by a 30° dihedral angle. The presence

of both the *cis* and *trans* isomers of the indolizine cyanine dyes as crystals and the ^{1}H NMR appearing as a single set of peaks suggests that both isomers are accessible and interconversion between *cis* and *trans* isomers is likely possible as was observed for prior squaraine derivatives.[25] Bond length analysis reveals a reasonably uniform bond length (weak alternation) when the indolizine-cyanine bond is compared to the bonds of the cyanine bridge. This bond uniformity is indicative of cyanine type structures and extends from the attachment point of the cyanine bridge to the indolizine across the π-bridge with lengths varying by less than 0.03 Å for all derivatives. The observed bond lengths (1.37-1.40 Å) are between that of an average single C-C bond (1.54 Å) and a double C-C bond (1.34 Å, **Table 1**). This bond length uniformity suggests these systems are more likely to exhibit π-π* optical transitions than n-π* optical transition and that the non-bonding electron lone pairs, which are often formally drawn on the nitrogens of the indolizine groups, are delocalized.

Table 1. Select crystal structure geometry measurements.

Dye	indz.-indz. Dihedral (°)	C1-C10 (Å)	C10-C11 (Å)	C11-C12 (Å)
C1	43	1.37 (1)	-	-
C3	175	1.38 (7)	1.39 (2)	-
C5	30	1.38 (3)	1.40 (2)	1.37 (5)

Absorption and emission studies were undertaken to analyze the optical properties of the dyes. First, the molar absorptivity and absorption curve features were analyzed for **C1**, **C3**, and **C5** to compare the effect of added methine spacers in several solvents (DCM, DMSO, 1:1 MeCN:H$_2$O, and MeCN) differing in polarity and protic nature (**Figure 7**, **Tables 2**, see appendix **Tables 14**, and **15**). The absorption maxima were found to shift to longer wavelength with

increasing number of methine groups (e.g. in DMSO λ_{max} values 652, 705, and 819 nm are observed for **C1**, **C3**, and **C5**, respectively). These maxima are likely from π-π* transitions based on bond length alternations observed from crystallography, DFT, and the high molar absorptivity values observed (see discussion below). This is a 23-26 nm red-shift for the **C5** derivative relative to the common indoline cyanine dye, **ICG**. Additionally, the molar absorptivity increased dramatically as the cyanine bridge length increased from 1 to 3 or more carbons. The twisted π-system of **C1** prevents a strong low-energy transition, limiting molar absorptivities from 11,000 to 27,000 $M^{-1}cm^{-1}$ for **C1** depending on solvent selection. **C3** and **C5** molar absorptivities are in stark contrast to this at up to 204,000 and 188,000 $M^{-1}cm^{-1}$, respectively. These values are similar to **ICG**, which has a maximum measured molar absorptivity of 238,000 $M^{-1}cm^{-1}$. A characteristic cyanine high-energy shoulder is observed for each of the dyes and this is attributed to vibronic transitions.[27] Both **C3** and **C5** exhibit similar molar absorptivity trends with solvents in the following order: DCM > DMSO > MeCN:H_2O > MeCN. These trends do not correlate to dielectric constants or dipole of
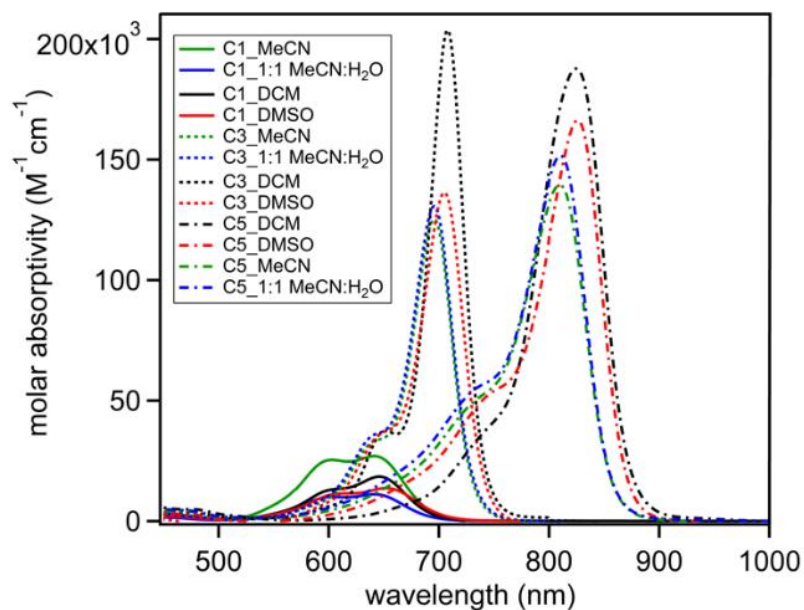
Figure 7. The molar absorptivities of **C1**, **C3**, and **C5** dyes in DCM, DMSO, MeCN, and 1:1 MeCN:H_2O measured at 1 x 10^{-5} M concentrations. See Figure S1 for the full visible range. Individual plots of the absorption and emission of **C1**, **C3**, and **C5** dyes in the four solvents are in the appendix (see appendix **Figures 37-39**).

Table 2. The molar absorptivity, absorption maximum, emission maximum, quantum yield, and Stokes shift for each dye in four solvents.

Dye	solvent	ε (M^{-1}cm^{-1})	λ_{max} abs (nm)	λ_{max} emis (nm)	Φ (%)	MB ($\varepsilon \times \Phi$)	Stokes shift (nm | eV | cm^{-1})
C1	MeCN	27,000	642	698	<1	≤300	56 | 0.15 | 1250
	1:1 MeCN:H_2O	11,000	641	698	<1	≤100	57 | 0.16 | 1270
	DMSO	14,000	652	846	<1	≤100	194 | 0.43 | 3517[a]
	DCM	18,000	646	693	<1	≤200	47 | 0.13 | 1050
C3	MeCN	126,000	695	725	<1	≤1,300	30 | 0.07 | 595
	1:1 MeCN:H_2O	133,000	696	727	<1	≤1,300	31 | 0.08 | 613
	DMSO	135,000	705	737	1.6	2,200	32 | 0.08 | 616

Compound	Solvent	ε	λ_{max}^{abs}	λ_{max}^{emis}	Φ	MB	MB
	DCM	204,000	708	741	<1	≤2,000	33 | 0.08 | 629
C5	MeCN	140,000	810	848	1.2	1,700	38 | 0.07 | 553
	1:1 MeCN:H$_2$O	151,000	811	840	<1	≤1,500	29 | 0.05 | 426
	DMSO	166,000	819	852	3.5	5,800	33 | 0.06 | 473
	DCM	188,000	825	868	2.2	4,100	43 | 0.07 | 600
PhOMe-C5	MeCN	94,000	799	845	1.3	1,200	46 | 0.08 | 681
	1:1 MeCN:H$_2$O	146,000	799	831	<1	≤1,500	32 | 0.06 | 482
	DMSO	162,000	816	840	2.7	4,400	24 | 0.04 | 350
	DCM	207,000	813	863	1.9	3,900	50 | 0.09 | 713
PhCN-C5	MeCN	122,000	799	854	<1	≤1,200	55 | 0.10 | 806
	1:1 MeCN:H$_2$O	100,000	805	851	<1	≤1,000	46 | 0.08 | 671
	DMSO	84,000	820	860	2.3	1,900	40 | 0.07 | 567
	DCM	151,000	812	870	2.0	3,000	58 | 0.10 | 821
IndzOMe-C5	MeCN	124,000	819	849	1.3	1,600	30 | 0.05 | 431
	1:1 MeCN:H$_2$O	138,000	821	859	<1	≤1,400	38 | 0.07 | 539
	DMSO	141,000	838	868	3.6	5,100	30 | 0.05 | 412
	DCM	151,000	823	876	<1	<1,500	53 | 0.09 | 735
ICG	1:1 MeCN:H$_2$O	238,000	785	816	9.1	21,700	31 | 0.06 | 484
	DMSO	211,000	797	835	17.1	36,100	38 | 0.07 | 571
PhIn$_2$SQ	DCM	181,000	716	766	2.1	3,800	50 | 0.11 | 912
*bis-t-*buPhIn$_2$SQ	DCM	216,000	716	736	9.5	20,500	20 | 0.05 | 380
TTD(T)$_2$	Toluene	12,000	624	765	16.8	2,000	141 | 0.37 | 2954
TPA-BBTD-TPA	Toluene	24,000	763	1065	7.1	1,700	302 | 0.46 | 3716
CH1055-PEG	H$_2$O	-	750	1055	0.3	-	305 | 0.48 | 3855

Absorption and emission curves for **PhOMe-C5**, **PhCN-C5**, and **PhIndzOMe-C5** are in the appendix (see appendix **Figures 39-41**). Data for **ICG** were collected under identical conditions as a benchmark. Data for PhIn$_2$SQ,[25] *bis-t-*buPhIn$_2$SQ,[25] TTD(T)$_2$,[24] TPA-BBTD-TPA,[28] and CH1055-PEG[10] are from literature reports. ε is molar absorptivity. λ_{max}^{abs} is the absorption curve low energy peak value. λ_{max}^{emis} is the emission curve peak value. Φ is the quantum yield. MB is molecular brightness. [a] This value is based on the smaller lower energy emission peak. A higher energy emission peak (715 nm) is also observed which would correspond to a Stokes shift of 63 nm, 0.17 eV.

Solvent, which indicates a subtler solvent-dye interaction is occurring to vary molar absorptivities (see appendix **Table 14**). **C1** follows a different molar absorptivity trend, and this deviation away from the pattern observed for **C3** and **C5** may originate from lack of planarity of the π-system of **C1**.

A host of additional solvents were analyzed for the **C1**, **C3**, and **C5** dyes to show solvent effects on absorption wavelength (see **Figures 8-10**). For each solvent analyzed via absorption spectroscopy, an emission spectrum in the same solvent was analyzed. For **C1**, the solvent had a significant effect on the absorption curve shape, with the shoulder at 600 nm changing intensity relative to the lower energy peak at 650 nm (**Figure 8**). THF shows the closest ratio of high-energy to lower-energy features nearing equal heights, while DCM shows the high-energy feature at about a 75% of the height of the low-energy feature. All the dyes were found to have a linear absorbance versus concentration dependence following the Beer-Lambert Law from low concentrations (<1 x 10^{-6} M) to high concentrations (>1 x 10^{-5} M), which suggests the solvent dependent features in the **C1** absorption spectrum are not due to aggregation. These results show that **C1** has significantly different ground-state solution conformations depending on solvent selection. The emission curve shape variation with solvent was even more dramatic. The emission maxima could be tuned over a ~200 nm range by solvent selection. THF and DMF represent the highest energy emission peaks near 650 nm, while DMSO, methanol, and ethanol all show peaks at wavelengths >800 nm, with DMSO being the most red-shifted at 850 nm. This is a 194 nm Stokes shift and represents a very large reorganization energy (0.43 eV) from the ground state to the excited state. All three of the solvents with the lowest energy emission spectrum peaks show dual emission behavior with an emission peak near 700 nm. This type of dichromic behavior has been observed previously with

non-symmetric cyanine dyes.[29] The low-energy emission is the dominant feature in MeOH, while the high-energy emission is dominant in DMSO. The remaining solvents all show a peak near 700 nm and typically show a shoulder at 750 nm, which mirrors the absorption spectrum, suggesting the higher energy absorption feature is vibronic in nature. The vast range of emission curve shapes and peak energies suggests a wide range of geometries are accessible in the excited-state and the excited-state geometry is exceptionally solvent dependent.

The quantum yield for **C1** was measured to be less than 1% in the same four solvents as the molar absorptivity studies (**Table 2**). This leads to a low molecular brightness upper limit of ≤300, as is expected from a molecule with a very large reorganization energy.

For the absorption curve profiles of **C3** and **C5**, solvent effects are not as dramatic as with **C1** (**Figures 9 & 10**). **C3** and **C5** show typical cyanine curve shapes with little energetic variation in the absorption curve maxima based on solvent choice (<20 nm change observed in the 12 solvents examined). The emission curves show a slight increase in solvent effect changes with a range of about 35 nm observed for **C3** and **C5**. Notably, the most red-shifted and most blue-shifted solvents change between these two derivatives, suggesting subtle differences in solvent interactions between these two dyes. Stokes shifts between 30 and 50 nm were observed for these dyes, which allows for use in some biological imaging applications.[30] Both **C3** and **C5** show >1% quantum yields with the highest values (1.6 and 3.5%, respectively) observed in DMSO. A high MB value of 5,800 is observed for **C5**. While the MB values for the indolizine-cyanine dyes were not as high as those reported for the ICG benchmark, it should be noted that these values can be improved dramatically through enhancing the emission quantum yield by selection of non-conjugated substituents, as was recently shown for CH1055-PEG.[15] Compared to other benchmark

materials such as D-A-D dyes based on squaraine (PhIn$_2$SQ and *bis-t*-buPhIn$_2$SQ) and thienothiadiazole (TTD(T)$_2$), **C5** is significantly more red shifted by >100 nm in absorption and emission spectrum maxima. The reorganization energy of **C5** is similar to that of the squaraine derivatives, which have large Stokes shifts for that class of materials (0.07 eV versus 0.05-0.11 eV). Despite being red shifted significantly with a larger Stokes shift, the MB of **C5** is higher than these comparison dyes even with the very high quantum yield of TTD(T)$_2$. Compared to one of the most red-shifted imaging materials, TPA-BBTD-TPA (and derivative CH1055-PEG), a significantly higher MB is observed for **C5** with a more red-shifted absorption maximum. Notably, a significantly more red-shifted emission is present with TPA-BBTD-TPA. Overall, compared to the benchmark materials analyzed, **C5** is a promising dye scaffold for future applications.

The remaining indolizine-cyanine dyes synthesized are analogues of **C5** and show comparable absorption maxima, emission maxima, quantum yields, and MB to the parent compound in most solvents (see appendix **Figures 39-41**). These derivatives (**PhOMe-C5**, **PhCN-C5**, and **IndzOMe-C5**) are dramatically different in substituent electronic nature with **PhOMe-C5** and **IndzOMe-C5** having a strong electron donating methoxy group and **PhCN-C5** having a strong electron withdrawing group. The lack of change in the absorption and emission spectrum suggests these derivatives do not have a strong effect on the π-conjugated system (see computational discussion below). These positions on the indolizine heterocycle and phenyl group of the indolizine have little effect on the optical properties of these dyes and are attractive positions for functionalization to introduce components such as water solubilizing groups or bioconjugation functionality.
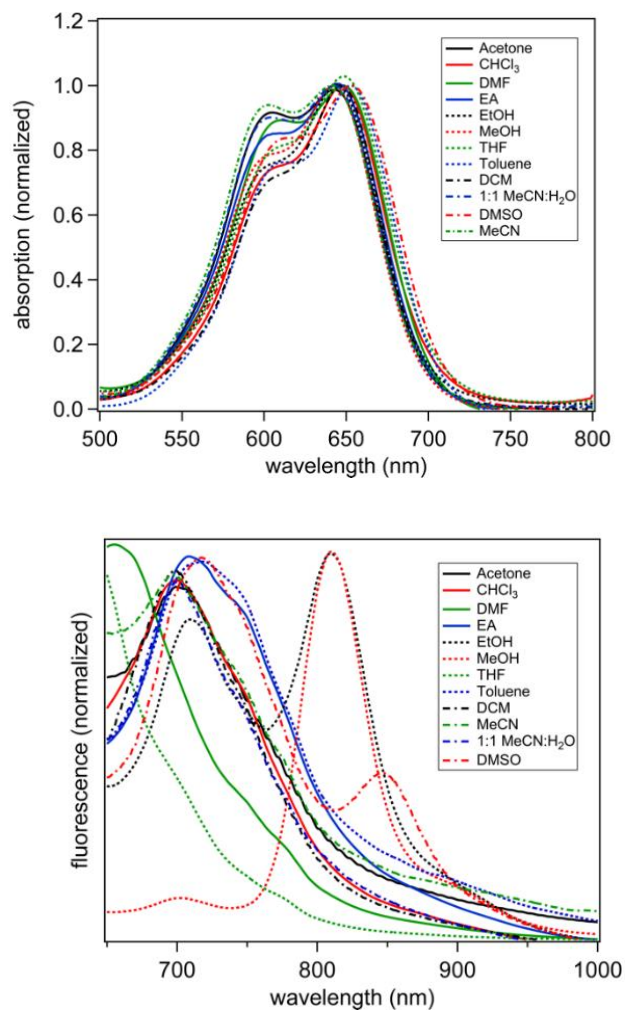
Figure 8. Absorption (top) and emission (bottom, fit with 0.1 LOESS function) spectra of **C1** in various solvents. Absorption spectra were collected at 1×10^{-5} M. Emission spectra were collected with excitation at 633 nm.
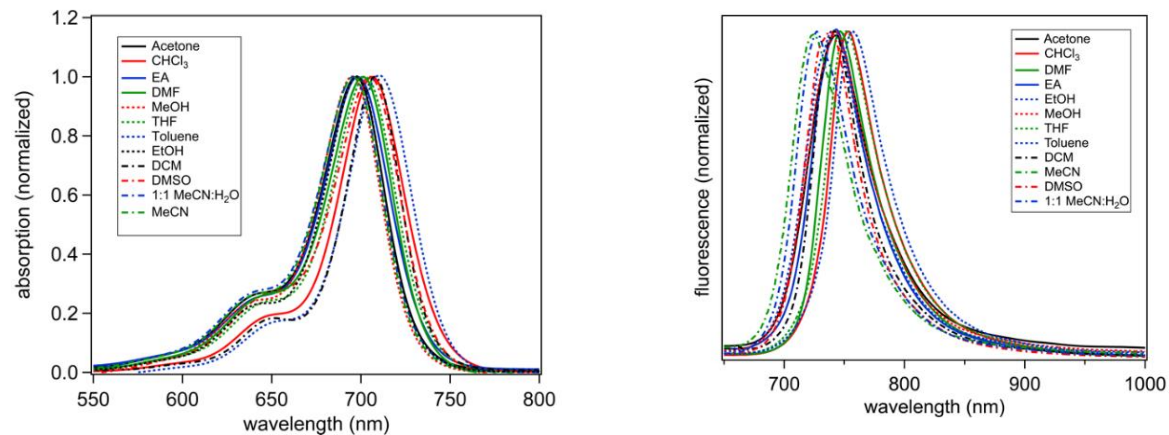
Figure 9. Absorption (left) and emission (right, fit with 0.1 LOESS function) spectra of **C3** in various solvents. Absorption spectra were collected at 1 x 10^{-5} M. Emission spectra were collected with excitation at 633 nm.
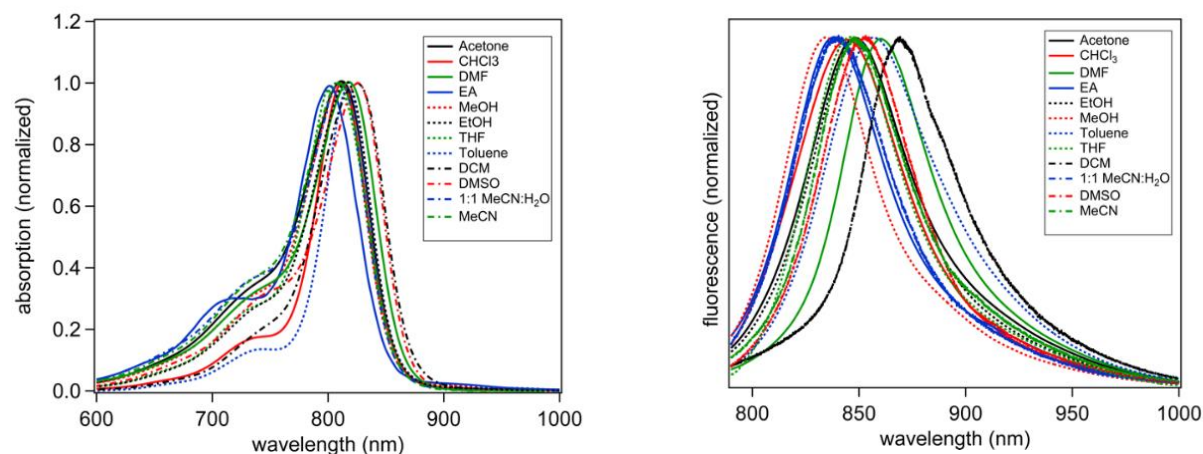
Figure 10. Absorption (left) and emission (right, fit with 0.1 LOESS function) spectra of **C5** in various solvents. Absorption spectra were collected at 1 x 10^{-5} M. Emission spectra were collected with excitation at 785 nm.

The **C5** derivatives show up to a 41 nm red shift relative to **ICG** in DMSO, indicating a deeper NIR light absorption as is desired for many applications (see appendix **Figures 42 & 43**). This red shift occurs despite a 2 methine shorter bridge for the C5 indolizine cyanine derivatives.

To better understand the role of the indolizine group and the optical properties of these dyes, calculations were performed using density functional theory (DFT) at the M06-2X/6-311G(d,p) level with the Gaussian 16 software package.[31-32] The SMD solvation model was used during geometry optimizations to better approximate the presence of MeCN.[33] Both the *cis* and *trans* isomers were analyzed since crystallography revealed the presence of *cis* isomers for **C1** and **C5** but the *trans* isomer of **C3**. A small energy difference was found between the ground state geometries of 1.0-4.4 kcal/mol with the *trans* isomer slightly lower in energy for **C1** and one of the *cis* isomers slightly lower in energy for **C3** and **C5** (see appendix). For all derivatives studied the highest occupied molecular orbital (HOMO) and lowest unoccupied molecular orbital (LUMO) were delocalized across the entire π-system, with significant orbital presence on both the methine bridge and on the indolizine donors (**Figure 11** and appendix **Figure 44**).
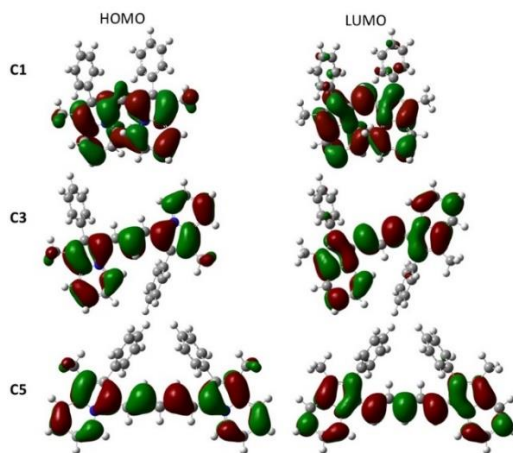
Figure 11. HOMO and LUMO images for **C1**, **C3**, and **C5** with an isovalue of 0.02.

It is noteworthy that the HOMO and LUMO are extended onto the conjugated indolizine heterocycle to a greater extent than is observed in the case of indoline cyanines.[34] This suggests the indolizine cyanine dyes may be electronically tuned more effectively than with indoline cyanines by careful substitution on the indolizine donor group.

For comparison to experimental trends, time dependent (TD)-DFT calculations were carried out at the same level of theory as the geometry optimizations (**Table 3**). TD-DFT shows a similar trend to the observed experimental data for the cis isomer with a close C7-C11 interaction for both λ_{max} and ε when compared with the vertical transition energies and oscillator strengths in MeCN: **C1** < **C3** < **C5** (**Table 3**, **Figure 3**). When the different conformers obtained from the crystal structure analysis are compared computationally, **C1** is red shifted relative to **C3**, and the energy of the vertical transition is significantly different than the experimental absorption spectrum maximum. As an example comparison, **C5** with the C7-C11 close interaction *cis* conformer shows theory and solution experiments within 0.12 eV. When the conformer observed via crystallography is computationally analyzed the comparison with solution experimentation shows a larger variation of 0.55 eV. We note that the energy difference between these geometries is small at 2 kcal/mol, and since ^{1}H NMR shows only a single isomer, rapid interconversion is likely possible. These transitions were found to be HOMO to LUMO π-π* transitions. To analyze the experimental emission spectrum data computationally, the excited-state geometry for each derivative was optimized. Similar to experimental data, **C5** was found to have the most red-shifted excited-state geometry vertical transition (labeled dye* vertical trans. In **Table 3**) and strongest oscillator strength (brightest emission). **C1** was computationally shown to have the largest Stokes shift, which is in good agreement with experimental data. Electron density difference mapping of the

22

three dyes was used to show where electrons are traveling from (red) and to (blue) upon photoexcitation (**Figure 12 &** appendix **Figure 45**). Green areas represent minimal electron movement. The maps show a delocalization of electron density across the cyanine π-bridge extending onto the full indolizine π-system in red, and a similar delocalization of areas accepting electron density on alternating atoms. No significant contribution from the phenyl group is observed on the electron density difference maps.

Table 3. TD-DFT values for the ground- and excited-state optimized geometries.

Dye	vertical trans. (eV, nm)	oscillator strength	dye* vertical trans. (eV, nm)	osc. Str. Dye*	Stokes shift (eV, nm)
C1 *cis*[a]	2.20, 561	0.79	1.78, 697	0.47	0.42, 136
C3 *trans*[a]	2.33, 533	1.11	2.18, 569	0.97	0.15, 36
C3 *cis*[b]	1.91, 648	1.49	1.74, 712	1.27	0.17, 64
C5 *cis*[b]	1.65, 752	2.06	1.51, 822	1.84	0.14, 70
C5 *cis*[a,c]	2.08, 596	1.52	2.03, 611	1.75	0.05, 15

[a] Conformation observed by crystallography. [b] C7-C11 interaction in Figure 1. [c] C7-C10 interaction in **Figure 3**.
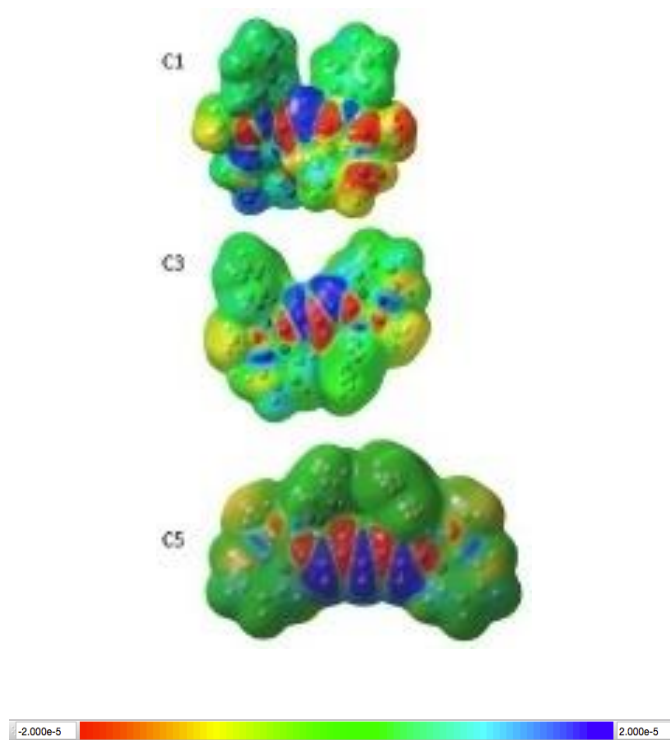
Figure 12. Electron density difference map. Red is where electrons originate from, blue is where they travel to upon photoexcitation, and green is neutral.

The predicted geometry changes from the ground state to the excited state were analyzed to determine the origin of the Stokes shift in these dyes. The ground state geometry shows a deviation of bond angles from ideal $120°$ sp^2 hybridized bong angles to wider values for all isomers (122-134° for the first two angles measured, **Table 4** & appendix **Table 16**). This is presumably to lower steric interactions between hydrogen atoms on the indolizine and cyanine bridge (or between the two indolizines for the case of **C1**). Despite the bond angle distortion, the nearest hydrogens are still well within a typical hydrogen bond distance (1.5-2.5 Å).

Table 4. Select computed bond angles, dihedral angles, and atom-atom distances.

Dye	angle 1 (°) GS | ES	angle 2 (°) GS | ES	angle 3 (°) GS | ES	angle 4 (°) GS | ES	dihedral (°) indz-cyanine GS | ES	dihedral (°) indz-indz GS | ES	H-H bond distance (Å) GS | ES
C1	128 | 123	134 | 125	N/A	N/A	15 | 27	35 | 50	2.7 | 3.6[a]
C3	128, 123 | 127, 122	131, 126 | 129, 123	120 | 123	N/A	2, 10 | 11, 22	15 | 32	1.8, 2.1 | 1.9, 2.1
C5	122 | 122	127 | 126	122 | 124	123 | 121	7 | 11	22 | 33	2.1 | 2.0

GS is ground state. ES is excited state. [a] Indicates H-H bond distance is between the two closest hydrogens of the indolizines. The structure below illustrates the bond angles being analyzed.
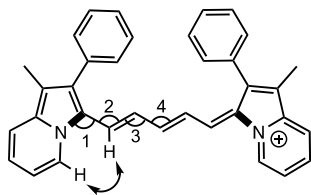
Upon photoexcitation, the bond angles adopt a closer to ideal geometry at 122-130°. These angles favor increased steric interactions between hydrogen atoms on indolizine and the cyanine bridge if the π-system were to remain planar. To relieve this increased strain, the indolizine-cyanine dihedral angle increases in the excited state by 4°-18° for all the conformers of **C3** and **C5** derivatives from nearer to planar in the ground state. This results in a less planar π-system, but does release steric strain, as evidenced by an increase in distance between nearest neighboring

hydrogens of about 0.1 Å (see appendix **Table 17**). Thus, the ground state geometry favors bond angle distortion with a more ideal dihedral angle across the π-system, while the excited state geometry favors a distorted dihedral angle across the π-system but gains more ideal bond angles (**Figure 13**). This change in geometry explains the increased Stokes shift for these indolizine cyanine derivatives relative to well-established indoline cyanines.
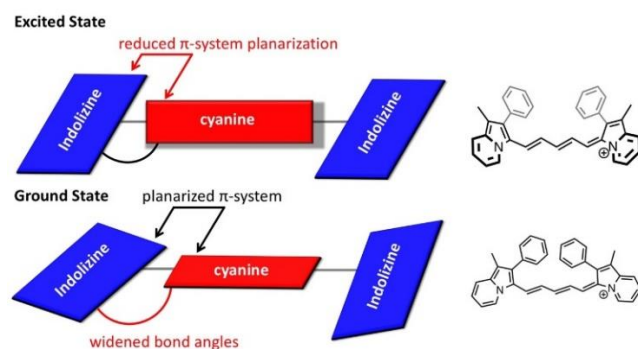
Figure 13. Illustration of geometry changes from the ground state to the excited state.

Conclusions:

Six NIR indolizine-cyanine dyes were designed, synthesized and characterized. UV-Vis-NIR absorption measurements show that increasing the methine bridge lengths leads to red-shifted absorptions. The indolizine-cyanine dyes show a red-shifted absorption relative to benchmark **ICG** despite two fewer methines.

This shows the critical role the indolizine groups can play in shifting absorption spectra as a conjugated donor group. The dyes were found to emit in the NIR region with the sterically congested dye **C1** showing the largest solvent effects and reorganization energies. The 5 methine group bridge of **C5** was found to lead to the largest quantum yields and a high MB value for a dye

emitting near 900 nm. Computational studies reveal that the ground state favors a planarized π-system with distorted bond angles while the excited state favors the opposite geometry. Importantly, the use of molecularly engineered steric interactions shows that significant Stokes shifts can be designed into a class of molecules known for minimal Stokes shifts while keeping a good quantum yield and red shifting the absorption and emission curves.

Experimental:

General Information. All commercially obtained reagents and solvents were used as received without further purification. It should be noted that the dyes were isolated as perchlorate salts, and perchlorate salts in general have been found explosive is some cases. Care is advised while handling all perchlorate salts. Thin-layer chromatography (TLC) was conducted with Sorbtech silica XHL TLC glass backed plates and visualized with UV. Flash column chromatography was performed using a CombiFlash Rf+ system. RediSep cartridges were charged with silica gel from Sobent Tech P60, 40-63 μm (230-400 mesh). ^{1}H and ^{13}C NMR spectra were recorded on a Bruker Avance-300 (300 MHz) spectrometer and a Bruker Avance-500 (500 MHz) spectrometer and are reported in ppm using solvent as an internal standard (DMSO at 2.50 ppm). Data reported as: s = singlet, d = doublet, t = triplet, q = quartet, p = pentet, m = multiplet, b = broad, ap = apparent, dd = doublet of doublets; coupling constant(s) in Hz; integration. UV-Vis Spectra were measured with a Cary 5000 UV-Vis-NIR spectrometer. HRMS spectra were obtained with a QTOF HRMS utilizing nanospray ionization. The mass analyzer was set to the 200-2000 Da range. Infrared spectra were recorded with an Agilent Cary 660 ATR-FTIR. For all derivatives, the excited-state lifetimes were found to be shorter than the response function of the instrument. The emission of the **C1** and **C3** derivatives were measured using a Horiba LabRam spectrometer with a 600

grooves/mm grating, CCD camera detection and an excitation laser of 633 nm. All other dyes were measured using the same instrument and a 785 nm excitation laser. The quantum efficiency of the detector was accounted for when measuring emission profiles. The relative quantum yields were obtained using this equation:

$$\Phi_{Sample} = \Phi_{Standard} * \frac{E_{Sample}}{E_{Standard}} * \frac{A_{Standard}}{A_{Sample}} * \frac{\eta_{Sample}^2}{\eta_{Standard}^2}$$

For the equation above, E is the sum of emission intensities and A is maximum absorbance. η is the refractive index of the solvent used and Φ denotes the quantum yield.[35] The standard used to obtain the relative quantum yields was Indocyanine Green (ICG) with a quantum yield of 14% in H_2O.[36] Diffraction data were collected at 90K on a Bruker D8 Venture dual microsource diffractometer using $MoK\alpha$ X-rays. Data scaling, merging, and absorption correction used well-established procedures.[36-37] Crystal structures were solved and refined using the Shelx programs.[38-39] Crystals of **C3** included some poorly defined solvent that was accounted for using SQUEEZE.[40]

(Z)-1-methyl-3-((1-methyl-2-phenylindolizin-3-yl)methylene)-2-phenyl-3H-indolizin-4-ium perchlorate (**C1**): To a round bottom flask equipped with a stir bar, **PhIndz** (1.00 g, 4.80 mmol) was added to acetic anhydride (48 mL) followed by perchloric acid (0.48 g, 4.80 mmol). The mixture was allowed to stir at room temperature for five minutes. Triethylorthoformate (**4**) (0.36 g. 2.40 mmol) was added along with triethylamine (0.58 g, 5.76 mmol). The reaction mixture was allowed to stir at room temperature for 24 hours before being subjected to a silica gel column with

a solvent gradient beginning with 40:60 dichloromethane:hexane and ending with 100% dichloromethane. The product was isolated as a red solid (0.48 g, 38%). ^{1}H NMR (300 MHz, DMSO-d6) δ 8.50 (s, 2H), 8.08-7.97 (m, 4H), 7.90-7.80 (m, 4H), 7.44-7.37 (m, 8H), 7.3 (t, J = 6.8 Hz, 1H), 2.38 (s, 6H). ^{13}C NMR was not obtained due to low solubility. IR (neat, cm^{-1}): 3598, 3534, 2916, 2665, 2329, 2092, 1777, 1621, 1586, 1464. HRMS m/z calculated for $C_{31}H_{25}N_2$ [M-ClO$_4$]$^+$: 425.2018, found 425.2019. Melting Point: 157-162 $^{\circ}$C.

(Z)-1-methyl-3-(3-(1-methyl-2-phenylindolizin-3-yl)allylidene)-2-phenyl-3H-indolizin-4-ium

perchlorate (**C3**): To a round bottom flask equipped with a stir bar, **PhIndz** (0.35 g, 1.69 mmol) was added to acetic anhydride (17.0 mL) followed by perchloric acid (0.169 g, 1.69 mmol). The mixture was allowed to stir at room temperature for five minutes. Malonaldehyde bis(dimethyl acetal) (**5**) (0.139 g, 0.845 mmol) was added along with triethylamine (0.205 g, 2.03 mmol). The reaction mixture was allowed to stir at room temperature for 24 hours before being subjected to a silica gel column with a solvent gradient beginning with a 50:50 dichloromethane:hexane solvent mixture and ending with 100% dichloromethane. The product was isolated as a gold solid (0.35 g, 76%). ^{1}H NMR (300 MHz, DMSO-d6) δ 7.99 (d, J = 8.5 Hz, 2H), 7.76-7.68 (m, 9H), 7.46-7.31 (m, 9H), 6.69 (t, J = 13.2 Hz, 1H), 2.19 (s, 6H). ^{13}C NMR was not obtained due to sparing solubility. IR (neat, cm^{-1}): 3109, 2993, 2817, 2669, 2582, 2330, 2116, 1618, 1555, 1533, 1454. HRMS m/z calculated for $C_{33}H_{27}N_2$ [M+H]$^+$: 451.2174, found 451.2197. Melting Point (dec.): 252-253 $^{\circ}$C.

(Z)-1-methyl-3-((2E,4E)-5-(1-methyl-2-phenylindolizin-3-yl)penta-2,4-dien-1-ylidene)-2-phenyl-

3H-indolizin-4-ium perchlorate (**C5**): To a round bottom flask equipped with a stir bar, **PhIndz** (1.00 g, 4.80 mmol) was added to acetic anhydride (48.0 mL) followed by perchloric acid (0.48 g,

4.80 mmol). The mixture was allowed to stir at room temperature for five minutes. (Phenylamino)pentadienylidene aniline HCl (**6**) (0.68 g. 2.40 mmol) was added along with triethylamine (0.58 g, 5.76 mmol). The reaction mixture was allowed to stir at room temperature for 24 hours before being subjected to a silica gel column with a solvent gradient beginning at 50:50 dichloromethane:hexane and ending with 100% dichloromethane. The product was isolated as a gold solid (1.1 g, 82%). ^{1}H NMR (300 MHz, DMSO-d6) δ 9.18 (d, J = 6.9 Hz, 2H), 8.03 (d, J = 13.6 Hz, 2H), 7.91 (d, J = 8.6 Hz, 2H), 7.70-7.54 (m, 8H), 7.37-7.25 (m, 8H), 5.91 (t, J = 12.5 Hz, 1H), 2.14 (s, 6H). ^{13}C NMR was not obtained due to sparing solubility. IR (neat, cm^{-1}): 3652, 2670, 2564, 2329, 2116, 1925, 1806, 1671, 1617, 1516, 1458. HRMS *m/z* calculated for $C_{35}H_{29}N_2$ [M]$^+$: 477.2331, found 477.2315. Melting Point (dec.): 176-179 $^°$C.

(Z)-2-(4-methoxyphenyl)-3-((2E,4E)-5-(2-(4-methoxyphenyl)-1-methylindolizin-3-yl)penta-2,4-dien-1-ylidene)-1-methyl-3H-indolizin-4-ium perchlorate (**PhOMe-C5**): To a round bottom flask equipped with a stir bar, **PhOMeIndz** (1.08 g, 4.54 mmol) was added to acetic anhydride (45.0 mL) followed by perchloric acid (0.46 g, 4.54 mmol). The mixture was allowed to stir at room temperature for five minutes. (Phenylamino)pentadienylidene aniline HCl (**6**) (0.65 g. 2.27 mmol) was added along with triethylamine (0.55 g, 5.45 mmol). The reaction mixture was allowed to stir at room temperature for 24 hours before being poured into ether (200 Ml). The pure product was insoluble in ether and was isolated by vacuum filtration as a red solid (0.81 g, 58%). ^{1}H NMR (300 MHz, DMSO-d6) δ 9.16 (d, J = 6.9 Hz, 2H), 7.90-7.85 (m, 2H), 7.70 (t, J = 15.6 Hz, 2H), 7.45-7.29 (m, 8H), 7.13 (d, J = 8.3 Hz, 6H), 6.42 (t, J = 11.5 Hz, 1H), 3.91 (s, 6H), 2.14 (s, 6H). ^{13}C NMR was not obtained due to sparing solubility. IR (neat, cm^{-1}): 3656, 3581, 3333, 2831, 2656,

2463, 2329, 2116, 1919, 1804, 1754, 1706, 1658, 1607, 1555, 1516, 1465. HRMS *m/z* calculated for $C_{37}H_{33}N_2O_2$ [M]$^+$: 537.2542, found 537.2516. Melting Point (dec.): 158-161 °C.

(Z)-2-(4-cyanophenyl)-3-((2E,4E)-5-(2-(4-cyanophenyl)-1-methylindolizin-3-yl)penta-2,4-dien-1-ylidene)-1-methyl-3H-indolizin-4-ium perchlorate (**PhCN-C5**): To a round bottom flask equipped with a stir bar, **PhCNIndz** (1.00 g, 4.31 mmol) was added to acetic anhydride (45.0 mL) followed by perchloric acid (0.432 g, 4.31 mmol). The mixture was allowed to stir at room temperature for five minutes. (Phenylamino)pentadienylidene aniline HCl (**6**) (0.613 g. 2.15 mmol) was added along with triethylamine (0.523 g, 5.17 mmol). The reaction mixture was allowed to stir at room temperature for 24 hours before being poured into ether (200 mL). The pure product was insoluble in ether and was isolated by vacuum filtration as a red solid (1.0 g, 77%). ^{1}H NMR (300 MHz, DMSO-d6) δ 9.19 (d, *J* = 6.8 Hz, 2H), 8.05 (d, *J* = 8.1 Hz, 4H), 7.98 (d, *J* = 8.6 Hz, 2H), 7.91 (d, *J* = 14.0 Hz, 2H), 7.76 (t, *J* = 7.6 Hz, 2H), 7.65 (d, *J* = 8.1 Hz, 4H), 7.44-7.36 (m, 4H), 6.21 (t, *J* = 13.2 Hz, 1H), 2.18 (s, 6H). ^{13}C NMR was not obtained due to sparing solubility. IR (neat, cm^{-1}): 3611, 3395, 2354, 2332, 2116, 1619, 1612, 1530, 1527, 1471. HRMS *m/z* calculated for $C_{37}H_{27}N_4$ [M]$^+$: 527.2236, found 527.2251. Melting Point (dec.): 187-191 °C.

(Z)-1-methyl-3-(3-(1-methyl-2-phenylindolizin-3-yl)allylidene)-2-phenyl-3H-indolizin-4-ium perchlorate (**IndzOMe-C5**): Part 1: *7-methoxy-1-methyl-2-phenylindolizine* (**4, PhIndzOMe**): To a round bottom flask equipped with a stir bar and a reflux condenser was added 2-ethyl-4-methoxypyridine (0.39 g, 2.81 mmol) and bromoacetophenone (0.84 g, 4.22 mmol) in acetone (5.62 mL). The mixture was heated to reflux in an oil bath for 24 hours. The reaction was monitored by TLC. Upon disappearance of the starting material **2**, water (5.62 mL) and sodium

bicarbonate (0.94 g, 11.2 mmol) were added to the reaction mixture. The mixture was heated at reflux in an oil bath for two hours. The crude product oiled out of solution and was extracted with dichloromethane to yield a brown oil that was immediately subjected to a rapid plug filtration through silica gel with 20:80 ethyl acetate:hexanes to yield an off white solid. Due to oxidative instability, the intermediate was carried forward to the next reaction without any further purification or characterization. To a round bottom flask equipped with a stir bar under nitrogen, the intermediate PhIndzOMe (0.25 g, 1.05 mmol) was added to acetic anhydride (10.5 mL) followed by perchloric acid (0.11 g, 1.05 mmol). The mixture was allowed to stir at room temperature for five minutes. (Phenylamino)pentadienylidene aniline HCl (**6**) (0.15 g. 0.52 mmol) was added along with triethylamine (0.13 g, 1.26 mmol). The reaction mixture was allowed to stir at room temperature for 3 hours before being subjected to a plug of silica with a solvent gradient from 100% dichloromethane to 50:50 ethyl acetate:dichloromethane. A final purification was performed by dissolving the concentrated product in a minimal about of dichloromethane followed by the addition of diethyl ether:hexanes (50:50) to yield the pure product as a green solid (0.03 g, 10%). ^{1}H NMR (300 MHz, DMSO-d6) δ 9.02 (d, J = 7.5 Hz, 2H), 7.73-7.53 (m, 10H), 7.33 (d, J = 7.2 Hz, 4H), 7.15-7.01 (m, 4H), 5.86 (t, J = 14.4 Hz, 1H), 4.01 (s, 6H), 2.10 (s, 6H). ^{13}C NMR was not obtained due to sparing solubility. IR (neat, cm^{-1}): 3788, 3691, 2917, 2633, 2329, 2116, 1797, 1775, 1630, 1527, 1444. HRMS m/z calculated for $C_{37}H_{33}N_2O_2$ [M]$^+$: 537.2542, found 537.2532. Melting Point (dec.): 162-165 $^{\circ}$C.

CHAPTER 3

3.1 COUNTER ANION EFFECT ON THE PHOTOPHYSICAL PROPERTIES OF EMISSIVE

INDOLIZINE-CYANINE DYES IN SOLUTION AND SOLID STATE

Adapted with the permission from **Jacqueline Gayton**, Shane Autry, Ryan C. Fortenberry,

Nathan I. Hammer, and Jared H. Delcamp *Molecules* **2018**, *23*, 3051. Copyright (2018) MDPI.

This project is a collaborative project between Dr. Delcamp's, Dr. Hammer's, and Dr. Fortenberry's group. Shane Autry contributed to the work by measuring the emission and quantum yield of the organic dyes. Dr. Ryan C. Fortenberry performed all computational studies presented. Jacqueline Gayton synthesized the cyanine anion exchanged dyes and performed characterizations.

ABSTRACT

Near-infrared emissive materials with tunable Stokes shifts and solid-state emission are needed for a number of active research areas and applications. To aid in addressing this need, a series of indolizine-cyanine compounds varying only the anions based on size, dipole, and hydrophilicity were prepared. The effect of the non-covalently bound anions on the absorption and emission properties of identical π-system indolizine-cyanine compounds were measured in solution and as thin films. Interestingly, the anion choice has a significantly influence on the Stokes shift and

molar absorptivities of the dyes in solution. In the solid-state, the anion choice was found to have an effect on the formation of aggregate states with higher energy absorptions than the parent compound. The dyes were found to be emissive in the NIR region with emissions peaking at near 900 nm for specific solvent and anion selections.

INTRODUCTION

Near infrared (NIR) emissive materials in both solution and the solid-state are in high demand with applications in biological imaging and optoelectronics [1-4, 6-7, 13, 41-44]. For non-invasive biological imaging an increased Stokes shift (the energetic difference between the absorption and emission maxima) is desirable to increase image resolution [10, 45]. Recently, we reported that Stokes shifts can be controlled through the molecular engineering of π-conjugated materials by the introduction of strategic dye steric elements and ground state ring strains [20, 24-25]. Presumably, non-covalently bound counter ion selection with charged π-systems could also be used to tune reorganization energies by altering the chromophore environment. The counter ion size would also be expected to have a significant impact on film morphologies and therefore influence solid-state emission properties.

Cyanine dyes are a common class of NIR emissive materials known for their intense molar absorptivities (ε) and high molecular brightness (MB = ε x ϕ, where ϕ is the quantum yield defined as number of photons emitted per number of photons absorbed) in the NIR region [1]. Cyanine dyes often suffer from small Stokes shifts and prior efforts have focused on increasing reorganization energies without loss of emission [11, 34]. Recently, we designed a series of cyanine dyes utilizing an indolizine donor in place of the common indoline donor [46]. A steric-induced deviation from typical bond angles along the cyanine backbone in the ground state geometry was found to reorganize to

34

more ideal bond angles in the excited state. The reorganization energy in changing from the ground state to the excited state geometry gave an increased Stokes shift (up to 60 nm) relative to common indoline cyanine Stokes shifts of $\geq$20 nm [11-12, 30, 47]. Thus, indolizine cyanine dyes are good candidates to evaluate the effects of non-covalent anions on the dye photophysical properties since the π-conjugated system is positively charged and significant reorganization energies can be adopted. Anion choice has been shown to have substantial effect on dye optical properties previously in literature [48-54]. To analyze the effects of anion selection on the recently reported indolizine cyanine dye **C5** [46], seven anions were targeted with varying size and charge distributions (**Figure 14**). Chloride (Cl^-), perchlorate (ClO_4^-), hexafluorophosphate (PF_6^-), and nitrate (NO_3^-) were selected as smaller sized ions. Trifluoromethanesulfonimide (TFSI), tetrakis[3,5-bis(trifluoromethyl)phenyl]borate (BARF), and tetraphenylborate (TPB) were selected as the largest anions studied. By systematic study of these anions with **C5**, the effects of anion properties on the conjugated system photophysical properties can be examined in both solution and the solid-state.
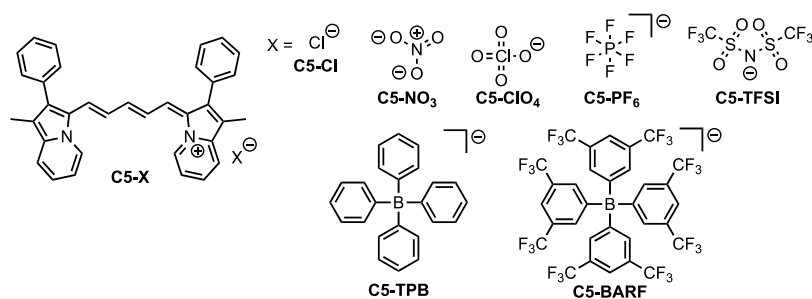
Figure 14. Dye **C5** with counter anions studied in this work.

Results and Discussion

First, the anions were analyzed computationally to determine ion volume, electrostatic surface potentials, and Mulliken population charges with the Gaussian 09 program[55] via B3LYP/6-31+G(d)[56-58] in a fashion similar to that done for determination of charge densities in common ions [59]. Comparing ion sizes by volume, the following order of ions is established from smallest to largest: $NO_3^- \approx Cl^- < ClO_4^- < PF_6^- < TFSI \ll TPB \ll BARF$ (**Table 5**). BARF is nearly double the size of the next largest ion, TPB, which is nearly double the size of TFSI. Comparing the range of anion sizes, Cl and NO_3 are more than 10 times smaller than BARF. This vast difference in size of the selected ions allows for the probing of anion size effects on dye emissive properties, which would be presumably heavily affected in the solid-state where the anion size plays a significant role in determination of dye-dye interaction distances.

Table 5. Calculated anion volumes.

Anion	Volume/Mole (cm³/mol)	Volume (cm³)
Cl^-	36.741	6.1011×10^{-23}
NO_3^-	35.092	5.8273×10^{-23}
ClO_4^-	52.148	8.6596×10^{-23}
PF_6^-	90.531	1.5033×10^{-22}
TFSI	130.771	2.1716×10^{-22}
TPB	246.294	4.0899×10^{-22}
BARF	414.785	6.8878×10^{-22}

The electrostatic surface potential maps for each of the anions are plotted with the WebMO graphical user interface[60] in **Figure 15** to see the outer atom charges, which interact most strongly with the cationic dye **C5**. Among the polyatomic anions studied NO_3^-, ClO_4^-, PF_6^-, and TFSI all show significant negative charge build up on the outer periphery of the anions. Mulliken population charges show the largest accumulation of negative charge on the outer atoms of the anion for PF_6^- with a charge of -0.734 on each of the F atoms (see appendix **Tables 39-44**). The trend then proceeds in the following order from most negative charge on peripheral atoms to least: PF_6^- > ClO_4^- > TFSI > NO_3^- >BARF> TPB. TPB is unique among the anions in that the outer most atoms (hydrogens) show a build-up of positive charge around the periphery of that anion. This is clearly displayed on the electrostatic surface potential map where the surface of the TPB anion is nearly completely blue indicating build-up of positive charge (**Figure 15**). Given the outer positive charge surrounding the TPB anion, it is expected to be very weakly attracted to the cationic C5 dye relative to the other anions with negative charge build-up on the surface.
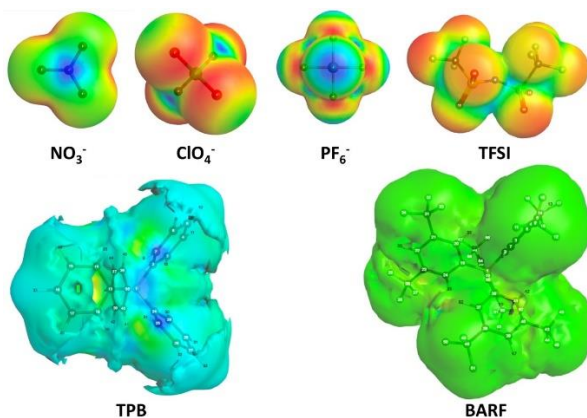
Figure 15. Electrostatic surface potentials of anions.

The target dyes were synthesized beginning from previously reported **C5-ClO₄** [46]. **C5-Cl** could be accessed from **C5-ClO₄** in high yield (95%) via a salt metathesis with tetrabutylammonium chloride (TBACl) in fluorobenzene (**Figure 16**). The significant solubility difference in **C5-ClO₄** (fluorobenzene soluble) and **C5-Cl** (fluorobenzene insoluble) suggests successful anion swap. **C5-Cl** was further purified with silica gel chromatography where the unique R_f of **C5-Cl** relative to **C5-ClO₄** further confirms ion exchange. The complete anion exchange is verified by metathesis reactions with **C5-Cl** and sodium salts of TPB and BARF which show quantitative anion exchange via ^{1}H NMR. If ClO_4^- were remaining, equal molar ratios of TBP or BARF to **C5** would not be observed. **C5-Cl** serves as a lynch pin intermediate in allowing access to **C5-NO₃**, **C5-PF₆**, **C5-TFSI**, **C5-TPB**, and **C5-BARF** from silver and sodium salts of the anions via metathesis reactions. The presence and quantification of the TPB and BARF anion could be confirmed by ^{1}H NMR. The presence of PF_6^-, TFSI and BARF were confirmed by ^{19}F NMR and the drastic solubility differences between **C5-Cl** and **C5-PF₆** or **C5-TFSI** suggests complete metathesis reactions. All dyes were purified via silica gel chromatography after metathesis reactions to remove any silver or sodium salts followed by filtration of the dyes through celite to remove any silica gel particles remaining in the sample due to the use of methanol as an elution solvent in most cases.
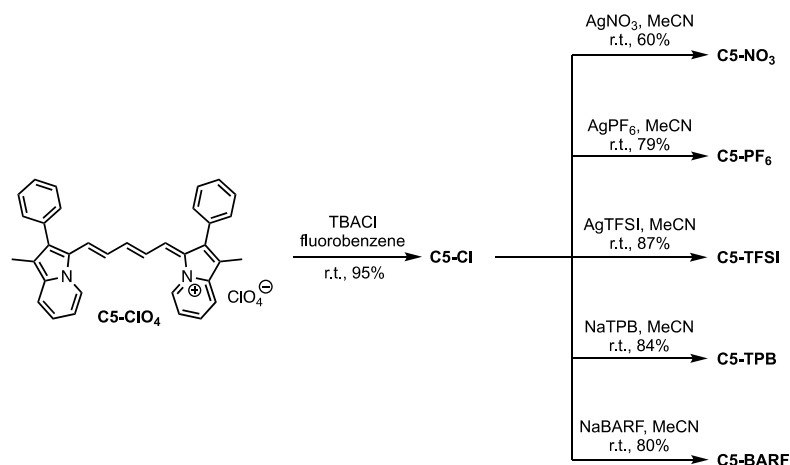
Figure 16. Synthetic route to the **C5** anion varied compounds.

With the target C5-anion varied compounds in hand, molar absorptivity and emission spectrum were measured for each dye in a polar aprotic solvent (acetonitrile, MeCN) and a low-polarity aprotic solvent (dichloromethane, DCM; **Figures 17**, appendix **Figures 57-58**; **Table 6**). The absorption curve shapes show sharp transitions at 810 nm in MeCN or 825 nm in DCM. The sharp transition shows a peak ½ width of only 75 nm (0.15 eV, 1176 cm^{-1}). The narrow transition is indicative of a π-π* transition as is commonly observed for many symmetric indoline cyanine dyes [61] rather than a charge transfer (CT) transition, which is typically much broader in this spectral region (>150 nm, >0.46 Ev, >3735 cm^{-1}) [20, 24]. Additionally, the curve shape for these dyes shows a high energy shoulder which is thought to be a characteristic vibronic feature of many indoline-cyanine dyes undergoing low energy π-π* transitions [27]. Anion selection has a dramatic effect on molar absorptivity in MeCN with a range of 141,000 to 66,000 M^{-1}cm^{-1} where ε is increasing in the following order: NO$_3^-$ < Cl$^-$ < PF$_6^-$ = TPB < BARF < ClO$_4^-$ < TFSI when an absorbance of 1 is reached. We note that the MeCN ε measurements via serial dilution reveal a positive deviation from the Beer Lambert Law, even at very low concentrations, while DCM shows linear absorbance

versus concentrations plots even to high absorbances near 3 in some cases (see appendix **Figures 59-70**). An example spectra set is provided at varying concentrations where new features are observed as concentrations change (see appendix **Figure 71**). The origin of this positive deviation is not obvious as the samples appear dissolved to the naked eye, although the possibility of non-observed solution aggregates exists. This non-linear behavior is observed even at low absorbances near the detection limit of the spectrometer used in these studies. The anion trend does not track with either simplistic analysis of anion size or charge localization and we note these factors as well as others such as dispersion forces may be in competition. The smallest anion and the largest anion had the highest molar absorptivities, and the order of anion charge localization is not mirrored in the molar absorptivity measurements as found via computational analysis. Significant dispersion forces with small ions may promote higher molar absorptivities and larger anions promote higher molar absorptivities through increased intermolecular spacing leading to two independent strong effects which does not allow for a definitive simple trend analysis. No significant change in molar absorptivity maximum (λ_{max}^{abs}) is observed with all compounds having a maximum absorbance at 810 nm in MeCN. In DCM, an even more dramatic molar absorptivity change is seen with anion choice ranging from 120,000 to 238,000 $M^{-1}cm^{-1}$. The anion trend in DCM is as follows: $NO_3^- <$ TPB $< Cl^- < PF_6 < ClO_4^- <$ TFSI $<$ BARF. This trend tracks reasonably well with anion size suggesting the influence of larger anions on π-system spacing places a dominate role. The three largest anions are in order of size with higher molar absorptivities than the remaining anions. The difference in MeCN and DCM can be rationalized as the less polar solvent (DCM) giving a stronger contact ion pairs between the anions and cations than the more polar MeCN. This tighter

ion pair shows a very dramatic ε change relative to the better solvated ions in MeCN. The anions in DCM again had no significant effect on λ_{max}^{abs} with all compounds absorbing at ~825 nm.
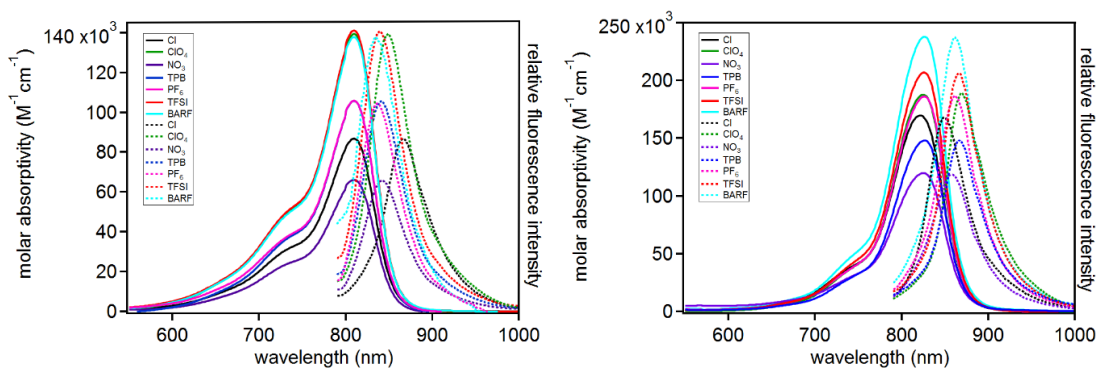
Figure 17. Molar absorptivity (solid lines) and emission intensity (dotted lines) for each dye in acetonitrile (left) and dichloromethane (right).

Table 6. Optical properties of each dye in acetonitrile and dichloromethane.

Dye	Solvent	Molar Abs. ($M^{-1}cm^{-1}$)	λ_{max}^{abs} (nm)	λ_{max}^{emis} (nm)	ϕ (%)	MB ($\varepsilon \times \phi$)	Stokes shift (nm | eV | cm^{-1})
C5-ClO₄	MeCN	140,000	810	848	1.2	1,700	38 | 0.07 | 553
	DCM	188,000	825	868	2.2	4,100	43 | 0.07 | 600
C5-Cl	MeCN	87,000	810	866	<1	<870	56 | 0.10 | 798

	DCM	170,000	821	849	<1	<1,700	28 | 0.05 | 402
C5-NO$_3$	MeCN	66,000	810	842	<1	<660	32 | 0.06 | 469
	DCM	120,000	825	856	<1	<1,200	31 | 0.06 | 439
C5-PF$_6$	MeCN	106,000	810	836	<1	<1,060	26 | 0.05 | 384
	DCM	186,000	826	862	<1	<1,860	36 | 0.07 | 506
C5-TFSI	MeCN	141,000	810	838	1.1	1,551	28 | 0.06 | 413
	DCM	207,000	826	866	<1	<2,070	40 | 0.07 | 559
C5-TPB	MeCN	106,000	810	840	1.2	1,272	30 | 0.06 | 441
	DCM	148,000	826	867	<1	<1,480	41 | 0.07 | 573
C5-BARF	MeCN	138,000	810	836	<1	<1,380	26 | 0.05 | 384
	DCM	238,000	826	861	<1	<2,380	35 | 0.06 | 492

The emissive properties of the dyes were also analyzed in both MeCN and DCM (**Table 6**). In MeCN, **C5-PF₆** and **C5-BARF** have the highest energy emission and **C5-Cl** has the lowest energy emission with the remaining anions following this energy trend: $PF_6^- \approx BARF > TFSI > TPB > NO_3^- > ClO_4^- >> Cl^-$. Since all the compounds have the same absorption energy, the Stokes shift values are directly correlated with the observed emission energy changes. **C5-Cl** has a 56 nm (0.10 eV, 798 cm^{-1}) Stokes shift which is the largest observed in the series. The smallest Stokes shift in MeCN was with **C5-PF₆** at half the energy of the chloride derivative (0.05 eV, 384 cm^{-1}). This change in energy of emission illustrates a larger geometry reorganization of the excited state in the presence of chloride relative to PF_6. In this polar solvent the localized anion has a larger effect on the geometry of the excited state, which may be due to a strong contact ion pairing being needed to keep the anion near the dye when dissolved in MeCN. The remaining anions are likely more readily dispersed in MeCN. Interestingly in the less polar DCM as solvent, the effect of the anions on emission energy changes substantially with a new order of increasing Stokes shift energies: $Cl^- > NO_3^- > BARF > PF_6^- > TFSI > TPB > ClO_4^-$. In this solvent, the chloride ion has the smallest Stokes shift (0.05 eV, 402 cm^{-1}) with ClO_4^- having nearly a twice as large of a Stokes shift at 0.09 eV (600 cm^{-1}). Thus, the effect of the anions on emission energy and absorption intensity, varies significantly with solvent as well as anion selection. These molar absorptivity and emission energy results in two different solvents with each set of anions highlights the importance of carefully comparing dyes in literature under identical conditions since both solvent and anion choice are non-innocent. In most cases, the dyes were too weakly emissive to accurately measure a quantum yield of emission. This is expected based on the Energy Gap Rule, which predicts that

as lower energy light is absorbed and emitted, thermal pathways start to dominate excited state energy loss mechanisms rather than photon emission [16-19]. However, despite the indolizine cyanines absorbing and emitting light significantly further into the NIR region than traditional indoline cyanines, several compounds were found to have quantum yields measured in excess of 1%. **C5-ClO₄** was found to be emissive in both MeCN and DCM at 1.2 and 2.2% ϕ, respectively. **C5-ClO₄** was the only compound found have a >1% quantum yield in DCM. **C5-TFSI** and **C5-TPB** were both emissive at 1.1 and 1.2% ϕ, respectively, in MeCN. These results suggest that ClO_4^-, TPB, and TFSI function most effectively in reducing thermal energy losses from the excited state dye. By analyzing molecular brightness of the compounds, both the intense absorption strength and quantum yield can be accounted for to generate a number valuable to applications of emissive materials where both components are critical such as biological imaging. The highest MB (4,100) was observed for **C5-ClO₄** in DCM due to a high ϕ and medium molar absorptivity relative to the other compounds in DCM. The highest MB confirmed in MeCN is also with **C5-ClO₄** and is significantly lower than that observed in DCM at 1,700. This lower MB is due to both a lower molar absorptivity in MeCN than DCM and a much lower quantum yield in MeCN. It should be noted that since the quantum yields are only reliably reported as <1% in several instances, the exact MB value is not known for many of the of the compounds and only a possible upper limit can be defined in **Table 6**.

In addition to solution studies, the solid-state absorption and emission properties were examined for each compound to determine the influence of anions on solid-state photophysical properties (**Figure 18**). Thin films of each dye were prepared by first dissolving each dye in a 1:1 mixture of acetonitrile:chlorobenzene (~0.01 M dye solution) and spin coating a glass slide. To

ensure the absorption spectrum were resulting from the dye and not the substrate, a non-normalized spectrum set is provided with the glass slide absorption which shows a clear difference (see appendix **Figure 72**). Additionally, films were made via spin coating from different solution concentrations which shows a significant change in absorption intensity and on a different surface (fluorine doped tin oxide (FTO)) with a different glass supplier (see appendix **Figures 73-75**). These control experiments suggest the absorption features are a result of the dye and not the substrate. The anion was found to have a significant effect on the absorption curve shape. **C5-TPB** was found to uniquely have a curve shape most resembling the solution spectrum with a large low energy feature and a presumably vibronic higher energy shoulder. The ratio of the shoulder feature to low energy transition differs significant from the solution measurements with a roughly 0.8:1 ratio in the solid state for **C5-TPB** and a 0.3:1 ratio in solution. Additionally, the absorption energy maximum has shifted significantly to 878 nm from solution measurements at 810 or 826 nm (**Table 7**). A host of reasons exist to explain this red-shift of film absorption relative to solution with examples such as a significant change in the π-conjugated system geometry in the ground state in the solid state relative to solution, excimer formation, π-stacking, and various aggregation phenomena.

Table 7. Optical properties of each dye on thin film.

Dye	λ_{max}^{abs} (nm)	Abs. High E: Low E Feature Ratio
C5-ClO$_4$	875	1:1
C5-Cl	750[a]	1:0.7
C5-NO$_3$	735[a]	1:0.8
C5-PF$_6$	778[a]	1:0.9

C5-TFSI	722[a]	1:0.7
C5-TPB	878[b]	0.8:1
C5-BARF	800[a]	1:1

[a] Indicates a lower energy shoulder is present near 875 nm. [b] Indicates a higher energy shoulder is present near 805 nm.

The remaining anions show an increase in the prominence of the higher energy shoulder region ranging from a near 1:1 ratio with the low energy feature for BARF and ClO_4^- to favoring of the higher energy feature for Cl^- anions at about 1:0.7. The unique behavior of the TPB anion is correlated to the unique electrostatic surface potential which shows a positive surface surrounding this anion. Presumably the positive surface charge of the TPB anion and the positive charge of the dye cation disrupt aggregation in the solid state due to electrostatic repulsion separating the π-conjugated systems. Attempts to obtain emission spectra form the solid state films proved to be difficult due to a weak emission signal.
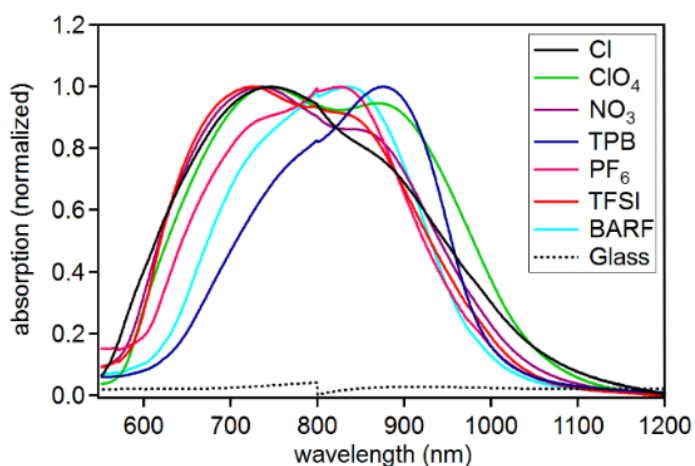
Figure 18. Solid-state absorption spectra for **C5-X** compounds.

Materials and Methods

All commercially obtained reagents and solvents were used as received without further purification. Thin-layer chromatography (TLC) was conducted with Sorbtech silica XHL TLC glass backed plates with a UV indication. TLCs were visualized with UV light (254 nm). Silica gel column chromatography was performed using silica gel from Sorbent Tech P60, and pre-packed Normal Phase Disposable RediSep columns on a Combi-Flash Rf+ system. ^{1}H and ^{19}F NMR spectra were recorded on a Bruker Avance-300 (300 MHz) spectrometer and a Bruker Avance-500 (500 MHz) spectrometer and are reported in ppm using solvent as an internal standard (DMSO at 2.5 ppm). Data reported as: s = singlet, d = doublet, t = triplet, q = quartet, p = pentet, m = multiplet, b = broad, ap = apparent, dd = doublet of doublets; coupling constant(s) in Hz; integration. UV-Vis Spectra were measured with a Cary 5000 UV-Vis-NIR spectrometer. HRMS spectra were obtained with a QTOF HRMS utilizing nanospray ionization. The mass analyzer was set to the 200-2000 Da range. Infrared spectra were recorded with an Agilent Cary 660 ATR-FTIR. Thin films of each dye were prepared with a spin coater (Laurell Technologies Corporation, Model WS-650MZ-23NPPB) on VWR 18x18 mm micro cover glass slides. Acquisition of emissive data was obtained using a Horiba LabRam Spectrometer with 785 nm diode laser excitation and dye concentrations of 1 x 10^{-5} M. The quantum efficiency of the detector was accounted for when measuring emission profiles. The relative quantum yields were obtained using the following equation:

$$\Phi_{Sample} = \Phi_{Standard} * \frac{E_{Sample}}{E_{Standard}} * \frac{A_{Standard}}{A_{Sample}} * \frac{\eta^2_{Sample}}{\eta^2_{Standard}}$$

For the equation above, E is the sum of emission intensities and A is maximum absorbance. The refractive index of the solvent used is accounted for with η and ϕ denotes the quantum yield [35]. The standard used to obtain the relative quantum yields was indocyanine green (ICG) taking the quantum yield to be 14% in H_2O as previously reported [62].

(Z)-1-methyl-3-((2E,4E)-5-(1-methyl-2-phenylindolizin-3-yl)penta-2,4-dien-1-ylidene)-2-phenyl-3H-indolizin-4-ium chloride (C5-Cl): To a round bottom flask equipped with a stir bar, **C5-ClO$_4$** (1.00 g, 1.73 mmol) was added and dissolved in fluorobenzene (0.35 M, 5.0 mL). Tetrabutylammonium chloride (0.47 g, 1.73 mmol) was then added. The mixture was allowed to stir at room temperature overnight. The reaction mixture was then filtered through syringe filters (MicroSolv Nylon, 13 mm diameter, 0.45 μm) to separate the fluorobenzene soluble material from the fine precipitate. The precipitate was then washed from the syringe filters with DCM. The DCM soluble material was then subjected to a silica column with a gradient of 100% DCM to 50:50 DCM:methanol. After concentration, the product was filtered through celite with DCM to remove silica that was dissolved by methanol on the column. The product was isolated as a red solid (0.84 g, 95%). ^{1}H NMR (300 MHz, DMSO-d$_6$) δ 9.18 (d, J = 6.9 Hz, 2H), 8.01 (d, J = 13.6 Hz, 2H), 7.91 (d, J = 8.6 Hz, 2H), 7.70-7.54 (m, 8H), 7.37-7.26 (m, 8H), 5.91 (t, J = 12.5 Hz, 1H), 2.14 (s, 6H). ^{13}C NMR was not obtained due to sparing solubility. IR (neat, cm^{-1}): 2800 (br), 2330, 1750 (br), 1619, 1517. HRMS (ESI) m/z calculated for $C_{35}H_{29}N_2$ [M]$^+$: 477.2331, found 477.2315.

(Z)-1-methyl-3-((2E,4E)-5-(1-methyl-2-phenylindolizin-3-yl)penta-2,4-dien-1-ylidene)-2-phenyl-3H-indolizin-4-ium nitrate (C5-NO$_3$): To a round bottom flask equipped with a stir bar, **C5-Cl** (0.020 g, 0.04 mmol) was added and dissolved in acetonitrile (0.008 M, 5.0 mL). Silver nitrate (0.007 g, 0.04 mmol) was then added to the mixture. The reaction mixture was then allowed

to stir at room temperature for 5 minutes. The reaction mixture was concentrated and directly subjected to silica column chromatography with a gradient from 100% DCM to 50:50 dichloromethane:methanol. The concentrated product was filtered through celite with DCM to remove silica that was dissolved by methanol on the column. The product was isolated as a red solid (0.013 g, 60%). ^{1}H NMR (300 MHz, DMSO-d$_6$) δ 9.16 (d, J = 6.9 Hz, 2H), 7.99 (d, J = 13.6 Hz, 2H), 7.89 (d, J = 8.6 Hz, 2H), 7.68-7.54 (m, 8H), 7.35-7.31 (m, 8H), 5.90 (t, J = 12.5 Hz, 1H), 2.13 (s, 6H). ^{13}C NMR was not obtained due to sparing solubility. IR (neat, cm^{-1}): 2700 (br), 2330, 2123, 1707 (br), 1619, 1559, 1517. HRMS (ESI) *m/z* calculated for C$_{35}$H$_{29}$N$_2$ [M]$^+$: 477.2331, found 477.2357.

(*Z*)-1-methyl-3-((*2E,4E*)-5-(1-methyl-2-phenylindolizin-3-yl)penta-2,4-dien-1-ylidene)-2-phenyl-3*H*-indolizin-4-ium hexafluorophosphate (C5-PF$_6$): To a round bottom flask equipped with a stir bar, (**C5-Cl**) (0.030 g, 0.06 mmol) was added and dissolved in acetonitrile (0.01 M, 5.0 mL). Silver hexafluorophosphate (0.012 g, 0.06 mmol) was then added to the mixture. The reaction mixture was allowed to stir at room temperature for 5 minutes. The reaction mixture was concentrated then subjected to a silica gel column chromatography with a gradient of 100% DCM to 50:50 dichloromethane:methanol. The concentrated product was filtered through celite with DCM to remove any silica that was dissolved by methanol on the column. The product was isolated as a red solid (0.031 g, 79%). ^{1}H NMR (300 MHz, DMSO) δ 9.09 (d, J = 6.9 Hz, 2H), 8.00 (d, J = 13.6 Hz, 2H), 7.88 (d, J = 8.6 Hz, 2H), 7.69-7.54 (m, 8H), 7.33-7.26 (m, 8H), 5.84 (t, J = 12.5 Hz, 1H), 2.15 (s, 6H). ^{19}F NMR (471 MHz, DMSO) δ -70.16 (d, J = 711.2 Hz). ^{13}C NMR was not obtained due to sparing solubility. IR (neat, cm^{-1}): 3100 (br), 2800 (br), 1800 (br), 1653, 1540. HRMS (ESI) *m/z* calculated for C$_{35}$H$_{29}$N$_2$ [M]$^+$: 477.2331, found 477.2315.

(*Z*)-1-methyl-3-((*2E*,*4E*)-5-(1-methyl-2-phenylindolizin-3-yl)penta-2,4-dien-1-ylidene)-2-phenyl-3*H*-indolizin-4-ium bis((trifluoromethyl)sulfonyl)amide (C5-TFSI): To a round bottom flask equipped with a stir bar, **C5-Cl** (0.03 g, 0.06 mmol) was added and dissolved in acetonitrile (0.012 M, 5.0 mL). Silver bis((trifluoromethyl)sulfonyl)amide (0.023 g, 0.06 mmol) was then added to the mixture. The reaction mixture was then allowed to stir at room temperature for 5 minutes. The reaction mixture was concentrated and subjected to silica gel column chromatography with a gradient of 100% DCM to 50:50 dichloromethane:methanol. The product was concentrated and filtered through celite with DCM to remove silica that was dissolved by methanol on the column. The product was isolated as a red solid (0.04 g, 87%). ^{1}H NMR (300 MHz, DMSO-d$_6$) δ 9.16 (d, *J* = 6.9 Hz, 2H), 8.00 (d, *J* = 13.6 Hz, 2H), 7.88 (d, *J* = 8.6 Hz, 2H), 7.68-7.56 (m, 8H), 7.37-7.25 (m, 8H), 5.73 (t, *J* = 12.5 Hz, 1H), 2.15 (s, 6H). ^{19}F NMR (471 MHz, DMSO) δ -78.70. ^{13}C NMR was not obtained due to sparing solubility. IR (neat, cm^{-1}): 2800 (br), 2335, 1750 (br), 1618, 1518. HRMS (ESI) *m/z* calculated for C$_{35}$H$_{29}$N$_2$ [M]$^+$: 477.2331, found 477.2315.

(*Z*)-1-methyl-3-((*2E*,*4E*)-5-(1-methyl-2-phenylindolizin-3-yl)penta-2,4-dien-1-ylidene)-2-phenyl-3*H*-indolizin-4-ium tetraphenylborate (C5-TPB): To a round bottom flask equipped with a stir bar, **C5-Cl** (0.02 g, 0.04 mmol) was added and dissolved in acetonitrile (0.008 M, 5.0 mL). Sodium tetraphenylborate (0.013 g, 0.04 mmol) was then added to the mixture. The reaction mixture was allowed to stir at room temperature for 5 minutes. The reaction mixture was concentrated and subjected to silica gel column chromatography with a gradient of 100% DCM to 50:50 dichloromethane:methanol. The concentrated product was filtered through celite with DCM to remove any silica that was dissolved by methanol on the column. The product was isolated as a

red solid (0.026 g, 84%). ^{1}H NMR (300 MHz, DMSO-d$_6$) δ 9.17 (d, $J = 6.9$ Hz, 2H), 8.01 (d, $J =$ 13.6 Hz, 2H), 7.90 (d, $J = 8.6$ Hz, 2H), 7.70-7.54 (m, 8H), 7.37-7.18 (m, 10H), 6.95-6.82 (m, 12H), 6.80-6.77 (m, 6 H), 5.93 (t, $J = 12.5$ Hz, 1H), 2.14 (s, 6H). ^{13}C NMR was not obtained due to sparing solubility. IR (neat, cm^{-1}): 2900 (br), 2336, 2152, 1857 (br), 1618, 1518. HRMS (ESI) *m/z* calculated for C$_{35}$H$_{29}$N$_2$ [M]$^+$: 477.2331, found 477.2315.

(*Z*)-1-methyl-3-((2*E*,4*E*)-5-(1-methyl-2-phenylindolizin-3-yl)penta-2,4-dien-1-ylidene)-2-phenyl-3*H*-indolizin-4-ium tetra(3,5-bis(trifluoromethyl)phenyl)borane (C5-BARF): To a round bottom flask equipped with a stir bar, **C5-Cl** (0.02 g, 0.04 mmol) was added and dissolved in acetonitrile (0.008 M, 5.0 mL). Sodium tetra(3,5-bis(trifluoromethyl)phenyl)borane (0.04 g, 0.04 mmol) was then added to the mixture. The reaction mixture was allowed to stir at room temperature for 5 minutes. The reaction mixture was concentrated and directly subjected to silica gel column chromatography with a gradient of 100% DCM to 50:50 dichloromethane:methanol. After concentration, the product was filtered through celite with DCM to remove silica that was dissolved by methanol on the column. The product was isolated as a red solid (0.03 g, 84%). ^{1}H NMR (300 MHz, DMSO-d$_6$) δ 9.17 (d, $J = 6.9$ Hz, 2H), 8.01 (d, $J = 13.6$ Hz, 2H), 7.90 (d, $J = 8.6$ Hz, 2H), 7.74-7.54 (m, 18H), 7.37-7.26 (m, 6H), 5.93 (t, $J = 12.5$ Hz, 1H), 2.14 (s, 6H). ^{19}F NMR (471 MHz, DMSO-d$_6$) δ -61.60. ^{13}C NMR was not obtained due to sparing solubility. IR (neat, cm^{-1}): 2918, 2852, 2800 (br), 2330, 2121, 1771, 1619, 1559, 1520. HRMS (ESI) *m/z* calculated for C$_{35}$H$_{29}$N$_2$ [M]$^+$: 477.2331, found 477.2303.

Conclusions

We have synthesized a series of seven compounds that differ only in anion size and electrostatic surface potentials. Anion selection has a dramatic effect on molar absorptivities,

behaviors depending on solvent selection, Stokes shifts variance, altered quantum yields, and solid state photophysics which are strongly affected. These results highlight the critical importance of strictly controlling the anion and the environment around the dye system when comparing optical properties of various dyes in the literature. DCM measurements are found to track with anion size showing that molar absorptivities can be significantly enhanced by a simple non-coordinating anion swap.

CHAPTER 4

4.1 INDOLIZINE-SQUARAINES:NIR FLUORESCENT MATERIALS WITH MOLECULAR

ENGINEERED STOKES SHIFTS

Adapted with the permission from Louis E. McNamara, Tana A. Rill, Aron J. Huckaba,

Vigneshraja Ganeshraj, **Jacqueline Gayton**, Rachael A. Nelson, Emily Anne Sharpe, Amala

Dass, Nathan I. Hammer, and Jared H. Delcamp *Chem. Eur. J.* **2017**, *23*, 12494. Copyright

(2017) Wiley.

(See appendix for permission license)

This project is a collaborative project between Dr. Delcamp's, Dr. Hammer's, and Dr.

Dass' group. Louis E. McNamara contributed to the work by measuring the emission and

quantum yield of the organic dyes and performing computational analyses. Tana A. Rill

synthesized some of the organic dyes as well as characterization of the dyes. Aron J. Huckaba

also synthesized some of the organic dyes as well as characterization of the dyes. Vigneshraja

Ganeshraj solved the crystal structure of the PhIndz dye. Jacqueline Gayton synthesized both the

cis and trans isomers of one of the organic dyes as well as characterization of both. Rachael A.

Nelson assisted in emission measurements. Emily Anne Sharpe assisted with the synthesis of the

organic dyes.

Abstract:

The development of deep red and near infrared emissive materials with high quantum yields is an important challenge. Several classes of squaraine dyes have demonstrated high quantum yields, but require significantly red-shifted absorptions to access the NIR window. Additionally, squaraine dyes have typically shown narrow Stokes shifts, which limits their use in living biological imaging applications due to dye emission interference with the light source. Through the incorporation of indolizine heterocycles we have synthesized novel indolizine squaraine dyes with increased Stokes shifts (up to >0.119 eV, >50 nm increase) and absorptions substantially further into the NIR region than an indoline squaraine benchmark (726 nm versus 659 nm absorption maxima). These materials have shown significantly enhanced water solubility, which is unique for squaraine dyes without water solubilizing substituents. Absorption, electrochemical, computational and fluorescence studies were undertaken and exceptional fluorescence quantum yields of up 12% were observed with emission curves extending beyond 850 nm.

INTRODUCTION

Near-infrared (NIR) absorbing and emitting materials have recently found a number of applications including secure displays, night vision goggles, tissue welding, telecommunications, biological imaging and more.[63-70] Among NIR materials, several donor-acceptor based designs have emerged including those based on cyanine, BODIPY, and squaraine.[71-76] Squaraines have been closely examined in many applications, such as organic solar cell applications, and are of interest for living fluorescence biological imaging applications.[63, 77-78] Ideally, for biological imaging, the NIR material would: (1) be water soluble, (2) absorb and emit photons within the

therapeutic window, 700 nm – 1400 nm, and (3) absorb and emit photons which are significantly different in energies.

Popular indoline donor-based squaraines (**1**) fall short of all of these goals (**Figure 19**). Their absorption often occurs outside the therapeutic window due to wider than desired optical band gaps and their absorption and emission peak intensities are separated by very small energies (<0.01 Ev). Hydrogen bonding approaches have shifted the absorption ranges for benzene based squaraines;[79] however, these dyes often fall short of the NIR window and have narrow absorption-emission peak separations. Water solubility is especially difficult for many squaraines despite having a charged donor and squaraine core, due to the anionic oxygen often being either shielded with hydrophobic groups or heavily hydrogen bonded with the appended donor group. Frequently, the addition of pendant water solubilizing groups are necessary to achieve significant water solubility. Despite these shortcomings, squaraine based dyes remain popular candidates for imaging research purposes as they represent low molecular weight NIR materials with relatively concise syntheses and exceptional molar absorptivities, which are commonly greater than 100,000 $M^{-1}cm^{-1}$.[80] We sought to address the deficiencies by substituting the indoline donor group with a more electron rich, fully conjugated indolizine donor group. Introduction of a sterically hindered donor with increased electron density may lead to significant separation of absorption and emission spectra, further extension of the absorption range into the therapeutic window, and increased water solubility through allowing hydrogen-bonding access to the charged squaraine core (**Figure 19**).
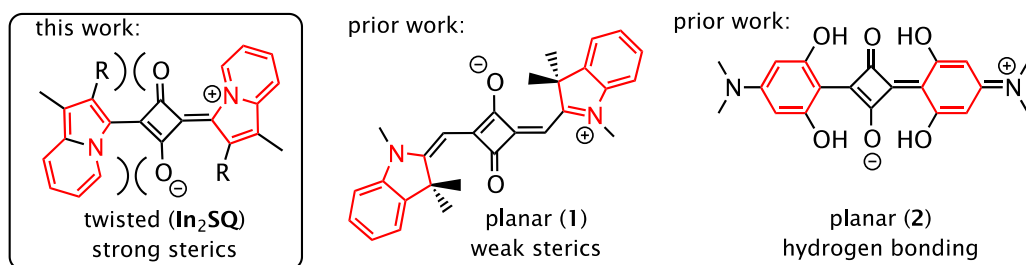
Figure 19. Example classes of popular D-A-D squaraines with the donor motifs highlighted in red.

Indolizines have been shown to yield improved performances in dye-sensitized solar cells owing to their exceptional donor strength when compared with common triphenylamine and alkyl amine-based donor groups within the donor-π bridge-acceptor framework.[81-83] The increase in relative donor strength is in part due to a nitrogen atom with three separate carbon bonds being incorporated into a building block with a fully planar geometry, a fully conjugated π-system involving the nitrogen loan-pair, reduced resonance stabilization energy of the aromatic indolizine, and the proaromatic nature of the indolizine building block in charge transfer systems. These properties are all attractive when selecting a donor for NIR imaging materials, which rely on strong intramolecular charge transfer events. To investigate the effects of different substituents on the dye's energetic properties and NIR emission, we have targeted twelve donor-acceptor-donor (D-A-D) dyes with the indolizine-squaraine-indolizine (**In₂SQ**) D-A-D core held constant (**Figure 20**). The substituents were varied from groups without π-electron contributions for steric analysis to a series of aryl substituents of various size baring electron donating, neutral and electron withdrawing groups for analysis of the influence of pendant aryl groups on the core structure. These substituents provide insight into the effects of substituent size, conjugation and electronic

contributions on the optical properties (molar absorptivity, excited-state lifetime and fluorescence quantum yield) of this new class of material.

The degree of planarity of the conjugated π-system plays a critical role on inducing significant Stokes-shifts. If the ground- and excited-state differ in planarity substantially, a geometry reorganization can occur after photoexcitation potentially leading to significant energy differences in the absorption and emission energies. The indolizine donor offers an nucleophilic position for EAS reactions at the 3-position with substituents at the 2-position and a fused ring in close proximity to the squaraine core allowing for the introduction of sterically demanding substituents to modulate the degree of planarity of the **In₂SQ** core and planarity at the 2-position substituent location, which should offer Stokes-shift tunability (**Figure 20**).
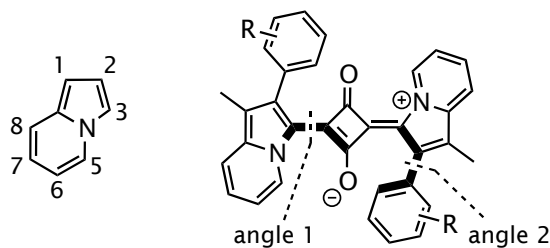
Figure 20. Position numbering convention for the indolizine building block and angles where dihedral steric interactions induce a significant deviation from a planar conjugated system. See **Table 9** for calculated twist angles.
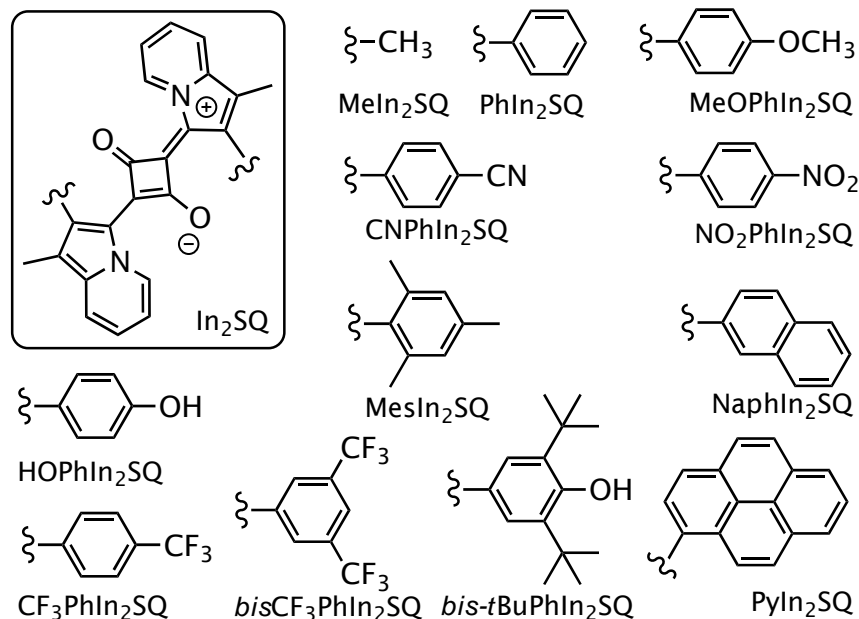
Figure 21. Indolizine-squaraine-indolizine (In$_2$SQ) based target NIR emissive materials.

MeIn$_2$SQ and PhIn$_2$SQ were selected as targets to compare a methyl versus an aryl substituent on the indolizine donors (**Figure 21**). The methyl substituent offers the smallest group, and a more planarized In$_2$SQ core. The phenyl group increases steric bulk near the squaraine core and may additionally expand the dye conjugated π-system through incorporating π-electrons from the phenyl ring. Large aryl substituted squaraine dyes (NaphIn$_2$SQ, PyIn$_2$SQ, *bis*CF$_3$PhIn$_2$SQ, *bis*^{t}BuPhIn$_2$SQ, MesIn$_2$SQ) and electronically variable substituted squaraine dyes (MeOPhIn$_2$SQ, CNPhIn$_2$SQ, NO$_2$PhIn$_2$SQ, HOPhIn$_2$SQ, CF$_3$PhIn$_2$SQ) were targeted to probe steric interactions and evaluate the effect of increased or decreased electron density on the aryl group in order to further probe the photophysical properties of these molecules.

The In$_2$SQ dye series was synthesized in a straight forward 2-step fashion from ethyl pyridine and alphabromo ketone derivatives (**Scheme 1**). Upon heating the bromide and pyridine starting

materials, *N*-alkylated salts were awarded which were insoluble in cold acetone. These pyridinium

salt intermediates were filtered, dissolved in an aqueous base solution, and heated to reflux. The

cyclization-condensation reaction proceeded to give neutral organic indolizine products, which

could be isolated through simple filtration upon cooling the solution. Finally, the indolizine

heterocycles were heated in the presence of squaric acid as a 2:1 ratio of indolizine:squaraine. The

resulting dark green reaction mixture gave an NMR and alumina TLC of analytically pure In2SQ

products upon addition of diethyl ether in many cases. In this manner, >1 gram scale was

demonstrated with no adverse effects on yield and no need for column chromatography for the

PhIn$_2$SQ derivative.

Results and Discussion

Two possible conformational isomers could result from the double condensation reaction with

squaric acid. Given the significant distance the two indolizine building blocks are separated by,

NMR may not show a substantial difference in the two possible isomers if both were present as a

mixture. To confirm the isomeric purity of the samples, a combined computational IR spectrum

prediction and experimental IR spectroscopy approach was employed. The B3LYP density

functional was employed with the 6-311g (d,p) basis set in order to calculate the modes and IR

intensities of both the cis and trans rotamer of PhIn$_2$SQ. The calculated modes were scaled by

0.975 in order to correct for the harmonic approximation. Modes were determined experimentally

by ATR-IR and compared to calculations of both rotamers (**Figure 22**). A mixture of the two

rotamers would show little difference according to the predicted spectrum since both rotamers are

similar except in the region between 1600 and 1800 cm^{-1}. In this region there is noticeably

difference between the cis and trans rotamer computationally with better agreement between the

experimental IR spectrum and the calculated modes for the cis rotamer, suggesting the cis rotamer is a product of the reaction (**Scheme 1**).

Scheme 1. Synthetic route to In$_2$SQ dyes.
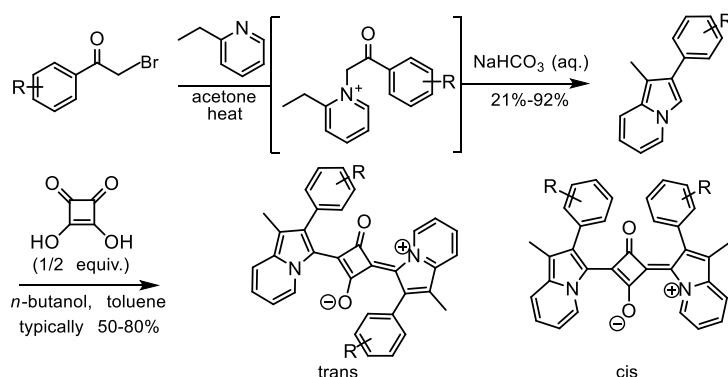
Since the majority of the IR spectrum (600-1600 cm^{-1}) is predicted to be similar for the cis and trans rotamers, the obvious peak confirming the cis rotamer presence that is not present for the predicted trans rotamer spectrum, cannot be used to exclude the presence of the trans rotamer in the mixture. As such, a variety of crystallization techniques were attempted, and the most successful crystallization attempt led to the formation of small (<0.5 mm) cubic crystals from the vapor diffusion of diethyl ether into chlorobenzene. These crystals, despite the small size, were X-ray quality and proved the presence of the trans rotamer (**Figure 23**). The crystal structure shows a significant dihedral angle between the phenyl and indolizine planes at 51° and a dihedral angle of 21° between the indolizine and squaraine plane. These results are further compared with computational results below.
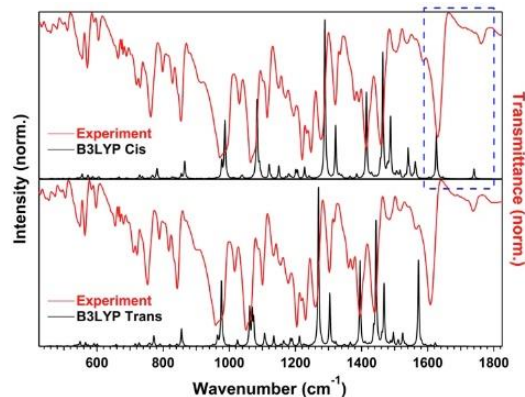
Figure 22. IR spectrum of PhIn$_2$SQ comparing the computational results for the cis rotamer (top, black) and the trans rotamer (bottom, black) to the experimental results (red).
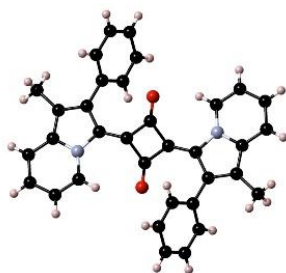
Figure 23. X-ray crystal structure representation for PhIn$_2$SQ as the trans rotamer.

The PyIn$_2$SQ derivative was unique among the synthesized derivatives in that the cis and trans rotamers were separable via silica gel chromatography with the trans rotamer eluting with a higher Rf value. Separation of these rotamers allowed for the comparison of a purified trans rotamer vibrational spectrum to the cis rotamer vibrational spectrum (see appendix **Figure 76**). For this rotamer, the peak at 1750 cm^{-1} is present for the cis rotamer similar to that predicted and observed for the PhIn$_2$SQ cis rotamer. This peak is not present for the trans rotamer experimentally, as predicted. The PyIn$_2$SQ was uniquely able to be studies as the purified cis rotamer, the purified trans rotamer and as a mixture. It is important to note however, that the rotational barrier to convert

61

from the cis to trans rotamer can be crossed at room temperature on the order of a day timescale. The existence of both rotamers could only be confirmed for PyIn$_2$SQ since no evidence of the cis isomer was obvious for the other derivatives.

Upon isolation of these novel dyes, the optical properties were probed by UV-Vis-NIR absorption spectroscopy to evaluate the effect the indolizine donor group in relation to the indoline standard (**1**). Comparison of MeIn$_2$SQ and **1** reveals a near 50 nm red-shift for the indolizine based dye (**Figure 24**). The 50 nm shift in absorption maxima to lower energy places these dyes in a more ideal range for use with non-invasive *in vivo* fluorescence imaging applications. Interesting, the absorption curve shape shows a very similar profile for both dyes with a strong, relatively sharp peak at low energy, followed by a weaker vibronic transition at slightly higher energy as a shoulder. Absorption spectra show a characteristic, intense absorption near 720 nm and no substantial absorption between 675 nm and 450 nm (see appendix **Figures 77 and 78**). MeIn$_2$SQ does show an extended absorption peak ½ height width of 45 nm (0.108 eV) versus 20 nm (0.076 eV) for benchmark **1** (**Figure 24**).
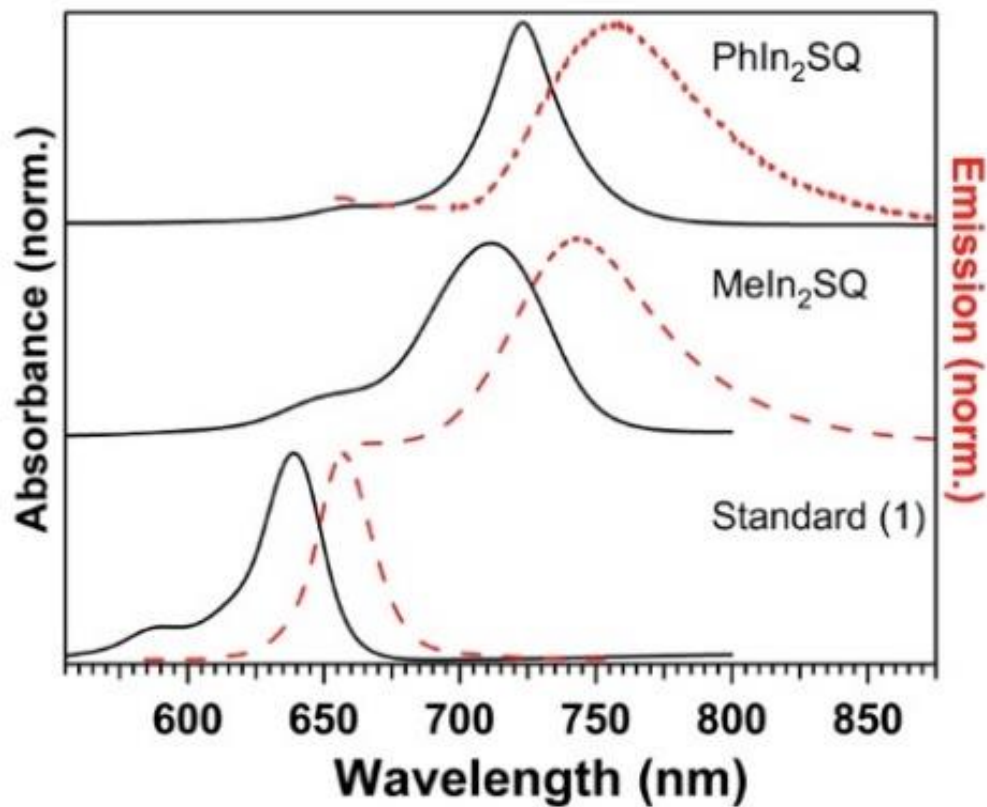
Figure 24. Comparison of UV-Vis-NIR absorption spectra (solid black lines) and emission spectra (dashed red lines) for **1**, MeIn$_2$SQ and PhIn$_2$SQ in toluene (see appendix for absorption and emission curves of all derivatives).

Table 8. Comparison of Stokes shifts, absorption, emission maxima, molar absorptivity, photoluminescent quantum yield and fluorescent lifetimes in toluene. *Indicates in DMSO.

Dye	Abs. Max. (nm)	Emis. Max. (nm)	Stokes Shift (nm, eV)	ε (M^{-1}cm^{-1})	Φ (%)	τ (ns)
MeIn$_2$SQ	712	738	26, 0.055	210,000	8.9	0.42
PhIn$_2$SQ	723	756	33, 0.075	181,000	3.7	0.45
NaphIn$_2$SQ	727	766	39, 0.087	150,000	5.3	0.45
PyIn$_2$SQ	729	757	28, 0.063	124, 000	10.5	1.11
PyIn$_2$SQ (trans)	730	756	26, 0.058	160,000	5.8	1.03
PyIn$_2$SQ (cis)	730	754	24, 0.054	110,000	12.1	1.46
MesIn$_2$SQ	724	735	11, 0.026	262,000	7.3	0.30
*Bis-t*BuPhIn$_2$SQ	722	770	48, 0.107	216,000	6.7	0.55
Bis-CF$_3$PhIn$_2$SQ	727	757	30, 0.068	260,000	12.0	0.79
CF$_3$PhIn$_2$SQ	727	765	38, 0.085	166,000	5.9	0.40
CNPhIn$_2$SQ	729	756	54, 0.119	213,000	5.8	0.65
NO$_2$PhIn$_2$SQ	732	769	37, 0.082	185,000	11.2	0.65
MeOPhIn$_2$SQ	723	761	38, 0.086	140,000	4.5	0.33
HOPhIn$_2$SQ*	723	756	33, 0.075	185,000	1.0	0.09
1	633	653	20, 0.050	229,000	16.0	2.40

Additionally, the indolizine group substituent influence on optical properties was evaluated based on electron donation ability, electron withdrawing ability, steric size and extended π-system size

for a variety of aryl groups. Comparison of a methyl versus a phenyl at the 2-position shows a 10 nm red-shift for the aryl substituted PhIn$_2$SQ dye. Among aryl groups however, a modest effect on absorption maxima position is observed with a close range varying by only 9 nm (723-732 nm) for the series in toluene. The absorption spectrum in dichloromethane was found to give similar absorption maxima shifted by about 6 nm to higher energy (see appendix for DCM results, **Table 45**). This suggests poor electronic coupling of the aryl group π-system with the squaraine π-system in the ground-state since strongly withdrawing and donating substituents have little effect on the absorption spectrum. A comparison of molar absorptivity of MeIn$_2$SQ and **1** shows a modest reduction in molar absorptivity for the indolizine-based dye (210,000 versus 229,000 M^{-1}cm^{-1} in toluene). A substantially larger effect on molar absorptivities was observed with indolizine substituent choice ranging from 110,000-262,000 M^{-1}cm^{-1} in toluene. Replacement of a methyl at the 2-position with a phenyl group reduces the dye's molar absorptivity from 210,000 to 181,000 M$^-$cm^{-1}. Expansion of the substituent π-system from phenyl to naphthyl further lowered the molar absorptivity by 31,000 M^{-1}cm^{-1} (from 181,000 to 150,000 M^{-1}cm^{-1}). Finally, pyrene substitution results in the lowest molar absorptivity of the series at 124,000 M^{-1}cm^{-1} for the mixture (**Figure 25**).
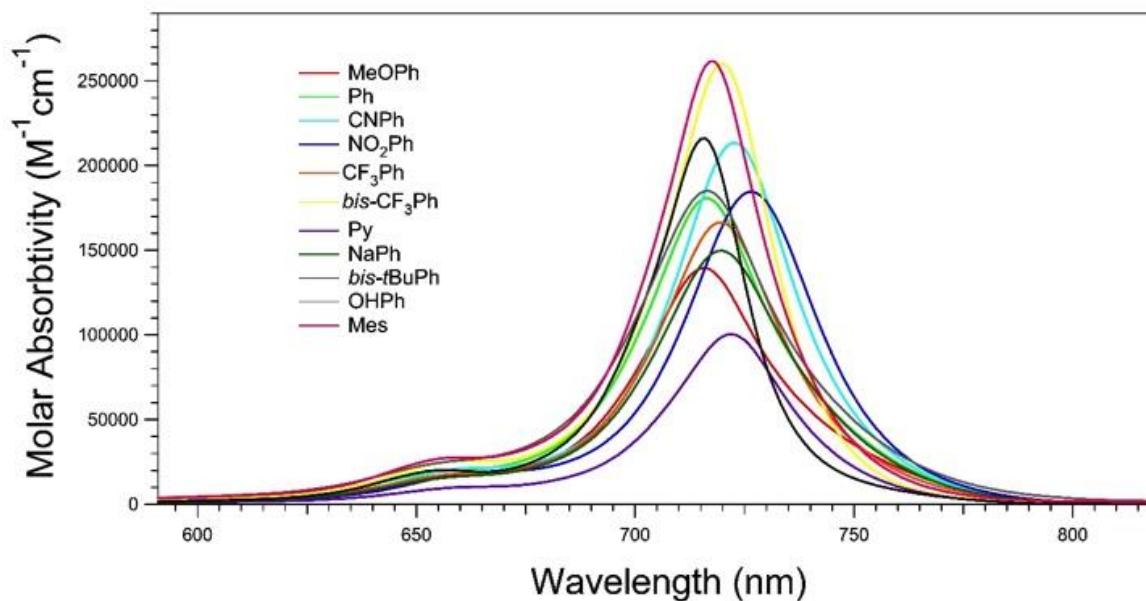
Figure 25. Comparison of molar absorptivities for all arylated dyes.

To probe if the lowering of molar absorptivity is a result of increasing the π-system size or a result of increasing steric bulk MesIn$_2$SQ, *bis-t*BuPhIn$_2$SQ and *bis*-CF$_3$PhIn$_2$SQ were evaluated as neutral, electron rich and electron deficient aryl groups. Increasing steric bulk leads to the highest molar absorptivities observed, exceeding those of the parent indolizine dye and the benchmark **1** by as much as 33,000 M^{-1}cm^{-1}. The MesIn$_2$SQ and *bis*-CF$_3$PhIn$_2$SQ had similar molar absorptivities of near 260,000 M^{-1}cm^{-1}, while the electron rich *bis-t*BuPhIn$_2$SQ gave a lower molar absorptivity of 216,000 M^{-1}cm^{-1}. To probe the lower molar absorptivity origin, a variety of electron donating (Ome, OH) and withdrawing (CN, NO$_2$, CF$_3$) substituents were evaluated at the para-position on each phenyl of PhIn$_2$SQ. However, no apparent trend emerged based on electronic considerations (**Table 8**).
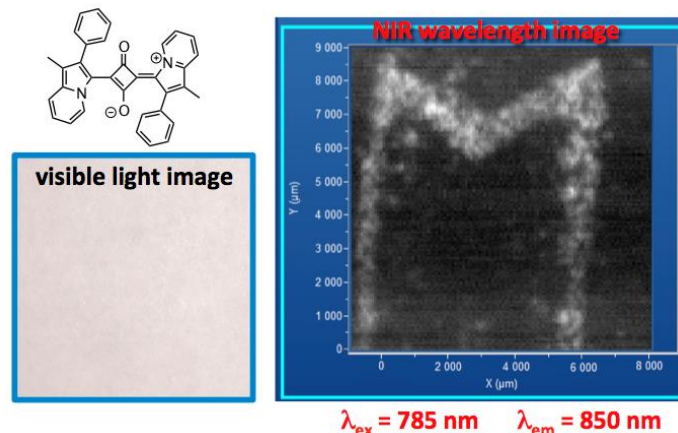
Figure 26. PhIn$_2$SQ Arranged in an "M" and covered by white filter paper.

Having established the desired red-shifting of the absorption spectrum in the therapeutic window (~700-1400 nm, dye absorption onsets ~750 nm) through the use of indolizine donors and retained high molar absorptivities, we next evaluated the emissive properties of the dyes in solution. The fluorescence spectra of the compounds were recorded in toluene and DCM. A large Stokes shift, the difference in energy between the absorption maximum and fluorescence maximum, is desirable for applications requiring significant separation between input and output energy, such as live fluorescence imaging. For this application specifically, molecules should also emit within the therapeutic window (~700-1400 nm). The emission maxima for these dyes were found to range from 756-777 nm with the exception of MesIn$_2$SQ, which emits at noticeably higher energy (735 nm). This gives Stokes shifts of around 30-50 nm or 0.063-0.119 eV for In$_2$SQ series (except MesIn$_2$SQ 11 nm, 0.026 eV), which is a significantly larger separation of input and output energies than observed for the benchmark **1** (12 nm, 0.034 eV) (**Table 8**). The absorption and emission of the most water soluble derivative, MeIn$_2$SQ, was also investigated by dissolving the dye in

minimal DMSO then diluting with water (see appendix **Figure 84**). A blue shift of the absorption spectrum is noted; however, no evidence of aggregation was observed based on absorption or emission curve shapes since there are no noticeable changes comparing water with organic solvents.

The excited-state lifetimes for the dyes in this series ranged from 0.30 ns to 0.79 ns with the longest excited-state lifetime from *bis*-CF$_3$PhIn$_2$SQ (0.79 ns) and the shortest excited-state lifetimes from MesIn$_2$SQ (0.30 ns) and MeOPhIn$_2$SQ (0.33 ns). It is noteworthy that the resonance withdrawing substituted dyes CNPhIn$_2$SQ and NO$_2$PhIn$_2$SQ have relatively long-lived excited-states (both at 0.65 ns) and the resonance donating substituted MeOPhIn$_2$SQ has a relatively short-lived excited-state. While all of the dyes show shorter excited-state lifetimes than the benchmark squaraine **1** (2.40 ns), this is expected as dyes emitting at lower energies typically have reduced excited-state lifetimes due to the Energy Gap Law.

The fluorescence quantum yield is one of the most important metrics for evaluating fluorescent materials, especially in the NIR range where Φ is typically very low, often <1%.[84] For a number of applications, Φ dictates the amount of dye needed for good image resolution and device performance. Interestingly, PyIn$_2$SQ was found to have a fluorescence quantum yield of >12%. This is a dramatic enhancement over what is commonly observed for materials emitting photons at energies lower than 800 nm, with notable exceptions[85-87]. The next highest Φ values were observed for *bis*-CF$_3$PhIn$_2$SQ (12%) and NO$_2$PhIn$_2$SQ (11%), with the remaining dyes emitting between 3.7%-8.9%. Even the lowest observed Φ for this series is a significant enhancement over that of many materials currently being evaluated for biological imaging purposes. Although substantially larger Stokes-shifts are observed compared to benchmark, **1,** with

less absorption and emission overlap, we do note that considerable overlap of absorption and emission curves is observed for the indolizine squaraine dyes, which can lead to re-absorption and diminished quantum yields. It is interesting that of the dyes evaluated computationally, PyIn$_2$SQ had a substantial influence of the HOMO^{-1} orbital (which is heavily influenced by the π-system of pyrene) on the vertical transition. Since the PyIn$_2$SQ dye has the highest quantum yield in the series, the modulation of the HOMO^{-1} to have a significant contribution to vertical transition upon transfer of charge to the LUMO may be a novel strategy for enhancing Φ values for NIR emissive materials. This suggests tuning lower level orbitals could have substantial influences on Φ values.

The solid-state absorption of all the dyes was also measured by diffuse reflectance spectroscopy. All of the dyes showed absorption in the 600-800 nm range in the solid state with several of the dyes' having absorption extending well into the 800-900 nm range (see appendix **Figure 82**). Solid-state emission of dyes in this range is useful for potential applications in secure display technologies (NIR OLEDs). As a demonstration for the use of these materials in as solid emitters, PhIn$_2$SQ powder was arranged in the shape of an "M", then covered with a white filter. As shown in **Figure 26**, under visible light irradiation only the filter is visible. However, under NIR irradiation at 785 nm through the white filter, an image of the PhIn$_2$SQ powder is clearly visible via NIR photon detection at 850 nm. The emission spectra of each dye in the solid state can be found in appendix **Figure 83**.

Substituent selection has relatively minor effects on absorption and emission energies. Electrochemical analysis was used to find if the substituents are effectively isolated from the In$_2$SQ π-system responsible for the observed absorption and emission energies. The electrochemical properties of the dyes are also critical for applications involving solar cells, display applications,

photochemical reactions and for assessing of the stability of the dyes under atmosphere. The dye ground-state oxidation potentials ($E_{(S+/S)}$) ranged from 1.26 to 1.44 V versus ferrocene and the excited-state oxidation potentials ($E_{(S+/S*)}$), varied from -0.88 V to -1.22 V. The ground-state reduction potentials ($E_{(S/S-)}$) show a similar range of potentials (-1.37 to -1.55 V). Interestingly, this indicates the substituents have tunable control of $E_{(S+/S)}$, $E_{(S/S-)}$ and $E_{(S+/S*)}$ energy levels without significantly altering the optical band gap energy (E_g^{opt}) which only varies by 0.04 Ev between dyes. In general, the dye substituents give the expected changes in energy levels where added π-electron density from aryl groups raise energy levels to more destabilized values and substituents withdrawing π-electron density lead to more stabilized energy levels (see appendix **Table 46**).

The observed Stokes shifts are hypothesized to be the result of a geometric reorganization in the excited-state to allow for increased planarization of the π-system. To evaluate this hypothesis, computational analysis was performed on PhIn$_2$SQ with DFT at the B3LYP/6-311g(*d,p*) level. Ground-state and excited-state geometries were first optimized, then TD-DFT at the B3LYP/6-311g(*d,p*) level was carried out to predict the vertical excitation (ground-state geometry) and relaxation energies (excited-state geometry), where the difference of these corresponds to a Stokes-shift. Provided reasonable agreement is observed between theory and experiment, the geometry changes from the ground to the excited-state can be analyzed to better understand the origin of the Stokes-shift observed.

In the ground state, the HOMO and LUMO were found to be delocalized throughout the indolizine-squaraine π-system with little orbital contribution from the indolizine substituents (**Figure 27**). The HOMO^{-1} orbital was found to be the first orbital with substantial contribution of

the indolizine-aryl substituent to the π-system (see appendix **Figure 85**). The indolizine-squaraine backbone is not fully planar and the PhIn$_2$SQ$_{trans}$ derivative was found to have a twist angle of 10 degrees between the indolizine plane and the squaraine plane which is in reasonable agreement with the crystallographic data collected (**Table 9**, **Figure 28**). Additionally, the aryl substituents have a substantial dihedral angle when compared to the plane of the indolizine (62 degrees for PhIn$_2$SQ$_{trans}$, in close agreement with crystallographic measurements). The twist angles and calculated energies are similar for PhIn$_2$SQ$_{cis}$ when compared with PhIn$_2$SQ$_{trans}$ (see appendix **Table 47**). The PyIn$_2$SQ$_{trans}$ derivative was also evaluated as it had the largest fluorescence quantum yield. PyIn$_2$SQ$_{trans}$ has similar dihedral angles to the PhIn$_2$SQ$_{trans}$ derivative with 8 degrees at the indolizine-squaraine planes and 72 degrees at the pyrene-indolizine planes.
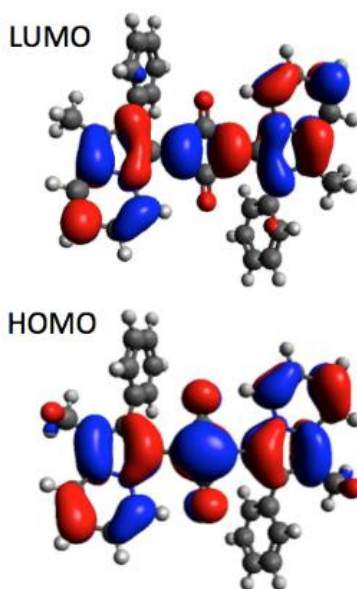
Figure 27. HOMO and LUMO orbitals for PhIn$_2$SQ as determined by B3LYP/6-311g(d,p) DFT geometry optimization.

Interestingly, PyIn$_2$SQ$_{cis}$ has a reduced indolizine-squaraine dihedral angle of only 2 degrees and an increased pyrene-indolizine dihedral angle of nearly perpendicular at 87 degrees (see appendix for cis rotamer values).

TD-DFT (B3LPY/6-311g(d,p)) was used to assess the orbital contributions to the vertical transition upon photoexcitation of electrons in the ground-state to the excited-state. The vertical excitation was found to be primarily composed of a HOMO to LUMO contribution (90% for PhIn$_2$SQ$_{trans}$, 98% for PhIn$_2$SQ$_{cis}$) with some contribution of the HOMO^{-1} to LUMO transition for the trans rotamers (8% for PhIn$_2$SQ$_{trans}$). The contribution of the HOMO^{-1} to LUMO transition was greatly increased for the large π-system pyrene substituted dye with 58% HOMO to LUMO and 36% HOMO^{-1} to LUMO for PyIn$_2$SQ$_{trans}$ and 20% and 72% for the respective orbital transitions for PyIn$_2$SQ$_{cis}$ (see appendix).

The substantial involvement of the HOMO^{-1} orbital highlights the importance of the aryl substituents in controlling the emissive properties of the indolizine-squaraine dye series. The MeIn$_2$SQ derivative also confirms the importance of the aryl groups as this compound shows a 98% HOMO to LUMO contribution to the lowest energy transition for both the trans and cis confirmers (**Table 9**).
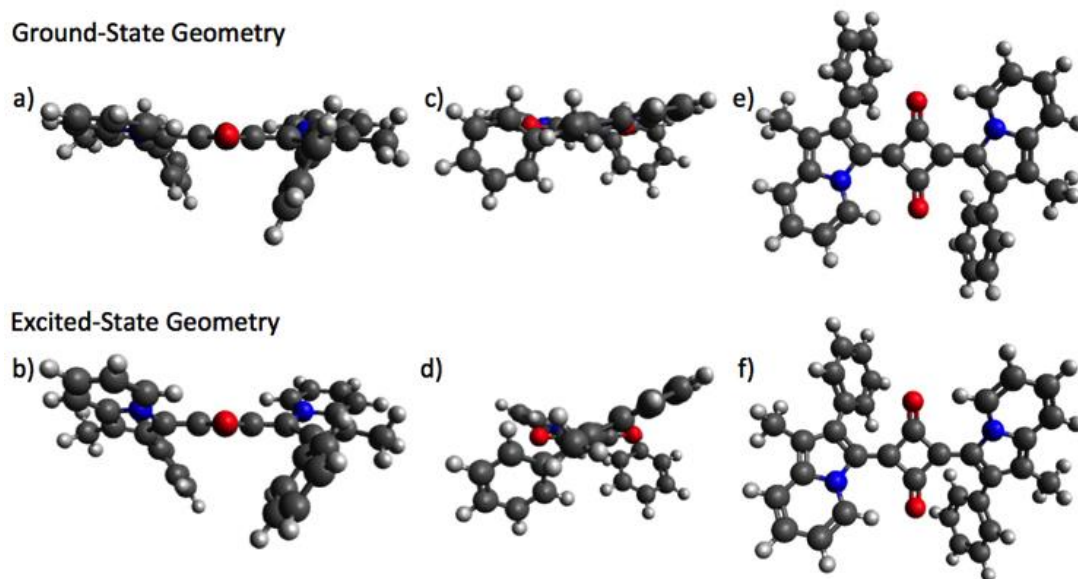
Figure 28. Comparison of the geometry of PhIn$_2$SQ in the ground and excited-state along the indolizine-squaraine-indolizine edge (a and b), along the indolizine edge (c and d), and of the π-system face (e and f), respectively.

The excited-state geometries were optimized with TD-DFT calculations on the PhIn$_2$SQ and PyIn$_2$SQ derivatives. In both cases (trans or cis), the indolizine substituent adopts a more planarized configuration with a 6-8 degree reduction in the dihedral angle. This observation suggests the aryl substituents may have a significant influence on the dye excited-state properties. Interestingly, the indolizine-squaraine dihedral angle substantially *increases* in the excited state. A substantial increase of the indolizine-squaraine dihedral angle is observed for PhIn$_2$SQ$_{trans}$ (17˚), PhIn$_2$SQ$_{cis}$ (12˚), PyIn$_2$SQ$_{trans}$ (7˚) and PyIn$_2$SQ$_{cis}$ (4˚).

Table 9. Dihedral angles, orbital contributions to vertical transitions, vertical transition energies and oscillator strengths computed with DFT and TD-DFT analysis at the B3LYP/6-311g(d,p) level.

dye	angle 1 (°)	angle 2 (°)	transition	contrib. (%)	vert. trans. (nm | eV)	oscillator strength
MeIn$_2$SQ	9°	-	H → L	98%	569 | 2.18	1.0118
PhIn$_2$SQ	10° (21°)[a]	62° (51°)[a]	H → L	90%	607 | 2.04	0.7524
			H^{-1} → L	8%		
PyIn$_2$SQ	8°	72°	H → L	58%	628 | 1.97	0.4171
			H^{-1} → L	36%		
			H^{-3} → L	5%		
MeIn$_2$SQ*	25	-	H → L	83%	676 | 1.83	0.5317
			H^{-1} → L	14%		
PhIn$_2$SQ*	27°	56°	H → L	78%	733 | 1.69	0.3689
			H^{-1} → L	19%		
PyIn$_2$SQ*	13°	66°	H → L	38%	758 | 1.64	0.1019
			H^{-1} → L	56%		
			H^{-3} → L	4%		

The reduced reorganization of the excited-state geometry for PyIn$_2$SQ relative to the ground-state geometry suggests the possibility of a higher fluorescence quantum yield for this dye is due to a better geometry overlap between the ground- and excited-states. Importantly, upon computational analysis of the MeIn$_2$SQ derivative, an increase in dihedral angle is still observed in the excited state (9° to 25^0) indicating the geometry reorganization is not the direct result of the aryl group on the indolizine. Additionally, no significant shifts in bond length are observed between the ground and excited-states, which indicates the driving force for the reorganization computationally observed is subtle.

A series of indolizine-squaraine based NIR fluorescent compounds, with emission maxima ranging from 730 to 770 nm, were synthesized and the optical properties studied. The dyes were studied with X-ray crystallography as well as IR spectroscopy to assess the presence of structural

rotamers. The NIR dyes were analyzed with electrochemical studies, UV−Vis-NIR spectroscopy, and fluorometry in a variety of solutions as well as in the solid-state. Compared to a benchmark indoline-squaraine compound, these materials are significantly red-shifted in absorption and emission spectrum values. Solution absorption and emission curves show Stokes shifts up to 50 nm and some of the highest fluorescence quantum yields known for emissive small molecules in this NIR region with significant Stokes-shifts (Φ>12%). Large Stokes shifts are desirable for living biological imaging applications to avoid background signals from the excitation source, and the squaraine-based dyes examined have demonstrated a large shift and high PLQE. DFT computational analysis shows the origin of this Stokes-shift to come from the molecular engineering of large dihedral angles within the π-system, which undergo significant changes when the excited-state geometry reorganizes.

Experimental General Information.

Photophysical Measurements: UV-Vis-NIR absorption spectra were all taken using a Cary 5000 UV-vis-NIR spectrometer. All dye solutions were stirred for at least 30 minutes with slight warming to fully dissolve the In_2SQ dyes. Solution phase photoluminescent quantum efficiencies (PLQE) were obtained using the optically dilute method described by Crosby and Demas.[88] All sample concentrations were on the order of 10^{-5} M to reduce reabsorption. The 647 nm line of a Kr+ ion laser was used as the excitation source, and zinc phthalocyanine ($\varphi = 0.30$ in 1% pyridine in toluene)[89] was used as a reference. Fluorescent lifetimes were obtained by exciting with the 485 nm line of a pulsed diode laser (fwhm <100 ps) and detecting with an avalanche photodiode.

Computational Analysis: MM2 energy minimization in ChemBio3D Ultra (version:13.0.2.3021) was used for the initial energy minimization of the TPz-based dyes. Dihedral angles for the relevant groups were set to values between the global minimum and the next local minimum on the conformational energy diagram as calculated by chemBio3D. Accurate geometry optimization were performed sequentially by density functional theory (DFT) using Guassian09[90] with the B3LYP[91-92] functional with the following basis sets: first 6-31g (d,p) and finally 6-311g (d,p). Dihedral angles were evaluated with the GaussView software on the fully optimized geometries. Time-dependent density functional theory (TD-DFT) computations were performed with optimized geometries and with the B3LYP functional and 6-311g (d,p) basis set to compute the vertical transition energies, oscillator strengths and orbital contributions to the vertical transitions.

Synthetic Materials and Instruments: All commercially obtained reagents and solvents were used as received without further purification. Thin-layer chromatography (TLC) was conducted with Analtech Alumina GF UV254 250 micron plates or Sorbtech Silica XHL TLC Plates with UV254 250 micron plates and visualized with UV irradiation when appropriate. Flash column chromatography was performed using Sorbent Tech P60, 40-63 μm (230-400 mesh). ^{1}H and ^{13}C NMR spectra were recorded on a Bruker Avance-300 (300 MHz) spectrometer and a Bruker Avance-500 (500 MHz) spectrometer and are reported in ppm using solvent as an internal standard (CDCl$_3$ at 7.26 ppm). Data reported as: s = singlet, d = doublet, t = triplet, q = quartet, p = pentet, m = multiplet, br = broad, ap = apparent, dd = doublet of doublets; coupling constant(s) in Hz; integration. UV-Vis Spectra were measured with a Cary 5000 UV-Vis-NIR spectrometer. Cyclic voltammetry was measured with a C-H Instruments 600E electrochemical analyzer. ATR-

IR were taken using an Agilent Technologies Cary 600 series FTIR Spectrometer. Crystal structure data was gathered with a Bruker APEX-II CCD diffractometer. The crystal was kept at 296 K during data collection. Using Olex2 software, the structure was solved with the ShelXT structure solution program using Direct Methods and refined with the XL refinement package using Least Squares minimization.

General Synthetic Procedure for Indolizine Heterocycle Synthesis: To a round bottom flask equipped with a stir bar and a reflux condenser was added 2-ethylpyridine (1.0 equiv.) and the desired alpha-bromoketone derivative (1.0 equiv.). After addition of acetone, the mixture was heated to 60°C or reflux for 16 hours. After cooling to room temperature, the white precipitate was filtered and washed with cold acetone. The solid was mixed with sodium bicarbonate and water and heated to reflux. After 2-7 hours, the solid formed is filtered and used in the next step without further purification.

General Synthetic Procedure for Squaraine Dye Double Condensation: To a flame dried round bottom flask equipped with a stir bar and reflux condenser was added 2.0 equivalents of the desired indolizine and 1.0 equivalent of squaric acid. A 1:1 mixture of toluene:*n*-butanol was added where the combined solvent mixture gave a concentration of 0.02 M. The mixture was vigorously degassed with N_2 for 10 minutes, then heated to reflux for 20 hours. After cooling to room temperature, approximately 10 times the reaction mixture volume of diethyl ether was added to precipitate out a green solid. The liquid was decanted to give the pure product. Alternatively, upon completion of the reflux time the mixture could be extracted with dichloromethane, washed with water three times, purified with alumina chromatography and a gradient solvent system

(dichlormethane:hexanes -> dichloromethane:methanol mixtures) and recrystallization from acetone/dichloromethane mixtures.

Specific Synthetic Procedures

1,2-dimethylindolizine (1): In a nitrogen filled round bottom flask equipped with a stir bar and a reflux condenser 2-ethylpyridine (2.00 g, 18.7 mmol) was mixed with chloroacetone (1.72 g, 18.7 mmol). The mixture was degassed with N_2 for 20 minutes, then heated to 130°C for 24 hours. The product was extracted with excess ethyl acetate and 2 M KOH and dried with sodium sulfate. The product was purified through aluminum oxide chromatography with 500 Ml hexanes to yield the pure product (0.386 g, 14%). ^{1}H NMR (500 MHz, CDCl$_3$) δ 7.76 (d, J = 7.5 Hz, 1H), 7.24 (d, J = 7.5 Hz, 1H), 7.10 (s, 1H), 6.55 (dd, J = 7.5 Hz, 4.0 Hz, 1H), 6.33 (ap t, J = 7.5 Hz, 1H), 2.26 (s, 6H). This compound has been previously synthesized and characterized through an alternative route.[93]

 (Z)-4-(1,2-dimethyl-3*H*-indolizin-4-ium-3-ylidene)-2-(1,2-dimethylindolizin-3-yl)-3-oxocyclobut-1-en-1-olate (MeIn₂SQ): To a flame dried round bottom flask equipped with a stir bar and reflux condenser, **1** (0.34 g, 2.34 mmol) was added then 3,4-dihydroxy-1,2-cyclobutanedione (0.12 g, 1.05 mmol) followed by purging with N_2 for 10 minutes. The mixture was dissolved in a degassed 1:1 mixture of toluene and n-butanol (squaric acid was 0.017 M in the mixture) and refluxed for 20 hours. The reaction mixture was then cooled to room temperature and 500 Ml diethyl ether was added to crash out a green solid. The liquid was centrifuged then decanted to yield the pure product as a black solid (0.24 g, 61%). ^{1}H NMR (500 MHz, CDCl$_3$) δ 10.35 (d, J = 7.0 Hz, 2H), 7.28 (d, J = 7.2 Hz, 2H), 7.15 (t, J = 6.8 Hz, 2H), 6.85 (t, J = 6.9 Hz, 2H), 2.81 (s,

6H), 2.21 (s, 6H). ^{13}C NMR was not obtained due to sparing solubility. IR (neat, cm^{-1}): 3392 (br), 1626, 1624. HRMS m/z calculated for C$_{24}$H$_{20}$N$_2$O$_2$ [M]$^+$: 368.1525, found 368.1563. UV-Vis (CH$_2$Cl$_2$) λ_{max} = 704 nm; UV-Vis (toluene) λ_{max} = 712 nm (ε = 210,000 M^{-1}cm^{-1}), λ_{onset} = 750 nm.

(Z)-4-(1-methyl-2-phenyl-3H-indolizin-4-ium-3-ylidene)-2-(1-methyl-2-phenylindolizin-3-yl)-3-oxocyclobut-1-en-1-olate (PhIn$_2$SQ): To a flame dried round bottom flask equipped with a stir bar and reflux condenser, 1-methyl-2-phenylindolizine **(2)**[23] was added (0.50 g, 2.4 mmol) then 3,4-dihydroxy-1,2-cyclobutanedione (0.137 g, 1.20 mmol) was added followed by purging with N$_2$ for 10 minutes. The mixture was dissolved in 136 mL 1:1 toluene:n-butanol then heated to 130°C for 15 hours. The mixture was cooled to room temperature, extracted with dichloromethane and washed three times with water. The product was purified through alumina chromatography with a gradient of 75:25 dichloromethane:hexanes then 98:2 dichloromethane:methanol and recrystallized in acetone and dichloromethane to yield a green solid (0.49 g, 82%). ^{1}H NMR (500 MHz, CDCl$_3$) δ 10.07 (d, J = 6.9 Hz, 2H), 7.5-7.40 (m, 6H), 7.39-7.35 (m, 6H), 7.19 (ap t, J = 6.0 Hz, 2H), 6.86 (ap t, J = 7.3 Hz, 2H), 2.18 (s, 6H). ^{13}C NMR (125 MHz, CDCl$_3$) δ 175.7, 168.5, 141.4, 137.6, 135.0, 134.7, 130.6, 127.6, 127.5, 126.9, 120.6, 118.2, 117.0, 114.9, 9.5. IR (neat, cm^{-1}): 3401 (br), 2356, 2329, 2038, 1633, 1616. HRMS m/z calculated for C$_{34}$H$_{25}$N$_2$O$_2$ [M+H]$^+$: 493.1916, found 493.1962. UV-Vis (CH$_2$Cl$_2$) λ_{max} = 716 nm; UV-Vis (toluene) λ_{max} = 723 nm (ε = 181,000 M^{-1}cm^{-1}), λ_{onset} = 755 nm.

2-bromo-1-mesitylethanone (3): To a round bottom flask equipped with a stir bar, mesitylene (10 mL, 96.4 mmol) was added and cooled to 0°C. After 10 minutes, aluminum trichloride (1.7 g, 13 mmol) was added and allowed to cool for 5 minutes. 2-bromoacetyl chloride was added drop wise (6.00 mL, 72.0 mmol). The solution turned from yellow to orange, and was stirred while warming

to room temperature for 15 hours. The reaction mixture was then poured into 100 mL cold H_2O and extracted twice with 150 mL Et_2O. The organic layer was washed with 50 mL saturated sodium bicarbonate, dried with magnesium sulfate, filtered and concentrated to yield a pure product (16.4 g, 94%). ^{1}H NMR (300 MHz, $CDCl_3$) 6.90 (s, 2H), 4.29 (s, 2H), 2.32 (s, 3H), 2.26 (s, 6H). This molecule has been previously synthesized through an alternate route.[94]

2-mesityl-1-methylindolizine (4): To a sealed pressure flask equipped with a stir bar and a reflux condenser was added **3** (2.41 g, 10 mmol) and 2-ethyl pyridine (1.14 mL, 10 mmol) in 0.5 M acetone (20 mL). The reaction mixture was heated to 150°C for 24 hours, then cooled to room temperature, poured into a 100 mL round bottom flask and dissolved in 70 mL H_2O and sodium bicarbonate (3.5 g, 40 mmol). The mixture was heated to 100°C for 2 hours, then cooled to room temperature, extracted with dichloromethane and concentrated. The product was passed through 200 mL SiO_2 using hexanes:DCM (70:30) and concentrated to yield a mixture of **3** and **4**. Due to the similar R_f values on SiO_2 of these compounds, the mixture was carried through to the next step. ^{1}H NMR (300 MHz, $CDCl_3$) δ 8.54 (d, J = 5.0 Hz, 1H), 7.62 (t, J = 7.5 Hz, 1H), 7.18 (d, J = 10.0 Hz, 1H), 7.62 (t, J = 7.5 Hz, 1H), 7.12 (d, J = 7.5 Hz, 1H), 6.88 (s, 2H), 6.81 (s, 1H), 2.31 (s, 3H), 2.24 (s, 6H), 2.29 (s, 3H).

(Z)-4-(2-mesityl-1-methyl-3H-indolizin-4-ium-3-ylidene)-2-(2-mesityl-1-methylindolizin-3-yl)-3-oxocyclobut-1-en-1-olate) (MesIn₂SQ): In a flame dried, round bottom flask equipped with a stir bar and a reflux condenser under N_2, **4** (0.10 g, 0.40 mmol) was dissolved in 4 mL 1:1 toluene:n-butanol. 3,4-dihydroxy-1,2-cyclobutanedione (0.023 g, 0.20 mmol) was added and the mixture was heated to reflux for 1.5 hours, cooled to room temperature and concentrated to yield a red solid. The solid was suspended in diethyl ether, centrifuged, and the supernatant was

decanted. The resulting solid was washed with hexanes (10 mL, 3 times) and dried to yield a bronze/red metallic in appearance solid (0.08 g, 70%). ^{1}H NMR (300 MHz, CDCl$_3$) δ 10.12 (d, J = 6.8 Hz, 2H), 7.31 (d, J = 8.7 Hz, 2H), 7.15 (t, J = 8.6 Hz, 2H), 6.93 (s, 4H), 6.83 (t, J = 6.8 Hz, 2H), 2.38 (s, 6H), 1.97 (s, 12H), 1.92 (s, 6H). IR (neat, cm^{-1}): 3411 (br), 1635, 1616. HRMS m/z calculated for C$_{40}$H$_{37}$N$_2$O$_2$ [M+H]$^+$: 577.2855, found 577.3189. UV-Vis (CH$_2$Cl$_2$) λ$_{max}$ = 717 nm; UV-Vis (toluene) λ$_{max}$ = 724 nm (ε = 262,000 M^{-1}cm^{-1}), λ$_{onset}$ = 750 nm.

1-methyl-2-(naphthalene-2-yl)indolizine (5): To a flame dried, N$_2$ filled round bottom flask equipped with a stir bar and a reflux condenser was added 2-ethyl pyridine (0.215 g, 2.01 mmol), 2-bromo-2-(naphthalene-2-yl)ethan-1-one (0.5 g, 2.01 mmol) and 8 mL acetone. The solution was heated to 60°C and stirred. After 16 hours, a white precipitate had formed and the solution was cooled to room temperature. The precipitate was filtered and washed with cold acetone, then combined with sodium bicarbonate (0.086 g, 8.04 mmol) and dissolved in 32 mL water. The mixture was heated to reflux. After 2 hours, a brown solid had formed. The solid was extracted with dichloromethane, washed three times with water, dried and concentrated to yield the pure product (0.153 g, 30%). ^{1}H NMR (300 MHz, CDCl$_3$) δ 7.96 (s, 1H), 7.95-7.80 (m, 4H), 7.68 (d, J = 8.3 Hz, 1H), 7.55-7.40 (m, 3H), 7.35 (d, J = 8.9 Hz, 1H), 6.63 (dd, J =8.9, 6.1 Hz, 1H), 6.44 (t, J = 6.6 Hz, 1H), 2.51 (s, 3H). ^{13}C NMR (75 MHz, CDCl$_3$) δ 133.7, 133.5, 132.1, 131.1,129.0, 127.9 (2 C), 127.7, 127.4, 126.9, 126.1, 125.5, 124.8, 117.6, 115.8, 110.2 (2 C), 105.8, 9.8. IR (neat, cm^{-1}): 3050, 2965, 2919, 2860, 1626, 1598. HRMS m/z calculated for C$_{19}$H$_{15}$NCs [M+Cs]$^+$: calculated 390.0259, found 390.0122.

(Z)-4-(1-methyl-2-(naphthaneln-2-yl)-3H-indolizin-4-ium-3-ylidene)-2-(1-methyl-2-(naphthalene-2-yl)indolizine-3-yl)-3-oxocyclobut-1-en-1-olate (NaphIn₂SQ): To a round bottom flask equipped with a stir bar and reflux condenser was added **5** (0.103 g, 0.401 mmol) and 3,4-dihydroxy-1,2-cyclobutanedione (0.023 g, 0.2 mmol). The flask was flushed with N_2 for 10 minutes. The solids were then dissolved in 23 mL 1:1 toluene:n-butanol, and heated to 130°C for 2 hours during which a red precipitate formed. The mixture was cooled to room temperature, 50 mL diethyl ether was added and the liquid was decanted from the precipitate. The solids were dissolved in warm dichloromethane and recrystallized three times, then suspended in diethyl ether and centrifuged to yield a metallic red appearing solid (0.102 g, 86%). ^{1}H NMR (300 MHz, CDCl₃) δ 9.95 (d, J = 6.3 Hz, 2H), 7.90-7.77 (m, 4H), 7.77-7.60 (m, 4H), 7.60-7.40 (m, 6H), 7.36 (d, J = 7.9 Hz, 2H), 7.17 (t, J = 7.5 Hz, 2H), 6.79 (t, J = 6.4 Hz, 2H), 2.21 (s, 6H). ^{13}C NMR was not obtained due to sparing solubility. IR (neat, cm^{-1}): 3350-1600 (br), 1594, 1435. HRMS m/z calculated for $C_{42}H_{28}N_2O_2Cs$ [M+Cs]: calculated 725.1205, found 725.0571. UV-Vis (CH₂Cl₂) λ_{max} = 720 nm; UV-Vis (toluene) λ_{max} = 727 nm (ε = 150,000 M^{-1}cm^{-1}), λ_{onset} = 760 nm.

2-bromo-1-(pyren-4-yl)ethanone (6): In a flame dried round bottom flask equipped with a stir bar under N_2, aluminum trichloride (0.34 g, 2.97 mmol) was suspended in 2 Ml dichloromethane and cooled to 0°C. 2-bromoacetyl chloride (0.215 Ml, 2.60 mmol) was added slowly, then pyrene (0.50 g, 2.47 mmol) was added. The solution turned a deep red and was warmed to room temperature while stirring. After 3.5 hours, the mixture was diluted with 50 Ml dichloromethane and washed with 25 Ml H_2O. The organic layer was separated, then dried with magnesium sulfate, filtered and concentrated to yield the pure product (0.77 g, 96%). ^{1}H NMR (300 MHz,

CDCl₃) δ 8.96 (d, J = 9.4 Hz, 1 H), 8.31 (d, J = 8.1 Hz, 1H), 8.28-7.95 (m, 7H), 4.71 (s, 2H).

This molecule has been previously synthesized through alternate reaction conditions.[95]

1-methyl-2-(pyren-1-yl)indolizine (7): In a round bottom flask equipped with a stir bar and a reflux condenser, 2-bromo-1-(pyren-4-yl)ethanone (**6**)[4] (4.1 g, 12.7 mmol) and 2-ethylpyridine (2.67 mL, 12.7 mmol) were dissolved in 25 mL of acetone and heated to reflux. The reaction intermediate crashed out of solution after 20 hours. The mixture was cooled to room temperature and the solid was collected by vacuum filtration. The solid was then dissolved in 25 mL of H_2O with sodium bicarbonate (4.3 g, 50.8 mmol) and heated at reflux for two hours. The final product crashed out of solution after two hours. The solution was cooled to room temperature and diluted with 50 mL of DCM and washed with H_2O. The organic layer was separated, then dried with magnesium sulfate, filtered and concentrated to yield the crude product. The product was passed through a plug of 200 mL of SiO_2 using ethyl acetate: DCM (30:70) to yield the pure product (0.95 g, 23%). ¹H NMR (500 MHz, CDCl₃) δ 8.28-8.10 (m, 7H), 8.04 (ap t, J = 7.3 Hz, 2H), 7.99 (d, J = 7.0 Hz, 1H), 7.53 (s, 1H), 7.49 (d, 1H), 6.72 (t, J = 7.8 Hz, 1H), 6.53 (t, J = 6.8 Hz, 1H), 2.25 (s, 3H). ¹³C NMR (125 MHz, CDCl₃) δ 131.6, 131.5, 131.2, 130.52, 130.5, 129.8, 128.9, 128.3, 127.6, 127.5, 127.4, 127.3, 126.3, 126.0, 125.0 (2C), 124.9, 124.8, 124.5, 117.7, 115.9, 111.9, 110.2, 108.2, 9.6. HRMS m/z calculated for $C_{19}H_{15}NCs$ [M+Cs]⁺: calculated 332.1439, found 332.1575. IR (neat, cm⁻¹): 3544, 3442, 3034, 2856, 1621, 1579,1451, 1367, 1302, 1098.

 (*E,Z*)-4-(1-methyl-2-(pyren-2-yl)-3*H*-indolizin-4-ium-3-ylidene)-2-(1-methyl-2-pyren-2-yl)indolizin-3-yl)-oxocyclobut-1-en-1-olate (PyIn₂SQ): In a round bottom flask equipped with a stir bar and a reflux condenser, 1-methyl-2-(pyren-1-yl)indolizine (**7**) (0.5 g, 1.51 mmol) and squaric acid (0.09 g, 0.75 mmol) were dissolved in 75 mL of a 1:1 toluene:butanol mixture. The

mixture was heated at reflux overnight under N_2. The mixture became green in color after heating overnight. The solvent was evaporated under reduced pressure. The solids were dispersed in ether and centrifuged. The ether was triturated off the solids and the solids were washed with hexane. Rotomers were confirmed to be present by ^{1}H NMR. The rotomers were separated by column chromatography with DCM to yield the pure trans rotamer (0.216 g, 39%) as the higher R_f and the pure cis rotamer (0.033 g, 6%) as the lower R_f. Even though the rotamers are separable by column chromatography, a mixture of the rotamers is obtained after storing for a day.

Trans rotamer: ^{1}H NMR (300 MHz, CDCl$_3$) δ 9.48 (d, $J = 9.0$, 2H), 8.30-7.70 (m, 16H), 7.48 (d, $J = 9.0$ Hz, 2H), 7.33 (m, 2H), 7.10 (t, $J = 9.0$ Hz, 2H), 6.44 (t, $J = 9.0$ Hz, 2H), 2.20 (s, 6H). ^{13}C NMR was not obtained due to sparing solubility. HRMS m/z calculated for $C_{54}H_{33}N_2O_2$ [M+H]$^+$: 741.2542, found 741.2977 with perfect isotope pattern match. UV-Vis (toluene), $\lambda_{max} = 730$ nm ($\varepsilon = 160{,}000$ M^{-1}cm^{-1}), $\lambda_{onset} = 756$ nm. IR (neat, cm^{-1}): 2955, 2920, 2852, 1729, 1604, 1431, 1392, 1368, 1297, 1257, 1226, 1205, 1050, 968, 842, 751, 717, 646, 545.

Cis rotamer: ^{1}H NMR (300 MHz, CDCl$_3$) δ 9.88 (br s, 2H), 8.66-6.40 (br m, 18H), 7.35-7.30 (br s, 2H), 7.20-7.00 (br s, 2H), 6.80-6.60 (br s, 2H), 2.20 (s, 6H). ^{13}C NMR was not obtained due to sparing solubility. HRMS m/z calculated for $C_{54}H_{33}N_2O_2$ [M + H]$^+$: 741.2542, found 741.2925. UV-Vis (toluene) $\lambda_{max} = 730$ nm ($\varepsilon = 110{,}000$ M^{-1}cm^{-1}), $\lambda_{onset} = 754$ nm. IR (neat, cm^{-1}): 2963, 2919, 2853, 1606, 1434, 1393, 1363, 1300, 1257, 1226, 1206, 1101, 1057, 975, 843, 792, 755, 717, 544.

Mixed UV-Vis (toluene) for mixture of rotamers: $\lambda_{max} = 729$ nm ($\varepsilon = 124{,}000$ M^{-1}cm^{-1}), $\lambda_{onset} = 757$ nm.

(Z)-4-(2-(4-methoxyphenyl)-1-methyl-3H-indolizin-4-ium-3-ylidene)-2-(2-(4-methoxyphenyl)-1-methylindolizin-3-yl)-3-oxocyclobut-1-en-1-olate (MeOPhIn$_2$SQ): To a flame dried round bottom flask equipped with a stir bar and Dean-Stark apparatus under N$_2$ was added 2-(4-methoxyphenyl)-1-methylindolizine **(8)**[23] (0.16 g, 0.69 mmol) and 3,4-dihydroxy-1,2-cyclobutanedione (0.04 g, 0.35 mmol). The mixture was degassed with N$_2$ for 10 minutes, then dissolved in 20 mL 1:1 toluene:n-butanol and heated to 130°C with stirring. After 6 hours, the reaction mixture was condensed, dissolved in dichloromethane, washed with 50 mL H$_2$O three times, dried with magnesium sulfate and condensed to yield a metallic dark green in appearance solid (0.11 g, 58%). ^{1}H NMR (300 MHz, CDCl$_3$) δ 10.10 (d, J = 6.8 Hz, 2H), 7.34 (d, J = 8.7 Hz, 2H), 7.25 (4H), 7.18 (ap t, J = 7.9 Hz, 2H), 6.97 (d, J = 8.6 Hz, 4H), 6.86 (t, J = 6.5 Hz, 2H), 3.87 (s, 6H), 2.19 (s, 6H). ^{13}C NMR (75 MHz, CDCl$_3$) δ 175.9, 168.3, 159.1, 141.5, 137.4, 134.9, 131.8, 127.1, 126.8, 120.7, 118.0, 116.9, 114.7, 113.2, 55.3, 9.6. IR (neat, cm^{-1}): 3395 (br), 1633. HRMS m/z calculated for C$_{36}$H$_{28}$N$_2$O$_4$ [M+H]$^+$: 553.2127, found 553.2237. UV-vis (CH$_2$Cl$_2$) λ_{max} = 716 nm; UV-Vis (toluene) λ_{max} = 723 nm (ε = 140,000 M^{-1}cm^{-1}), λ_{onset} = 760 nm.

4-(1-methylindolizin-2-yl)phenol (9): To a flame dried round bottom flask equipped with a stir bar and a reflux condenser was added 2-bromo-4-hydroxyacetophenone (1.00 g, 4.65 mmol), 2-ethyl pyridine (0.498 g, 4.65 mmol) and 18.6 mL of acetone. The mixture was heated to 60°C and stirred during which time a fine white precipitate formed. After 18 hours, the mixture was cooled to room temperature and the precipitate was filtered off and washed with cold acetone. The precipitate was then added with sodium bicarbonate (1.56 g, 18.6 mmol) and 18.6 mL water to a round bottom flask, and the mixture was heated and stirred for 2 hours at reflux. After 2 hours, a dark brown oil had formed. The oil was extracted with dichloromethane, washed 3 times

with 50 mL water, dried with sodium sulfate and condensed to yield an orange solid (0.356 g, 35%). ^{1}H NMR (300 MHz, CDCl$_3$) δ 7.82 (d, J = 7.0 Hz, 1H), 7.39 (d, J = 8.5 Hz, 2H), 7.36-7.26 (m, 2H), 6.90 (d, J = 8.5 Hz, 2H), 6.59 (t, J = 7.7 Hz, 1H), 6.38 (t, J = 6.7 Hz, 1H), 2.40 (s, 3H). ^{13}C NMR (75 MHz, CDCl$_3$) δ 154.4, 131.1, 130.1, 128.9, 128.9, 124.9, 117.6, 115.8, 115.6, 110.1, 109.7, 105.6, 9.8. IR (neat, cm^{-1}): 3309.2, 1619.9, 1608.3.

(Z)-4-(2-(4-hydroxyphenyl)-1-methyl-3_H_-indolizin-4-ium-3-ylidene)-2-(2-(4-hydroxyphenyl)-1-methylindolizin-3-yl)-3-oxocyclobut-1-en-1-olate (HOPhIn$_2$SQ): In a round bottom flask equipped with a stir bar and a reflux condenser was added **(9)** (0.326 g, 1.46 mmol) and 3,4-dihydroxy-1,2-cyclobutanedione (0.075 g, 0.657 mmol) dissolved in 80 mL of 1:1 toluene:_n_-butanol. The mixture was heated to 130°C and stirred for 6 hours. ^{1}H NMR (300 MHz, DMSO-d$_6$) δ 9.92 (d, J = 7.1 Hz, 2H), 9.5 (s, 2H), 7.72 (d, J = 9.2 Hz, 2H), 7.43, (t, J = 7.2 Hz, 2H), 7.14 (d, J = 8.6 Hz, 4H), 7.20-7.10 (m, 6H), 6.82 (d, J = 8.6 Hz, 4H), 2.21 (s, 6H). ^{13}C NMR was not obtained due to sparing solubility. IR (neat, cm^{-1}): 3397.89, 1641.09, 1639.16. HRMS m/z calculated for C$_{34}$H$_{24}$N$_2$O$_4$ [M]$^+$: 524.1736, found 524.1722. UV-Vis (DMSO) λ_{max} = 723 nm (ε = 185,000 M^{-1}cm^{-1}), λ_{onset} = 765 nm.

2,6-di-_tert_-butyl-4-(1-methylindolizin-2-yl)phenol (10): To a flame dried round bottom flask equipped with a stir bar and a reflux condenser was added 2-ethylpyridine (0.137 mL, 1.2 mmol), 2-bromo-1-(3,5-di-tert-butyl-4-hydroxy-phenyl)-ethanone (0.393 g, 1.2 mmol) and 1.6 mL of acetone. The reaction mixture was heated to 65°C for 12 hours, then cooled to 0°C. The resulting precipitate was filtered and washed with cold acetone, then suspended in 2 mL H$_2$O. Sodium bicarbonate was added (0.403 g, 4.8 mmol), then the mixture was heated to 110°C for 2 hours. The mixture was cooled to room temperature, extracted with dichloromethane, washed 3

times with water and dried with sodium bicarbonate and concentrated to yield the pure product

(0.083 g, 21%). ^{1}H NMR (500 MHz, CDCl$_3$) δ 7.84 (br s, 1H), 7.4-7.2 (m, 4H), 6.58 (br s, 1H),

6.38 (br s, 1H), 5.18 (s, 1H), 2.42 (s, 3H), 1.49 (s, 18H). ^{13}C NMR (75 MHz, CDCl$_3$) δ 152.8,

136.1, 131.1, 130.2, 127.2, 125.7, 124.9, 117.5, 115.7, 110.0, 109.7, 105.5, 34.6, 30.6, 9.9. IR

(neat, cm^{-1}): 3627, 2942, 2908, 2864. HRMS m/z calculated for C$_{23}$H$_{29}$NO [M+H]$^+$: 336.2327,

found 336.2327.

(Z)-4-(2-(3,5-di-tert-butyl-4-hydroxyphenyl)-1-methyl-3H-indolizin-4-ium-3-ylidene)-2-(2-(3,5-di-tert-butyl-4-hydroxyphenyl)-1-methylindolizin-3-yl-3-oxocyclobut-1-en-1-olate (bis-tBuPhIn$_2$SQ): To a flame dried round bottom flask equipped with a stir bar and a reflux condenser was added **(10)** (69.0 mg, 0.206 mmol), 3,4-dihydroxy-1,2-cyclobutanedione (10.5 mg, 0.0925 mmol), butanol (5.88 mL), and toluene (5.88 mL). The reaction was heated to 130°C for 15 hours, then cooled to room temperature. The reaction was extracted with dichloromethane, washed three times with water and dried with magnesium sulfate. The product was purified through silica gel chromatography in dichloromethane, and then triturated in ethyl acetate to give a red solid (58.0 mg, 84% yield). ^{1}H NMR (300 MHz, CDCl$_3$) δ 9.90 (d, J = 6.9 Hz, 2H), 7.37 (d, J = 8.6 Hz, 2H), 7.25-7.10 (m, 6H), 6.77 (t, J = 6.2 Hz, 2H), 2.32 (s, 6H) 1.48 (s, 36H). ^{13}C NMR was not obtained due to sparing solubility. IR (neat, cm^{-1}): 3419 (br), 1653. HRMS m/z calculated for C$_{50}$H$_{56}$N$_2$O$_4$ [M]$^+$: 748.4240, found 748.4153. UV-vis (CH$_2$Cl$_2$) λ$_{max}$ = 716 nm; UV-Vis (toluene) λ$_{max}$ = 722 nm (ε = 216,000 M^{-1}cm^{-1}), λ$_{onset}$ = 750 nm.

1-methyl-2-(4-trifluoromethyl)phenyl)indolizine (11): To a flame dried, round bottom flask equipped with a stir bar and a reflux condenser was added 2-ethyl pyridine (1.07 mL, 9.33 mmol) and 2-bromo-1-(4-(trifluoromethyl)-phenyl)ethanone (2.49 g, 9.33 mmol) dissolved in 20

mL of acetone and heated to reflux. After 22 hours, the reaction mixture was cooled to room temperature and concentrated. The resulting solid was dissolved in 20 Ml H_2O and sodium bicarbonate (3.13 g, 37.3 mmol). The mixture was refluxed for 2 hours and cooled to room temperature during which dark crystals formed. The crystals were filtered and washed with cold water to yield the pure product (2.36 g, 92%). ^{1}H NMR (500 MHz, CDCl$_3$) δ 7.86 (d, J = 6.0 Hz, 1H), 7.67 (d, J = 8.0 Hz, 2H), 7.62 (d, J = 8.0 Hz, 2H), 7.41 (s, 1H), 7.34 (d, J = 9.0 Hz, 1H), 6.64 (ap t, J = 6.5 Hz, 1H), 6.45 (t, J = 6.5 Hz, 1H). ^{13}C NMR (75 MHz, CDCl$_3$) δ 149.0, 139.9, 136.5, 131.3, 128.7, 127.5, 125.0 (q, J = 270 Hz, C-F coupling), 124.8, 117.6, 116.2, 110.6, 110.1, 105.7, 9.6. IR (neat, cm^{-1}): 3400 (br), 3070, 2920, 1684, 1616. HRMS *m/z* calculated for $C_{16}H_{12}F_3N$ [M+H]$^+$: 276.1000, found 276.1318.

(Z)-4-(1-methyl-2-(4-(trifluoromethyl)phenyl)-3*H*-indolizin-4-ium-3-ylidene)-2-(1-methyl-2-(4-(trifluoromethyl)phenyl)indolizin-3-yl)-3-oxocyclobut-1-en-1-olate (CF₃PhIn₂SQ): To a flame dried, round bottom flask equipped with a stir bar and condenser under N_2 was added **(11)** (0.10 g, 0.36 mmol) and 3,4-dihydroxy-1,2-cyclobutanedione (0.021 g, 0.18 mmol) were in 4 mL of 1:1 toluene:*n*-butanol and heated to reflux. After 24 hours, the reaction mixture was cooled to room temperature and a dark green precipitate formed. Diethyl ether was added and a metallic yellow/bronze precipitate was observed. The mixture was centrifuged and the resulting supernatant was decanted. To purify, diethyl ether was again added to the precipitate to give a suspension which was centrifuged and the supernatant was decanted 2 additional times. Then, the precipitate was washed with hexanes to yield a metallic green solid (0.01 g, 9%). ^{1}H NMR (300 MHz, CDCl$_3$) δ 10.14 (d, J = 6.9 Hz, 2H), 7.65 (d, J = 8.4 Hz, 4H), 7.45-7.35 (m, 6H), 7.24 (t, J = 6.8 Hz, 2H), 6.92 (t, J = 6.9 Hz, 2H), 2.16 (s, 6H). ^{13}C NMR (75 MHz, CDCl$_3$) δ 175.4, 167.4, 141.5, 138.4,

136.1, 135.0, 130.9 (2C), 127.5, 124.7 (q, J = 270 Hz, C-F coupling), 124.5, 120.6, 119.0, 117.3, 115.6, 9.6. IR (neat, cm^{-1}): 3381 (br), 1616. HRMS m/z calculated for $C_{36}H_{22}F_6N_2O_2$ [M]: 628.1585, found 628.1810. UV-vis (CH_2Cl_2) λ_{max} = 720 nm; UV-Vis (toluene) λ_{max} = 727 nm (ε = 166,000 $M^{-1}cm^{-1}$), λ_{onset} = 760 nm.

2-(3,5-bis(trifluoromethyl)phenyl)-1-methylindolizine (12): To a flame dried round bottom flask equipped with a stir bar and a reflux condenser was added 1-(3,5-bis(trifluoromethyl)phenyl)-2-bromoethan-1-one (0.8 g, 2.38 mmol), 2-ethyl pyrinine (0.255 g, 2.38 mmol) and 10 mL of acetone. The mixture was heated to 60°C and stirred, during which a white precipitate formed. After 16 hours, the solution was cooled to room temperature, and the white precipitate was filtered off and washed with cold acetone. The precipitate was then combined with sodium bicarbonate (0.802 g, 9.55 mmol) in a round bottom flask and dissolved in 10 mL of water. The solution was heated to 100°C and stirred for 2 hours. After 2 hours a brown oil had formed, and was extracted with dichloromethane. The organic layer was washed three times with water, dried with magnesium sulfate and concentrated to yield the pure product (0.69 g, 84% yield). ^{1}H NMR (300 MHz, CDCl$_3$) δ 7.94 (s, 2H), 7.87 (d, J = 6.9 Hz, 1H), 7.79 (s, 1H), 7.46 (s, 1H), 7.35 (d, J = 9.0 Hz, 1H), 6.67 (ap t, J = 6.7 Hz, 1H), 6.48 (t, J = 6.7 Hz, 1H), 2.43 (s, 3H). ^{13}C NMR (75 MHz, CDCl$_3$) δ 138.4, 132.0, 131.6, 131.4, 128.3, 126.1, 124.8, 123.7 (q, J = 271 Hz, C-F coupling), 117.7, 116.5, 110.9, 110.1, 105.6, 9.3. IR (neat, cm^{-1}): 3232 (br), 2923, 2866, 1617. HRMS m/z calculated for $C_{17}H_{11}F_6N$ [M+H]$^+$: 344.0874, found 344.0860.

(Z)-4-(2-(3,5-bis(trifluoromethyl)phenyl)-1-methyl-3H-indolizin-4-ium-3-ylidene)-2-(2-(3,5,-bis(trifluoromethyl)phenyl)-1-methylindolizin-3-yl)-3-oxocyclobut-1-en-1-olate (bisCF3PhIn2SQ): To a N$_2$ filled, round bottom flask equipped with a stir bar and a reflux

condenser was added **(12)** (0.235 g, 0.685 mmol), 3,4-dihydroxy-1,2-cyclobutanedione (0.0389 g, 0.342 mmol) and 40 mL of 1:1 toluene:*n*-butanol. The mixture was heated to 130°C and stirred. After 6 hours, the mixture was cooled to room temperature and 50 Ml diethyl ether was added to precipitate a dark solid. The liquid was decanted and the solids were collected. To purify, the solids were dissolved in hot dichloroethane and hot filtered. The solution was cooled to room temperature, and dark solids precipitated at the bottom of the flask. The solids were separated from the supernatant to yield the pure metallic appearing product (0.24 g, 90% yield). ^{1}H NMR (300 MHz, CDCl$_3$) δ 9.99 (d, J = 6.3 Hz, 2H), 7.90 (s, 2H), 7.74 (s, 4H), 7.45 (d, J = 8.6 Hz, 2H), 7.30 (t, J = 7.6, 2H), 7.0 (t, J = 6.7 Hz, 2 H), 2.23 (s, 6H). ^{13}C NMR was not obtained due to sparing solubility. IR (neat, cm^{-1}): 3415, 1574, 1556. HRMS m/z calculated for C$_{38}$H$_{20}$F$_{12}$N$_2$Cs [M+Cs]$^+$:897.0388, found 897.0547. UV-Vis (CH$_2$Cl$_2$) λ$_{max}$ = 720 nm; UV-Vis (toluene) λ$_{max}$ = 727 nm (ε = 260,000 M^{-1}cm^{-1}), λ$_{onset}$ = 755 nm.

1-methyl-2-(4-nitrophenyl)indolizine (13): To a flame dried round bottom flask equipped with a stir bar and a reflux condenser was added 2-bromo-4'-nitroacetophenone (1.0 g, 4.10 mmol), 2-ethyl pyridine (0.439 g, 4.10 mmol) and 16.4 mL of acetone. The mixture was heated to 60°C and stirred. After 16 hours, the solution was cooled to room temperature, and the white precipitate was filtered off and washed with cold acetone. The precipitate was then combined with sodium bicarbonate (1.38 g, 16.4 mmol) in a round bottom flask and dissolved in 16.4 mL water. The solution was heated to 100°C and stirred for 2 hours. After 2 hours a brown oil had formed, and was extracted with dichloromethane. The organic layer was washed three times with water, dried with sodium sulfate and concentrated. To purify, the product was filtered through silica with 1:1 dichloromethane:hexanes and concentrated to yield a orange powder (0.237 g, 23%). ^{1}H NMR

(300 MHz, CDCl$_3$) δ 8.27 (d, J = 8.7 Hz, 2H), 7.86 (d, J = 6.8 Hz, 1H), 7.67 (d, J = 8.7 Hz, 2H), 7.46 (s, 1H), 7.35, (d, J = 9.2 Hz, 1H), 6.66 (t, J = 6.7 Hz, 1H), 6.47 (t, J = 6.5 Hz, 1H), 2.46 (s, 3H). ^{13}C NMR (75 MHz, CDCl$_3$) δ 146.1, 143.2, 131.5, 128.7, 126.6, 124.8, 123.9, 117.8, 116.5, 111.0, 110.4, 105.9, 9.8. IR (neat, cm^{-1}): 3361, 3109, 1595. HRMS m/z calculated for C$_{15}$H$_{13}$O$_2$N$_2$ [M+H]$^+$:253.0977, found 253.0960.

(Z)-4-(1-methyl-2-)4-nitrophenyl)-3_H_-indolizin-4-ium-3-ylidene)-2-)1-methyl-2-(4-nitrophenyl)indolizin-3-yl)-3-oxocyclobut-1-en-1-olate (NO₂PhIn₂SQ): To a N$_2$ filled round bottom flask equipped with a stir bar and a reflux condenser was added **(13)** (0.118 g, 0.468 mmol), 3,4-dihydroxy-1,2-cyclobutanedione (0.027 g, 0.234 mmol) and 13.4 mL of toluene:*n*-butanol. The mixture was heated to 130°C and stirred. After 24 hours the mixture was cooled to room temperature and 50 mL of 1:1 diethyl ether:hexanes was added. A red solid precipitated and the liquid was decanted off. The solids were filtered from dichloromethane after the hot solution reached room temperature and concentrated to yield a metallic appearing red solid (0.088 g, 64%). ^{1}H NMR (300 MHz, CDCl$_3$) δ 10.13 (d, J = 5.2 Hz, 2H), 8.28 (d, J = 8.6 Hz, 4H), 7.46 (d, J = 8.9 Hz, 4H), 7.43 (d, J = 9.9 Hz, 2 H), 7.26 (m, 2H), 6.96 (t, J = 6.5 Hz, 2 H), 2.18 (s, 6H). ^{13}C NMR was not obtained due to sparing solubility. IR (neat, cm^{-1}): 3408, 1653, 1617. UV-Vis (CH$_2$Cl$_2$) λ_{max} = 726 nm; UV-Vis (toluene) λ_{max} = 732 nm (ε = 185,000 M^{-1}cm^{-1}), λ_{onset} = 765 nm.

4-(1-methylindolizin-2-yl)benzonitrile (14): To a flame dried round bottom flask equipped with a stir bar and a reflux condenser was added 4-(2-bromoacetyl)benzonitrile (0.5 g, 2.23 mmol), 2-ethylpyridine (0.256 mL, 2.23 mmol) and 5 mL of acetone. The mixture was then heated to 60°C and stirred for 16 hours to yield a white precipitate. The reaction mixture was then cooled to room temperature, and the precipitate was filtered off, rinsed with cold acetone and dried. The solid was

then dissolved in 5 mL H_2O with sodium bicarbonate (0.75 g, 8.93 mmol). The solution was heated to 100°C, during which a brown precipitate formed. After 3 hours, the precipitate was extracted with 50 mL dichloromethane, washed 3 times with water, dried with magnesium sulfate and condensed to yield a dark brown solid (0.283 g, 54%). ^{1}H NMR (300 MHz, CDCl$_3$) δ 7.85 (d, J = 6.9 Hz, 1H), 7.70 (d, J = 8.6 Hz, 2H), 7.62 (d, J = 8.3 Hz, 2H), 7.42 (s, 1H), 7.34 (d, J = 9.0 Hz, 1H), 6.65 (dd, J = 9.2, 6.0 Hz, 1H), 6.46 (t, J = 6.7 Hz, 1H), 2.43 (s, 1H). ^{13}C NMR (75 MHz, CDCl$_3$) δ 141.1, 132.3, 131.4, 128.8, 127.0, 124.9, 119.3, 117.7, 116.9, 110.9, 110.2, 109.5, 105.7, 9.8. IR (neat, cm^{-1}): 3100, 2912, 2842, 2219. HRMS m/z calculated for $C_{16}H_{13}N_2$ [M+H]$^+$:233.1079, found 233.0682.

(Z)-4-(2-(4-cyanophenyl)-1-methyl-3H-indolizin-4-ium-3-ylidene)-2-(2-(4-cyanophenyl)-1-methylindolizin-3-yl)-3-oxocyclobut-1-en-1-olate (CNPhIn₂SQ): To a flame dried, N_2 flushed round bottom flask was added **(14)** (0.153 g, 0.659 mmol), 3,4-dihydroxy-1,2-cyclobutanedione (0.037 g, 0.33 mmol), and 38 mL of 1:1 toluene:n-butanol. The reaction mixture was heated to 130°C with a reflux condenser for 2.5 hours, during which a green solid precipitated. The precipitate was extracted with dichloromethane, then condensed. To purify, the solid suspended in hot hexanes and filtered three times, then suspended in diethyl ether and centrifuged. The resulting supernatant was decanted off to yield a metallic green solid (0.23 g, 46%). ^{1}H NMR (300 MHz, CDCl$_3$) δ 10.12 (d, J = 7.0 Hz, 2H), 7.72 (d, J = 8.3 Hz, 4H), 7.50-7.30 (m, 6H), 7.26 (m, 2H), 6.96 (m, 2H), 2.17 (s, 6H). ^{13}C NMR was not obtained due to sparing solubility. IR (neat, cm^{-1}): 3390, 2913, 2846, 2373, 2346, 2217, 1604, 1596. HRMS m/z calculated for $C_{36}H_{22}N_4O_2Cs$ [M+Cs]$^+$:675.0797, found 675.0160. UV-Vis (CH$_2$Cl$_2$) λ_{max} = 723 nm; UV-Vis (toluene) λ_{max} = 729 nm (ε = 213,000 M^{-1}cm^{-1}), λ_{onset} = 760 nm.

CHAPTER 5

5.1 DONOR-ACCEPTOR-DONOR NIR II EMISSIVE RHODINDOLIZINE DYE SYNTHESIZED BY C-H BOND FUNCTIONALIZATION

This project is a collaborative project between Dr. Delcamp's group and Dr. Hammer's group, where Austin L. Dorris and Shane A. Autry contributed to the work by measuring the emission and quantum yield of the rhodindolizine dye. Chathuranga S.L. Rathnamala contributed by optimizing reaction conditions to obtain the rhodindolizine dyes in higher yields. Jacqueline Gayton contributed by making the first rhodindolzine dye. William Meador contributed to the project by synthesizing the indolizine donors.

ABSTRACT:

A NIR II emissive dye was synthesized by the C-H bond functionalization of 1-methyl-2-phenylindolizine with 3,6-dibromoxanthene. The rhodindolizine (**RhIndz**) spirolactone product was non-fluorescent; however, upon opening of the lactone ring by the formation of the ethyl ester derivative, the fluorophore absorbs at 920 nm and emits at 1092 nm, which are both in the NIR II region. In addition, 4-cyanophenyl- (**CNRhIndz**) and 4-methoxyphenyl-substituted rhodindolizine (**MeORhIndz**) could also be prepared by the C-H activation reaction.

INTRODUCTION:

Photoluminescent materials in the near-infrared I (NIR I) (~ 0.7 μm – 0.9 μm) and near-infrared II (NIR II) (~ 0.9 μm – 1.7 μm) region of the electromagnetic spectrum have applications in many areas such as optical recording, laser filters, thermal writing displays, bioimaging, NIR photography, photodynamic therapy, and solar cells.[2-4, 41, 44, 96-101] Among these applications, NIR I and NIR II materials are desirable for tissue imaging due to the deeper penetration of light, minimal tissue damage, and high spatial resolution as a result of low autofluorescence in the NIR I and NIR II regions.[5, 10, 13, 42, 45, 102] There are several examples of NIR I dyes derived from common fluorescent dye scaffolds such as cyanine,[1, 30, 103-106] phthalocyanine and porphyrin,[101, 107-108] squaraine,[25, 109-111] BODIPY analogs,[112-114] benzo[c]heterocycle,[115] and xanthene derivatives.[101, 116-119] Among these common scaffolds, xanthene-based dyes are widely explored due to their outstanding photophysical properties and stimuli responses. Consequently, they have been

modified to achieve absorption and emission wavelengths in the NIR I region. For example, replacing the bridged oxygen atom of the xanthene scaffold to phosphorous[120] or silicon[121] leads to a reduced optical energy gap into the NIR I region. Subsequently, there are a number of examples
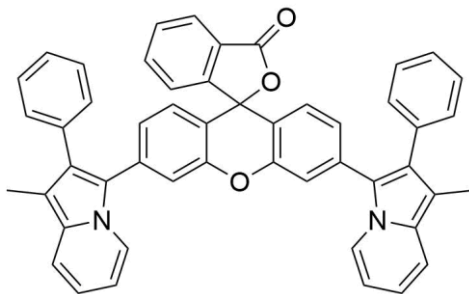
Figure 29. Rhodindolizine structure

from our group,[122] and others,[123-124] that have demonstrated strong atom substitution effects with various xanthene-based dyes. In addition, Yuan and coworkers have developed several NIR I dyes with moderate to high quantum yields by extending the π-conjugation of the xanthene scaffold.[125-126] In contrast, while there are several examples of NIR I emissive dyes, there are only a few NIR II fluorophores available.[5, 10, 13, 15, 26, 43, 45, 97, 127-128] Nanoparticles and quantum dots have shown interesting photophysical properties as NIR II fluorophores with very high quantum efficiencies;[129-130] however, these nanoparticles tend to be insoluble, slow to excrete from the body, and accumulate in the spleen and liver, making them non-ideal therapeutic agents in many cases.[131-132] In this regard, small molecule organic dyes are attractive for clinical applications because of their tendency to metabolize in the cells and low toxicity.[10, 103-104] Recently, researchers have sought different strategies to develop NIR II organic emissive dyes such as combining donor and acceptor groups.[20, 24, 28, 133] This approach is well-developed for organic electronic devices, and

this strategy has been successful in producing low bandgap molecules. The choice of a good donor – acceptor pair can significantly lower the optical bandgap of a dye due to the promotion of charge transfer events.[99, 134] Indolizines are gaining use in dye-sensitized solar cells as the donor due to a good donor strength compared to ubiquitous triphenylamine donors and other alkyl amine-based donor groups.[23, 26, 135-136] The excellent donor strength of indolizines is a result of several factors such as, having a nitrogen atom with three separate single bonds creating a fully planar geometry, a fully conjugated π-scaffold with the nitrogen lone pair, low stabilization energy, and a pro-aromatic nature.[23, 26, 137] Owing to the excellent photophysical properties of xanthene-based dyes and their electron accepting ability, we have designed a donor-acceptor-donor NIR II fluorescent dye by coupling the 3-position of the electron rich indolizine to the 3 and 6 positions of the electron poor xanthene using the C-H bond functionalization reaction (**Figure 29**).

C-H bond functionalization/activation has emerged as a very useful method for the formation of sp^2 – hybridized C-C bonds. C-H activation synthetic routes have an advantage over the classical cross-coupling approaches in that additional synthetic steps to activate the carbon site and the production of toxic by-products are avoided.[138-140] C-H functionalization can be highly tolerant of many functional groups, which makes it desirable for the preparation of drugs and natural products. However, since there are usually many C-H bonds on the substrates, selectivity can be challenging. While C-H functionalization on sp^2 – hybridized carbon centers has been widely developed for the preparation of conjugated compounds for applications in organic devices, only a few examples have been reported for the synthesis of photoluminescent dyes.[20] For instance, Verbelen et al. have developed several BODIPY dyes by radical C-H arylation and alkylation.[141-142] They have also reported the direct palladium catalyzed C-H activation at the 3- and 3,5-positions of a BODIPY

derivative that resulted in high fluorescence quantum yields ($\phi > 0.85$).[143] Perumal and coworkers have reported tetra-substituted olefinic xanthene dyes with aggregation induced emission (AIE) properties, which were synthesized by a tandem Pd-catalyzed 6-exo-dig cyclization followed by a C-H activation reaction.[144] Gryko and coworkers have prepared indolizine-based dyes by a double C-H activation of electron deficient indolizines with the electron rich dibromoarenes, fluorene and thiophene.[145] They obtained the desired bis-indolizine products in 58% and 47% yield respectively.

Herein, we reported the first NIR II xanthene-based dye, which was prepared by the C-H bond functionalization reaction of 1-methyl-2-phenylindolizine with 3′,6′-dibromofluoran (a xanthene derivative). The specific methyl/phenyl substitution pattern on the indolizine was selected as these groups allow for a simple synthesis of an electron rich indolizine with prolonged ambient stability. The target dye is inspired by the popular rhodamine dyes; however, the xanthene core is attached to carbon atoms of indolizine (**Figure 29**), instead of nitrogen atoms, which is common to the rhodamine structure. Interestingly, 3',6'-bis(1-methyl-2-phenylindolizin-3-yl)-3*H*-spiro[2-benzofuran-1,9'-xanthen]-3-one, which is referred to as rhodindolizine (**RhIndz**) from here on, undergoes the typical molecular optical switching between the closed spirocyclic ring structure and the open-form that is commonly observed for rhodamine dyes. **RhIndz** shows intense absorption and emission in the NIR II region of the spectrum, which is desirable for biological imaging. To analyze the substituent effects on the C-H activation reaction, substituted indolizines containing both electron withdrawing and electron donating groups on the phenyl ring were investigated.

RESULTS AND DISCUSSION:

The C-H bond functionalization is an attractive method for preparing 3-substituted indolizine since preparing/isolating 3-haloindolizines, which are common precursors to other classical cross coupling reagents such as organoboron and organotin reagents is challenging. Furthermore, the direct borylation at the 3-position of the indolizine is also challenging, while the C-H bond functionalization at the 3-position of indolizine has been reported.[145,71] The synthesis of **RhIndz** begins with the known 3,6-ditriflated fluorescein (1) reported by Lavis and coworkers.[72] The intermolecular C-H bond functionalization of 1-methyl-2-phenylindolizine with the 3,6-ditriflated xanthene derivative was explored by varying the catalyst, ligand, base, additive, solvent, temperature and time according to **Table 10** and appendix **Table 48**. We began our study with PdCl$_2$(PPh$_3$)$_2$ (10 mol %) as the catalyst, potassium acetate (KOAc) (5.2 equiv.) as the base, and N-methyl-2-pyrrolidone (NMP) as the solvent at 80 °C for 6.5 h (**Table 10, Entry 1**). For these conditions, 5% of the desired disubstituted product (**2a**) and 10% of undesired monosubstituted product (**2b**) were isolated. Increasing the time to 17 h only slightly increased the yield of the desired product (**Table 10, Entry 2**). Notably, changing the base to cesium carbonate (Cs$_2$CO$_3$), potassium *tert*-butoxide (KO^{t}Bu), or sodium *tert*- butoxide (NaO^{t}Bu) yielded trace or no product (appendix **Table 48, Entries 1-3**). In fact, the ditriflated xanthene precursor was converted to fluorescein by a de-triflation process that was previously observed by Rogers et al.,[146] with the recovery of the indolizine starting material. When the catalyst was changed to Pd(OAc)$_2$ (10 mol %) with triphenylphosphine (PPh$_3$) (20 mol %) as the ligand, KOAc (3 equiv) as the base in DMF at 150 °C for 18 h – 20 h, only the desired product **2a** was obtained in 14% isolated yield (**Table

10, Entry 3). The yield of the desired product increased to 22% when Xphos (20 mol %) was used

as the ligand in place of PPh$_3$ at 100 °C (**Table 10, Entry 4**).

Table 10. Optimization of reaction conditions for xanthene ditriflate
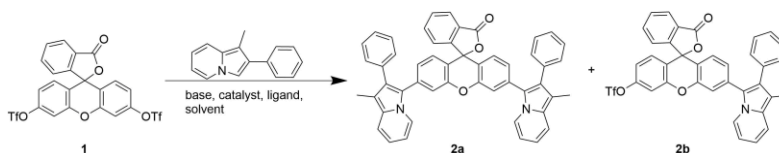
entry	catalyst	ligand	KOAc (equiv)	temp (°C)	time (h)	(%)[a] 2a:2b
1	PdCl$_2$(PPh$_3$)$_2$	None	(5.2)	80	6.5	5:10
2	PdCl$_2$(PPh$_3$)$_2$	None	(5.2)	80	18	8:17
3	Pd(Oac)$_2$	PPh$_3$	(3.0)	150	20	14:0
4	Pd(Oac)$_2$	Xphos	(6.0)	100	20	22:20
5[b]	Pd(Oac)$_2$	Xphos	(6.0)	100	20	5:6
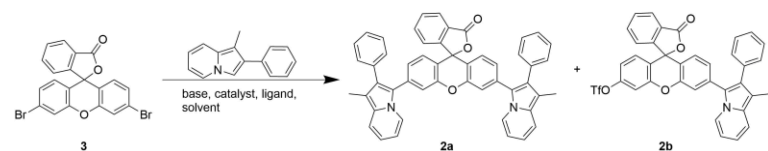
Reactions are carried out in a sealed tube under nitrogen atmosphere in the presence of **1** (0.083 mmol), 1-methyl-2-phenylindolizine (0.167 mmol), NMP (entries 1 and 2) or DMF as solvent (0.34 – 2.0 mL), catalyst (10 mol %), ligand (20 mol %when added), and KOAc. [a]Isolated yields (%) were reported for **2a** and **2b**.[b]Pivalic acid added (30 mol %).

The work of Fagnou and coworkers has shown the direct arylation of electron rich indolizines with

trialkylphosphines;[147] however, with (^{t}Bu)$_2$PMeHBF$_4$ added as the ligand, no product was obtained

(appendix **Table 48, Entry 4**). In fact, the addition of pivalic acid (30 mol %) or any condition

that requires strong bases such as K$_2$CO$_3$, Cs$_2$CO$_3$ and KO^{t}Bu, including the conditions reported

by Ozawa and coworkers that use Pd(dba)$_3$·CHCl$_3$ adduct (10 mol %) as the catalyst,[148] resulted in

only trace or no product at all (appendix **Table 48, Entries 5 – 10**). In all cases, mostly unreacted

starting materials were recovered.

While the target dye is accessible from the xanthene ditriflate precursor with yields high

enough for photophysical studies, the C-H bond functionalization of 1-methyl-2-phenylindolizine

with 3′,6′-dibromofluoran[75] was investigated to determine if the reaction yield could be improved

(**Table 11**). Beginning with one of the highest yielding conditions from the ditriflate study in Table

1, 3′,6′-dibromofluoran (**3**) and 1-methyl-2-phenylindolizine were subjected to PdCl$_2$(PPh$_3$)$_2$ (10 mol %) as the catalyst, KOAc (5.2 equiv) as the base, and NMP as the solvent at 80 °C for 18 h. From these reaction conditions, the desired product was isolated in 23% yield (**Table 11, Entry 1**). Changing the base to Cs$_2$CO$_3$ did not affect the yield (**Table 11, Entry 2**), and there was no observable conversion with NaO^{t}Bu (see appendix **Table 49, Entry 1**). However, by increasing the reaction temperature and time to 110 °C and 24 h respectively, the desired product could be isolated in 35% yield (**Table 11, Entry 3**). Further increase in the temperature to 150 °C did not improve the yield (**Table 11, Entry 4**). Again, Fagnou's conditions or the use of Xphos only lowered the percent conversion after 18 h (see appendix **Table 49, Entries 2 & 3**). To the best of our knowledge, this is the first known case of a xanthene-based C(sp^2)-C(sp^2) bond C-H activation cross-coupling reaction, and this route sets a precedent for the rapid access of aryl-xanthene derivatives. Furthermore, our yields were comparable to the literature where bis-indolizine products were prepared by C-H bond functionalization.[70]

Table 11. Optimization of reaction conditions with 3′,6′-dibromofluoran (**3**)

entry	catalyst	base (equiv)	temp (°C)	time (h)	yield (%)[a]
1	PdCl$_2$(PPh$_3$)$_2$	KOAc (5.2)	80	18	23
2	PdCl$_2$(PPh$_3$)$_2$	Cs$_2$CO$_3$ (5.2)	80	18	23
3	PdCl$_2$(PPh$_3$)$_2$	KOAc (5.2)	110	24	35
4	PdCl$_2$(PPh$_3$)$_2$	KOAc (5.2)	150	24	35

Unless otherwise specified, the reaction was carried out in a sealed tube under nitrogen atmosphere in the presence of **3** (0.11 mmol), 1-methyl-2-phenylindolizine (0.24 mmol), NMP solvent (0.34 – 2 Ml), PdCl$_2$(PPh$_3$)$_2$ (10 mol %), and base, for 18 – 24 h at 80 °C – 150 °C. [a]Isolated yields (%) reported for **2a**.

In order to probe the substrate scope with respect to the C-H bond functionalization of the indolizine coupling partner, the electronic effects on the reaction was investigated. As such, the C-H bond functionalization of six phenyl-substituted 1-methyl-2-phenylindolizine containing electron donating and withdrawing groups were investigated in comparison with the parent 1-methyl-2-phenylindolizine using the optimized conditions from **Table 12**. 4-Cyanophenyl-substituted rhodindolizine (**CN RhIndz**) was obtained in comparative yield relative to **RhIndz** (30% versus 35% respectively) indicating that the resonance withdrawing CN group is tolerated in this reaction. However, 4-trifluoromethylphenyl-substituted (**CF₃RhIndz**), 4-nitrophenyl-substituted rhodindolizine (**NO₂RhIndz**) and 3,5-ditrifluoromethylphenyl-substituted (**diCF₃RhIndz**), led to low or trace amounts of the corresponding products. The origin of the low yields is not obvious, but it is notable that the starting materials, compound **3** and indolizine precursors were not consumed during the reaction. Modifying the phenyl group with the electron donating phenol substituent led to only trace product, presumably due to the reaction not tolerating acidic functionality (**Table 12, Entry 5**.) On the other hand, the methoxy derivative gave a reasonable yield (20%) of the desired product (**Table 12, Entry 6**).

With **RhIndz** in hand, the reactivity of the spirolactone functionality was explored. Interestingly, upon exposure to strong Bronsted acids the lactone ring resisted ring opening. However, the ring opened acid chloride derivative could be prepared directly from the lactone using POCl₃ in refluxing 1,2-dichloroethane (**Scheme 2**),[76] which was reacted with anhydrous ethanol to form the ethyl ester (**10**). Having accessed both the ring closed (**2a**) and ring open (**10**) forms, the photophysical properties of these derivatives were investigated.

Table 12. Substrate Scope with Substituted Indolizines

di-substituted Prod   mono-substituted Prod
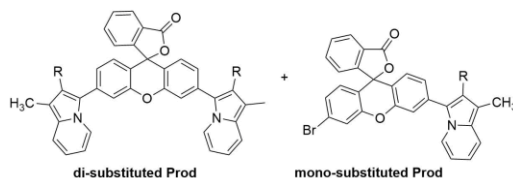
compound	R group	yield (%) di : mono
CNRhIndz 4	4-CNPh	30 : 14
CF₃RhIndz 5	4-CF₃Ph	11 : 6
NO₂RhIndz 6	4-NO₂Ph	trace
diCF₃RhIndz 7	3,5-bisCF₃Ph	trace
HORhIndz 8	4-OHPh	trace
MeORhIndz 9	4-OmePh	20:0

The absorption maximum for **RhIndz** is 375 nm (see appendix **Figure 86**). However, upon the formation of the ethyl ester, a large bathochromic shift of 550 nm occurs shifting the maximum absorption to 920 nm, which is within the NIR II region. The dye also displays a high molar absorptivity of 97,500 $M^{-1}cm^{-1}$, which is critical for a practical molecular brightness (MB). Excitingly, dye **10** also exhibits an emission peak at ~1092 nm in the NIR II region, which is almost 200 nm Stokes shift (**Figure 30**). This observed emission is broad extending from 950 nm to just beyond 1400 nm in dichloromethane with a quantum yield (Φ) of ~0.03% when using a cyanine references dye (C5).[105] While this Φ appears low, we stress that very few molecular emissive materials exist in this region.[97] Additionally, a range of solvent polarities were evaluated to access the polarity of **RhIndz** in the ground-state via absorption spectroscopy and in the excited-state via fluorescence spectroscopy (see appendix **Figure 87**). Both the absorption and emission maxima varied by < 0.04 Ev in energy for solvents ranging in dipole from 3.96 debye to 0.36 debye and with dielectric constants ranging from 46.7 to 3.96.

These very large ranges of solvent properties show very small changes in the absorption maxima, which indicates minimal conformational or localized charge density changes occurring in the ground or excited state of **10** due to the solvent properties.

Scheme 2. Synthesis of RhIndz ethyl ester **10** from RhIndz **2a**
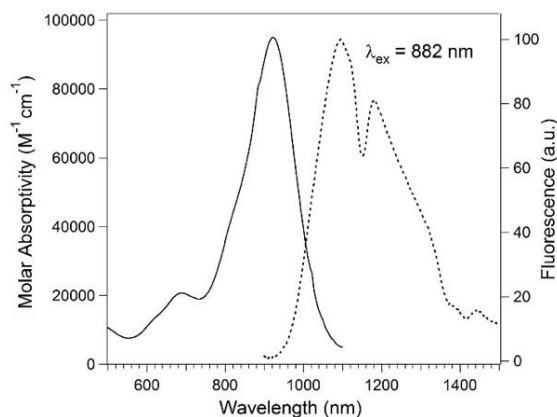
Figure 30. Molar absorptivity and emission of RhIndz ethyl ester in dichloromethane. Note: the drop in the emission spectrum at ~1150 nm is a possible spectrometer artifact (see appendix **Figure 88**).

In conclusion, we have demonstrated the use of C-H bond functionalization reaction to prepare NIR II emissive dyes by the combination of the electron rich indolizine donor with the electron poor xanthene core. The best condition found was PdCl$_2$(PPh$_3$)$_2$ catalyst with KOAc base and NMP as solvent at 110 °C. CNRhIndz and MeORhIndz were also prepared by the C- bond

activation reaction; while CF$_3$RhIndz, (diCF$_3$)RhIndz and OHRhIndz only gave trace amounts of the product, with recovery of the starting materials.

The RhIndz dye, while not a typical rhodamine structure with N-xanthene bonds, was non-fluorescent in the closed spirocyclic structure; however, with the formation of the opened ethyl ester derivative, the fluorophore possessed absorption and emission within the NIR II region with high molar absorptivity and a Φ of ~0.03%. To the best of our knowledge, this is the first xanthene-based emissive dye with photophysical properties in the NIR II region.

EXPERIMENTAL SECTION

All chemicals and solvents were purchased from commercial suppliers and used without further purification unless otherwise specified. ^{1}H NMR (500 MHz) and ^{13}C NMR (500 MHz) spectra were recorded in deuterated solvents on a Bruker AVANCE 500 NMR Spectrometer. J values are expressed in Hz and quoted chemical shifts are in ppm downfield from tetramethylsilane (TMS) reference using the residual protonated solvents as an internal standard. The signals have been designated as follows: s (singlet), d (doublet), t (triplet), m (multiplets). High resolution mass spectra (HRMS) were determined on Bruker-micrOTOF-Q II Mass Spectrometer. Absorption spectra were acquired using a Cary 5000 UV-Vis-NIR spectrophotometer in a 1-cm quartz cell. Fluorescence spectra were acquired using a Horiba QuantaMaster 8075-21 spectrofluorometer with xenon lamp excitation and liquid nitrogen cooled indium gallium arsenide solid state detector. The choice of 882 nm excitation was chosen to coincide with a Xe emission peak. The relative quantum yield of the rhodindolizine dye was calculated using a technique previously outlined by Miller et al.[77]A cyanine dye was chosen as the standard due to the similar

absorption and emissive regions. The dye, C5, has a known quantum yield of 2.2%.[78] The absorbance point for the quantum yield was chosen because of similar overlap in the absorption spectra between the standard and the rhodindolizine dye.

An excitation wavelength of 870 nm was used for both the C5 and rhodindolizine dyes. Both samples were solvated in DCM to a 10 mM concentration.

3-oxo-3H-spiro[isobenzofuran-1,9'-xanthene]-3',6'-diylbis(trifluoromethanesulfonate) (**1**) was prepared according to literature procedure.[72] *3',6'-dibromofluoran* (**3**) was prepared according to literature procedure. [75]

Representative procedure for the preparation of **RhIndz** (**2a**) (**Table 10**)

Compound **1** (50 mg, 0.083 mmol), 1-methyl-2-phenylindolizine (35 mg, 0.167 mmol), solvent (0.34 – 2.0 mL), catalyst (5 – 10 mol %), base, and additives (pivalic acid) were placed in a microwave sealed tube, flushed with nitrogen and heated for 12 – 24 h at 80 – 150 °C according to Table 1. The reactions were monitored by TLC and NMR. Once it was determined that the reaction conversion has plateaued, the crude was diluted with 30 mL of dichloromethane and washed with water (5 x 10 mL). The crude product was dried over anhydrous sodium sulfate, filtered, and concentrated under reduced pressure.

3',6'-bis(1-methyl-2-phenylindolizin-3-yl)-3H-spiro[2-benzofuran-1,9'-xanthen]-3-one (2a)

The crude product was purified by column chromatography on silica gel (hexane: ethyl acetate, 70:30) to give the product (**2a**) as a light-yellow solid in 20% yield (12 mg). ^{1}H NMR (500 MHz, CD$_2$Cl$_2$) δ 8.11 (d, J = 7.2 Hz, 2H), 8.00 (d, J = 7.6 Hz, 1H), 7.73 (td, J = 7.6, 1.1 Hz, 1H), 7.68 –

7.63 (m, 1H), 7.40 (d, *J* = 9.0 Hz, 2H), 7.33 – 7.20 (m, 13H), 6.97 (dd, *J* = 8.2, 1.7 Hz, 2H), 6.78 (d, *J* = 8.2 Hz, 2H), 6.73 – 6.68 (m, 2H), 6.46 (t, *J* = 6.7 Hz, 2H), 2.31 (d, *J* = 4.5 Hz, 6H).

^{13}C{1H}NMR (126 MHz, CD$_2$Cl$_2$) δ 169.6, 153.3, 152.0, 135.82, 135.79, 135.1, 131.4, 131.2, 130.6, 129.3, 128.8, 128.6, 127.1, 126.9, 126.3, 126.2, 125.6, 124.6, 124.5, 124.3, 122.5, 120.4, 119.6, 118.7, 118.1, 117.9, 117.7, 117.2, 111.2, 108.2, 82.8, 9.5. HRMS-ESI-TOF (*m/z*): [M+H]$^+$ calcd for C$_{50}$H$_{34}$N$_2$O$_3$H 711.2642 found 711.2642.

3'-(1-methyl-2-phenylindolizin-3-yl)-3-oxo-3H-spiro[2-benzofuran-1,9'-xanthen]-6'-yl

trifluoromethanesulfonate (2b)

The crude product was purified by column chromatography on silica gel (hexane: ethyl acetate, 70:30) to give the product (**2b**) as a light-yellow solid in 22% yield (12 mg). ^{1}H NMR (500 MHz, CD$_2$Cl$_2$) δ 8.14 (s, 1H), 8.03 (d, *J* = 6.6 Hz, 1H), 7.73 (s, 1H), 7.68 (d, *J* = 7.0 Hz, 1H), 7.54 (s, 1H), 7.41 (d, *J* = 7.7 Hz, 1H), 7.28 (d, *J* = 36.9 Hz, 8H), 7.00 (d, *J* = 7.4 Hz, 1H), 6.90 (d, *J* = 22.3 Hz, 1H), 6.81 (d, *J* = 8.0 Hz, 1H), 6.71 (s, 1H), 6.47 (s, 1H), 2.32 (s, 3H). ^{13}C{1H} NMR (126 MHz, CD$_2$Cl$_2$) δ 169.4, 153.2, 152.8, 152.3, 151.9, 135.86, 135.85, 135.8, 135.14, 135.12, 131.47 131.45, 131.2, 130.6, 129.5, 129.3, 128.8, 128.7, 126.9, 126.4, 125.6, 124.6, 122.5, 120.3, 118.8, 118.2, 118.1, 117.9, 117.2, 111.3, 111.0, 108.2, 82.4, 9.5. HRMS-ESI-TOF (*m/z*): [M+K]$^+$ calcd for C$_{36}$H$_{22}$F$_3$NO$_6$SK 692.0752 found 692.0751.

Representative procedure for the preparation RhIndz and phenyl-substituted RhIndz (**Table 11** and **Table 12**)

The reaction was carried out in a sealed tube under nitrogen atmosphere in the presence of 3',6'-dibromofluoran (**3**) (0.458 g, 1 mmol), 1-methyl-2-phenylindolizine (0.456 g, 2.2 mmol), solvent

(3 mL), catalyst 10 mol %), base, and additives (PivOH) for 18 – 24 h at 110 °C. The reactions were monitored by TLC and ^{1}H NMR. Once it was determined that the reaction conversion had plateaued, the crude was diluted with 30 mL of dichloromethane and washed with water (5 x 10 Ml). The crude product was dried over anhydrous sodium sulfate, filtered, and concentrated under reduced pressure. The crude product was purified by column chromatography on silica gel (hexane: ethyl acetate, 70:30) to give the product (**2a**) as a light-yellow solid in 35% yield (244 mg).

4-(3-{3'-[2-(4-cyanophenyl)-1-methylindolizin-3-yl]-3-oxo-3H-spiro[2-benzofuran-1,9'-xanthen]-6'-yl}-1-methylindolizin-2-yl)benzonitrile (**4a**)

Yellow solid, 30 % yield, (25 mg). ^{1}H NMR (500 MHz, CD$_2$Cl$_2$) δ 8.09 (d, J = 7.1 Hz, 2H), 8.03 (d, J = 7.6 Hz, 1H), 7.77 (t, J = 7.5 Hz, 1H), 7.68 (t, J = 7.5 Hz, 1H), 7.59 (d, J = 8.1 Hz, 4H), 7.42 (d, J = 9.0 Hz, 2H), 7.33 (d, J = 8.0 Hz, 4H), 7.28 (d, J = 7.7 Hz, 1H), 7.22 (s, 2H), 6.93 (d, J = 8.2 Hz, 2H), 6.82 (d, J = 8.2 Hz, 2H), 6.76 – 6.71 (m, 2H), 6.50 (t, J = 6.8 Hz, 2H), 2.32 (s, 6H). ^{13}C{1H} NMR (126 MHz, CD$_2$Cl$_2$) δ 169.5, 153.2, 152.0, 141.1, 135.9, 134.5, 132.5, 131.8, 131.7, 130.7, 129.2, 127.3, 127.0, 126.5, 125.7, 124.5, 122.5, 120.6, 119.6, 118.9, 118.4, 118.3, 117.7, 111.9, 110.5, 108.1, 82.5, 9.5. HRMS-ESI-TOF (*m/z*): [M+K]$^+$ calcd for C$_{52}$H$_{32}$N$_4$O$_3$K 799.2106 found 799.2106

3'-(2-(4-cyanophenyl)-1-methylindolizin-3-yl)-3-oxo-3H-spiro[2-benzofuran-1,9'-xanthen]-6'-yltrifluormethanesufonate (**4b**)

Yellow solid, 14 % yield, (9 mg). ^{1}H NMR (300 MHz, CD$_2$Cl$_2$) δ 8.11 (d, J = 7.2 Hz, 1H), 8.04 (d, J = 7.4 Hz, 1H), 7.79 – 7.72 (m, 1H), 7.72 – 7.65 (m, 1H), 7.61 (s, 1H), 7.59 (s, 1H), 7.57 – 7.54 (m, 1H), 7.43 (d, J = 9.0 Hz, 1H), 7.38 – 7.30 (m, 3H), 7.26 (d, J = 5.6 Hz, 2H), 7.00 – 6.91 (m,

2H), 6.85 (d, J = 8.2 Hz, 1H), 6.74 (dd, J = 8.7, 6.5 Hz, 1H), 6.50 (t, J = 6.8 Hz, 1H), 2.33 (d, J = 2.8 Hz, 3H). ^{13}C{1H} NMR (126 MHz, CD$_2$Cl$_2$) δ 169.6, 153.4, 152.1, 152.0, 142.8, 141.1, 135.9, 134.4, 132.5, 131.8, 131.8, 130.7, 129.21, 129.16, 127.3, 126.8, 126.4, 125.7, 124.5, 123.3, 122.5, 120.7, 119.6, 119.3, 119.0, 118.4, 118.3, 117.7, 116.2, 111.9, 110.5, 108.1, 82.4, 9.6. HRMS-ESI-TOF (m/z): [M+K]$^+$ calcd for C$_{36}$H$_{21}$BrN$_2$O$_3$K 609.0808 found 609.0877

3',6'-bis(2-(3,5-bis(trifluoromethyl)phenyl)-1-methylindolizin-3-yl)-3H-spiro[2-benzofuran-1,9'-xanthen]-3-one (**5a**)

Brown solid, 11% yield (10 mg). ^{1}H NMR (300 MHz, CD$_2$Cl$_2$) δ 8.09 (d, J = 7.2 Hz, 2H), 8.02 (d, J = 7.5 Hz, 1H), 7.78 – 7.72 (m, 1H), 7.70 – 7.64 (m, 1H), 7.57 (d, J = 8.1 Hz, 4H), 7.42 (d, J = 9.0 Hz, 2H), 7.36 (d, J = 8.0 Hz, 4H), 7.29 (d, J = 7.6 Hz, 1H), 7.23 (d, J = 1.5 Hz, 2H), 6.96 (dd, J = 8.2, 1.6 Hz, 2H), 6.82 (d, J = 8.2 Hz, 2H), 6.73 (dd, J = 8.9, 6.5 Hz, 2H), 6.52 – 6.45 (m, 2H), 2.32 (s, 6H). ^{13}C{1H} NMR (126 MHz, CD$_2$Cl$_2$) δ 169.5, 153.2, 152.1, 140.0, 135.9, 134.7, 131.6, 131.5, 130.7, 129.1, 128.8, 128.5, 127.6, 127.0, 126.4, 126.2, 125.7, 125.6, 125.5, 124.6, 124.0, 122.5, 120.6, 118.9, 118.3, 118.2, 117.6, 111.7, 108.2, 82.6, 9.5. HRMS-ESI-TOF (m/z): [M+H]$^+$ calcd for C$_{52}$H$_{32}$F$_6$N$_2$O$_3$H 847.2389 found 847.2389

3'-(1-methyl-2-(4-(trifluoromethyl)phenyl)108ppearance-3-yl)-3-oxo-3H-spiro[2-benzofuran-1,9'-xanthen]-6'-yltrifluoromethan esulfonate (**5b**)

Brown solid, 6% yield (5 mg). ^{1}H NMR (300 MHz, CD$_2$Cl$_2$) δ 8.11 (d, J = 7.2 Hz, 1H), 8.04 (d, J = 7.3 Hz, 1H), 7.71 (dt, J = 20.2, 7.2 Hz, 2H), 7.62 – 7.51 (m, 3H), 7.47 – 7.23 (m, 6H), 6.99 (d, J = 8.1 Hz, 1H), 6.93 (d, J = 8.1 Hz, 1H), 6.85 (d, J = 8.2 Hz, 1H), 6.78 – 6.69 (m, 1H), 6.49 (t, J = 6.7 Hz, 1H), 2.33 (s, 3H). ^{13}C{1H} NMR (126 MHz, CD$_2$Cl$_2$) δ 169.6, 153.4, 152.11, 152.06,

142.8, 140.0, 135.9, 134.7, 131.6, 131.5, 130.7, 129.2, 129.1, 128.5, 127.6, 126.9, 126.4, 125.7, 125.57, 125.55, 124.5, 123.2, 122.5, 120.6, 119.3, 119.0, 118.3, 118.2, 117.5, 116.2, 111.7, 108.2, 82.4, 9.6. HRMS-ESI-TOF (*m/z*): [M+K]$^+$ calcd for $C_{36}H_{21}BrF_3NO_3K$ 690.0288 found 690.0284

3',6'-bis(2-(4-methoxyphenyl)-1-methylindolizin-3-yl)-3H-spiro[2-benzofuran-1,9'-xanthen]-3-one (**9a**)

Pale Green solid, 20 % yield (17 mg). ^{1}H NMR (500 MHz, CD$_2$Cl$_2$) δ 8.11 (d, *J* = 7.1 Hz, 2H), 8.01 (d, *J* = 7.6 Hz, 1H), 7.74 (t, *J* = 7.4 Hz, 1H), 7.66 (t, *J* = 7.3 Hz, 1H), 7.39 (d, *J* = 8.9 Hz, 2H), 7.31 – 7.23 (m, 3H), 7.13 (t, *J* = 9.3 Hz, 4H), 6.96 (d, *J* = 8.2 Hz, 2H), 6.85 (d, *J* = 7.1 Hz, 4H), 6.78 (d, *J* = 8.1 Hz, 2H), 6.68 (dd, *J* = 15.7, 7.7 Hz, 2H), 6.44 (t, *J* = 6.7 Hz, 2H), 3.79 (s, 6H), 2.29 (s, 6H). ^{13}C NMR (126 MHz, CD$_2$Cl$_2$) δ 169.6, 158.9, 153.3, 152.0, 135.8, 135.3, 132.2, 131.5, 130.6, 128.9, 128.8, 127.9, 127.1, 126.3, 125.6, 124.6, 122.4, 120.3, 118.7, 118.0, 117.8, 117.1, 114.1, 111.1, 108.2, 82.8, 55.7, 9.5. HRMS-ESI-TOF (*m/z*): [M+K]$^+$ calcd for $C_{52}H_{38}N_2O_5K$ 809.2412 found 809.2411

(Z)-3-(9-(2-(ethoxycarbonyl)phenyl)-6-(1-methyl-2-phenylindolizin-3-yl)-3H-xanthen-3-ylidene)-1-methyl-2-phenyl-3H-indolizin-4-ium (**10**)

Compound **2a** (80 mg, 0.112 mmol) was transferred to a 150 mL two neck round bottom flask and flushed with nitrogen thoroughly for 10 minutes. 1,2-Dichloroethane (4.8 mL) and POCl$_3$ (0.03 mL) were added to the flask and the reaction was refluxed for 4 h. The reaction mixture was allowed to cool to room temperature and concentrated under reduced pressure to give a green solid, which was used in the next step without further purification. The reaction mixture was thoroughly flushed with nitrogen for 10 min, followed by the addition of dry ethanol (3.0 mL), and stirring at

50 ºC for 24 h. The reaction mixture was concentrated under reduced pressure and the solid was dissolved in chloroform (20 mL). The organic layer was washed with water (8 x 10 mL), dried over anhydrous sodium sulfate, filtered and concentrated under reduced pressure to give a green solid. The solid was then washed with hot hexane (20 x 5 mL), and recrystallize from hexane: ethyl acetate mixture to give 28 mg of a green solid in 34% yield. ^{1}H NMR (500 MHz, CD$_2$Cl$_2$) δ 8.32 (s, 1H), 8.11 (d, J = 5.9 Hz, 1H), 8.01 (d, 1H), 7.79 (s, 2H), 7.73 (s, 1H), 7.66 (t, 1H), 7.57 (s, 1H), 7.41 (s, 4H), 7.27 (dd, J = 29.1, 13.4 Hz, 10H), 6.93 (d, J = 26.1 Hz, 2H), 6.83 (d, J = 6.4 Hz, 1H), 6.78 (d, J = 7.4 Hz, 1H), 6.70 (t, 1H), 6.46 (t, 1H), 4.09 (q, 2H), 2.35 – 2.23 (m, 6H), 1.31 (t, 3H). ^{13}C{1H} NMR (126 MHz, CDCl$_3$) δ 165.4, 161.2, 157.1, 142.7, 137.5, 135.3, 134.7, 134.6, 134.4, 133.9, 133.3, 131.3, 131.2, 131.1, 130.9, 130.8, 130.7, 130.2, 129.3, 129.1, 129.0, 128.8, 128.5, 128.4, 127.8, 126.6, 126.0, 125.4, 124.9, 124.0, 122.2, 122.14, 122.09, 118.34, 118.30, 117.9, 117.4, 116.9, 115.1, 114.3, 113.1, 111.0, 107.9, 61.9, 22.9, 14.3, 9.4. HRMS-ESI-TOF (m/z): [M]$^{+}$ calcd for C$_{52}$H$_{39}$N$_2$O$_3$$^{+}$ 739.2955 found 739.2924

CHAPTER 6

6.1 WATER SOLUBLE NIR ABSORBING AND EMITTING INDOLIZINE CYANINE AND

INDOLIZINE SQUARAINE DYES FOR BIOLOGICAL IMAGING

Adapted with the permission from William E. Meador, Shane A. Autry, Riley Bessetti,

Jacqueline Gayton, Alex Flynt, Nathan I. Hammer, and Jared H. Delcamp.; *J. Org. Chem.*

2020, *85*, 4089-4095. Copyright (2020) American Chemical Society.

(See appendix for permission license.)

This project is a collaborative project between Dr. Delcamp's group and Dr. Hammer's group at the University of Mississippi as well as Dr. Flynt's lab at the University of Southern Mississippi. William Meador contributed to the project by synthesizing the dyes and writing the manuscript. Shane Autry contributed to the work by measuring the emission and quantum yield of the organic dyes. Riley Bessetti contributed by performing all biological studies. Jacqueline Gayton contributed by synthesizing the squaraine dye.

ABSTRACT

Organic dyes that absorb and emit in the near-infrared (NIR) region are potentially noninvasive, high-resolution, and rapid biological imaging materials. Indolizine donor-based cyanine and squaraine dyes with water-solubilizing sulfonate groups were targeted in this study due to strong absorptions and emissions in the NIR region. As previously observed for nonwater-soluble derivatives, the indolizine group with water-solubilizing groups retains a substantial shift toward longer wavelengths for both absorption and emission with squaraines and cyanines relative to classically researched indoline donor analogues. Very high quantum yields (as much as 58%) have been observed with absorption and emission >700 nm in fetal bovine serum. Photostability studies, cell culture cytotoxicity, and cell uptake specificity profiles were all studied for these dyes, demonstrating exceptional biological imaging suitability.

INTRODUCTION

Near-infrared (NIR) emissive materials are intensely researched due to a plentiful number of practical applications, including biological imaging,[1−8] photodynamic therapy[,1,9−12] telecommunications,[13−15] secure displays, which can be coupled to night vision technologies,[16−18] and many other innovative areas of research.[5,19−21] NIR biological imaging agents use low-energy photons in a spectral region where tissue is readily penetrated at a maximal depth optically.[4,10,22,23] The desirable properties of biological imaging dyes include (1) absorbing and emitting light in the "therapeutic window" ranging from 700 to 1400 nm, (2) a significant Stokes shift to enable high-precision imaging, (3) efficient absorption and emission of photons through both a high molar absorptivity and quantum yield, and (4) water solubility. While there are many exciting dye design

prospects being pursued in the literature,[2] exceptional NIR emissive materials are still needed for practical biological imaging since current dyes fall short of meeting all of the desired criteria simultaneously. Among NIR emissive dyes, squaraines[21,24] and cyanines[19,25] are ubiquitous.[1,3,26] Previous research has frequently investigated indoline donor-based cyanine and squaraine dyes with indocyanine green (ICG) having been awarded FDA approval several decades ago.[27,28] Both of these classes of dyes need design strategies that allow access to longer wavelength NIR photons in aqueous environments.[2] In fact, the indoline squaraine absorbs outside the therapeutic window, which renders it impractical for use as a noninvasive biological imaging agent.[29] To deepen the NIR absorbing properties of these dye classes, designs capable of extending the π-system through a conjugated donor (such as indolizine) are attractive.[29–32] Recent photophysical studies using proaromatic indolizine donors in place of indoline donors show redshifting of the absorption and emission profiles of these dyes firmly into the therapeutic window in nonaqueous environments (C5 and SQ compared to ICG and indoline squaraine, respectively; **Figure 31**).[29–32] These studies indicated that in the case of phenyl-indolizine derivatives, the phenyl group does not play a significant role in tuning the absorption or emission energy values of the NIR indolizine dyes.[29,30] This enables the use of the phenyl group to append water-soluble functionality without perturbing the core chromophore properties of the dyes, permitting the probing of the photophysical properties of the dyes in aqueous environments. Sulfonate-substituted dyes, SO_3C5 and SO_3SQ, were targeted given the water-solubilizing properties of sulfonate groups and FDA approval for human use by way of ICG (**Figure 31**). This work aims to compare the photophysical properties of SO3C5, SO3SQ, and benchmark ICG in a biologically relevant medium
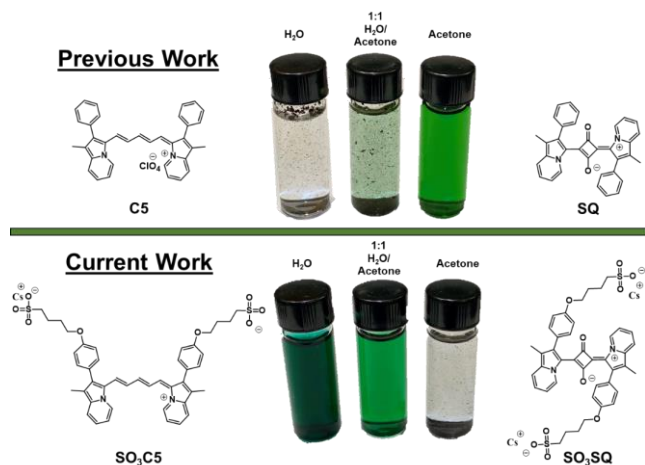
Figure 31. Current work demonstrating water solubility of indolizine cyanine and indolizine

SYNTHESIS

The target dyes were synthesized in two steps from previously reported indolizine phenol **1** (**Scheme 3**).[29] First, **1** was alkylated with butane sultone (**2**) in the presence of base to give sulfonate indolizine **3**. Interestingly, this reaction required a careful selection of solvent and base to avoid significant side product formation as a carbon alkylated product (see appendix **Table 52**). Intermediate **3** is common to both SO$_3$C5 and SO$_3$SQ target dyes. The target sulfonate indolizine cyanine dye (SO$_3$C5) is synthesized by reacting **3** with the methine bridge linker **4** in the presence of perchloric acid and acetic anhydride at room temperature similar to previously reported conditions in the literature.[30] The target sulfonate indolizine squaraine (SO$_3$SQ) is synthesized via an electrophilic aromatic substitution/condensation reaction between sulfonate indolizine **3** and squaric acid (**5**). Importantly, during optimization of the condensation reaction, it was found that the addition of small amounts of water led to an increase in product formation. Ultimately, running

114

the reaction in nondried laboratory-grade methanol gave the highest yields (see appendix **Table 53**). Both target dyes are formed in an approximately 50% overall yield in this route over two steps.
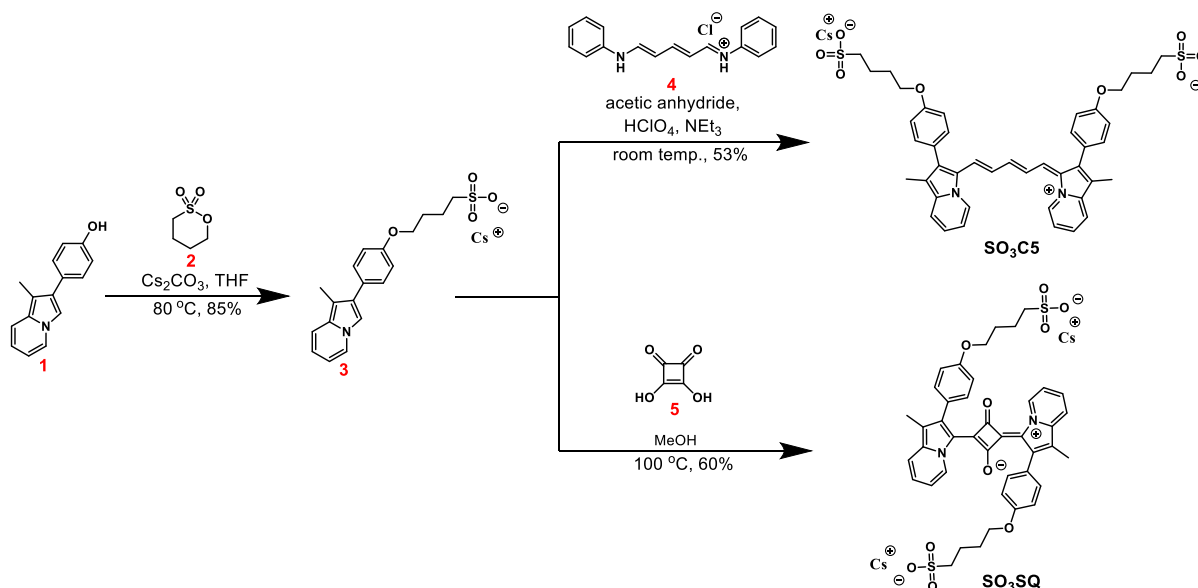
Scheme 3. Synthetic route towards target dyes, **SO₃C5** and **SO₃SQ**.

RESULTS AND DISCUSSION

With SO₃C5 and SO₃SQ in hand, absorption and emission studies were undertaken for comparison to ICG as a benchmark reference dye (**Figure 32**, appendix **Figures 89&90** ; **Table 13**). Dimethyl sulfoxide (DMSO) and MeOH were also selected as solvents, which allows for the comparison of **SO₃C5** and **SO₃SQ** to the previously reported dyes C5 and SQ, respectively (see appendix **Table 51** for solubility data).[29,30] H_2O and fetal bovine serum (FBS) were selected as well due to the biological relevance and for a convenient analysis of how these dyes will behave with biological

matrix elements in place, as has been previously reported in the literature.[4,33,34] The absorption

profiles of both dyes in DMSO and MeOH are not significantly changed relative to the previously

published dyes with no sulfonate groups.[29,30] The absorption curves in H_2O and FBS are similar to

the curves observed in DMSO and MeOH for **SO₃SQ**; however, the absorption curve of **SO₃C5**

in water deviates shape significantly, which is likely due to aggregation in water (see appendix

Figure 91). Upon changing concentrations, no significant evidence of aggregate disruption could

be observed down to concentrations near the detection limit of the spectrometer (see appendix

Figure 92). Notably, the evidence of aggregation of **SO₃SQ** (modest amounts) and ICG

(significant amounts) in H_2O at concentrations of $\geq 10^{-5}$ M is apparent at higher-energy

wavelengths when the absorption curves are overlaid with curves at 10^{-6} M in H_2O, which appear

to have disrupted aggregate features (see appendix **Figures 93&94**).[35] It should be noted that while

all three dyes were observed to form aggregates in H_2O via dynamic light scattering analysis at 5

$\times 10^{-6}$ M (see appendix **Figure 103**), **SO₃C5** is the only dye that shows a significant impact of this

aggregative behavior from the absorption profile. Interestingly, upon dissolving **SO₃C5** in FBS,

the original curve shape observed in DMSO and MeOH is regained with a notable red shift of the

λ_{max} value by about 40 nm (**Figure 32**). FBS is commonly used in photophysical studies for NIR

dyes intended for biological use as the albumin proteins help to better separate dye molecules from

one another as is dramatically demonstrated here. The disruption of aggregation under biologically

relevant conditions is encouraging as it leads to the minimization of thermal relaxations resulting
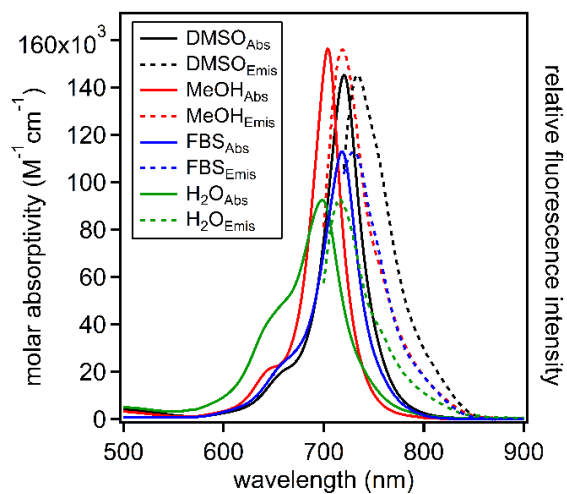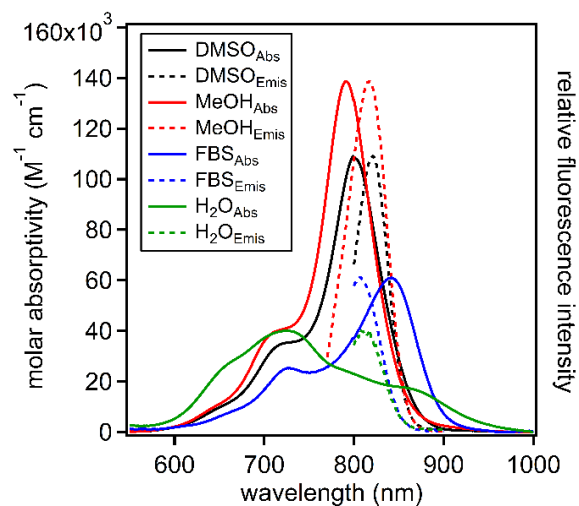
Figure 32. Vis-NIR region molar absorptivity and normalized fluorescence emission of **SO₃C5** (top) and **SO₃SQ** (bottom) in DMSO, MeOH, H₂O, and FBS.

in increased quantum yields. For comparison, the curve shape of ICG retains the same profile in all four solvents (see appendix **Figure 91**). The molar absorptivities are similar for **SO₃C5** and **SO₃SQ** in MeOH and DMSO at approximately $110{,}000-150{,}000$ M^{-1} cm^{-1} (**Figure 32** and **Table**

13). In H_2O and FBS, the **SO₃C5** molar absorptivities drop substantially to ~60,000 M^{-1} cm^{-1} or less. For **SO₃SQ** in H_2O or FBS, the molar absorptivities remain significantly higher at

Table 13. Optical properties of **SO₃C5**, **SO₃SQ**, and ICG in water, fetal bovine serum (FBS), methanol, and DMSO.

Dye	Solvent	Abs. max. [nm]	Emis. Max. [nm]	Stokes shift [nm | eV | cm⁻¹]	ε [M⁻¹ cm⁻¹]	Φ [%]	MB [ε × Φ]
SO₃C5	DMSO	801	821	20 | 0.04 | 304	109,000	2.0	2,180
	MeOH	791	817	26 | 0.05 | 403	139,000	0.3	420
	FBS	842	808	---	61,000	0.1	60
	Water	726	808	---	40,000	0.05	20
SO₃SQ	DMSO	720	734	14 | 0.03 | 265	145,000	8.6	12,500
	MeOH	704	719	15 | 0.04 | 296	156,000	0.8	1,250
	FBS	719	730	11 | 0.03 | 210	113,000	58.3	65,900
	Water	698	716	18 | 0.04 | 360	93,000	0.3	280
ICG	DMSO	794	825	31 | 0.06 | 473	211,000	11.0	23,200
	MeOH	784	819	35 | 0.07 | 545	230,000	4.3	9,900
	FBS	798	827	29 | 0.05 | 439	174,000	9.3	16,200
	Water	779	812	33 | 0.06 | 522	157,000	0.5	780

113,000−93,000 M^{-1} cm^{-1}. The molar absorptivity values and order of λ_{max} values follow the same trend for **SO₃SQ** and ICG with each of the four solvents. **SO₃C5** deviates from this trend with obvious aggregation in water-based solutions. Compared to ICG, the λ_{max} of **SO₃C5** is shifted toward lower energy values (~15 nm), and the λ_{max} of **SO₃SQ** is shifted toward higher energy by about 100 nm (0.21 eV, **Table 13**). Fluorescence spectroscopy was probed with each of the dyes to understand the excited-state behavior. Prior reports on **C5** and **SQ** in organic solvents such as dichloromethane have shown Stokes shifts of 43 and 50 nm, respectively (taken as the difference between the λ_{max}abs and λ_{max}emis).[29−31] The Stokes shifts of both sulfonate dyes decreased to ≤26 nm (≤400 cm^{-1}) in all solvents where single molecule behavior is likely occurring. As the magnitude of the Stokes shift is directly related to the reorganization energy of the dye, the decrease in the Stokes shift demonstrates that there is smaller reorganization energy of **SO₃SQ** and **SO₃C5** relative to the non-sulfonate substituted dyes. Stokes shifts for **SO₃C5** could not be determined in FBS and H_2O due to the presence of multiple species due to aggregation, leading to apparent emission energies higher than the lowest energy features of the combined absorption spectrum of all monomer and aggregate states. This suggests that in aqueous solvents, the higher energy absorption feature of **SO₃C5** corresponds to the observed emission, while the lower-energy absorption feature is either weakly emissive or has an emission beyond the InGaAs fluorimeter detection limit. Quantum yields (Φ) for each dye were calculated as relative values with respect to ICG in DMSO at 11.0% as the benchmarking system (**Table 13**).[36] The quantum yields for ICG in water, MeOH, and FBS were calculated with respect to ICG in DMSO. Previously reported quantum yields for **C5** in organic solvents ranged from 2 to 3.6%;[30,31] however, **SO₃C5** shows Φ values below 1% in all three protic solvents examined. In DMSO, a Φ of 2% is observed, which is

similar to the values observed for the parent **C5** structure. The Φ data for **SO₃SQ** is exceptionally intriguing. In water or methanol, the Φ of **SO₃SQ** is 9000 M^{-1} cm^{-1}). **SO₃SQ** shows an MB value of >65,000 M^{-1} cm^{-1} in FBS, which is dramatically larger than the substantial 23,000 M^{-1} cm^{-1} value for ICG and is likely one of the largest values in this spectral region known in the literature.
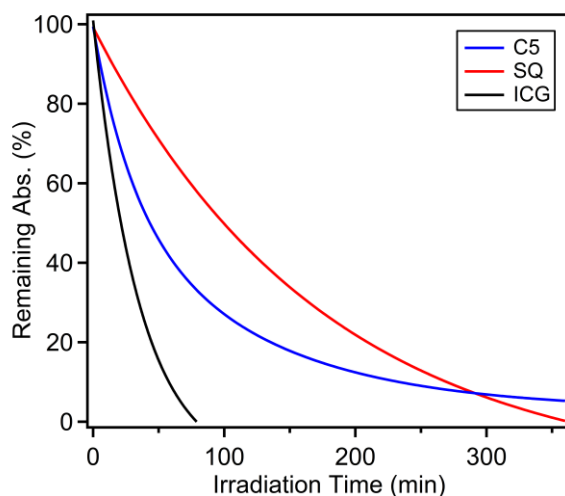
Figure 33. Photostability of **SO₃C5**, **SO₃SQ**, and ICG in water.

This indicates that significantly less dye (∼3× less) would be needed with **SO₃SQ** to generate the same amount of signal as ICG. A key desirable property of biological imaging dyes is prolonged photostability.[37] To probe this, **SO₃C5**, **SO₃SQ**, and ICG were dissolved in water under an ambient atmosphere at a concentration of 1×10^{-6} M and irradiated with a solar simulated light-emitting diode (LED) spectrum from 400 to 1100 nm with white light irradiation (**Figures 33** and appendix **Figures 95−97**). Under these conditions, ICG has a half-life of approximately 35 min with complete consumption by 80 min. Both **SO₃C5** and **SO₃SQ** show a higher photostability than ICG with half-lives of 50 and 100 min, respectively. The higher photostability of **SO₃SQ** can be attributed, in part, to the squaraine structure being devoid of double-substituted alkenes, which are

120

known to undergo various degradation pathways with ICG.[38] In MeOH, **SO₃SQ** and ICG are exceptionally stable with half-lives >24 h (see appendix **Figures 99−102**). **SO₃C5** is notably less stable than ICG or **SO₃SQ** in MeOH where the dye appears to be deaggregated, which suggests that the aggregate states of **SO₃C5** in water could impart some photostability since this dye is more stable than ICG in water. Overall, **SO₃SQ** has a likely record quantum yield in this spectral region, a high molar absorptivity, an exceptional molecular brightness, and the highest photostability measured in this study in H_2O. Finally, the cytotoxicity and cellular uptake of **SO₃C5** and **SO₃SQ** were examined with human (HEK293) and Drosophila (S2) tissue culture cells (Figure 34). HEK cells are a human cell line grown at physiological conditions found in mammals. Performance and cytotoxicity of the dyes in HEK cells inform in vivo biocompatibility for clinical and veterinary settings for use in diagnostic or therapeutic technologies. In contrast, S2 cells grow at a lower temperature under normal atmospheric conditions and are derived from invertebrates (fruit fly embryos). Dye behavior in these cells is a proxy for understanding the environmental impact of these compounds. Both **SO₃C5** and **SO₃SQ** show < 25% HEK cell death at or below 2 mM concentrations. At high dye loadings (10 mM), cell death is near 30%, which indicates that these dyes are relatively benign toward a human cell line. A similar trend is observed with the cytotoxicity studies of the S2 cell line, although ≥2 mM **SO₃C5** and 10 mM **SO₃SQ** show >50% cell death. S2 cells are more phagocytically active compared to HEK293 cells, which may explain greater sensitivity to the dyes. This suggests that low-to-moderate concentrations of the dyes are not toxic to animal cells. **SO₃C5** and **SO₃SQ** cell uptake studies were undertaken with LysoTracker by comparing the fluorescence overlap of each NIR dye with LysoTracker. With these studies, the **SO₃C5** dye shows a Pearson's correlation coefficient of 0.9, indicating that HEK cells largely

uptake this dye into the cell lysosomes. A similarly high Pearson's correlation coefficient is observed for **SO₃SQ** and S2 cells at 0.7. This shows that nonfavorable interactions of the dye with cell organelles are minimized.
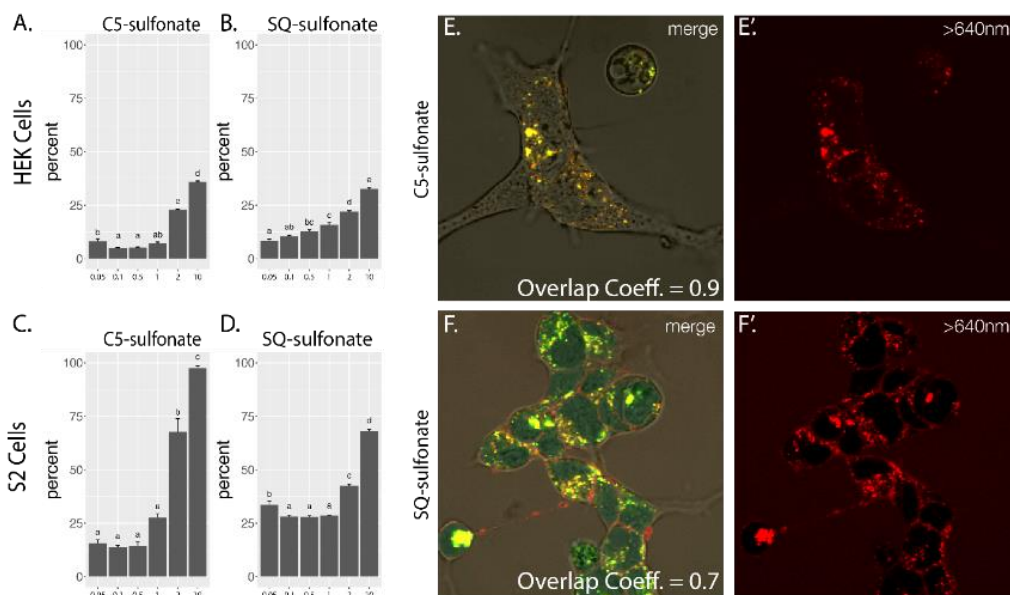
Figure 34. Interaction of **SO₃C5** and **SO₃SQ** dyes with human (HEK) and *Drosophila* (S2) cells. A-D) Percent cytotoxicity for each combination as determined by LDH assay. X-axis values are Mm. Error bars represent standard error, and letter denote significance groups determined by TukeyHSD (p ≤ 0.05). E-F) Confocal images of live HEK and S2 (F) cells after exposure to dye and lysotracker®. Left panels are merge of bright field, lysotracker (green), and dye (red). Dye fluorescence alone is right (E',F'). Overlap coefficient shows colocalization between dye and lystotracker®.

CONCLUSION

The need for biological imaging dyes that absorb and emit strongly in the NIR region is of paramount importance to society since this could enable noninvasive, nontoxic, and rapid imaging of medical patients and biological specimens. Indolizine donor-based cyanine and squaraine dyes with attached sulfonate groups were synthesized to provide a direct comparison in biological medium to benchmark ICG. The increased donor strength of the indolizine compared to that of the indoline allowed for these dyes to have a more red-shifted absorption and emission than their indoline counterparts. **SO₃SQ** demonstrated a remarkable quantum yield of 58.3% (MB of > 65,000) in FBS, which is notable in that this is representative of the optical properties inside of a biological medium. **SO₃C5** shows significant concentration-independent aggregation effects in water, while **SO₃SQ** shows minimal aggregation in water. Prolonged irradiation studies demonstrate that both of the indolizine dyes have a significantly higher photostability than ICG in water. Cell culture studies exhibited high specificity for lysosomal uptake with overlap coefficients of 0.9 and 0.7 for **SO₃C5** and **SO₃SQ**, respectively, as well as low levels of cytotoxicity. The high molecular brightness, simple synthesis, prolonged photostability, and low toxicity of **SO₃SQ** show that it is an attractive potential NIR biological imaging material with very high metrics significantly surpassing the benchmark ICG over a range of tests.

EXPERIMENTAL SECTION

All commercially obtained reagents and solvents were used as received without further purification. All heating was done in an oil bath. Thin layer chromatography (TLC) was conducted with Merck KGaA TLC silica gel 60 RP-18 F254S glass-backed plates and visualized with UV.

Flash column chromatography was performed using a CombiFlash Rf + system. RediSep cartridges were charged with silica gel from RediSep Rf reversed-phase C18, 40−63 μm (230−400 mesh). ^{1}H and ^{13}C NMR spectra were recorded on a Bruker Ascend-300 (300 MHz) spectrometer and are reported in ppm using solvent as an internal standard (DMSO-d_6 at 2.50 ppm and CD$_3$OD-d_4 at 3.31 ppm). Data are reported as s = singlet, d = doublet, t = triplet, q = quartet, p = pentet, m = multiplet, b = broad, ap = apparent, dd = doublet of doublets, dt = doublet of triplets; coupling constant(s) are in Hz; integration. UV−vis−NIR spectra were measured with a Cary 5000 UV−vis−NIR spectrometer. For photostability studies, samples were irradiated with a Class AAA Rated G2V pico LED solar simulator providing a spectral range from 400 to 1100 nm at 100 mW cm^{-2} . High-resolution mass spectrometry (HRMS) spectra were obtained with a quadrupole time-of-flight (QTOF) HRMS utilizing nanospray ionization. The mass analyzer was set to the 200−2000 Da range. Infrared spectra were recorded with an Agilent Cary 660 attenuated total reflection-Fourier transform infrared (ATR-FTIR) spectrometer. All emission data was obtained using a Horiba PTI fluorimeter. Excitation wavelengths were achieved by passing white light through a dual-grating system. Photons were collected through a photomultiplier tube. The relative quantum yields were obtained using this equation:

$$\Phi_{sample} = \Phi_{standard} \cdot \frac{E_{sample}}{E_{standard}} \cdot \frac{A_{sample}}{A_{standard}} \cdot \frac{\eta^2_{sample}}{\eta^2_{standard}}$$

For the equation above, E is the sum of emission intensities and A is the maximum absorbance, η is the refractive index of the solvent used, and Φ denotes the quantum yield. The standard used to obtain the relative quantum yields was indocyanine green (ICG) with a quantum yield of 11% in DMSO.[36] HEK293 cells were grown in standard conditions (37°C, 5% CO$_2$) in Dulbecco's

modified Eagle's medium (DMEM) media supplemented with 10% FBS. S2 cell cultures were maintained in S2 media with 10% FBS at 25°C. Dye cytotoxicity was determined with a CyQUANT LDH Cytotoxicity Assay KitTM Invitrogen using a BioTek SynergyTM H1 microplate reader. Cells were imaged with a Zeiss LSM 510 META laser scanning confocal microscope following a 24 h exposure to dyes. Lysosome was visualized with a LysoTracker Green DND-26 (Invitrogen) following the manufacturer's protocols.

Cesium 4-(4-(1-Methylindolizin-2-yl)phenoxy)butane-1-sulfonate (**3**). To a flame-dried round-bottom flask equipped with a stir bar and reflux condenser that had been purged with N_2 for 10 min were added 4-(1-methylindolizin-2-yl)phenol (**1**) (1.00 g, 4.48 mmol),[29] Cs_2CO_3 (3.65 g, 11.20 mmol), and 1,4-butane sultone (**2**) (1.15 mL, 11.20 mmol). The reaction mixture was dissolved in tetrahydrofuran (THF) (140 mL) and heated to 80 °C in an oil bath for 16 h. The reaction mixture was cooled down to room temperature and yielded a light brown precipitate. Ethyl acetate was added (100 mL) to further precipitate the product, which was subsequently filtered to yield the crude material. The crude mixture was purified by recrystallization in water to yield a pure golden brown metallic in appearance solid (1.87 g, 85%). ^{1}H NMR (300 MHz, DMSO-d_6) δ 8.13 (d, J = 6.9 Hz, 1H), 7.63 (s, 1H), 7.42 (d, J = 8.7 Hz, 2H) 7.37 (d, J = 9.1 Hz, 1H), 6.99 (d, J = 8.7 Hz, 2H), 6.60 (dd, J = 8.1, 7.2 Hz, 1H), 6.45 (dt, J = 7.1, 1.2 Hz, 1H), 3.98 (t, J = 5.8 Hz, 2H), 2.46 (t, J = 7.1 Hz, 2H), 2.34 (s, 3H), 1.85−1.65 (m, 4H). ^{13}C NMR (300 MHz, DMSO-d_6) δ 157.3, 130.2, 129.1, 127.8, 127.8, 125.2, 117.0, 115.6, 114.6, 109.8, 109.7, 104.2, 67.3, 51.1, 28.1, 22.0, 9.7. HRMS m/z calculated for $C_{19}H_{20}NO_4S$ [M−Cs]$^-$: 358.1119, found 358.1128. IR (neat, cm^{-1}): 3413, 3310, 3064, 3048, 2931, 2860, 1675, 1611, 1535, 1515. Melting point (dec.): 226−232°C.

Cesium-4-(4-(1-Methyl-3-((1E,3E)-5-((Z)-1-methyl-2-(4-(4-sulfonatobutoxy)phenyl)-3H-indolizin-4-ium-3-ylidene)-penta-1,3-dien-1-yl)indolizin-2-yl)phenoxy)butane-1-sulfonate

(**SO₃C5**). To a round-bottom flask equipped with a stir bar was added cesium 4-(4-(1-methylindolizin-2-yl)phenoxy)butane-1-sulfonate (**3**) (0.50 g, 1.02 mmol) to acetic anhydride (10.2 mL) followed by perchloric acid (0.088 mL, 1.02 mmol) and N-[5-(phenylamino)- 2,4-pentadienylidene]aniline monohydrochloride (**4**) (0.15 g, 0.51 mmol). The mixture was then sonicated and stirred until all of the starting material appeared to have been consumed in this first phase of the reaction (about 10 min). When the starting material was no longer visible, the reaction was allowed to stir for another 10 min before the addition of triethylamine (0.17 mL, 1.22 mmol). The reaction mixture quickly turned green and was allowed to stir for 2 h before diethyl ether was added to precipitate the crude product. The precipitate was filtered and rinsed once more with diethyl ether, collecting the solids. The solids were purified via reversed-phase column chromatography beginning with 100% H_2O and gradually transitioning to 40:60 ethanol/H_2O. The water was removed by blowing air over the surface of the solution to avoid heating. The pure product was yielded as a dark green solid (250 mg, 53%). ^{1}H NMR (300 MHz, CD₃OD-d₄) δ 8.89 (d, J = 6.8 Hz, 2H), 7.73 (d, J = 8.6 Hz, 2H), 7.66−7.54 (m, 4H), 7.42−7.22 (m, 7H), 7.12 (d, J = 8.5 Hz, 4H), 6.57 (t, J = 13.1 Hz, 2H), 4.16 (t, J = 5.9 Hz, 4H), 2.95 (t, J = 7.0 Hz, 4H), 2.20 (s, 6H), 2.14−1.94 (m, 8H). ^{13}C NMR (300 MHz, CD₃OD-d₄) δ 168.4, 160.9, 144.4, 140.1, 135.6, 132.6, 131.3, 129.7, 127.4, 126.2, 122.5, 121.2, 119.4, 118.0, 116.1, 68.9, 52.4, 29.5, 23.1, 9.3. HRMS m/z calculated for $C_{43}H_{44}CsN_2O_8S_2$ [M + H]$^+$: 913.1588, found 913.1606. IR (neat, cm^{-1}): 3375 (br), 3099, 3070, 3033, 2917, 2861, 1651, 1611, 1521, 1508. UV−vis−NIR (DMSO) λ_{max} =

801 nm; UV−vis−NIR (MeOH) λ_{max} = 791 nm; UV−vis−NIR (H_2O) λ_{max} = 726 nm; UV−vis−NIR (FBS) λ_{max} = 842 nm. Melting point (dec.): 211−217°C.

Cesium-(Z)-4-(4-(1-Methyl-3-(3-(1-methyl-2-(4-(4-sulfonatobutoxy)phenyl)-3H-indolizin-4-ium-3-ylidene)-2-oxido-4-oxocyclobut-1-en-1-yl)indolizin-2-yl)phenoxy)-butane-1-sulfonate

(**SO₃SQ**). To a pressure flask equipped with a stir bar were added cesium 4-(4-(1-methylindolizin-2-yl)phenoxy)-butane-1-sulfonate (**3**) (0.100 g, 0.204 mmol) and 3,4-dihydroxy-1,2-cyclobutanedione (**5**) (0.012 g, 0.102 mmol). The reagents were dissolved in 10 mL methanol and degassed with N_2 for 10 min. The reaction mixture was then heated to 100 °C in an oil bath for 6 h. The reaction mixture was then concentrated, and the solids were further purified via reversed-phase column chromatography beginning with 100% H_2O and gradually transitioning to 40:60 ethanol/H_2O. The water was removed by blowing air over the surface of the solution as the product appeared to be sensitive to heat. The pure product was yielded following this step as a metallic red solid in appearance (65 mg, 60%). ^{1}H NMR (300 MHz, CD₃OD-d₄) δ 9.76 (d, J = 6.9 Hz, 2H), 7.57 (d, J = 8.7 Hz, 2H), 7.37 (dd, J = 6.8, 1.0 Hz, 2H), 7.23 (d, J = 8.6 Hz, 4H), 7.04−6.95 (m, 6H), 4.13 (t, J = 6.0 Hz, 4H), 2.95 (t, J = 7.0 Hz, 4H), 2.21 (s, 6H), 2.12−1.83 (m, 8H). ^{13}C NMR (300 MHz, CD₃OD-d₄) δ 177.8, 166.1, 160.1, 143.2, 138.6, 134.9, 132.9, 128.9, 127.7, 121.0, 119.5, 118.4, 116.1, 114.8, 68.7, 52.5, 29.6, 23.1, 9.5. HRMS m/z calculated for $C_{42}H_{39}N_2O_{10}S_2$ [M−2Cs + 2H]⁻: 795.2052, found 795.2050. IR (neat, cm^{-1}): 3398 (br), 3068, 3038, 2919, 2864, 1733, 1600, 1570, 1523. UV−vis−NIR (DMSO) λ_{max} = 720 nm; UV−vis−NIR (MeOH) λ_{max} = 704 nm; UV−vis−NIR (H_2O) λ_{max} = 699 nm; UV−vis−NIR (FBS) λ_{max} = 719 nm. Melting point: 240−244°C.

All photostability studies were conducted at a concentration of 1×10^{-6} M to maintain consistency and deter any aggregative effects throughout the photodecomposition process. The samples were irradiated with a white LED lamp providing a spectral range from 400 to 1100 nm. The experiment was allowed to take place under ambient conditions without any further precautions to remove oxygen from the system. UV−vis−NIR was used to periodically measure the decline in absorption with respect to the λ_{max}. The photostability in methanol was conducted over a period of 24 h, while the photostability in water was conducted over a period of just 6 h as the photodecomposition was observed within a shorter time frame.

CHAPTER 7

7.1 OVERALL CONCLUSION

In conclusion, the indolizine donor can greatly impact the properties of commonly used NIR emissive material backbones. The indolizine-cyanine dyes show a red-shifted absorption relative to benchmark **ICG** despite two fewer methines which shows the critical role the indolizine groups can play in shifting absorption spectra as a conjugated donor group. The dyes were found to emit in the NIR region with the sterically congested dye **C1** showing the largest solvent effects and reorganization energies. The 5 methine group bridge of **C5** was found to lead to the largest quantum yields and a high MB value for a dye emitting near 900 nm. In addition, counter anion choice was also found to tune both the solution and solid state properties with a larger anion generating the most single molecule-like solid state absorption. The indolizine-squaraine based NIR fluorescent compounds, with emission maxima ranging from 730 to 770 nm, showed Stokes shifts up to 50 nm and some of the highest fluorescence quantum yields known for emissive small molecules in this NIR region with significant Stokes-shifts ($\Phi > 12\%$). DFT computational analysis shows the origin of this Stokes-shift to come from the molecular engineering of large dihedral angles within the π-system, which undergo significant changes when the excited-state geometry reorganizes. The indolizine-xanthene based dye, while not a typical rhodamine structure with N-xanthene bonds, was non-fluorescent in the closed spirocyclic structure; however, with the formation of the opened ethyl ester derivative, the fluorophore possessed absorption and emission

within the NIR II region with high molar absorptivity and a quantum yield of ~0.03%. To the best of our knowledge, this is the first xanthene-based emissive dye with photophysical properties in the NIR II region. The water soluble **SO₃SQ** demonstrated a remarkable quantum yield of 58.3% (MB of >65,000) in FBS which is notable in that this is representative of the dye's performance inside of a biological medium. Irradiation studies demonstrate that both of the indolizine dyes have a significantly higher photostability than ICG in water.

LIST OF REFERENCES

1.   Shindy, H. A., Fundamentals in the chemistry of cyanine dyes: A review. *Dyes and Pigments* **2017,** *145*, 505-513.

2.   Xue, J.; Li, C.; Xin, L.; Duan, L.; Qiao, J., High-efficiency and low efficiency roll-off near-infrared fluorescent OLEDs through triplet fusion. *Chemical Science* **2016,** *7* (4), 2888-2895.

3.   Tuong Ly, K.; Chen-Cheng, R.-W.; Lin, H.-W.; Shiau, Y.-J.; Liu, S.-H.; Chou, P.-T.; Tsao, C.-S.; Huang, Y.-C.; Chi, Y., Near-infrared organic light-emitting diodes with very high external quantum efficiency and radiance. *Nature Photonics* **2016,** *11* (1), 63-68.

4.   Suzuki, H., Organic Light-Emitting Materials and Devices for Optical Communicaiton Technology. *Journal of Photochemistry and Photobiology A: Chemistry* **2004,** *166*, 155-161.

5.   Yang, Z.; Sharma, A.; Qi, J.; Peng, X.; Lee, D. Y.; Hu, R.; Lin, D.; Qu, J.; Kim, J. S., Super-resolution fluorescent materials: an insight into design and bioimaging applications. *Chemical Society Reviews* **2016,** *45*, 4651-4667.

6.   Keereweer, S.; Van Driel, P. B. A. A.; Snoeks, T. J. A.; Kerrebijn, J. D. F.; Baatenburg de Jong, R. J.; Vahrmeijer, A. L.; Sterenborg, H. J. C. M.; Löwik, C. W. G. M., Optical image-guided cancer surgery: challenges and limitations. *Clinical Cancer Research* **2013,** *19*, 3745-54.

7.   Escobedo, J. O.; Rusin, O.; Lim, S.; Strongin, R. M., NIR dyes for bioimaging applications. *Current Opinion in Chemical Biology* **2010,** *14* (1), 64-70.

8.   Bricks, J. L.; Slominskii, Y. L.; Panas, I. D.; Demchenko, A. P., Fluorescent J-aggregates of cyanine dyes: basic research and applications review. *Methods Appl Fluoresc* **2017,** *6* (1), 012001.

9.   Shi, C.; Wu, J. B.; Pan, D., Review on near-infrared heptamethine cyanine dyes as theranostic agents for tumor imaging, targeting, and photodynamic therapy. *J Biomed Opt* **2016,** *21* (5), 50901.

10.   Antaris, A. L.; Chen, H.; Cheng, K.; Sun, Y.; Hong, G.; Qu, C.; Diao, S.; Deng, Z.; Hu, X.; Zhang, B.; Zhang, X.; Yaghi, O. K.; Alamparambil, Z. R.; Hong, X.; Cheng, Z.; Dai, H., A small-molecule dye for NIR-II imaging. *Nature Materials* **2016,** *15*, 235-42.

11.   Peng, X.; Song, F.; Lu, E.; Wang, Y.; Zhou, W.; Fan, J.; Gao, Y., Heptamethine Cyanine Dyes with a Large Stokes Shift and Strong Fluorescence: A Paradigm for Excited-State Intramolecular Charge Transfer. *Journal of the American Chemical Society* **2005,** *127*, 4170-4171.

12.   Han, J.; Engler, A.; Qi, J.; Tung, C. H., Ultra Pseudo-Stokes Shift Near Infrared Dyes Based on Energy Transfer. *Tetrahedron Letters* **2013,** *54*, 502-505.

13.   Smith, A. M.; Mancini, M. C.; Nie, S., Bioimaging: second window for in vivo imaging. *Nature Nanotechnology* **2009,** *4*, 710-1.

14.   Pham, W.; Cassell, L.; Gillman, A.; Koktysh, D.; Gore, J. C., A near-infrared dye for multichannel imaging. *Chemical Communications* **2008,** (16), 1895-7.

15.   Antaris, A. L.; Chen, H.; Diao, S.; Ma, Z.; Zhang, Z.; Zhu, S.; Wang, J.; Lozano, A. X.; Fan, Q.; Chew, L.; Zhu, M.; Cheng, K.; Hong, X.; Dai, H.; Cheng, Z., A high quantum yield molecule-protein complex fluorophore for near-infrared II imaging. *Nature Communications* **2017,** *8*, 15269.

16.   Siebrand, W., Radiationless Transitions in Polyatomic Molecules. I. Calculation of Franck—Condon Factors. *The Journal of Chemical Physics* **1967,** *46* (2), 440-447.

17.   Siebrand, W., Radiationless Transitions in Polyatomic Molecules. II. Triplet-Ground-State Transitions in Aromatic Hydrocarbons. *The Journal of Chemical Physics* **1967,** *47* (7), 2411-2422.

18.   Caspar, J. V.; Sullivan, B. P.; Kober, E. M.; Meyer, T. J., Application of the Energy Gap Law to the Decay of Charge Transfer Excited-States. Solvent Effects. *Chemical Physics Letters* **1982,** *91*, 91-95.

19.   Englman, R.; Jortner, J., The Energy Gap Law for Radiationless Transitions in Large Molecules. *Molecular Physics* **1970,** *18*, 145-164.

20.   McNamara, L. E.; Liyanage, N.; Peddapuram, A.; Murphy, J. S.; Delcamp, J. H.; Hammer, N. I., Donor-Acceptor-Donor Thienopyrazines via Pd-Catalyzed C-H Activation as NIR Fluorescent Materials. *The Journal of Organic Chemistry* **2016,** *81*, 32-42.

21.   Alander, J. T.; Kaartinen, I.; Laakso, A.; Patila, T.; Spillmann, T.; Tuchin, V. V.; Venermo, M.; Välisuo, P., A review of indocyanine green fluorescent imaging in surgery. *International Journal of Biomedical Imaging* **2012,** *2012*, 940585.

22.   Alander, J. T.; Villet, O. M.; Pätilä, T.; Kaartinen, I. S.; Lehecka, M.; Nakaguchi, T.; Suzuki, T.; Tuchin, V., *Fluorescence Imaging for Surgeons: Review of Indocyanine Green Imaging in Surgery*. Springer, Cham, 2015.

23.   Huckaba, A. J.; Giordano, F.; McNamara, L. E.; Dreux, K. M.; Hammer, N. I.; Tschumper, G. S.; Zakeeruddin, S. M.; Grätzel, M.; Nazeeruddin, M. K.; Delcamp, J. H., Indolizine-Based Donors as Organic Sensitizer Components for Dye-Sensitized Solar Cells. *Advanced Energy Materials* **2015,** *5*, 1401629.

24.   Zhang, Y.; Autry, S. A.; McNamara, L. E.; Nguyen, S. T.; Le, N.; Brogdon, P.; Watkins, D. L.; Hammer, N. I.; Delcamp, J. H., Near-Infrared Fluorescent Thienothiadiazole Dyes with Large Stokes Shifts and High Photostability. *The Journal of Organic Chemistry* **2017,** *82*, 5597-5606.

25.   McNamara, L. E.; Rill, T. A.; Huckaba, A. J.; Ganeshraj, V.; Gayton, J.; Nelson, R. A.; Sharpe, E. A.; Dass, A.; Hammer, N. I.; Delcamp, J. H., Indolizine-Squaraines: NIR Fluorescent Materials with Molecularly Engineered Stokes Shifts. *Chemistry - A European Journal* **2017,** *23*, 12494-12501.

26.   Huckaba, A. J.; Yella, A.; McNamara, L. E.; Steen, A. E.; Murphy, J. S.; Carpenter, C. A.; Puneky, G. D.; Hammer, N. I.; Nazeeruddin, M. K.; Grätzel, M.; Delcamp, J. H., Molecular Design Principles for Near-Infrared Absorbing and Emitting Indolizine Dyes. *Chemistry - A European Journal* **2016,** *22* (43), 15536-15542.

27.   Mustroph, H.; Towns, A., Fine Structure in Electronic Spectra of Cyanine Dyes: Are Sub-Bands Largely Determined by a Dominant Vibration or a Collection of Singly Excited Vibrations? *ChemPhysChem* **2018,** *19* (9), 1016-1023.

28.   Qian, G.; Dai, B.; Luo, M.; Yu, D.; Zhan, J.; Zhang, Z.; Ma, D.; Wang, Z. Y., Band Gap Tunable, Donor-Acceptor-Donor Charge-Transfer Heteroquinoid-Based Chromophores: Near Infrared Photoluminescence and Electroluminescence. *Chemistry of Materials* **2008,** *20*, 6208-6215.

29.   Bai, M.; Achilefu, S., Synthesis and spectroscopy of near infrared fluorescent dyes for investigating dichromic fluorescence. *Bioorganic & Medicinal Chemistry Letters* **2011,** *21* (1), 280-4.

30.   Dost, T. L.; Gressel, M. T.; Henary, M., Synthesis and Optical Properties of Pentamethine Cyanine Dyes with Carboxylic Acid Moieties. *Analytical Chemistry Insights* **2017,** *12*, 1-6.

31.   Frisch, M. J.; Trucks, G. W.; Schlegel, H. B.; Scuseria, G. E.; Robb, M. A.; Cheeseman, J. R.; Scalmani, G.; Barone, V.; Petersson, G. A.; Nakatsuji, H.; Li, X.; Caricato, M.; Marenich, A. V.; Bloino, J.; Janesko, B. G.; Gomperts, R.; Mennucci, B.; Hratchian, H. P.; Ortiz, J. V.; Izmaylov, A. F.; Sonnenberg, J. L.; Williams-Young, D.; Ding, F.; Lipparini, F.; Egidi, F.; Goings, J.; Peng, B.; Petrone, A.; Henderson, T.; Ranasinghe, D.; Zakrzewski, V. G.; Gao, J.; Rega, N.; Zheng, G.; Liang, W.; Hada, M.; Ehara, M.; Toyota, K.; Fukuda, R.; Hasegawa, J.; Ishida, M.; Nakajima, T.; Honda, Y.; Kitao, O.; Nakai, H.; Vreven, T.; Throssell, K.; Montgomery Jr., J. A.; Peralta, J. E.; Ogliaro, F.; Bearpark, M. J.; Heyd, J. J.; Brothers, E. N.; Kudin, K. N.; Staroverov, V. N.; Keith, T. A.; Kobayashi, R.; Normand, J.; Raghavachari, K.; Rendell, A. P.; Burant, J. C.; Iyengar, S. S.; Tomasi, J.; Cossi, M.; Millam, J. M.; Klene, M.; Adamo, C.; Cammi, R.; Ochterski, J. W.;

Martin, R. L.; Morokuma, K.; Farkas, O.; Foresman, J. B.; Fox, D. J., *Gaussian 16, Revision A.03* **2016**, Gaussian, Inc., Wallingford CT.

32.	Zhao, Y.; Truhlar, D. G., The M06 suite of density functionals for main group thermochemistry, thermochemical kinetics, noncovalent interactions, excited states, and transition elements: two new functionals and systematic testing of four M06-class functionals and 12 other functionals. *Theoretical Chemistry Accounts* **2008,** *120* (1-3), 215-241.

33.	Marenich, A. V.; Cramer, C. J.; Truhlar, D. G., Universal Solvation Model Based on Solute Electron Density and on a Continuum Model of

the Solvent Defined by the Bulk Dielectric Constant and Atomic Surface Tensions. *Journal of Physical Chemistry B* **2009,** *113*, 6378-6396.

34.	Cao, J.; Fan, J.; Sun, W.; Guo, Y.; Wu, H.; Peng, X., The photoprocess effects of an amino group located at different positions along the polymethine chain in indodicarbocyanine dyes. *RSC Advances* **2017,** *7* (49), 30740-30746.

35.	Williams, A. T. R.; Winfield, S. A.; Miller, J. N., Relative fluorescence quantum yields using a computer-controlled luminescence spectrometer. *Analyst* **1983,** *108*, 1067-1071.

36.	APEX3; "Programs for X-Ray Data Collection and Reduction" Bruker-AXS Inc.: Madison, W., USA, **2016**.

37.	Krause, L.; Herbst-Irmer, R.; Sheldrick, G. M.; Stalke, D., Comparison of silver and molybdenum microfocus X-ray sources for single-crystal structure determination. *Journal of Applied Crystallography* **2015,** *48*, 3-10.

38.	Sheldrick, G. M., Crystal structure refinement with SHELXL. *Acta Crystallographica Section C Structural Chemistry* **2015,** *71*, 3-8.

39.	Sheldrick, G. M., SHELXT - integrated space-group and crystal-structure determination. *Acta Crystallographica Section A Foundations and Advances* **2015,** *71*, 3-8.

40.	Spek, A. L., PLATON SQUEEZE: a tool for the calculation of the disordered solvent contribution to the calculated structure factors. *Acta Crystallographica Section C Structural Chemistry* **2015,** *71*, 9-18.

41.	Berezin, M. Y.; Achilefu, S., Fluorescence Lifetime Measurements and Biological Imaging. *Chemical Reviews* **2010,** *110*, 2641-2684.

42.	Guo, Z.; Park, S.; Yoon, J.; Shin, I., Recent progress in the development of near-infrared fluorescent probes for bioimaging applications. *Chemical Society Reviews* **2014,** *43* (1), 16-29.

43.	Zhao, J.; Zhong, D.; Zhou, S., NIR-I-to-NIR-II fluorescent nanomaterials for biomedical imaging and cancer therapy. *Journal of Materials Chemistry B* **2018,** *6* (3), 349-365.

44.	Yao, L.; Zhang, S.; Wang, R.; Li, W.; Shen, F.; Yang, B.; Ma, Y., Highly Efficient Near-Infrared Organic Light-Emitting Diode Based on a Butterfly-Shaped Donor–Acceptor Chromophore with Strong Solid-State Fluorescence and a Large Proportion of Radiative Excitons. *Angewandte Chemie International Edition* **2014,** *53*, 2119-2123.

45.	Sun, Y.; Qu, C.; Chen, H.; He, M.; Tang, C.; Shou, K.; Hong, S.; Yang, M.; Jiang, Y.; Ding, B.; Xiao, Y.; Xing, L.; Hong, X.; Cheng, Z., Novel benzo-bis(1,2,5-thiadiazole) fluorophores for in vivo NIR-II imaging of cancer. *Chemical Science* **2016,** *7*, 6203-6207.

46.	Gayton, J.; Autry, S. A.; Meador, W.; Parkin, S.; Hill, G.; Hammer, N. I.; Delcamp, J. H., Indolizine-Cyanine Dyes: Near Infrared Emissive Cyanine Dyes with Increased Stokes Shifts *Manuscript Under Review* **2018**.

47.	Ashitate, Y.; Levitz, A.; Park, M. H.; Hyun, H.; Venugopal, V.; Park, G.; El Fakhri, G.; Henary, M.; Gioux, S.; Frangioni, J. V.; Choi, H. S., Endocrine-specific NIR fluorophores for adrenal gland targeting. *Chemical Communications* **2016,** *52* (67), 10305-8.

48.   Bouit, P.-A.; Aronica, C.; Toupet, L.; Guennic, B. L.; Andraud, C.; Maury, O., Continuous Symmetry Breaking Induced by Ion Pairing Effect in Heptamethine Cyanine Dyes: Beyond the Cyanine Limit. *Journal of the American Chemical Society* **2010,** *132*, 4328-4335.

49.   Bates, M.; Lunt, R. R., Organic Salt Photovoltaics. *Sustainable Energy Fuels* **2017,** *1*, 955-968.

50.   Li, Z. a.; Mukhopadhyay, S.; Jang, S.-H.; Brédas, J.-L.; Jen, A. K. Y., Supramolecular Assembly of Complementary Cyanine Salt J-Aggregates. *Journal of the American Chemical Society* **2015,** *137*, 11920-11923.

51.   De Jonghe-Risse, J.; Heier, J.; Nüesch, F.; Moser, J. E., Ultrafast charge transfer in solid-state films of pristine cyanine borate and blend with fullerene. *Journal of Materials Chemistry A* **2015,** *3*, 10935-10941.

52.   Zhang, H.; Jenatsch, S.; De Jonghe, J.; Nüesch, F.; Steim, R.; Véron, A. C.; Hany, R., Transparent Organic Photodetector using a Near-Infrared Absorbing Cyanine Dye. *Scientific Reports* **2015,** *5*, 9439.

53.   Veron, A. C.; Zhang, H.; Linden, A.; Nuesch, F.; Heier, J.; Hany, R.; Geiger, T., NIR-absorbing heptamethine dyes with tailor-made counterions for application in light to energy conversion. *Organic Letters* **2014,** *16* (4), 1044-7.

54.   Makha, M.; Schwaller, P.; Strassel, K.; Anantharaman, S. B.; Nuesch, F.; Hany, R.; Heier, J., Insights into photovoltaic properties of ternary organic solar cells from phase diagrams. *Science and Technology of Advanced Materials* **2018,** *19* (1), 669-682.

55.   Frisch, M. J.; Trucks, G. W.; Schlegel, H. B.; Scurseria, G. E.; Robb, M. A.; Cheeseman, J. R.; Scalmani, G.; Barone, V.; Mennucci, B.; Petersson, A.; Nakatsuji, H.; Caricato, M.; Li, X.; Hratchian, H. P.; Izmaylov, A. F.; Bloino, J.; Zheng, G.; Sonnenberg, J. L.; Hada, M.; Ehara, M.; Toyota, K.; Fukuda, R.; Hasegawa, J.; Ishida, M.; Nakajima, T.; Honda, Y.; Kitao, O.; Nakai, H.; Vreven, t.; Montgomery Jr., J. A.; Peralta, J. E.; Ogliaro, F.; Bearpark, M.; Heyd, J. J.; Brothers, E.; Kudin, K. N.; Staroverov, V. N.; Kobayashi, R.; Normand, J.; Raghavachari, K.; Rendell, A.; Burant, J. C.; Iyengar, S. S.; Tomasi, J.; Cossi, M.; Rega, N.; Millam, J. M.; Klene, M.; Knox, J. E.; Cross, J. B.; Bakken, V.; Adamo, C.; Jaramillo, J.; Gomperts, R.; Stratmann, R. E.; Yazyev, O.; Austin, A. J.; Cammi, R.; Pomelli, C.; Ochterski, J. W.; Martin, R. L.; Morokuma, K.; Zakrzewski, V. G.; Voth, G. A.; Salvador, P.; Dannenberg, J. J.; Dapprich, S.; Daniels, A. D.; Farkas, O.; Foresman, J. B.; Ortiz, J. V.; Cioslowski, J.; Fox, D. J., *Gaussian, Inc.* **2009,** *Wallingford, CT, USA*, Gaussian09 Revision D.01.

56.   Becke, A. D., Density-functional thermochemistry. III. The role of exact exchange. *The Journal of Chemical Physics* **1993,** *98*, 5648-5652.

57.   Lee, C.; Yang, W.; Parr, R. G., Development of the Colle-Salvetti correlation-energy formula into a functional of the electron density. *Physical Review B* **1988,** *37* (2), 785-789.

58.   Hehre, W. J.; Ditchfield, R.; Pople, J. A., Self—Consistent Molecular Orbital Methods. XII. Further Extensions of Gaussian—Type Basis Sets for Use in Molecular Orbital Studies of Organic Molecules. *The Journal of Chemical Physics* **1972,** *56* (5), 2257-2261.

59.   Hurst, M. O.; Fortenberry, R. C., Factors affecting the solubility of ionic compounds. *Computational and Theoretical Chemistry* **2015,** *1069*, 132-137.

60.   Schmidt, J. R. P., W.F. WebMO Enterprise, version 14.0; WebMO LLC: Holland, MI, USA, 2014.

61.   Pascal, S.; Haefele, A.; Monnereau, C.; Charaf-Eddin, A.; Jacquemin, D.; Le Guennic, B.; Andraud, C.; Maury, O., Expanding the polymethine paradigm: evidence for the contribution of a bis-dipolar electronic structure. *Journal of Physical Chemistry A* **2014,** *118* (23), 4038-47.

62.   Reindl, S.; Penzkofer, A.; Gong, S.-H.; Landthaler, M.; Szeimies, R. M.; Abels, C.; Bäumler, W., Quantum Yield of Triplet Formation for Indocyanine Green. *Journal of Photochemistry and Photobiology A: Chemistry* **1997,** *105*, 65-68.

63.   Beverina, L.; Salice, P., Squaraine Compounds: Tailored Design and Synthesis towards a Variety of Material Science Applications. *European Journal of Organic Chemistry* **2010,** *2010* (7), 1207-1225.

64.   Ajayaghosh, A., Chemistry of Squaraine-Derived Materials: Near-IR Dyes, Low Band Gap Systems, and Cation Sensors. *Accounts of Chemical Research* **2005,** *38* (6), 449-459.

65.   Bigelow, R. W.; Freund, H.-J., An MNDO and CNDO / S(S + DES CI) study on the structural and electronic properties of a model squaraine dye and related cyanine. *Chemical Physics* **1986,** *107* (2), 159-174.

66.   Chen, C.-T.; Marder, S. R.; Cheng, L.-T., Syntheses and Linear and Nonlinear Optical Properties of Unsymmetrical Squaraines with Extended Conjugation. *Journal of the American Chemical Society* **1994,** *116* (7), 3117-3118.

67.   Wu, Y.; Zhu, W., Organic sensitizers from D-[small pi]-A to D-A-[small pi]-A: effect of the internal electron-withdrawing units on molecular absorption, energy levels and photovoltaic performances. *Chemical Society Reviews* **2013,** *42* (5), 2039-2058.

68.   Mishra, A.; Fischer, M. K. R.; Bäuerle, P., Metal-Free Organic Dyes for Dye-Sensitized Solar Cells: From Structure: Property Relationships to Design Rules. *Angewandte Chemie International Edition* **2009,** *48* (14), 2474-2499.

69.   Kuang, D.; Uchida, S.; Humphry-Baker, R.; Zakeeruddin, S. M.; Grätzel, M., Organic Dye-Sensitized Ionic Liquid Based Solar Cells: Remarkable Enhancement in Performance through Molecular Design of Indoline Sensitizers. *Angewandte Chemie International Edition* **2008,** *47* (10), 1923-1927.

70.   Suzuki, H., Organic light-emitting materials and devices for optical communication technology. *Journal of Photochemistry and Photobiology A: Chemistry* **2004,** *166* (1–3), 155-161.

71.   Kim, H. M.; Cho, B. R., Small-Molecule Two-Photon Probes for Bioimaging Applications. *Chemical Reviews* **2015,** *115* (11), 5014-5055.

72.   Eldo, J.; Ajayaghosh, A., New Low Band Gap Polymers: Control of Optical and Electronic Properties in near Infrared Absorbing π-Conjugated Polysquaraines. *Chemistry of Materials* **2002,** *14* (1), 410-418.

73.   Sreejith, S.; Carol, P.; Chithra, P.; Ajayaghosh, A., Squaraine dyes: a mine of molecular materials. *Journal of Materials Chemistry* **2008,** *18* (3), 264-274.

74.   Ajayaghosh, A., Donor-acceptor type low band gap polymers: polysquaraines and related systems. *Chemical Society Reviews* **2003,** *32* (4), 181-191.

75.   Hao, Y.; Wood, C. J.; Clark, C. A.; Calladine, J. A.; Horvath, R.; Hanson-Heine, M. W.; Sun, X. Z.; Clark, I. P.; Towrie, M.; George, M. W.; Yang, X.; Sun, L.; Gibson, E. A., Can aliphatic anchoring groups be utilised with dyes for p-type dye sensitized solar cells? *Dalton Trans* **2016,** *45* (18), 7708-19.

76.   Hu, L.; Yan, Z.; Xu, H., Advances in synthesis and application of near-infrared absorbing squaraine dyes. *RSC Advances* **2013,** *3* (21), 7667-7676.

77.   Alander, J. T.; Kaartinen, I.; Laakso, A.; P, T.; #228; til; Spillmann, T.; Tuchin, V. V.; Venermo, M.; V, P.; lisuo, A review of indocyanine green fluorescent imaging in surgery. *Journal of Biomedical Imaging* **2012,** *2012*, 7-7.

78.   Luo, S.; Zhang, E.; Su, Y.; Cheng, T.; Shi, C., A review of NIR dyes in cancer targeting and imaging. *Biomaterials* **2011,** *32* (29), 7127-7138.

79.   Kamat, P. V.; Das, S.; Thomas, K. G.; George, M. V., Photochemistry of squaraine dyes. 1. Excited singlet, triplet, and redox states of bis[4-(dimethylamino)phenyl]squaraine and bis[4-(dimethylamino)-2-hydroxyphenyl]squaraine. *The Journal of Physical Chemistry* **1992,** *96* (1), 195-199.

80.	Law, K. Y.; Bailey, F. C., Squaraine chemistry. Synthesis, characterization, and optical properties of a class of novel unsymmetrical squaraines: [4-(dimethylamino)phenyl](4'-methoxyphenyl)squaraine and its derivatives. *The Journal of Organic Chemistry* **1992,** *57* (12), 3278-3286.

81.	Huckaba, A. J.; Giordano, F.; McNamara, L. E.; Dreux, K. M.; Hammer, N. I.; Tschumper, G. S.; Zakeeruddin, S. M.; Grätzel, M.; Nazeeruddin, M. K.; Delcamp, J. H., Indolizine-Based Donors as Organic Sensitizer Components for Dye-Sensitized Solar Cells. *Advanced Energy Materials* **2015,** *5* (7), 1401629-n/a.

82.	Huckaba, A. J.; Yella, A.; Brogdon, P.; Scott Murphy, J.; Nazeeruddin, M. K.; Gratzel, M.; Delcamp, J. H., A low recombination rate indolizine sensitizer for dye-sensitized solar cells. *Chemical Communications* **2016,** *52* (54), 8424-8427.

83.	Huckaba, A. J.; Yella, A.; McNamara, L. E.; Steen, A. E.; Murphy, J. S.; Carpenter, C. A.; Puneky, G. D.; Hammer, N. I.; Nazeeruddin, M. K.; Grätzel, M.; Delcamp, J. H., Molecular Design Principles for Near-Infrared Absorbing and Emitting Indolizine Dyes. *Chemistry – A European Journal* **2016,** *22* (43), 15536-15542.

84.	Antaris, A. L.; Chen, H.; Cheng, K.; Sun, Y.; Hong, G.; Qu, C.; Diao, S.; Deng, Z.; Hu, X.; Zhang, B.; Zhang, X.; Yaghi, O. K.; Alamparambil, Z. R.; Hong, X.; Cheng, Z.; Dai, H., A small-molecule dye for NIR-II imaging. *Nat Mater* **2016,** *15* (2), 235-242.

85.	Sassi, M. e. a., Near-infrared roll-off-free electroluminescence from highly stable diketopyrrolopyrrole light emitting diodes. *Sci. Rep.* **2016,** (6), 34096.

86.	Fischer, G. M.; Ehlers, A. P.; Zumbusch, A.; Daltrozzo, E., Near-Infrared Dyes and Fluorophores Based on Diketopyrrolopyrroles. *Angewandte Chemie International Edition* **2007,** *46* (20), 3750-3753.

87.	Wiktorowski, S.; Rosazza, C.; Winterhalder, M. J.; Daltrozzo, E.; Zumbusch, A., Water-soluble pyrrolopyrrole cyanine (PPCy) NIR fluorophores. *Chemical Communications* **2014,** *50* (36), 4755-4758.

88.	Crosby, G. A.; Demas, J. N., Measurement of photoluminescence quantum yields. Review. *Journal of Physical Chemistry* **1971,** *75* (8), 991-1024.

89.	Vincett, P. S.; Voigt, E. M.; Rieckhoff, K. E., Phosphorescence and Fluorescence of Phthalocyanines. *Journal of Chemical Physics* **1971,** *55* (8), 4131-4140.

90.	Frisch, M. J.; Trucks, G. W.; Schlegel, H. B.; Scuseria, G. E.; Robb, M. A.; Cheeseman, J. R.; Scalmani, G.; Barone, V.; Mennucci, B.; Petersson, G. A.; Nakatsuji, H.; Caricato, M.; Li, X.; Hratchian, H. P.; Izmaylov, A. F.; Bloino, J.; Zheng, G.; Sonnenberg, J. L.; Hada, M.; Ehara, M.; Toyota, K.; Fukuda, R.; Hasegawa, J.; Ishida, M.; Nakajima, T.; Honda, Y.; Kitao, O.; Nakai, H.; Vreven, T.; Montgomery Jr., J. A.; Peralta, J. E.; Ogliaro, F.; Bearpark, M. J.; Heyd, J.; Brothers, E. N.; Kudin, K. N.; Staroverov, V. N.; Kobayashi, R.; Normand, J.; Raghavachari, K.; Rendell, A. P.; Burant, J. C.; Iyengar, S. S.; Tomasi, J.; Cossi, M.; Rega, N.; Millam, N. J.; Klene, M.; Knox, J. E.; Cross, J. B.; Bakken, V.; Adamo, C.; Jaramillo, J.; Gomperts, R.; Stratmann, R. E.; Yazyev, O.; Austin, A. J.; Cammi, R.; Pomelli, C.; Ochterski, J. W.; Martin, R. L.; Morokuma, K.; Zakrzewski, V. G.; Voth, G. A.; Salvador, P.; Dannenberg, J. J.; Dapprich, S.; Daniels, A. D.; Farkas, Ö.; Foresman, J. B.; Ortiz, J. V.; Cioslowski, J.; Fox, D. J. *Gaussian 09*, Gaussian, Inc.: Wallingford, CT, USA, 2009.

91.	Becke, A. D., Density‐functional thermochemistry. III. The role of exact exchange. *Journal of Chemical Physics* **1993,** *98* (7), 5648-5652.

92.	Lee, C.; Yang, W.; Parr, R., Phys. l Rev. B 37, 785 (1988);(b) AD Becke. *Phys. Rev. A* **1988,** *38*, 3098.

93.	Siriwardana, A. I.; Kamada, M.; Makamura, I.; Yamamoto, Y., Palladium-Catalyzed Addition of Nitrogen Pronucleophiles to Alkylidenecyclopropanes. *The Journal of Organic Chemistry* **2005,** *70*, 5932-5937.

94.   Lee, Y. S.; Chuang, S. H.; Huang, L. Y.; Lai, C. L.; Lin, Y. H.; Yang, J. Y.; Liu, C. W.; Yang, S. C.; Lin, H. S.; Chang, C. C.; Lai, J. Y.; Jian, P. S.; Lam, K.; Chang, J. M.; Lau, J. Y.; Huang, J. J., Discovery of 4-aryl-N-arylcarbonyl-2-aminothiazoles as Hec1/Nek2 inhibitors. Part I: optimization of in vitro potencies and pharmacokinetic properties. *Journal of Medicinal Chemistry* **2014,** *57*, 4098-110.

95.   Spijker, N. M.; van den Braken-van Leersum, A. M.; Lugtenburg, J.; Cornelisse, J., A Very Convenient Synthesis of Cyclopenta[cd]pyrene. *The Journal of Organic Chemistry* **1990,** *55*, 756-758.

96.   Yao, J. H.; Chi, C.; Wu, J.; Loh, K.-P., Bisanthracene Bis(dicarboxylic imide)s as Soluble and Stable NIR Dyes. *Chemistry – A European Journal* **2009,** *15* (37), 9299-9302.

97.   Jin, T., Review—Recent Progress in NIR Fluorophores Emitting over 1000 nm for Bioimaging. *ECS Journal of Solid State Science and Technology* **2019,** *8* (1), R9-R13.

98.   Fabian, J., Near-Infrared Absorbing Dyes. *Chem. Rev.* **1992,** *92*, 1197-1226.

99.   Qian, G.; Wang, Z. Y., Near-infrared organic compounds and emerging applications. *Chemistry, an Asian journal* **2010,** *5* (5), 1006-29.

100.   Barlow, S.; Brédas, J.-L.; Getmanenko, Y. A.; Gieseking, R. L.; Hales, J. M.; Kim, H.; Marder, S. R.; Perry, J. W.; Risko, C.; Zhang, Y., Polymethine materials with solid-state third-order optical susceptibilities suitable for all-optical signal-processing applications. *Mater. Horiz.* **2014,** *1* (6), 577-581.

101.   Detty, M. R.; Gibson, S. L.; Wagner, S. J., Current clinical and preclinical photosensitizers for use in photodynamic therapy. *J Med Chem* **2004,** *47* (16), 3897-915.

102.   Zhang, X. D.; Wang, H.; Antaris, A. L.; Li, L.; Diao, S.; Ma, R.; Nguyen, A.; Hong, G.; Ma, Z.; Wang, J.; Zhu, S.; Castellano, J. M.; Wyss-Coray, T.; Liang, Y.; Luo, J.; Dai, H., Traumatic Brain Injury Imaging in the Second Near-Infrared Window with a Molecular Fluorophore. *Advanced Materials* **2016,** *28*, 6872-6879.

103.   Braun, A. B.; Wehl, I.; Kölmel, D. K.; Schepers, U.; Bräse, S., New Polyfluorinated Cyanine Dyes for Selective NIR Staining of Mitochondria. *Chemistry – A European Journal* **2019,** *25* (34), 7998-8002.

104.   Gayton, J.; Autry, S. A.; Meador, W.; Parkin, S. R.; Hill, G. A.; Hammer, N. I.; Delcamp, J. H., Indolizine-Cyanine Dyes: Near Infrared Emissive Cyanine Dyes with Increased Stokes Shifts. *The Journal of Organic Chemistry* **2019,** *84*, 687-697.

105.   Gayton, J. N.; Autry, S.; Fortenberry, R. C.; Hammer, N. I.; Delcamp, J. H., Counter Anion Effect on the Photophysical Properties of Emissive Indolizine-Cyanine Dyes in Solution and Solid State. *Molecules* **2018,** *23* (12), 3051.

106.   Davydenko, I.; Barlow, S.; Sharma, R.; Benis, S.; Simon, J.; Allen, T. G.; Cooper, M. W.; Khrustalev, V.; Jucov, E. V.; Castaneda, R.; Ordonez, C.; Li, Z.; Chi, S. H.; Jang, S. H.; Parker, T. C.; Timofeeva, T. V.; Perry, J. W.; Jen, A. K.; Hagan, D. J.; Van Stryland, E. W.; Marder, S. R., Facile Incorporation of Pd(PPh3)2Hal Substituents into Polymethines, Merocyanines, and Perylene Diimides as a Means of Suppressing Intermolecular Interactions. *Journal of the American Chemical Society* **2016,** *138*, 10112-10115.

107.   Kuimova, M. K.; Collins, H. A.; Balaz, M.; Dahlstedt, E.; Levitt, J. A.; Sergent, N.; Suhling, K.; Drobizhev, M.; Makarov, N. S.; Rebane, A.; Anderson, H. L.; Phillips, D., Photophysical properties and intracellular imaging of water-soluble porphyrin dimers for two-photon excited photodynamic therapy. *Organic & Biomolecular Chemistry* **2009,** *7* (5), 889-896.

108.   Nesterova, I. V.; Verdree, V. T.; Pakhomov, S.; Strickler, K. L.; Allen, M. W.; Hammer, R. P.; Soper, S. A., Metallo-Phthalocyanine Near-IR Fluorophores: Oligonucleotide Conjugates and Their Applications in PCR Assays. *Bioconjugate Chemistry* **2007,** *18* (6), 2159-2168.

109.   Patwari, J.; Sardar, S.; Liu, B.; Lemmens, P.; Pal, S. K., Three-in-one approach towards efficient organic dye-sensitized solar cells: aggregation suppression, panchromatic absorption and resonance energy transfer. *Beilstein J Nanotechnol* **2017,** *8*, 1705-1713.

110.   Umezawa, K.; Citterio, D.; Suzuki, K., Water-soluble NIR Fluorescent Probes Based on Squaraine and Their Application for Protein Labeling. *Analytical Sciences* **2008,** *24*, 213-217.

111.   Lambert, C.; Scherpf, T.; Ceymann, H.; Schmiedel, A.; Holzapfel, M., Coupled oscillators for tuning fluorescence properties of squaraine dyes. *Journal of the American Chemical Society* **2015,** *137*, 3547-57.

112.   Staudinger, C.; Breininger, J.; Klimant, I.; Borisov, S. M., Near-infrared fluorescent aza-BODIPY dyes for sensing and imaging of pH from the neutral to highly alkaline range. *Analyst* **2019,** *144* (7), 2393-2402.

113.   Sakamoto, N.; Ikeda, C.; Yamamura, M.; Nabeshima, T., alpha-Bridged BODIPY oligomers with switchable near-IR photoproperties by external-stimuli-induced foldamer formation and disruption. *Chemical Communications* **2012,** *48*, 4818-20.

114.   Yamazawa, S.; Nakashima, M.; Suda, Y.; Nishiyabu, R.; Kubo, Y., 2,3-Naphtho-Fused BODIPYs as Near-Infrared Absorbing Dyes. *The Journal of Organic Chemistry* **2016,** *81*, 1310-5.

115.   Lu, Y.; Sun, Q.; Zhang, Z.; Tang, L.; Shen, X.; Xue, S.; Yang, W., New frog-type Dibenzo[a,c][1,2,5]thiadiazolo[3,4-i]phenazine heterocyclic derivatives with aggregation-enhanced one- and two-photon excitation NIR fluorescence. *Dyes and Pigments* **2018,** *153*, 233-240.

116.   Wang, L. G.; Munhenzva, I.; Sibrian-Vazquez, M.; Escobedo, J. O.; Kitts, C. H.; Fronczek, F. R.; Strongin, R. M., Altering Fundamental Trends in the Emission of Xanthene Dyes. *The Journal of Organic Chemistry* **2019,** *84* (5), 2585-2595.

117.   Sun, Y. Q.; Liu, J.; Lv, X.; Liu, Y.; Zhao, Y.; Guo, W., Rhodamine-inspired far-red to near-infrared dyes and their application as fluorescence probes. *Angew Chem Int Ed Engl* **2012,** *51* (31), 7634-6.

118.   Myochin, T.; Hanaoka, K.; Iwaki, S.; Ueno, T.; Komatsu, T.; Terai, T.; Nagano, T.; Urano, Y., Development of a series of near-infrared dark quenchers based on Si-rhodamines and their application to fluorescent probes. *J Am Chem Soc* **2015,** *137* (14), 4759-65.

119.   Davies, K. S.; Linder, M. K.; Kryman, M. W.; Detty, M. R., Extended rhodamine photosensitizers for photodynamic therapy of cancer cells. *Bioorg Med Chem* **2016,** *24* (17), 3908-3917.

120.   Fukazawa, A.; Suda, S.; Taki, M.; Yamaguchi, E.; Grzybowski, M.; Sato, Y.; Higashiyama, T.; Yamaguchi, S., Phospha-fluorescein: a red-emissive fluorescein analogue with high photobleaching resistance. *Chemical Communications* **2016,** *52* (6), 1120-1123.

121.   Fu, M.; Xiao, Y.; Qian, X.; Zhao, D.; Xu, Y., A design concept of long-wavelength fluorescent analogs of rhodamine dyes: replacement of oxygen with silicon atom. *Chemical Communications* **2008,** (15), 1780-1782.

122.   Best, Q. A.; Sattenapally, N.; Dyer, D. J.; Scott, C. N.; McCarroll, M. E., pH-Dependent Si-Fluorescein Hypochlorous Acid Fluorescent Probe: Spirocycle Ring-Opening and Excess Hypochlorous Acid-Induced Chlorination. *Journal of the American Chemical Society* **2013,** *135* (36), 13365-13370.

123.   Kushida, Y.; Nagano, T.; Hanaoka, K., Silicon-substituted xanthene dyes and their applications in bioimaging. *Analyst* **2015,** *140* (3), 685-695.

124.   Butkevich, A. N.; Mitronova, G. Y.; Sidenstein, S. C.; Klocke, J. L.; Kamin, D.; Meineke, D. N. H.; D'Este, E.; Kraemer, P.-T.; Danzl, J. G.; Belov, V. N.; Hell, S. W., Fluorescent Rhodamines and Fluorogenic Carbopyronines for Super-Resolution STED Microscopy in Living Cells. *Angewandte Chemie International Edition* **2016,** *55* (10), 3290-3294.

125.   Yuan, L.; Lin, W.; Zhao, S.; Gao, W.; Chen, B.; He, L.; Zhu, S., A Unique Approach to Development of Near-Infrared Fluorescent Sensors for in Vivo Imaging. *Journal of the American Chemical Society* **2012,** *134* (32), 13510-13523.

126.   Yuan, L.; Lin, W.; Yang, Y.; Chen, H., A Unique Class of Near-Infrared Functional Fluorescent Dyes with Carboxylic-Acid-Modulated Fluorescence ON/OFF Switching: Rational Design, Synthesis, Optical Properties, Theoretical Calculations, and Applications for Fluorescence Imaging in Living Animals. *Journal of the American Chemical Society* **2012,** *134* (2), 1200-1211.

127.   Cosco, E. D.; Caram, J. R.; Bruns, O. T.; Franke, D.; Day, R. A.; Farr, E. P.; Bawendi, M. G.; Sletten, E. M., Flavylium Polymethine Fluorophores for Near- and Shortwave Infrared Imaging. *Angewandte Chemie International Edition* **2017,** *56* (42), 13126-13129.

128.   Wang, W.; Ma, Z.; Zhu, S.; Wan, H.; Yue, J.; Ma, H.; Ma, R.; Yang, Q.; Wang, Z.; Li, Q.; Qian, Y.; Yue, C.; Wang, Y.; Fan, L.; Zhong, Y.; Zhou, Y.; Gao, H.; Ruan, J.; Hu, Z.; Liang, Y.; Dai, H., Molecular Cancer Imaging in the Second Near-Infrared Window Using a Renal-Excreted NIR-II Fluorophore-Peptide Probe. *Adv Mater* **2018**, e1800106.

129.   Zebibula, A.; Alifu, N.; Xia, L.; Sun, C.; Yu, X.; Xue, D.; Liu, L.; Li, G.; Qian, J., Ultrastable and Biocompatible NIR-II Quantum Dots for Functional Bioimaging. *Advanced Functional Materials* **2018,** *28* (9), 1703451.

130.   Ma, Z.; Wan, H.; Wang, W.; Zhang, X.; Uno, T.; Yang, Q.; Yue, J.; Gao, H.; Zhong, Y.; Tian, Y.; Sun, Q.; Liang, Y.; Dai, H., A theranostic agent for cancer therapy and imaging in the second near-infrared window. *Nano Research* **2019,** *12* (2), 273-279.

131.   Hong, G.; Antaris, A. L.; Dai, H., Near-infrared fluorophores for biomedical imaging. *Nature Biomedical Engineering* **2017,** *1*, 0010.

132.   Zhang, Y.; Zhang, Y.; Hong, G.; He, W.; Zhou, K.; Yang, K.; Li, F.; Chen, G.; Liu, Z.; Dai, H.; Wang, Q., Biodistribution, pharmacokinetics and toxicology of Ag2S near-infrared quantum dots in mice. *Biomaterials* **2013,** *34* (14), 3639-3646.

133.   Yang, Q.; Ma, Z.; Wang, H.; Zhou, B.; Zhu, S.; Zhong, Y.; Wang, J.; Wan, H.; Antaris, A.; Ma, R.; Zhang, X.; Yang, J.; Zhang, X.; Sun, H.; Liu, W.; Liang, Y.; Dai, H., Rational Design of Molecular Fluorophores for Biological Imaging in the NIR-II Window. *Advanced Materials* **2017,** *29* (12), 1605497.

134.   Kinnibrugh, T. L.; Salman, S.; Getmanenko, Y. A.; Coropceanu, V.; Porter, W. W., 3rd; Timofeeva, T. V.; Matzger, A. J.; Bredas, J. L.; Marder, S. R.; Barlow, S., Dipolar Second-Order Nonlinear Optical Chromophores Containing Ferrocene, Octamethylferrocene, and Ruthenocene Donors and Strong pi-Acceptors: Crystal Structures and Comparison of pi-Donor Strengths. *Organometallics* **2009,** *28* (5), 1350-1357.

135.   Cheema, H.; Baumann, A.; Loya, E. K.; Brogdon, P.; McNamara, L. E.; Carpenter, C. A.; Hammer, N. I.; Mathew, S.; Risko, C.; Delcamp, J. H., Near-Infrared-Absorbing Indolizine-Porphyrin Push-Pull Dye for Dye-Sensitized Solar Cells. *ACS Appl Mater Interfaces* **2019,** *11* (18), 16474-16489.

136.   Huckaba, A. J.; Yella, A.; Brogdon, P.; Scott Murphy, J.; Nazeeruddin, M. K.; Grätzel, M.; Delcamp, J. H., A Low Recombination Rate Indolizine Sensitizer for Dye-Sensitized Solar Cells. *Chemical Communications* **2016,** *52*, 8424-8427.

137.   Brogdon, P.; Giordano, F.; Puneky, G. A.; Dass, A.; Zakeeruddin, S. M.; Nazeeruddin, M. K.; Grätzel, M.; Tschumper, G. S.; Delcamp, J. H., A Computational and Experimental Study of Thieno[3,4-b]thiophene as a Proaromatic π-Bridge in Dye-Sensitized Solar Cells. *Chemistry - A European Journal* **2016,** *22*, 694-703.

138.   Chen, X.; Engle, K. M.; Wang, D.-H.; Yu, J.-Q., Palladium(II)-Catalyzed C☐H Activation/C☐C Cross-Coupling Reactions: Versatility and Practicality. *Angewandte Chemie International Edition* **2009,** *48* (28), 5094-5115.

139.   Daugulis, O.; Do, H.-Q.; Shabashov, D., Palladium- and Copper-Catalyzed Arylation of Carbon–Hydrogen Bonds. *Accounts of Chemical Research* **2009,** *42* (8), 1074-1086.

140.   Davies, H. M. L.; Morton, D., Collective Approach to Advancing C–H Functionalization. *ACS Central Science* **2017,** *3* (9), 936-943.

141.   Verbelen, B.; Boodts, S.; Hofkens, J.; Boens, N.; Dehaen, W., Radical C☐H Arylation of the BODIPY Core with Aryldiazonium Salts: Synthesis of Highly Fluorescent Red-Shifted Dyes. *Angewandte Chemie International Edition* **2015,** *54* (15), 4612-4616.

142.   Verbelen, B.; Cunha Dias Rezende, L.; Boodts, S.; Jacobs, J.; Van Meervelt, L.; Hofkens, J.; Dehaen, W., Radical C☐H Alkylation of BODIPY Dyes Using Potassium Trifluoroborates or Boronic Acids. *Chemistry – A European Journal* **2015,** *21* (36), 12667-12675.

143.   Verbelen, B.; Leen, V.; Wang, L.; Boens, N.; Dehaen, W., Direct palladium-catalysed C–H arylation of BODIPY dyes at the 3- and 3,5-positions. *Chemical Communications* **2012,** *48* (73), 9129-9131.

144.   Nandakumar, A.; Perumal, P. T., Tetrasubstituted Olefinic Xanthene Dyes: Synthesis via Pd-Catalyzed 6-exo-dig Cyclization/C–H Activation of 2-Bromobenzyl-N-propargylamines and Solid State Fluorescence Properties. *Organic Letters* **2013,** *15* (2), 382-385.

145.   Koszarna, B.; Matczak, R.; Krzeszewski, M.; Vakuliuk, O.; Klajn, J.; Tasior, M.; Nowicki, J. T.; Gryko, D. T., Direct arylation of electron-poor indolizines. *Tetrahedron* **2014,** *70* (2), 225-231.

146.   Roger, J.; Doucet, H., Aryl triflates: useful coupling partners for the direct arylation of heteroaryl derivatives via Pd-catalyzed C–H activation–functionalization. *Organic & Biomolecular Chemistry* **2008,** *6* (1), 169-174.

147.   Liégault, B.; Lapointe, D.; Caron, L.; Vlassova, A.; Fagnou, K., Establishment of Broadly Applicable Reaction Conditions for the Palladium-Catalyzed Direct Arylation of Heteroatom-Containing Aromatic Compounds. *The Journal of Organic Chemistry* **2009,** *74* (5), 1826-1834.

148.   Wakioka, M.; Kitano, Y.; Ozawa, F., A Highly Efficient Catalytic System for Polycondensation of 2,7-Dibromo-9,9-dioctylfluorene and 1,2,4,5-Tetrafluorobenzene via Direct Arylation. *Macromolecules* **2013,** *46* (2), 370-374.

APPENDIX

APPENDIX A: FIGURES AND TABLES

Table 14. Dielectric constant and dipole values for solvents used in photophysical studies.

Solvent	Dielectric constant	Dipole (D)
DMSO	46.7	3.96
MeCN	37.5	3.92
DMF	38	3.82
Acetone	21	2.88
Water	80	1.85
Ethyl Acetate	6.0	1.78
THF	7.5	1.75
Methanol	33	1.70
Ethanol	24.6	1.69
Dichloromethane	9.1	1.60
Chloroform	4.8	1.04
Toluene	2.4	0.36

Table 15. The solubility of each dye in the series and ICG in various solvents where (PS) represents partial solubility and (IS) represents insolubility.

Solvent Solubility (mg/mL)														
Dye	MeCN	2:1 MeCN:H_2O	1:1 MeCN:H_2O	10:1 MeCN:H_2O	MeOH	Acetone	Toluene	CHCl3	DMF	EtOH	EA	THF	DMSO	DCM
C1	0.58	1.79	5.00	0.95	1.86	2.38	0.07	0.54	7.00	1.25	0.95	0.90	6.50	2.10
C3	1.00	1.47	0.37	1.22	0.35	0.85	0.02 (PS)	0.60	6.75	0.05 (PS)	0.06 (PS)	0.03 (PS)	5.50	0.50
C5	1.89	0.86	0.43	2.17	0.32	2.45	0.04 (PS)	1.87	8.00	0.18	0.04 (PS)	0.03 (PS)	4.00	2.80
PhOMeIndz-C5	2.78	1.30	0.43	4.00	0.29	1.25	(IS)	3.43	10.5	0.05 (PS)	0.05 (PS)	0.11	10.5	2.50
PhCNIndz-C5	0.48	0.18	0.15	0.70	0.15	0.22	0.04 (PS)	0.28	7.25	0.04 (PS)	0.04 (PS)	0.04 (PS)	8.00	0.30
PhIndzOMe-C5	2.50	0.55	0.20	2.75	0.13	0.22	0.02 (PS)	0.50	5.50	0.03 (PS)	0.03 (PS)	0.03 (PS)	5.50	1.20
ICG	0.04 (PS)	8.50	9.50	1.80	10.0	(IS)	(IS)	(IS)	1.40	0.05 (PS)	(IS)	(IS)	18.0	(IS)
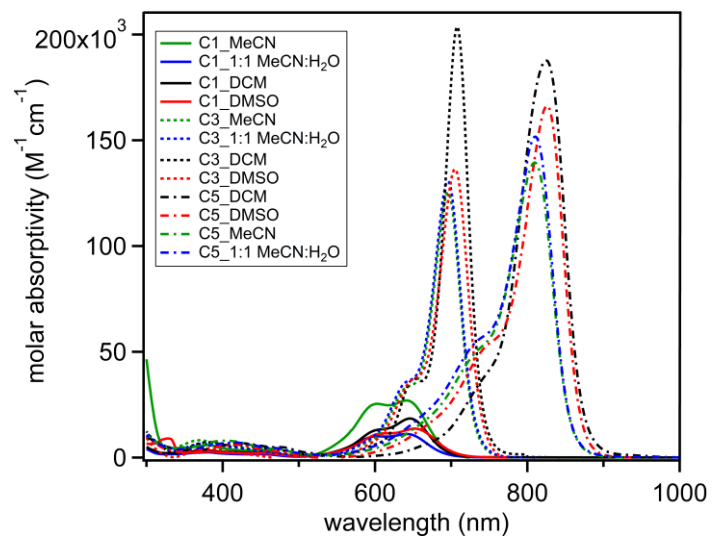
Figure 35. UV-Vis-NIR molar absorptivity of **C1**, **C3**, and **C5** in various solvents with window expanded from 300-1000 nm.
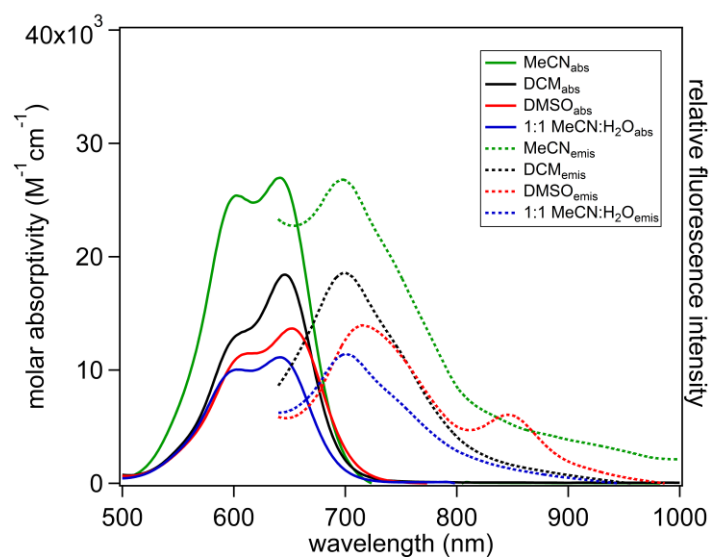
Figure 36. C1 UV-Vis-NIR molar absorptivity (solid lines) and normalized emission spectrum (dotted lines) in 4 solvents
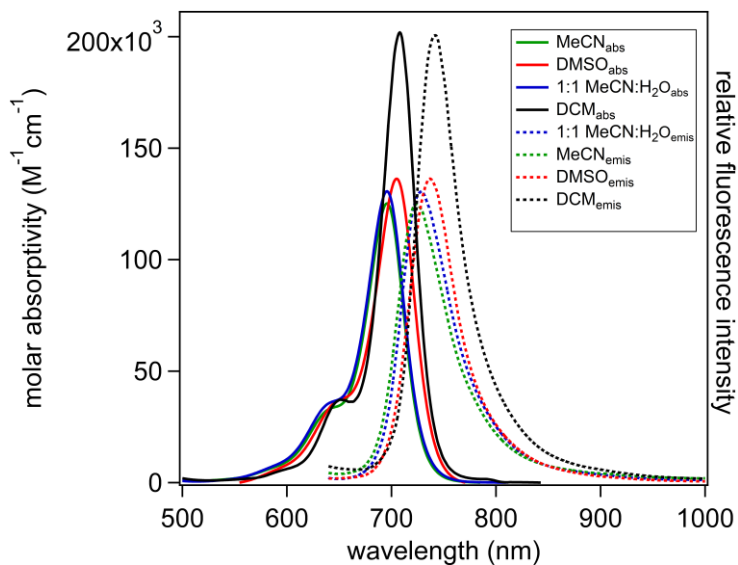
Figure 37. C3 UV-Vis-NIR molar absorptivity (solid lines) and normalized emission spectrum (dotted lines) in 4 solvents.
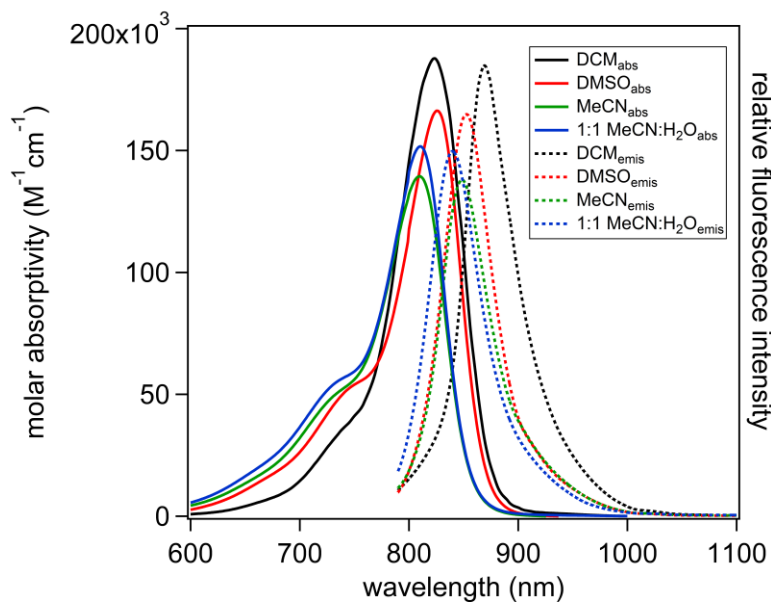
Figure 38. C5 UV-Vis-NIR molar absorptivity (solid lines) and normalized emission spectrum (dotted lines) in 4 solvents.
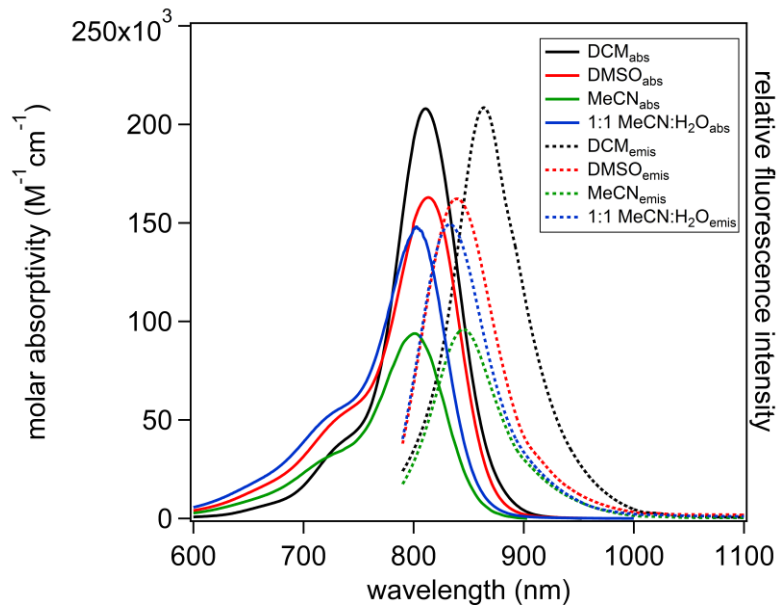
Figure 39. PhOMe-C5 UV-Vis-NIR molar absorptivity (solid lines) and normalized emission spectrum (dotted lines) in 4 solvents.
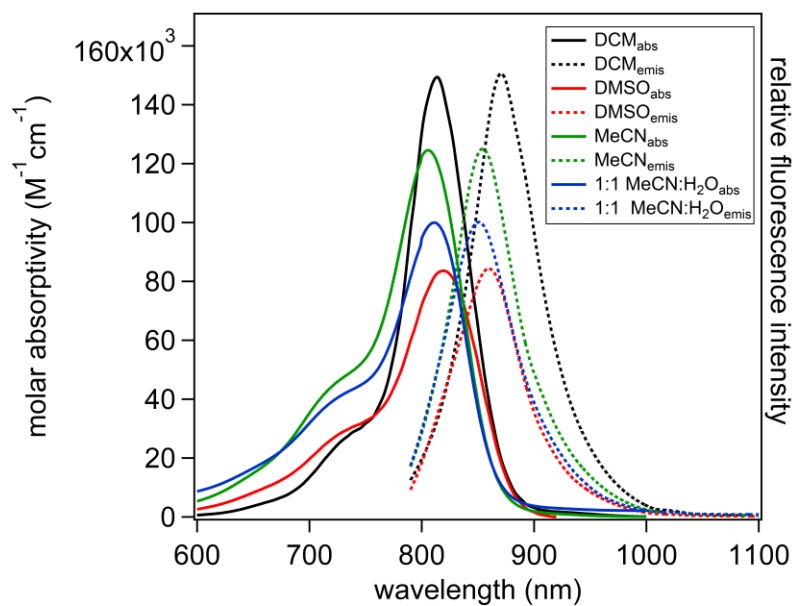
Figure 40. PhCN-C5 UV-Vis-NIR molar absorptivity (solid lines) and normalized emission spectrum (dotted lines) in 4 solvents.
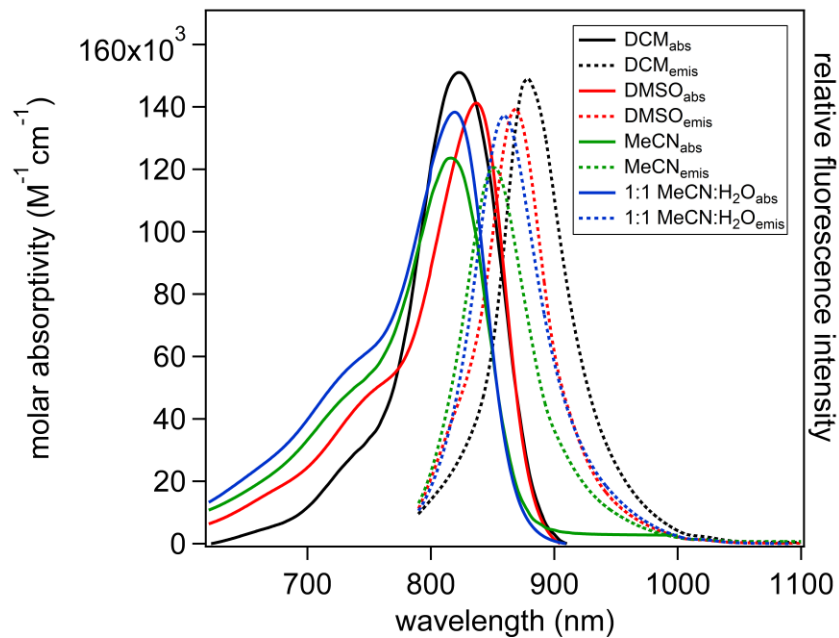
Figure 41. IndzOMe-C5 UV-Vis-NIR molar absorptivity (solid lines) and normalized emission spectrum (dotted lines) in 4 solvents.
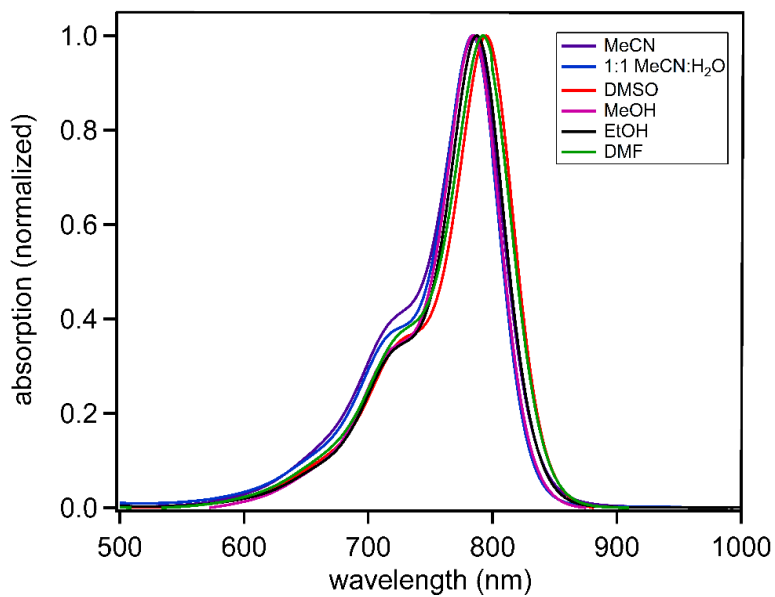
Figure 42. ICG UV-Vis-NIR absorbance in several solvents.
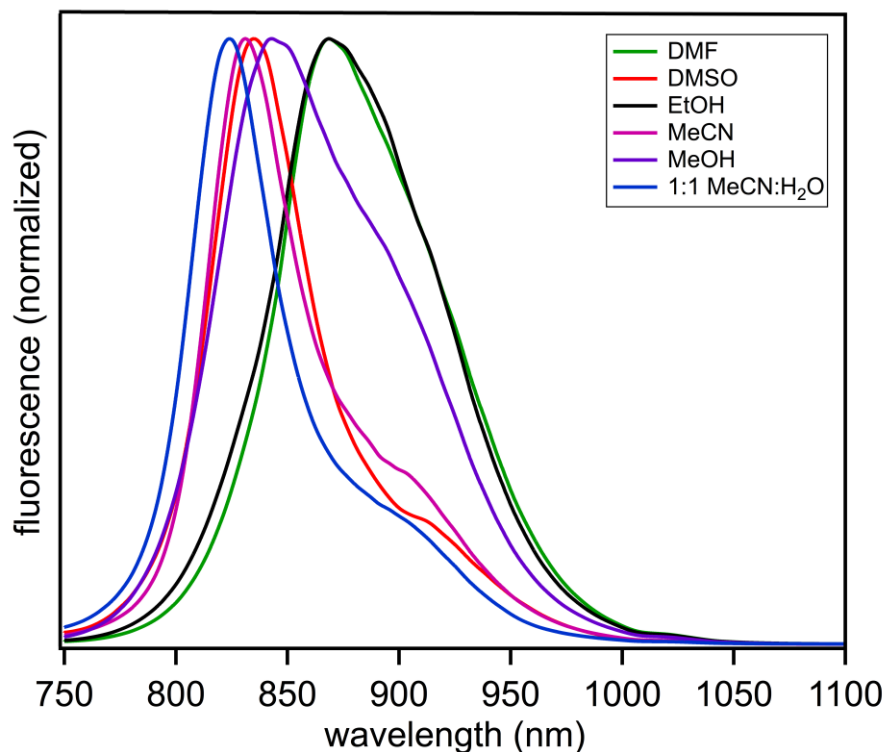
Figure 43. ICG normalized emission spectrum in several solvents.

Table 16. Select computed bond angles. See below **Table 17** for an illustration of the angles.

dye	angle 1 (°) GS | ES	angle 2 (°) GS | ES	angle 3 (°) GS | ES	angle 4 (°) GS | ES
C1 cis	128 | 123	134 | 125	N/A	N/A
C3 cis-7	129 | 127	133 | 129	118 | 121	N/A
C3 trans-7, 6	128, 123 | 127, 122	131, 126 | 129, 123	120 | 123	N/A
C5 cis-7	128 | 127	132 | 129	119 | 122	125 | 122
C5 cis-6	122 | 122	127 | 126	122 | 124	123 | 121
C5 trans-7, 6	128, 122 | 127, 122	133, 128 | 130, 126	120, 121 | 122, 123	125 | 123

Cis and trans refer to the relative orientation of the two indolizine groups.

Table 17. Select computed dihedral angles and atom-atom distances.

dye	dihedral (°) indz-cy GS | ES	dihedral (°) indz-indz GS | ES	H-H bond distance (Å) GS | ES
C1 cis	15 | 27	35 | 50	2.7 | 3.6[a]
C3 cis-7	3 | 21	8 | 2	1.8 | 2.0
C3 trans-7, 6	2, 10 | 11, 22	15 | 32	1.8, 2.1 | 1.9, 2.1
C5 cis-7	2 | 20	10 | 0	1.9 | 2.0
C5 cis-6	7 | 11	22 | 33	2.1 | 2.0
C5 trans-7, 6	3, 7 | 12, 15	12 | 35	1.9, 2.0 | 2.0, 2.0

Cis and trans refer to the relative orientation of the two indolizine groups.
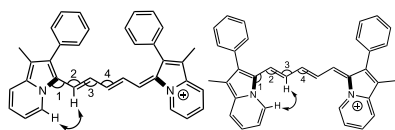
cis-6 conformer   cis-7 conformer
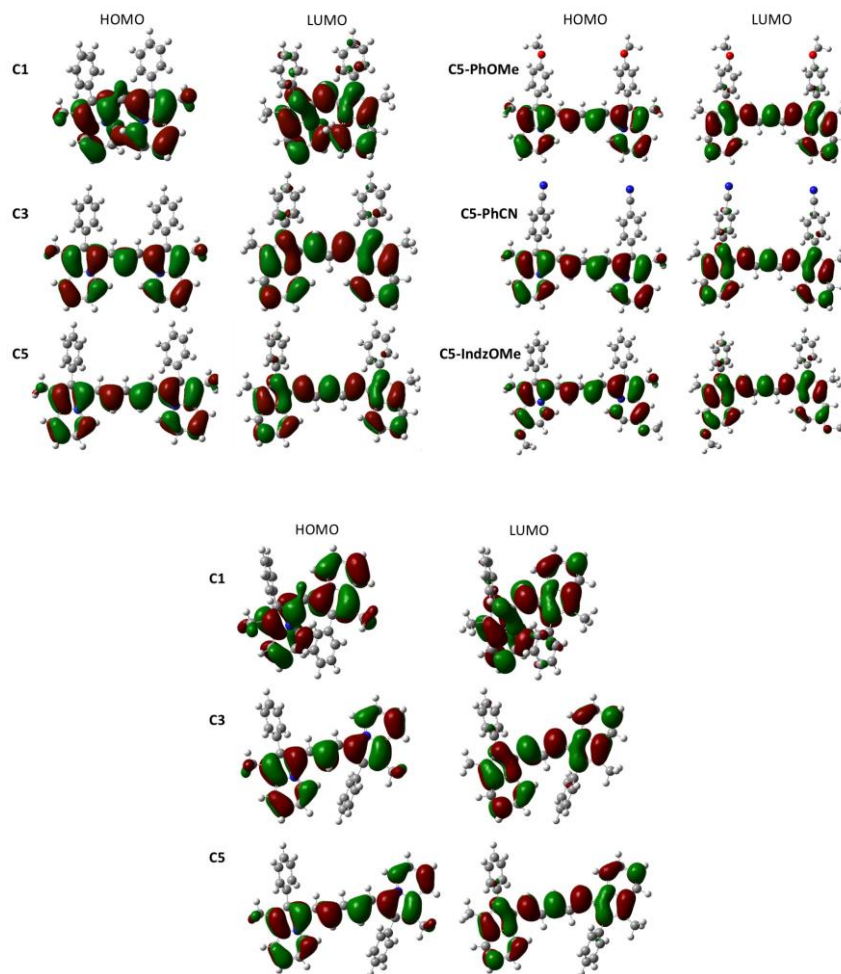
Figure 44. HOMO-LUMO diagrams of **C1**, **C3**, **C5**, **PhOMe-C5**, **PhCN-C5**, and **IndzOMe-C5**.

The left two columns of HOMO-LUMO orbitals are shown as the cis-7 conformers, and the right

column is shown as the trans conformer. Isovalues of 0.02 are shown above.

cis-7 conformers
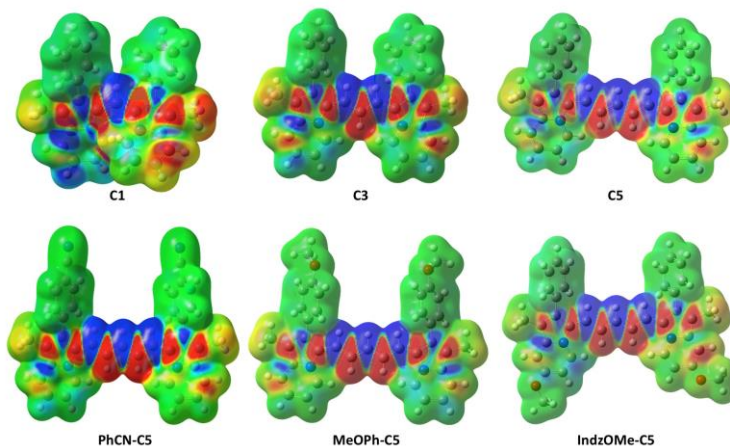
Trans conformers
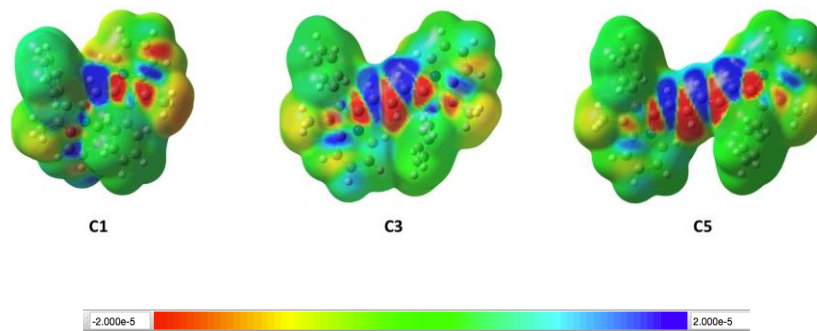
Figure 45. Electron density difference maps for **C1**, **C3**, **C5**, **PhCN-C5**, **PhOMe-C5**, and **IndzOMe-C5.** Red is where electrons originate from, blue is where they travel to upon photoexcitation, and green is neutral. Top dyes are in the cis-7 conformation as illustrated under Table 17, and the bottom row dyes are in the trans conformation.

Table 18. TD-DFT values for the ground- and excited-state optimized geometries for variable conformations.

dye	vertical trans. (eV, nm)	oscillator strength	dye* vertical trans. (eV, nm)	osc. str. dye*	Stokes shift (eV, nm)
C1 cis	2.20, 561	0.79	1.78, 697	0.47	0.42, 136
C3 cis-7	1.91, 648	1.49	1.74, 712	1.27	0.17, 64
C3 trans	2.33, 533	1.11	2.18, 569	0.97	0.15, 36
C5 cis-7	1.65, 752	2.06	1.51, 822	1.84	0.14, 70
C5 cis-6	2.08, 596	1.52	2.03, 611	1.75	0.05, 15
C5 trans	2.15, 576	1.78	2.04, 606	1.64	0.11, 30

Table 19. Table of total energies and relative energies of ground state conformers.

dye	relative energy (kcal/mol)	energy (Hartree)
C1 cis	2.00	-1305.4230007
C1 trans	0.00	-1305.4261922
C3 cis-7	0.00	-1382.8119535
C3 trans-7, 6	4.44	-1382.8190310
C5 cis-7	1.98	-1460.2026484
C5 cis-6	0.00	-1460.2058166
C5 trans-7, 6	0.94	-1460.2043175

Table 20. Table of cartesian coordinates X,Y,Z of **C1** cis ground state. All energies are given in Hartrees.

C1 cis Ground State XYZ

Energy =-1305.5110025			
No Imaginary Frequencies			
	X	**Y**	**Z**
C	-2.89302400	-1.86501300	-0.66078200
C	-3.42069900	-3.07221900	-1.12208200
C	-2.56830900	-4.02451200	-1.63818800
C	-1.19025000	-3.75937300	-1.73163300
C	-0.68732300	-2.57501600	-1.26489200
C	-1.24217000	-0.37781900	-0.20570600
C	-2.52063500	0.24683800	0.03831500
C	-3.51878800	-0.67038500	-0.18644600
H	-4.49096300	-3.22740500	-1.07700100
H	-2.96031300	-4.96673600	-1.99964500
H	-0.51181100	-4.47110100	-2.18117100
H	0.34918300	-2.28973100	-1.36974300
N	-1.52783500	-1.66843000	-0.69074200
C	-2.69104800	1.64038800	0.49245100
C	-3.46639100	1.92752100	1.61982700
C	-2.09572900	2.69283000	-0.21309800
C	-3.63618300	3.24300500	2.03856600

H	-3.92500700	1.11542000	2.17344400
C	-2.26644300	4.00616900	0.20858400
H	-1.51005700	2.48025200	-1.10192300
C	-3.03531900	4.28366500	1.33611400
H	-4.23525900	3.45437900	2.91660700
H	-1.80200900	4.81297300	-0.34645400
H	-3.16700000	5.30797600	1.66473500
C	-4.99739700	-0.51366700	-0.04282500
H	-5.35937700	-1.00244900	0.86618400
H	-5.27141400	0.54028400	0.00615100
H	-5.51495300	-0.96697200	-0.89134300
C	2.98743800	-1.79392800	0.67156900
C	0.79921300	-2.63414900	1.19329800
C	1.34746200	-3.80704400	1.62727500
C	2.74291200	-4.00718200	1.55855000
C	3.55803800	-2.99845100	1.10414900
C	3.56125000	-0.56937300	0.24382500
C	2.51410000	0.30262800	0.00204600
C	1.27621100	-0.38127000	0.22113200
H	-0.25058200	-2.40085500	1.29193800
H	0.69413800	-4.56479300	2.03750800
H	3.16902100	-4.94283600	1.89762600
H	4.63603400	-3.09771700	1.08888700

154

C	5.03042600	-0.34569900	0.07836400
H	5.50845600	-0.10753900	1.03301000
H	5.51249000	-1.24150200	-0.31916700
H	5.22107800	0.48066300	-0.60767900
N	1.60701600	-1.66533100	0.66296700
C	2.61647700	1.69559900	-0.46780100
C	3.50968200	2.57550900	0.15556400
C	1.83635100	2.16361500	-1.53293000
C	3.61156300	3.89483800	-0.26955700
H	4.11025100	2.22512800	0.98780800
C	1.93998000	3.48488000	-1.95485800
H	1.16303300	1.48530800	-2.04566100
C	2.82549700	4.35367100	-1.32361100
H	4.30199200	4.56708400	0.22637800
H	1.33315100	3.83247900	-2.78295100
H	2.90547300	5.38291100	-1.65343900
C	-0.00101700	0.16477000	0.06073000
H	-0.01506300	1.24614500	0.16463100

Table 21. Table of cartesian coordinates X,Y,Z of **C1** cis excited state. Energy is given in Hartrees.

C1 cis Excited State XYZ

Energy= -1305.436231

No imaginary Frequency			
	X	**Y**	**Z**
C	-2.54474900	-1.69325500	-1.17019600
C	-2.81686600	-2.93897000	-1.72913100
C	-1.77201000	-3.70700100	-2.21257200
C	-0.45488300	-3.20127000	-2.19363000
C	-0.19815700	-1.97702400	-1.64055600
C	-1.18064600	-0.02515600	-0.42685900
C	-2.53876800	0.38174600	-0.24648100
C	-3.37239000	-0.64941700	-0.66395400
H	-3.84367600	-3.27878400	-1.78375100
H	-1.96888400	-4.67942100	-2.64605700
H	0.36182700	-3.75627300	-2.63453200
H	0.77618600	-1.50807100	-1.65341500
N	-1.22277200	-1.28031900	-1.06128200
C	-2.94673000	1.65038500	0.38066200
C	-3.89377800	1.65879600	1.41126900
C	-2.39929600	2.86561000	-0.04739400
C	-4.28193800	2.85632000	2.00143800
H	-4.31322000	0.72121600	1.75937500
C	-2.78908600	4.06156000	0.54481100
H	-1.68128700	2.87352400	-0.86082300
C	-3.73046200	4.06004300	1.57063100

H	-5.01217500	2.84850500	2.80235700
H	-2.36138300	4.99589100	0.20029300
H	-4.03338900	4.99276000	2.03197000
C	-4.86159100	-0.71554600	-0.62256300
H	-5.20919300	-1.23028200	0.27889900
H	-5.29388800	0.28589800	-0.62446800
H	-5.24515800	-1.26487700	-1.48491100
C	2.43861700	-1.88460600	1.14371700
C	0.07011000	-2.08358400	1.52355900
C	0.25839900	-3.32907200	2.05936500
C	1.55106100	-3.88905600	2.10846800
C	2.64196600	-3.15324100	1.67778900
C	3.32546700	-0.86492700	0.68884800
C	2.54512100	0.20162100	0.25096400
C	1.17193700	-0.14651700	0.38914700
H	-0.88427200	-1.57580900	1.51626000
H	-0.59472100	-3.85799500	2.46167600
H	1.69437500	-4.87798200	2.52522100
H	3.65250100	-3.53317100	1.76222200
C	4.80957500	-0.99916300	0.67295400
H	5.24165000	-0.68138100	1.62747700
H	5.09993300	-2.03845000	0.50790600
H	5.24771300	-0.38135900	-0.11247600

157

N	1.13930800	-1.41873600	0.99363800
C	3.02780600	1.46062000	-0.34347500
C	4.07968700	2.16008100	0.25949700
C	2.46128600	1.96920000	-1.51908700
C	4.55224800	3.34253000	-0.29869900
H	4.51616600	1.78214400	1.17743600
C	2.93636300	3.15182900	-2.07432800
H	1.66019800	1.42618900	-2.00840100
C	3.98157500	3.84215900	-1.46590900
H	5.36404800	3.87601200	0.18189100
H	2.49342900	3.53106000	-2.98794100
H	4.35022700	4.76394300	-1.90056500
C	0.01451500	0.56432400	0.01492400
H	0.06094200	1.64600200	0.07861600

Table 22. Table of cartesian coordinates X,Y,Z of **C1** trans ground state. Energy is given in Hartrees.

C1 Trans Ground State XYZ

Energy: -1305.426192			
No Imaginary Frequencies			
	X	**Y**	**Z**
C	-1.96144690	-2.20699452	-0.74579396

C	-1.95786366	-3.56751107	-1.06424159
C	-0.81769138	-4.12809029	-1.59443526
C	0.31182799	-3.32650737	-1.84853567
C	0.29218414	-2.00052874	-1.51910927
C	-1.05683390	-0.14031655	-0.54324576
C	-2.45886982	-0.07833160	-0.19762023
C	-2.99499556	-1.33888886	-0.27111422
H	-2.85391446	-4.14928573	-0.89332918
H	-0.79443324	-5.18170413	-1.84185113
H	1.20145233	-3.74121051	-2.30050738
H	1.11013113	-1.32167286	-1.70743072
N	-0.81479582	-1.47011525	-0.93567861
C	-3.15487748	1.15864754	0.20247671
C	-3.79800270	1.24436767	1.43888606
C	-3.19154338	2.25430149	-0.66660089
C	-4.46121625	2.41010487	1.80360345
H	-3.76631437	0.39833695	2.11644153
C	-3.85801888	3.41681673	-0.30026716
H	-2.72422598	2.17660525	-1.64314443
C	-4.49084499	3.49689821	0.93647406
H	-4.95485880	2.46967090	2.76568388
H	-3.89611827	4.25548101	-0.98466958
H	-5.01199653	4.40263684	1.22070850

159

C	-4.39422448	-1.78354728	0.00705311
H	-4.44393091	-2.40316608	0.90638046
H	-5.04629615	-0.92270258	0.15064974
H	-4.78707396	-2.37221255	-0.82537701
C	3.21320853	2.06161486	-0.02307390
C	1.37841280	3.35927345	-0.85196086
C	2.17719238	4.45942877	-0.93246207
C	3.53909359	4.37579947	-0.55755699
C	4.05320704	3.18469787	-0.11785560
C	3.44937099	0.72999089	0.39486856
C	2.25100826	0.04246090	0.27768444
C	1.24464757	0.94016286	-0.21177484
H	0.34677771	3.35769137	-1.17159046
H	1.75950594	5.38397533	-1.30501187
H	4.17261854	5.24934351	-0.63839136
H	5.09549212	3.08031339	0.15298321
C	4.75309678	0.24829453	0.94913997
H	5.44603247	-0.04631673	0.15606081
H	5.23517425	1.03182225	1.53661347
H	4.60074474	-0.61326002	1.59944255
N	1.88440721	2.18437407	-0.36979205
C	2.03656168	-1.34618068	0.72297827
C	2.93246544	-2.34840609	0.33353306

C	0.94967364	-1.68539467	1.53508690
C	2.72958432	-3.66641232	0.72243155
H	3.77754898	-2.09193710	-0.29616541
C	0.74452314	-3.00500173	1.91605269
H	0.26804678	-0.91064823	1.86976101
C	1.62847284	-3.99929174	1.50452787
H	3.42995117	-4.43313784	0.41401965
H	-0.09824201	-3.25698173	2.54845865
H	1.46881470	-5.02650751	1.80876862
C	-0.14930861	0.87756284	-0.34760207
H	-0.65492497	1.83093842	-0.20948702

Table 23. Table of cartesian coordinates X,Y,Z of **C3 cis-7** ground state. Energy is given in

Hartrees.

C3 cis-7 Ground State XYZ

Energy = -1382.9024343			
No Imaginary Frequency			
	X	Y	Z
C	-4.47012500	-1.74666900	-0.09735400
C	-5.26229700	-2.90032100	-0.15960000
C	-4.65955800	-4.12184200	-0.33489300
C	-3.25695800	-4.19746100	-0.45936400
C	-2.49873200	-3.06361500	-0.39797600

C	-2.53345500	-0.56531500	-0.10579000
C	-3.64363600	0.34007600	0.03728000
C	-4.81970400	-0.37638000	0.05636400
H	-6.33584400	-2.79872800	-0.06484100
H	-5.25510900	-5.02468700	-0.38327900
H	-2.76002900	-5.14548200	-0.61218100
H	-1.42961100	-3.08105200	-0.51314500
N	-3.09698200	-1.85184600	-0.20812700
C	-3.52436500	1.80699500	0.14503700
C	-4.15659300	2.48461000	1.19315200
C	-2.80634100	2.54291500	-0.80503900
C	-4.06558900	3.86841100	1.29324500
H	-4.70930500	1.92013700	1.93635800
C	-2.71821300	3.92681500	-0.70305000
H	-2.33041200	2.02888700	-1.63306800
C	-3.34566800	4.59224700	0.34655700
H	-4.55516700	4.38106000	2.11302400
H	-2.16286000	4.48546700	-1.44752500
H	-3.27574600	5.67090100	0.42531100
C	-6.22660000	0.11501300	0.17358000
H	-6.62068800	-0.04388000	1.18158300
H	-6.28292200	1.18144400	-0.04633200
H	-6.87922300	-0.41522600	-0.52390100

C	4.44408100	-1.79366800	0.14887200
C	2.44199400	-3.09151200	0.30902700
C	3.18245500	-4.23307300	0.41400400
C	4.59192900	-4.17368100	0.37248500
C	5.21787600	-2.95832100	0.24902600
C	4.81587600	-0.42689400	0.04219500
C	3.64629100	0.30210000	-0.01107800
C	2.52342100	-0.59196300	0.05049600
H	1.36740800	-3.09510500	0.36348200
H	2.66703600	-5.17575800	0.53532200
H	5.17262500	-5.08397200	0.45184100
H	6.29647700	-2.86663700	0.23637600
C	6.23127700	0.04869200	-0.03056000
H	6.69897200	0.06045100	0.95829800
H	6.82566800	-0.60867000	-0.66938100
H	6.27918200	1.05910000	-0.43781900
N	3.06454700	-1.88601100	0.15215300
C	3.55115000	1.76858700	-0.14571500
C	4.25885700	2.59454300	0.73461100
C	2.78487900	2.35543600	-1.15952500
C	4.19280800	3.97769300	0.61010400
H	4.85157200	2.14678400	1.52494300
C	2.72159400	3.73920800	-1.28226800

	X	Y	Z
H	2.25306800	1.72470900	-1.86350800
C	3.42288900	4.55316100	-0.39716100
H	4.74113700	4.60620800	1.30214500
H	2.12821700	4.18102500	-2.07436400
H	3.37242700	5.63141300	-0.49407000
C	1.18845900	-0.20653600	0.03602200
H	1.07114600	0.87246800	0.10066000
C	-0.00225900	-0.92208300	-0.07331600
H	0.00431200	-1.98446200	-0.23156700
C	-1.19745200	-0.20208200	-0.02663300
H	-1.07503800	0.86807700	0.12106000

Table 24. Table of cartesian coordinates X,Y,Z of **C3 cis-7** excited state. Energy is given in

Hartrees.

C3 cis-7 Excited State XYZ

Energy = -1382.835669		
No Imaginary Frequency		
X	Y	Z
C	-4.28940836	-1.85603519	-0.19128327
C	-4.91663130	-3.09095023	-0.34628376
C	-4.17948408	-4.24955308	-0.20431698
C	-2.81155249	-4.17136437	0.13155838
C	-2.20594352	-2.95397365	0.27283387

C	-2.51841505	-0.46830829	0.16468559
C	-3.70481551	0.31907604	0.01231016
C	-4.78283378	-0.52158789	-0.21803410
H	-5.97771606	-3.11443902	-0.56140590
H	-4.65336879	-5.21589709	-0.32185829
H	-2.22598162	-5.06488276	0.29948048
H	-1.17811535	-2.84673472	0.58067446
N	-2.92196582	-1.81024258	0.05947153
C	-3.74580341	1.79307513	0.04479989
C	-4.70532540	2.44636831	0.82712397
C	-2.85729326	2.56180878	-0.71738026
C	-4.77063512	3.83511212	0.85183143
H	-5.39255848	1.86005932	1.42746651
C	-2.92462517	3.95020356	-0.69044442
H	-2.12421796	2.06852401	-1.34611280
C	-3.87957615	4.59067380	0.09487832
H	-5.51583503	4.32688043	1.46630757
H	-2.23367486	4.53237838	-1.28920531
H	-3.93027728	5.67309677	0.11479284
C	-6.20684600	-0.16505835	-0.48473248
H	-6.80450519	-0.21353475	0.43109138
H	-6.28586757	0.84798887	-0.88163996
H	-6.64849226	-0.85785720	-1.20397921

C	4.28950544	-1.85852760	-0.12958043
C	2.21195066	-2.94075641	0.39401238
C	2.81774570	-4.16196318	0.29143393
C	4.18226939	-4.25088841	-0.05579263
C	4.91684843	-3.09748827	-0.24628652
C	4.78158639	-0.52533841	-0.20305037
C	3.70465221	0.32217622	0.00783952
C	2.51993781	-0.46067602	0.19092966
H	1.18828139	-2.82120643	0.71314255
H	2.23581159	-5.04928027	0.50003610
H	4.65624855	-5.22041766	-0.14239082
H	5.97633814	-3.12769807	-0.46841273
C	6.20346768	-0.17842159	-0.49180003
H	6.80838332	-0.19898597	0.42031760
H	6.63843921	-0.89410293	-1.19250348
H	6.28019727	0.82161990	-0.92078127
N	2.92406476	-1.80519554	0.12910417
C	3.74418696	1.79640612	-0.00917401
C	4.71327174	2.47592740	0.73841689
C	2.84488324	2.53908120	-0.78455751
C	4.77759606	3.86473146	0.71607858
H	5.40900875	1.91015082	1.34858926
C	2.91125587	3.92762531	-0.80453981

H	2.10409750	2.02513448	-1.38706667
C	3.87593254	4.59433920	-0.05368296
H	5.53052493	4.37704276	1.30376705
H	2.21177407	4.48918537	-1.41301640
H	3.92587519	5.67685456	-0.07033810
C	1.21780248	0.01939729	0.39367259
H	1.16767120	1.06011415	0.70098881
C	0.00285132	-0.62732282	0.15045335
H	0.01138587	-1.59148262	-0.34110043
C	-1.21872224	0.01031801	0.38287805
H	-1.17511764	1.04691930	0.70434480

Table 25. Table of cartesian coordinates X,Y,Z of **C3 trans** ground state. Energy is given in

Hartrees.

C3 trans Ground State XYZ

Energy = -1382.819031			
No Imaginary Frequencies			
	X	**Y**	**Z**
C	-3.73634928	-1.80807194	0.33972777
C	-4.13883332	-3.13278521	0.55261375
C	-3.21036827	-4.14149775	0.47599176
C	-1.87150763	-3.83582805	0.15513976
C	-1.49237464	-2.54064263	-0.04999149

C	-2.26033958	-0.14278894	-0.08638625
C	-3.58214906	0.41351062	0.02537401
C	-4.47605088	-0.59300698	0.31060524
H	-5.17953872	-3.33077709	0.77308181
H	-3.50488486	-5.16962665	0.64210620
H	-1.12665885	-4.61203916	0.05128882
H	-0.49228841	-2.28071854	-0.35707228
N	-2.40719517	-1.53480718	0.07680856
C	-3.89425282	1.84602213	-0.12405105
C	-4.58440851	2.52494360	0.88375014
C	-3.52474460	2.53583202	-1.28334745
C	-4.89416616	3.87118240	0.73687047
H	-4.86377338	1.99501371	1.78757158
C	-3.83937341	3.88117137	-1.42873580
H	-3.01620346	2.00487856	-2.08092574
C	-4.52236126	4.55083383	-0.41851941
H	-5.42591416	4.39018089	1.52480308
H	-3.56227150	4.40408019	-2.33593225
H	-4.76980401	5.59889146	-0.53393565
C	-5.95510162	-0.50819788	0.51172118
H	-6.22469081	-0.64765532	1.56215767
H	-6.32732225	0.46502603	0.19311512
H	-6.47169832	-1.27506465	-0.06997079

C	4.84717232	1.27406231	0.23513557
C	3.44349039	3.21095599	0.19706210
C	4.53302445	4.01726717	0.33736461
C	5.82577324	3.45224857	0.43159219
C	5.97874780	2.09044327	0.38445375
C	4.69629326	-0.13685787	0.15358176
C	3.34945723	-0.39173307	0.00706559
C	2.63134823	0.84511366	0.00163298
H	2.43589032	3.59334144	0.13505619
H	4.38999221	5.08765379	0.38047644
H	6.68701451	4.09710508	0.54709630
H	6.95100479	1.62168896	0.46292470
C	5.82961592	-1.11064436	0.18051127
H	6.56938703	-0.87311255	-0.58779112
H	6.33769974	-1.09891828	1.14826545
H	5.46706711	-2.12240495	0.00056106
N	3.60122500	1.85662288	0.13320433
C	2.75541889	-1.73169742	-0.20746594
C	2.29012274	-2.08954669	-1.47642535
C	2.67509547	-2.65342553	0.83712493
C	1.76114241	-3.35569373	-1.69776408
H	2.35649055	-1.37378264	-2.28828503
C	2.13886467	-3.91936047	0.61541396

	X	Y	Z
H	3.03427559	-2.37581098	1.82170396
C	1.68830741	-4.27394069	-0.65195727
H	1.42097088	-3.63173276	-2.68865833
H	2.08906884	-4.63157781	1.43015298
H	1.29922377	-5.26945502	-0.83175204
C	1.26928151	1.11800860	-0.08710339
H	0.97077168	2.15666650	-0.20677187
C	0.24527181	0.18426013	-0.02588498
H	0.50920524	-0.83885757	0.17794034
C	-1.08491569	0.58515769	-0.14561638
H	-1.25800847	1.65253259	-0.26420043

Table 26. Table of cartesian coordinates X,Y,Z of **C3 trans** excited state. Energy is given in

Hartrees.

C3 trans Excited State XYZ

Energy: -1382.735727 Hartrees		
No Imaginary Frequency		
X	Y	Z
C	3.53690970	-1.88084210	-0.61527575
C	3.79492158	-3.20642585	-0.96976899
C	2.78746234	-4.14813691	-0.87870005
C	1.51994595	-3.76706737	-0.38984283
C	1.27352236	-2.46232328	-0.05196420

C	2.23739827	-0.14280045	0.07096548
C	3.58664467	0.31719610	-0.07703639
C	4.37230487	-0.73207089	-0.53096289
H	4.79134462	-3.47347314	-1.30444828
H	2.97644383	-5.17989084	-1.15315603
H	0.72561552	-4.49109347	-0.25374292
H	0.34221616	-2.14646592	0.40005944
N	2.25280540	-1.52180783	-0.21565851
C	4.02745567	1.70051387	0.17052372
C	4.75957652	2.39505498	-0.80023090
C	3.74143602	2.33257877	1.38816008
C	5.19244241	3.69482838	-0.55974488
H	4.97231430	1.91588515	-1.75189938
C	4.17503695	3.63229659	1.62616612
H	3.20115051	1.78789279	2.15840078
C	4.90032218	4.31602328	0.65245968
H	5.75578378	4.22457425	-1.32113201
H	3.95749633	4.10777355	2.57723566
H	5.24125915	5.32904043	0.83995470
C	5.83245077	-0.73022073	-0.84676405
H	6.01169369	-0.68423257	-1.92734204
H	6.32185231	0.13254098	-0.38939206
H	6.31638765	-1.63714956	-0.47096082

C	-4.83323862	1.30390930	-0.37393266
C	-3.45096454	3.27315177	-0.28380720
C	-4.53630119	4.06019314	-0.55090095
C	-5.80958582	3.46980273	-0.73065492
C	-5.95126281	2.10022296	-0.64995901
C	-4.65426728	-0.09779580	-0.22998673
C	-3.31143351	-0.31513742	0.06259481
C	-2.63149832	0.94142427	0.07932685
H	-2.44978254	3.66360784	-0.15568149
H	-4.40259769	5.13207658	-0.62898770
H	-6.66885177	4.09626063	-0.94229810
H	-6.91159093	1.62032832	-0.80350437
C	-5.75430727	-1.10451043	-0.32228254
H	-6.66980662	-0.73118700	0.14665062
H	-5.99261722	-1.34720617	-1.36451015
H	-5.46966214	-2.03264685	0.17925755
N	-3.60523602	1.92034260	-0.17504066
C	-2.71202373	-1.61526019	0.42082520
C	-2.06668388	-1.77602198	1.65748906
C	-2.81858553	-2.71543306	-0.43716910
C	-1.55633464	-3.01499269	2.03096870
H	-1.98858161	-0.92645391	2.33020530
C	-2.29932696	-3.95400318	-0.06493755

H	-3.30729867	-2.59475997	-1.40001638
C	-1.67499031	-4.10871161	1.17116401
H	-1.07872860	-3.13227720	2.99871958
H	-2.39483347	-4.80079150	-0.73749909
H	-1.29193626	-5.07949578	1.47143705
C	-1.27125171	1.25876793	0.25864924
H	-1.00312419	2.27636325	0.53543868
C	-0.23790753	0.34056548	0.06715530
H	-0.50972445	-0.62107076	-0.34977217
C	1.10778496	0.65594614	0.28626411
H	1.33868312	1.67777697	0.57913326

Table 27. Table of cartesian coordinates X,Y,Z of **C5 cis-6** ground state. Energy is given in Hartrees.

C5 cis-6 Ground State XYZ

Energy: -1460.205817			
No Imaginary Frequency			
	X	**Y**	**Z**
C	5.97605200	-0.99258300	-0.10009000
C	4.97826500	-3.16205800	-0.23548200
C	6.20857000	-3.73274600	-0.36793400
C	7.36881500	-2.92426100	-0.36895500
C	7.25006000	-1.56474000	-0.23764100

C	5.55125100	0.35343500	0.05635100
C	4.17604400	0.33599500	0.15325000
C	3.71036800	-1.01215000	0.04614300
H	4.06505000	-3.73735100	-0.23302900
H	6.27902600	-4.80608300	-0.47278000
H	8.34329700	-3.38227200	-0.47622000
H	8.11410300	-0.91310600	-0.23927400
C	6.47206600	1.52783600	0.13497200
H	7.22879000	1.38212500	0.90969600
H	6.99167100	1.68812800	-0.81337500
H	5.91316000	2.43264900	0.37245600
N	4.86333900	-1.80913200	-0.09669600
C	3.31741900	1.51826000	0.38381700
C	2.68415600	1.69121500	1.61708800
C	3.13531000	2.46807900	-0.62163300
C	1.86722300	2.79291800	1.83476900
H	2.83216800	0.95461200	2.39912000
C	2.31475300	3.56993500	-0.40171500
H	3.62956100	2.33378100	-1.57731800
C	1.67856300	3.73141500	0.82392600
H	1.38211600	2.92278400	2.79447000
H	2.17730900	4.30306500	-1.18745700
H	1.04438800	4.59244600	0.99725300

174

C	2.42606600	-1.55001100	0.02023000
H	2.34558800	-2.63371200	-0.01368800
C	1.22430400	-0.85654400	0.01341800
H	1.21646800	0.22613900	0.00515200
C	0.00007900	-1.51838000	0.00002900
H	0.00009400	-2.60811900	-0.00013900
C	-1.22416700	-0.85657600	-0.01316400
H	-1.21637700	0.22610700	-0.00457500
C	-2.42590800	-1.55007500	-0.02019200
H	-2.34540300	-2.63378100	0.01349200
C	-4.17596000	0.33588800	-0.15316500
C	-5.55118200	0.35324200	-0.05636100
C	-5.97591500	-0.99279700	0.10003900
C	-3.31745000	1.51823500	-0.38373400
C	-3.13589400	2.46838000	0.62150800
C	-2.68385800	1.69103200	-1.61686300
C	-2.31561100	3.57042700	0.40152000
H	-3.63038300	2.33420400	1.57708800
C	-1.86718800	2.79291100	-1.83461100
H	-2.83143000	0.95417200	-2.39873800
C	-1.67912400	3.73176200	-0.82398400
H	-2.17862200	4.30381800	1.18709600
H	-1.38183400	2.92264900	-2.79420400

175

	X	Y	Z
H	-1.04519600	4.59296200	-0.99738300
C	-4.97802000	-3.16221400	0.23554700
C	-7.24990300	-1.56501800	0.23749400
C	-7.36859700	-2.92454400	0.36880900
H	-8.34306300	-3.38260600	0.47600400
C	-6.20830700	-3.73296500	0.36789800
H	-6.27871200	-4.80630100	0.47278300
H	-8.11397700	-0.91342300	0.23906700
H	-4.06477400	-3.73745600	0.23322800
C	-3.71022200	-1.01223900	-0.04605500
N	-4.86315800	-1.80928500	0.09671300
C	-6.47212100	1.52753600	-0.13513600
H	-5.91324100	2.43250000	-0.37209400
H	-7.22842300	1.38191000	-0.91029200
H	-6.99224500	1.68748300	0.81298400

Table 28. Table of cartesian coordinates X,Y,Z of **C5 cis-6** excited state. Energy is given in Hartrees.

C5 cis-6 Excited State XYZ

Energy: -1460.126655 Hartrees			
No Imaginary Frequency			
	X	Y	Z
C	-5.97459600	0.87348800	-0.10168000

C	-5.09258800	3.09908200	-0.28914600
C	-6.35409800	3.59695200	-0.45775300
C	-7.46694700	2.72321600	-0.44893600
C	-7.27248300	1.37024100	-0.27532500
C	-5.46596100	-0.43683900	0.10070100
C	-4.08840300	-0.33228500	0.22723800
C	-3.70881400	1.04158800	0.08239700
H	-4.20929000	3.72318000	-0.29563500
H	-6.48289100	4.66281700	-0.60042200
H	-8.46665000	3.12041900	-0.58455400
H	-8.10275100	0.67249200	-0.27456900
C	-6.31212200	-1.66478900	0.19878300
H	-7.19063100	-1.48865100	0.82773600
H	-6.67029800	-1.98681300	-0.78585100
H	-5.74201800	-2.48898900	0.63332500
N	-4.90696100	1.75868500	-0.10270000
C	-3.17449800	-1.45825100	0.50702400
C	-2.38691900	-1.46893500	1.66607600
C	-3.10132700	-2.54059600	-0.37630900
C	-1.52882600	-2.53188500	1.92310800
H	-2.44941300	-0.63425700	2.35930600
C	-2.24322000	-3.60573800	-0.11566400
H	-3.71031600	-2.53474000	-1.27623200

177

C	-1.45359900	-3.60111900	1.03107900
H	-0.92335500	-2.53067800	2.82392300
H	-2.19318800	-4.43894300	-0.80997600
H	-0.78418300	-4.43130400	1.23452700
C	-2.45948800	1.67957900	0.04969300
H	-2.44702300	2.76709800	0.03414200
C	-1.21946600	1.04382100	0.01255200
H	-1.17895300	-0.04016500	-0.02648000
C	-0.00001000	1.72775500	-0.00000800
H	-0.00000900	2.81805900	0.00002900
C	1.21944100	1.04381900	-0.01260800
H	1.17892500	-0.04017000	0.02635400
C	2.45946700	1.67957800	-0.04969900
H	2.44699800	2.76709600	-0.03408100
C	4.08839900	-0.33227700	-0.22723500
C	5.46595500	-0.43681800	-0.10067300
C	5.97457700	0.87351500	0.10170300
C	3.17451500	-1.45826000	-0.50702400
C	3.10133700	-2.54059000	0.37632600
C	2.38697000	-1.46897900	-1.66609900
C	2.24325500	-3.60575000	0.11567800
H	3.71030200	-2.53470800	1.27626600
C	1.52890100	-2.53194800	-1.92313400

H	2.44947100	-0.63431500	-2.35934400
C	1.45366500	-3.60116500	-1.03108600
H	2.19321700	-4.43894400	0.81000400
H	0.92345600	-2.53076800	-2.82396700
H	0.78426600	-4.43136400	-1.23453700
C	5.09255300	3.09910700	0.28910400
C	7.27245800	1.37027800	0.27536500
C	7.46691100	2.72325700	0.44895400
H	8.46660900	3.12046900	0.58458500
C	6.35405700	3.59698800	0.45772800
H	6.48284200	4.66285700	0.60037000
H	8.10273000	0.67253400	0.27463600
H	4.20925400	3.72320400	0.29554800
C	3.70879500	1.04159600	-0.08241500
N	4.90693700	1.75870500	0.10269100
C	6.31212600	-1.66476400	-0.19872300
H	5.74205700	-2.48895500	-0.63332700
H	7.19068300	-1.48860900	-0.82760500
H	6.67022800	-1.98681300	0.78593000

Table 29. Table of cartesian coordinates X,Y,Z of **C5 cis-7** ground state. Energy is given in

Hartrees.

C5 cis-7 Ground State XYZ

Energy= -1460.2927992			
No Imaginary Frequencies			
	X	**Y**	**Z**
C	-5.68650400	-1.71683000	-0.08396200
C	-6.47977000	-2.87127200	-0.13331700
C	-5.89131700	-4.08051800	-0.41123200
C	-4.50515500	-4.14239900	-0.66745100
C	-3.74558300	-3.00942300	-0.61532100
C	-3.75310300	-0.53432600	-0.18953000
C	-4.84842600	0.36652500	0.04992300
C	-6.02165100	-0.35287000	0.13650700
H	-7.54281900	-2.77964900	0.04947500
H	-6.48773000	-4.98327600	-0.45016800
H	-4.02538600	-5.07750600	-0.92138900
H	-2.69574200	-3.00422300	-0.85137800
N	-4.32504800	-1.81497500	-0.29786300
C	-4.72120100	1.82908200	0.19713600
C	-5.29142100	2.47433300	1.29992500
C	-4.05903800	2.59391900	-0.77018200
C	-5.19529000	3.85477900	1.43537000

H	-5.79967500	1.88751000	2.05735400
C	-3.96606900	3.97447000	-0.63310400
H	-3.63073200	2.10444100	-1.63827400
C	-4.53238500	4.60769800	0.46991900
H	-5.63674200	4.34202000	2.29695100
H	-3.45544000	4.55599600	-1.39185100
H	-4.45902000	5.68379900	0.57587200
C	-7.41549500	0.13414300	0.37155500
H	-7.72739200	-0.03318500	1.40661700
H	-7.49201600	1.20205800	0.16499000
H	-8.12064200	-0.39286500	-0.27543900
C	5.69691900	-1.71409400	0.23412300
C	3.72584600	-3.06417100	0.37486500
C	4.49425900	-4.18080100	0.52802200
C	5.90343100	-4.08372700	0.52458500
C	6.49858400	-2.85575500	0.38462200
C	6.03353900	-0.34411200	0.09288900
C	4.84380200	0.35029100	-0.01331900
C	3.74654100	-0.57028100	0.05529600
H	2.65081000	-3.09892300	0.39166100
H	4.00133400	-5.13469000	0.65568900
H	6.50584600	-4.97548700	0.64292800
H	7.57440400	-2.73499100	0.39515000

C	7.43589700	0.17225300	0.04028400
H	7.87286600	0.24499700	1.04055900
H	8.06983400	-0.49376600	-0.54965800
H	7.46587400	1.16402300	-0.41231800
N	4.31864000	-1.84339900	0.20890200
C	4.71614700	1.80901000	-0.19842500
C	5.38049500	2.68112000	0.67131900
C	3.96554500	2.34326900	-1.25219100
C	5.28750900	4.05736200	0.49696000
H	5.96154100	2.27459100	1.49207100
C	3.87578100	3.72020600	-1.42540500
H	3.46727200	1.67618300	-1.94721900
C	4.53416800	4.58011200	-0.55080000
H	5.80202300	4.72185600	1.18135600
H	3.29568400	4.12079800	-2.24861500
H	4.46319300	5.65294700	-0.68720400
C	2.39693900	-0.22180500	0.01320600
H	2.25007000	0.85586000	0.02314200
C	1.22841800	-0.96723500	-0.05559300
H	1.21891000	-2.04516800	-0.13274200
C	-0.00583400	-0.31285200	-0.07191600
H	-0.00203700	0.77458200	-0.01498800
C	-1.23757800	-0.95379200	-0.15851800

H	-1.23427900	-2.03422800	-0.20143100
C	-2.40691700	-0.19573500	-0.14438900
H	-2.25167800	0.87547600	-0.03951500

Table 30. Table of cartesian coordinates X,Y,Z of **C5 cis-7** excited state. Energy is given in

Hartrees.

C5 cis-7 Excited State XYZ

Energy = -1460.234632			
No Imaginary frequencies			
	X	**Y**	**Z**
C	5.52333230	-1.83903333	0.16045641
C	6.15612029	-3.07716881	0.28032167
C	5.41992223	-4.23233877	0.12557871
C	4.04620247	-4.14965811	-0.18788446
C	3.43602639	-2.93185654	-0.29282759
C	3.74761124	-0.44769277	-0.14175397
C	4.93809857	0.33686137	0.00711220
C	6.01821405	-0.50674895	0.20611909
H	7.22049735	-3.10175631	0.47819784
H	5.89657785	-5.20027382	0.21564546
H	3.46000607	-5.04075713	-0.36598270
H	2.40387173	-2.81971005	-0.58226635
N	4.15325924	-1.79032638	-0.06722118

C	4.98202967	1.81117607	-0.00194551
C	5.92783100	2.47376882	-0.79326360
C	4.11249328	2.57047577	0.79088497
C	5.99805896	3.86238109	-0.79705872
H	6.60029035	1.89442871	-1.41667982
C	4.18524752	3.95896237	0.78541114
H	3.39057019	2.06964244	1.42643856
C	5.12610206	4.60866243	-0.00911605
H	6.73220407	4.36136872	-1.41898967
H	3.50965004	4.53394789	1.40808984
H	5.18086672	5.69107689	-0.01228259
C	7.44729997	-0.15738756	0.45973329
H	8.03707251	-0.20633862	-0.46097968
H	7.53488775	0.85377684	0.85944866
H	7.89197444	-0.85377131	1.17381499
C	-5.52333860	-1.83901343	0.16055010
C	-3.43601317	-2.93187279	-0.29251049
C	-4.04620872	-4.14966152	-0.18754041
C	-5.41995203	-4.23232315	0.12583088
C	-6.15614844	-3.07713673	0.28045407
C	-6.01823067	-0.50673463	0.20609854
C	-4.93810332	0.33686896	0.00712719
C	-3.74760150	-0.44768753	-0.14162427

184

H	-2.40383252	-2.81977183	-0.58186483
H	-3.45999912	-5.04076977	-0.36555192
H	-5.89661791	-5.20025054	0.21592485
H	-7.22054128	-3.10169984	0.47824780
C	-7.44734114	-0.15738151	0.45959478
H	-8.03711797	-0.20675102	-0.46109370
H	-7.89194978	-0.85352490	1.17395468
H	-7.53500284	0.85392857	0.85891657
N	-4.15324986	-1.79031827	-0.06703506
C	-4.98202842	1.81117803	-0.00202465
C	-5.92776184	2.47373012	-0.79345235
C	-4.11254089	2.57052627	0.79081909
C	-5.99798832	3.86234411	-0.79733529
H	-6.60017435	1.89435504	-1.41688858
C	-4.18528751	3.95900902	0.78525460
H	-3.39066036	2.06972912	1.42645090
C	-5.12608693	4.60867000	-0.00937642
H	-6.73209326	4.36129512	-1.41934302
H	-3.50972394	4.53403007	1.40793777
H	-5.18084365	5.69108435	-0.01261059
C	0.00000180	0.02113764	-0.36538279
H	-0.00001517	1.02630246	-0.78071161
C	1.22453143	-0.60170477	-0.10966202

185

H	1.18734209	-1.59470805	0.32580749
C	2.44660583	0.03563823	-0.32569717
H	2.40108277	1.08247057	-0.61316174
C	-1.22451126	-0.60172138	-0.10958686
C	-2.44659340	0.03563361	-0.32556058
H	-1.18728110	-1.59471563	0.32589314
H	-2.40106416	1.08246489	-0.61302933

Table 31. Table of cartesian coordinates X,Y,Z of **C5 trans** ground state. Energy is given in

Hartrees.

C5 trans Ground State XYZ

Energy: -1460.204318			
No Imaginary Frequencies			
	X	**Y**	**Z**
C	-5.26001277	-1.71416719	-0.12168560
C	-5.85099272	-2.98582759	-0.15235665
C	-5.08032319	-4.08352528	-0.44015974
C	-3.70716601	-3.91967854	-0.72763600
C	-3.14403299	-2.67827544	-0.69023579
C	-3.54908453	-0.23593763	-0.27309264
C	-4.77056588	0.47763092	-0.02942818
C	-5.80868891	-0.42252423	0.08941718

H	-6.91053395	-3.07063715	0.05044580
H	-5.52192543	-5.07116301	-0.46621943
H	-3.09016790	-4.76560830	-0.99534056
H	-2.11680467	-2.49503907	-0.95393713
N	-3.90233924	-1.59249535	-0.35833647
C	-4.87045987	1.94340560	0.09035235
C	-5.44986525	2.51903187	1.22423927
C	-4.41089300	2.77327624	-0.93734680
C	-5.56150779	3.89961914	1.33103071
H	-5.79957950	1.87839803	2.02615666
C	-4.52695875	4.15347765	-0.82911960
H	-3.98830591	2.32937701	-1.83232988
C	-5.10029456	4.71847541	0.30547318
H	-6.00848174	4.33659838	2.21549426
H	-4.18052331	4.78779365	-1.63590685
H	-5.19308477	5.79440256	0.38774185
C	-7.25890287	-0.15556137	0.33835945
H	-7.54893312	-0.43388173	1.35520506
H	-7.48007790	0.90265031	0.20173077
H	-7.88407007	-0.72381182	-0.35413089
C	6.08142872	1.18694934	-0.08927833
C	4.67542357	3.11671449	-0.21332197
C	5.77000537	3.92363135	-0.30261005

C	7.06753311	3.36219519	-0.28653738
C	7.21902883	2.00353260	-0.18197403
C	5.93024331	-0.22017781	0.03311216
C	4.57747759	-0.47922511	0.09293577
C	3.85437764	0.75105980	-0.00471564
H	3.66650517	3.49980921	-0.22353378
H	5.62736781	4.99168700	-0.38574901
H	7.93356984	4.00691158	-0.35896614
H	8.19534964	1.53680751	-0.17125739
C	7.06635596	-1.18730393	0.11887100
H	7.62210616	-1.23050304	-0.82154859
H	7.76642571	-0.90051503	0.90731493
H	6.69732743	-2.18833820	0.34053817
N	4.82926875	1.76532448	-0.10247291
C	3.97324489	-1.81566638	0.28033064
C	4.05501672	-2.77534723	-0.72906611
C	3.33606682	-2.13382122	1.48240627
C	3.49393587	-4.03483478	-0.54393754
H	4.55285664	-2.52790183	-1.66000739
C	2.77949411	-3.39299340	1.66592212
H	3.28139869	-1.38952157	2.26931565
C	2.85504146	-4.34408888	0.65165031
H	3.56185677	-4.77508556	-1.33177667

H	2.29543458	-3.63611998	2.60400581
H	2.42664074	-5.32807945	0.79866474
C	2.49239416	1.02840125	-0.06496064
H	2.20899955	2.07750637	-0.09426943
C	1.43673213	0.12742523	-0.11407567
H	1.62408915	-0.93901829	-0.12536659
C	0.12194303	0.58000039	-0.16530946
H	-0.04549357	1.65649643	-0.15605106
C	-1.00158746	-0.24138317	-0.22815536
H	-0.83180426	-1.30928444	-0.21562739
C	-2.27502592	0.31778749	-0.24226182
H	-2.30493374	1.40261781	-0.16994240

Table 32. Table of cartesian coordinates X,Y,Z of **C5 trans** excited state. Energy is given in Hartrees.

C5 trans Excited State XYZ

Energy: -1459.782024			
No Imaginary Frequency			
	X	**Y**	**Z**
C	-5.00323400	-1.80830100	-0.46362900
C	-5.42721000	-3.12704500	-0.66445900
C	-4.54979100	-4.05672700	-1.18092500

189

C	-3.24045800	-3.66036400	-1.53868600
C	-2.83449200	-2.37122500	-1.33129000
C	-3.49222300	-0.10889500	-0.46770200
C	-4.77063900	0.40540700	-0.07299900
C	-5.68399400	-0.63779300	-0.03442900
H	-6.44931300	-3.38978800	-0.41461800
H	-4.86757400	-5.08118600	-1.33939100
H	-2.55232800	-4.35844200	-1.99958300
H	-1.87282800	-1.99664800	-1.64970200
N	-3.68478000	-1.47143800	-0.75041300
C	-5.03289600	1.81210400	0.27587100
C	-5.66212700	2.13636100	1.48401300
C	-4.68044200	2.84328400	-0.60526300
C	-5.92771000	3.46309700	1.80621200
H	-5.92578200	1.34240700	2.17729700
C	-4.94713200	4.16902800	-0.28102800
H	-4.22150300	2.59646000	-1.55932100
C	-5.56988500	4.48150900	0.92566000
H	-6.41170800	3.70239500	2.74760300
H	-4.67951400	4.95847100	-0.97613000
H	-5.78007100	5.51609400	1.17692200
C	-7.13248400	-0.59331700	0.33239000
H	-7.30535600	-0.96996800	1.34717900

H	-7.50663100	0.43197200	0.28817200
H	-7.73003100	-1.20356400	-0.35213700
C	6.18392900	0.98576300	-0.21147700
C	4.97067000	3.00322800	-0.69073100
C	6.14362800	3.67298100	-0.89848400
C	7.37852500	2.99614200	-0.76043700
C	7.39307700	1.65983000	-0.42463600
C	5.87924000	-0.35542900	0.14190800
C	4.49767000	-0.45683200	0.23287700
C	3.91552800	0.81280400	-0.08364500
H	4.00020000	3.46885400	-0.79741900
H	6.10892300	4.71976000	-1.17419300
H	8.30783500	3.52905000	-0.92769200
H	8.32235300	1.10945800	-0.32645000
C	6.90407300	-1.40892600	0.41326100
H	7.30503100	-1.83130600	-0.51542600
H	7.74643400	-1.00110600	0.98066700
H	6.46903000	-2.22750400	0.99136600
N	4.99227800	1.68428600	-0.33587000
C	3.76126200	-1.66030300	0.66476700
C	3.94055700	-2.87684300	-0.00287300
C	2.90379400	-1.61060600	1.77291600
C	3.26749500	-4.01964200	0.42122900

191

H	4.60142300	-2.91857500	-0.86445500
C	2.23295300	-2.75239100	2.19431200
H	2.77202300	-0.67047700	2.30189000
C	2.41198700	-3.95927700	1.51821800
H	3.41315200	-4.95721700	-0.10577700
H	1.57827900	-2.70438900	3.05880300
H	1.89198000	-4.85160500	1.85203400
C	2.58355700	1.23825800	-0.20054400
H	2.39894100	2.30792600	-0.27352300
C	1.46294200	0.40957100	-0.25821300
H	1.60101600	-0.66766700	-0.26540700
C	0.15718100	0.90242900	-0.32988000
H	0.00246200	1.98141000	-0.32555400
C	-0.96671800	0.07091200	-0.39836400
H	-0.78227000	-0.99930800	-0.36809500
C	-2.26853700	0.57237200	-0.41642600
H	-2.37523500	1.64756000	-0.28816600

192

Table 33. Crystal data and structure refinement for **C1**.

Identification code	m18097	
Empirical formula	C33 H28 Cl N3 O4	
Formula weight	566.03	
Temperature	90.0(2) K	
Wavelength	0.71073 Å	
Crystal system, space group	Monoclinic, P2(1)/n	
Unit cell dimensions	a = 13.2027(4) Å	alpha = 90 deg.
	b = 8.2361(2) Å	beta = 90.564(1) deg.
	c = 24.8945(6) Å	gamma = 90 deg.
Volume	2706.87(12) Å^3	
Z, Calculated density	4, 1.389 Mg/m^3	
Absorption coefficient	0.187 mm^{-1}	
F(000)	1184	
Crystal size	0.320 x 0.160 x 0.040 mm	
Theta range for data collection	2.887 to 27.497 deg.	
Limiting indices	-17<=h<=16, -10<=k<=10, -32<=l<=30	
Reflections collected / unique	30828 / 6215 [R(int) = 0.0666]	
Completeness to theta = 25.242	99.8 %	
Absorption correction	Semi-empirical from equivalents	
Max. and min. transmission	0.958 and 0.673	
Refinement method	Full-matrix least-squares on F^2	
Data / restraints / parameters	6215 / 0 / 374	
Goodness-of-fit on F^2	1.047	
Final R indices [I>2sigma(I)]	R1 = 0.0403, wR2 = 0.0948	
R indices (all data)	R1 = 0.0539, wR2 = 0.1035	
Extinction coefficient	0.0021(6)	
Largest diff. peak and hole	0.389 and -0.507 e.A^{-3}	

Table 34. Atomic coordinates (x 10^4) and equivalent isotropic displacement parameters (A^2 x 10^3)

for **C1**. U(eq) is defined as one third of the trace of the orthogonalized Uij tensor.

	x	y	z	U(eq)
N1	5608(1)	8302(2)	8320(1)	12(1)
N2	4249(1)	5004(2)	8702(1)	12(1)
C1	5183(1)	7524(2)	7873(1)	12(1)
C2	5838(1)	7833(2)	7433(1)	12(1)
C3	6665(1)	8729(2)	7620(1)	13(1)

C4	7030(1)	9999(2)	8549(1)	16(1)
C5	6644(1)	10202(2)	9053(1)	18(1)
C6	5707(1)	9483(2)	9182(1)	17(1)
C7	5195(1)	8557(2)	8818(1)	14(1)
C8	6503(1)	9061(2)	8168(1)	13(1)
C9	7603(1)	9228(2)	7327(1)	18(1)
C10	4256(1)	6676(2)	7866(1)	12(1)
C11	3794(1)	5700(2)	8237(1)	12(1)
C12	2760(1)	5137(2)	8231(1)	12(1)
C13	2596(1)	4203(2)	8675(1)	14(1)
C14	3804(1)	3247(2)	9430(1)	18(1)
C15	4796(1)	3289(2)	9606(1)	19(1)
C16	5524(1)	4144(2)	9312(1)	18(1)
C17	5244(1)	4990(2)	8861(1)	15(1)
C18	3528(1)	4102(2)	8969(1)	14(1)
C19	1653(1)	3349(2)	8842(1)	21(1)
C20	5682(1)	7191(2)	6886(1)	12(1)
C21	6002(1)	8094(2)	6442(1)	15(1)
C22	5897(1)	7479(2)	5925(1)	17(1)
C23	5452(1)	5977(2)	5839(1)	18(1)
C24	5114(1)	5076(2)	6273(1)	17(1)
C25	5238(1)	5670(2)	6793(1)	14(1)
C26	1991(1)	5596(2)	7823(1)	14(1)
C27	2153(1)	5372(2)	7273(1)	16(1)
C28	1419(1)	5846(2)	6900(1)	20(1)
C29	516(1)	6520(2)	7071(1)	21(1)
C30	334(1)	6700(2)	7616(1)	20(1)
C31	1072(1)	6260(2)	7989(1)	17(1)
Cl1	2701(1)	3230(1)	5519(1)	18(1)
O1	2562(1)	3480(2)	6082(1)	36(1)
O2	2951(1)	4725(2)	5262(1)	36(1)
O3	1787(1)	2605(2)	5294(1)	54(1)
O4	3518(1)	2108(2)	5450(1)	46(1)
N1S	7561(1)	6295(2)	8976(1)	32(1)
C1S	8163(1)	6543(2)	9297(1)	22(1)
C2S	8930(2)	6819(2)	9710(1)	31(1)
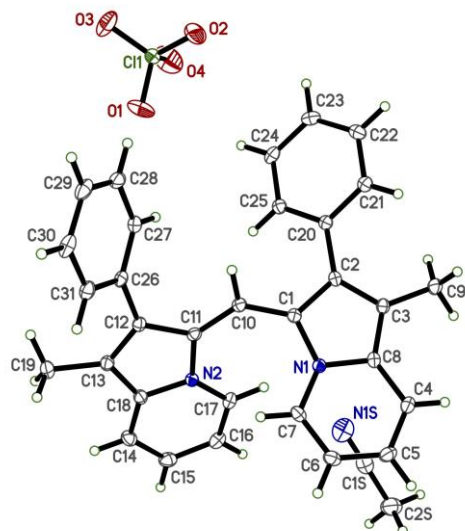
Figure 46. C1 thermal ellipsoid plot at 50% probability for a single **C1** molecule with added

hydrogens.
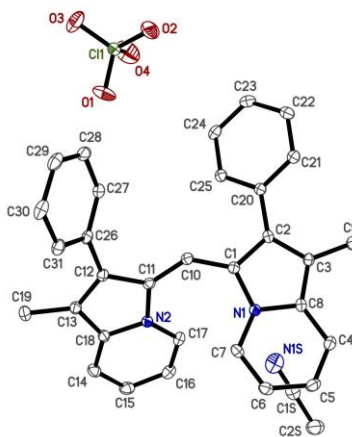
Figure 47. C1 thermal ellipsoid plot at 50% probability for a single **C1** molecule.
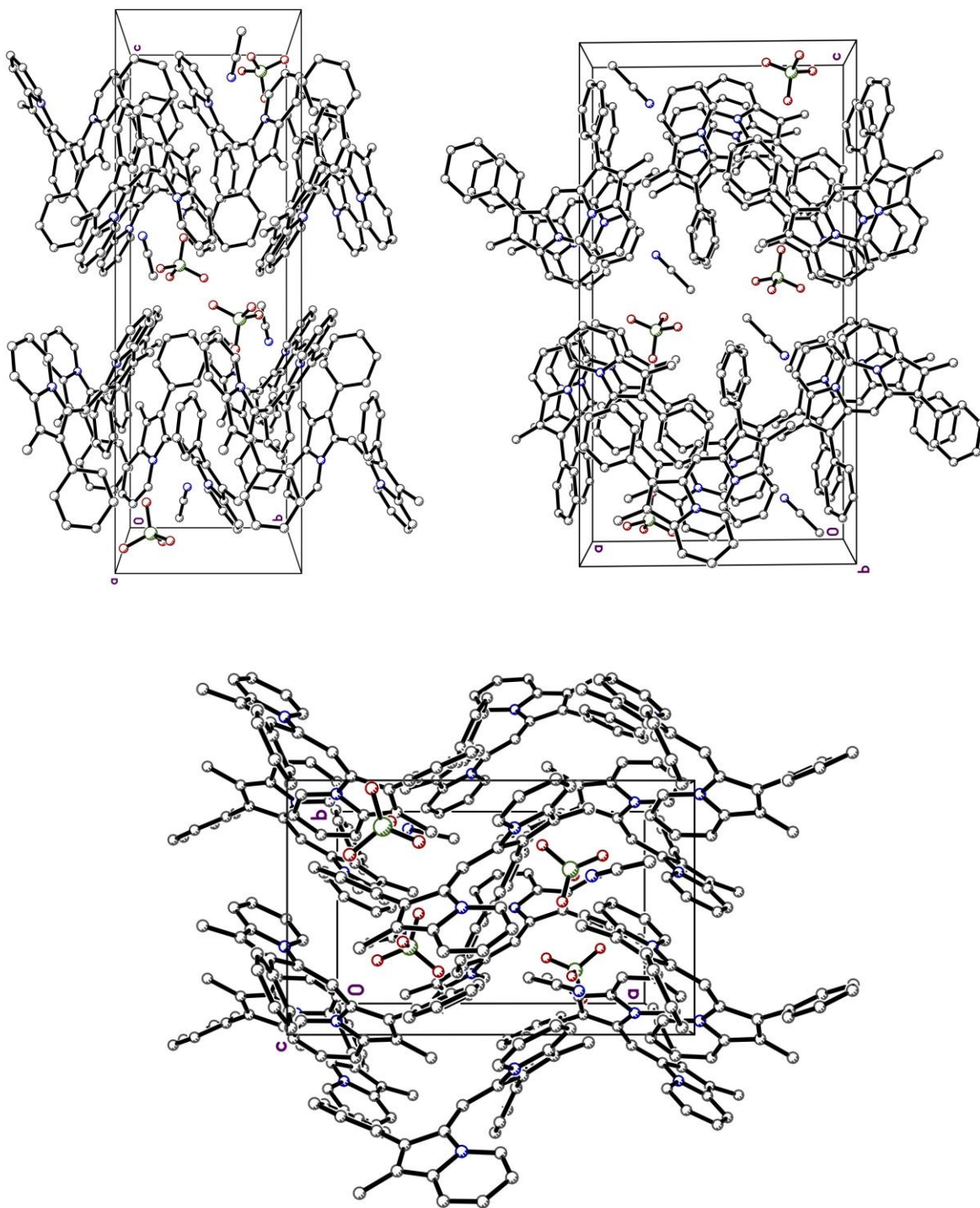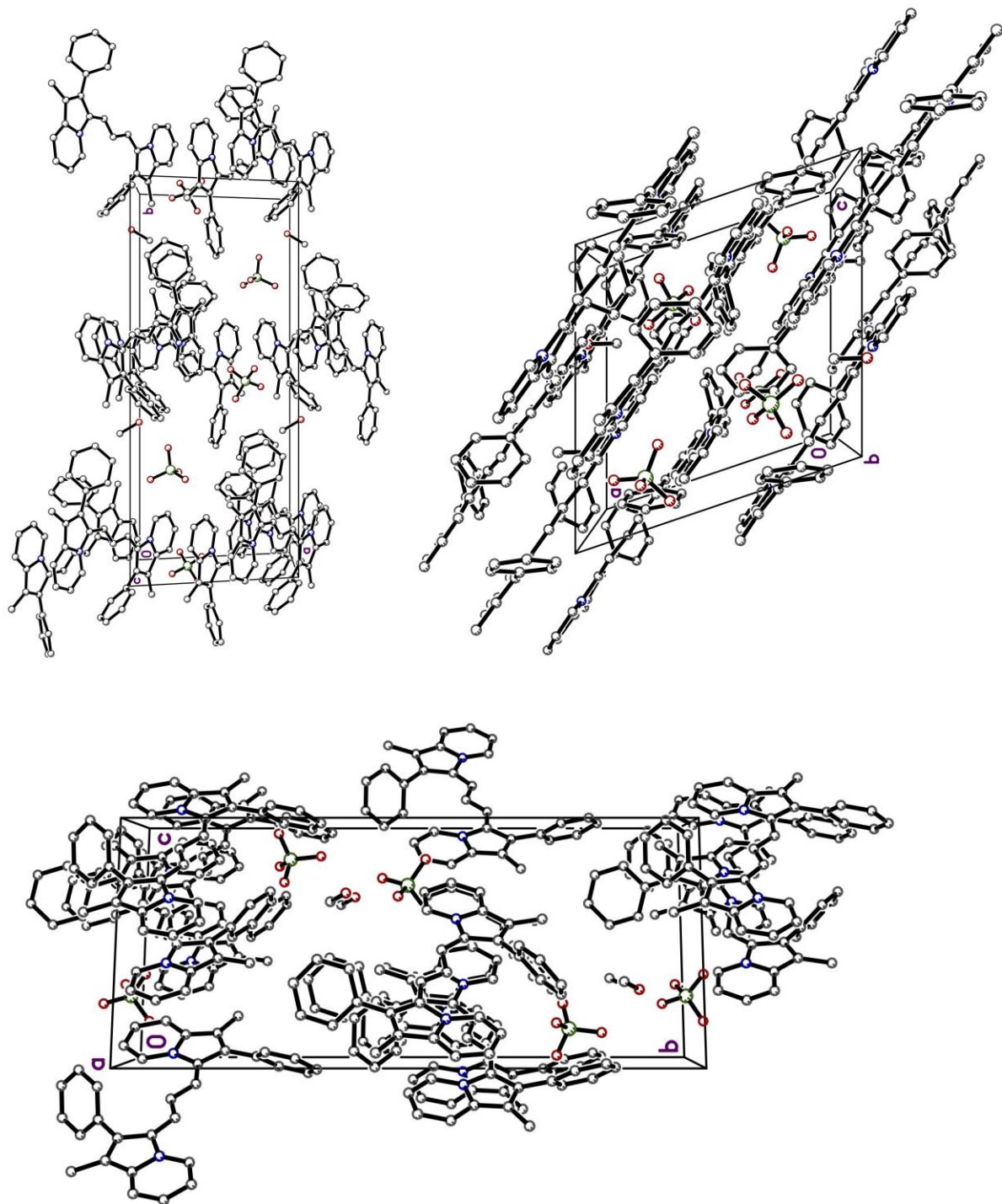
Figure 48. Crystal packing structure for **C1** from three different perspectives.

Table 35. Crystal data and structure refinement for **C3**.

Identification code	m18106s
Empirical formula	C33.50 H29 Cl N2 O4.50
Formula weight	567.04
Temperature	90.0(2) K
Wavelength	0.71073 A
Crystal system, space group	Monoclinic, P2(1)
Unit cell dimensions	a = 11.2142(6) Å alpha = 90 deg.
	b = 25.3615(11) Å beta = 108.702(2) deg.
	c = 11.4422(7) Å gamma = 90 deg.
Volume	3082.4(3) $Å^3$
Z, Calculated density	4, 1.222 Mg/m^3
Absorption coefficient	0.164 mm^{-1}
F(000)	1188
Crystal size	0.300 x 0.200 x 0.150 mm
Theta range for data collection	2.501 to 27.476 deg.
Limiting indices	-14<=h<=14, -32<=k<=32, -14<=l<=14
Reflections collected / unique	84864 / 14089 [R(int) = 0.0495]
Completeness to theta = 25.242	99.8 %
Absorption correction	Semi-empirical from equivalents
Max. and min. transmission	0.942 and 0.893
Refinement method	Full-matrix least-squares on F^2
Data / restraints / parameters	14089 / 87 / 784
Goodness-of-fit on F^2	1.057
Final R indices [I>2sigma(I)]	R1 = 0.0509, wR2 = 0.1365
R indices (all data)	R1 = 0.0610, wR2 = 0.1436
Absolute structure parameter	0.092(14)
Extinction coefficient	n/a
Largest diff. peak and hole	0.277 and -0.404 $e.A^{-3}$

Table 36. Atomic coordinates (x 10^4) and equivalent isotropic displacement parameters (A^2 x 10^3)

for **C3**. U(eq) is defined as one third of the trace of the orthogonalized Uij tensor.

	x	y	z	U(eq)
N1A	5240(3)	5638(1)	2076(3)	20(1)
N2A	1518(3)	5803(1)	5881(3)	25(1)
C1A	4856(4)	5216(2)	2679(3)	23(1)
C2A	5381(3)	4751(1)	2310(3)	21(1)
C3A	6024(3)	4885(1)	1521(3)	22(1)
C4A	6500(4)	5795(2)	759(3)	24(1)
C5A	6318(4)	6328(2)	845(4)	27(1)
C6A	5586(4)	6515(2)	1547(4)	26(1)
C7A	5057(4)	6176(2)	2152(4)	25(1)
C8A	5966(3)	5450(2)	1394(3)	22(1)
C9A	6714(4)	4535(2)	890(4)	23(1)
C10A	4120(4)	5232(2)	3448(3)	24(1)
C11A	3510(4)	5648(2)	3813(3)	24(1)
C12A	2872(4)	5565(2)	4660(3)	24(1)
C13A	2262(3)	5942(2)	5135(3)	24(1)
C14A	2190(3)	6506(2)	5038(3)	24(1)
C15A	1426(4)	6695(2)	5679(4)	26(1)
C16A	256(4)	6209(2)	6966(4)	31(1)
C17A	-6(4)	5719(2)	7335(4)	32(1)
C18A	501(4)	5263(2)	6959(4)	30(1)
C19A	1261(4)	5308(2)	6237(4)	26(1)
C20A	1012(3)	6252(2)	6216(4)	25(1)
C21A	1111(4)	7256(2)	5878(4)	33(1)
C22A	5237(4)	4210(2)	2711(4)	26(1)
C23A	4797(4)	3812(2)	1834(4)	30(1)
C24A	4700(6)	3294(2)	2214(5)	48(1)
C25A	4999(6)	3175(2)	3416(6)	55(2)
C26A	5441(6)	3560(2)	4307(5)	49(1)
C27A	5565(4)	4082(2)	3957(4)	31(1)
C28A	2898(4)	6847(2)	4430(4)	26(1)
C29A	4223(4)	6832(2)	4820(4)	28(1)
C30A	4889(4)	7159(2)	4290(4)	33(1)
C31A	4244(4)	7511(2)	3338(4)	34(1)
C32A	2936(5)	7529(2)	2956(4)	35(1)
C33A	2271(4)	7204(2)	3503(4)	29(1)

N1B	2813(3)	5923(1)	-470(3)	20(1)
N2B	-995(3)	5924(1)	3274(3)	25(1)
C1B	2285(3)	6372(1)	-82(3)	22(1)
C2B	2731(3)	6817(1)	-585(3)	22(1)
C3B	3490(3)	6650(2)	-1256(3)	22(1)
C4B	4109(4)	5717(2)	-1727(4)	25(1)
C5B	3996(4)	5184(2)	-1493(4)	26(1)
C6B	3282(4)	5035(2)	-761(4)	25(1)
C7B	2685(4)	5396(2)	-261(3)	23(1)
C8B	3533(3)	6090(2)	-1195(3)	21(1)
C9B	4174(4)	6976(2)	-1923(4)	27(1)
C10B	1523(3)	6382(2)	673(3)	22(1)
C11B	1051(4)	5987(2)	1234(3)	24(1)
C12B	245(4)	6105(2)	1908(3)	25(1)
C13B	-279(3)	5748(2)	2529(3)	23(1)
C14B	-224(3)	5181(2)	2650(3)	26(1)
C15B	-857(4)	5031(2)	3447(3)	28(1)
C16B	-2109(4)	5570(2)	4570(4)	32(1)
C17B	-2450(4)	6085(2)	4769(4)	34(1)
C18B	-2021(4)	6507(2)	4234(4)	34(1)
C19B	-1316(4)	6432(2)	3485(4)	29(1)
C20B	-1356(4)	5499(2)	3826(3)	25(1)
C21B	-1063(4)	4490(2)	3846(4)	34(1)
C22B	2462(4)	7370(2)	-360(4)	27(1)
C23B	3443(4)	7730(2)	78(4)	32(1)
C24B	3206(5)	8246(2)	324(5)	40(1)
C25B	1989(6)	8421(2)	135(5)	47(1)
C26B	989(5)	8068(2)	-338(5)	46(1)
C27B	1225(4)	7550(2)	-579(4)	34(1)
C28B	353(4)	4813(2)	1988(4)	29(1)
C29B	-60(4)	4797(2)	692(4)	35(1)
C30B	471(5)	4443(2)	82(5)	45(1)
C31B	1423(6)	4106(2)	734(6)	49(2)
C32B	1835(5)	4118(2)	2014(5)	43(1)
C33B	1298(4)	4470(2)	2640(4)	33(1)
Cl1C	6822(1)	4945(1)	7311(1)	38(1)
O1C	5914(4)	5236(3)	6389(4)	82(2)
O2C	7347(4)	5263(2)	8383(3)	62(1)
O3C	7787(4)	4786(2)	6841(4)	57(1)
O4C	6209(5)	4491(2)	7620(5)	77(1)
Cl1D	2284(8)	2745(3)	8529(6)	40(1)
O1D	1089(9)	2512(6)	8261(17)	108(5)
O2D	3179(11)	2544(4)	9627(8)	64(3)

199

O3D	2150(12)	3303(3)	8678(10)	56(3)
O4D	2733(14)	2651(3)	7530(8)	75(3)
Cl1E	2000(11)	2693(5)	8492(10)	40(1)
O1E	1282(11)	2312(5)	8856(12)	46(3)
O2E	3310(11)	2621(7)	9120(20)	75(6)
O3E	1605(18)	3199(5)	8797(16)	58(4)
O4E	1720(20)	2647(5)	7205(10)	76(5)
C1M	-813(7)	3631(3)	6594(8)	78(2)
O1M	341(4)	3916(2)	6923(4)	62(1)
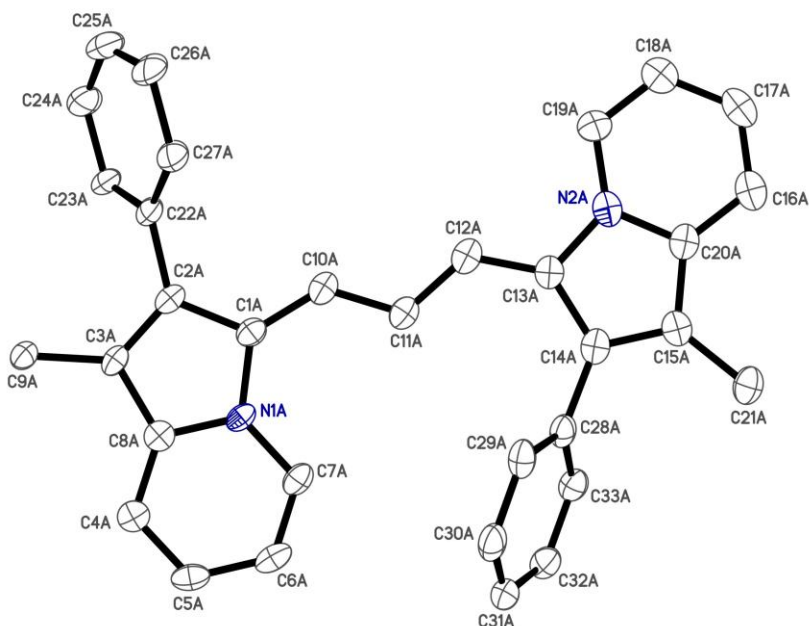
Figure 49. C3 molecule A thermal ellipsoid plot at 50% probability for a single **C3** molecule A.
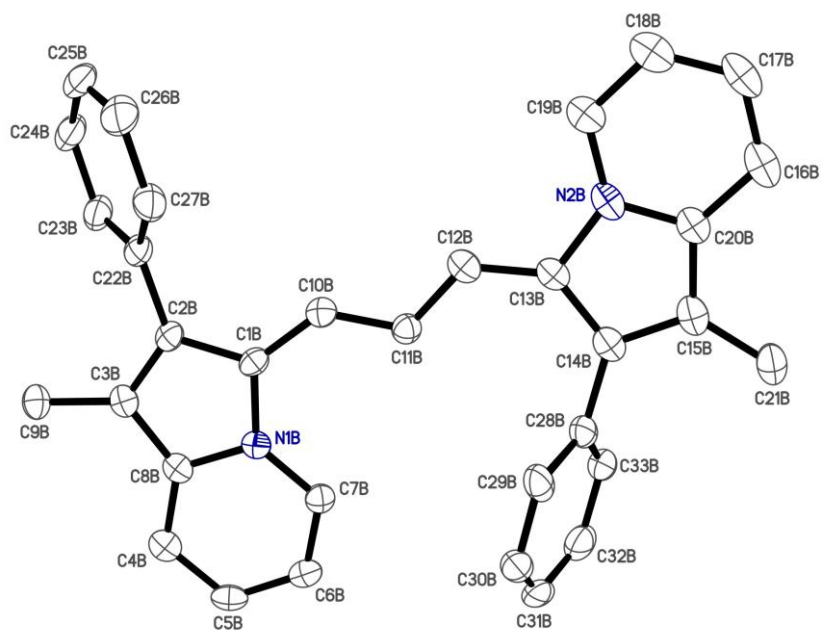
Figure 50. **C3** molecule B thermal ellipsoid plot at 50% probability for a single **C3** molecule B.
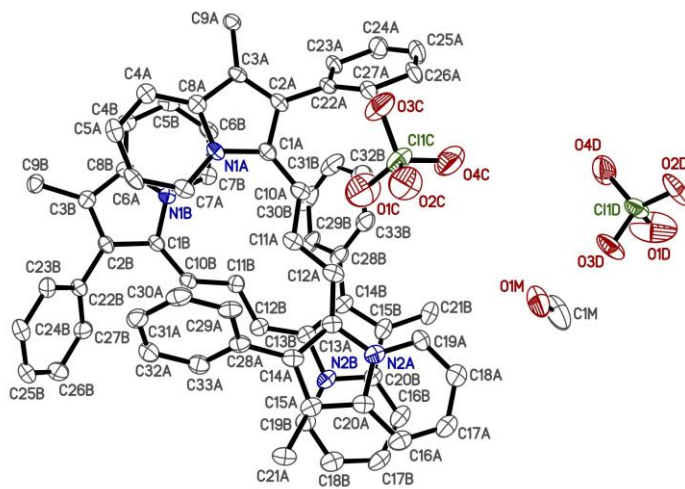
Figure 51. **C3** thermal ellipsoid plot at 50% probability for a molecule A and B of **C3**.
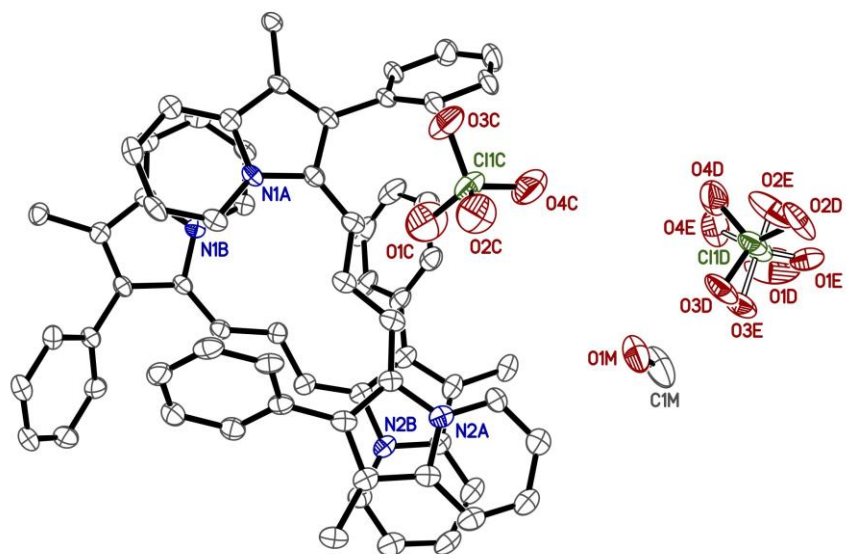
Figure 52. C3 thermal ellipsoid plot at 50% probability for a molecule A and B of **C3** with a reduced atom label count.

Figure 53. Crystal packing structure for **C3** from three different perspectives.

Table 37. Crystal data and structure refinement for **C5**.

Identification code	m18112	
Empirical formula	C37 H32 Cl N3 O4	
Formula weight	618.10	
Temperature	90.0(2) K	
Wavelength	0.71073 Å	
Crystal system, space group	Monoclinic, P2(1)/n	
Unit cell dimensions	a = 8.4563(2) Å	alpha = 90 deg.
	b = 23.5963(5) Å	beta = 99.308(1) deg.
	c = 16.0089(4) Å	gamma = 90 deg.
Volume	3152.31(13) Å^3	
Z, Calculated density	4, 1.302 Mg/m^3	
Absorption coefficient	0.167 mm^{-1}	
F(000)	1296	
Crystal size	0.260 x 0.220 x 0.180 mm	
Theta range for data collection	2.569 to 27.498 deg.	
Limiting indices	-10<=h<=10, -30<=k<=30, -20<=l<=20	
Reflections collected / unique	60046 / 7220 [R(int) = 0.0283]	
Completeness to theta = 25.242	99.8 %	
Absorption correction	Semi-empirical from equivalents	
Max. and min. transmission	0.942 and 0.879	
Refinement method	Full-matrix least-squares on F^2	
Data / restraints / parameters	7220 / 0 / 410	
Goodness-of-fit on F^2	1.032	
Final R indices [I>2sigma(I)]	R1 = 0.0365, wR2 = 0.0954	
R indices (all data)	R1 = 0.0413, wR2 = 0.0994	
Extinction coefficient	0.0026(6)	
Largest diff. peak and hole	0.297 and -0.412 e.Å^{-3}	

Table 38. Atomic coordinates (x 10^4) and equivalent isotropic displacement parameters (Å^2 x 10^3) for **C5**. U(eq) is defined as one third of the trace of the orthogonalized Uij tensor.

	x	y	z	U(eq)
N1	9856(1)	5071(1)	1250(1)	17(1)
N2	71(1)	5210(1)	3757(1)	20(1)
C1	8602(1)	5405(1)	1485(1)	17(1)
C2	9002(1)	5981(1)	1317(1)	18(1)
C3	10409(2)	5994(1)	997(1)	20(1)

C4	12280(1)	5186(1)	669(1)	21(1)
C5	12513(2)	4610(1)	724(1)	22(1)
C6	11396(2)	4266(1)	1051(1)	22(1)
C7	10074(2)	4498(1)	1306(1)	20(1)
C8	10944(1)	5422(1)	950(1)	18(1)
C9	11295(2)	6497(1)	747(1)	28(1)
C10	7326(1)	5168(1)	1801(1)	18(1)
C11	6084(1)	5465(1)	2091(1)	20(1)
C12	4877(1)	5199(1)	2424(1)	20(1)
C13	3696(2)	5502(1)	2765(1)	21(1)
C14	2518(1)	5241(1)	3122(1)	20(1)
C15	1396(1)	5507(1)	3558(1)	19(1)
C16	1330(1)	6054(1)	3924(1)	20(1)
C17	10(2)	6081(1)	4341(1)	23(1)
C18	-2174(2)	5341(1)	4492(1)	26(1)
C19	-2681(2)	4804(1)	4269(1)	28(1)
C20	-1794(2)	4466(1)	3782(1)	28(1)
C21	-437(2)	4670(1)	3535(1)	24(1)
C22	-785(1)	5557(1)	4228(1)	22(1)
C23	-428(2)	6558(1)	4876(1)	32(1)
C24	7995(1)	6477(1)	1455(1)	18(1)
C25	6851(2)	6684(1)	806(1)	26(1)
C26	5841(2)	7122(1)	959(1)	32(1)
C27	5989(2)	7365(1)	1755(1)	31(1)
C28	7142(2)	7168(1)	2400(1)	27(1)
C29	8131(2)	6724(1)	2255(1)	23(1)
C30	2499(2)	6521(1)	3934(1)	23(1)
C31	4124(2)	6441(1)	4236(1)	31(1)
C32	5187(2)	6888(1)	4263(1)	40(1)
C33	4669(2)	7422(1)	3992(1)	40(1)
C34	3062(2)	7510(1)	3713(1)	46(1)
C35	1984(2)	7064(1)	3690(1)	37(1)
Cl1	16221(1)	3539(1)	1313(1)	20(1)
O1	16251(1)	3983(1)	699(1)	26(1)
O2	16436(2)	3002(1)	931(1)	44(1)
O3	17495(1)	3625(1)	2015(1)	34(1)
O4	14716(1)	3548(1)	1609(1)	52(1)
N1S	13194(3)	3832(1)	3628(1)	69(1)
C1S	14064(2)	3478(1)	3561(1)	41(1)
C2S	15206(2)	3029(1)	3492(1)	47(1)
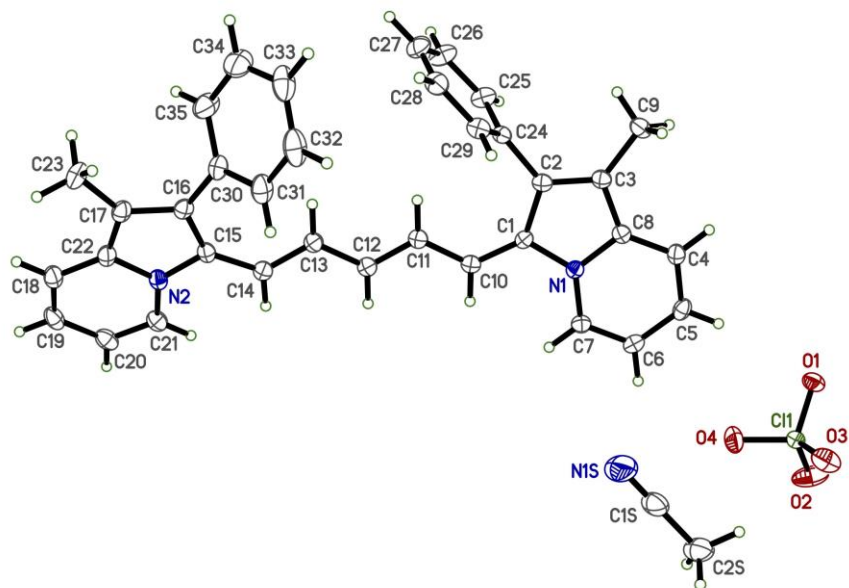
Figure 54. C5 thermal ellipsoid plot at 50% probability for a single **C5** molecule with added hydrogens.
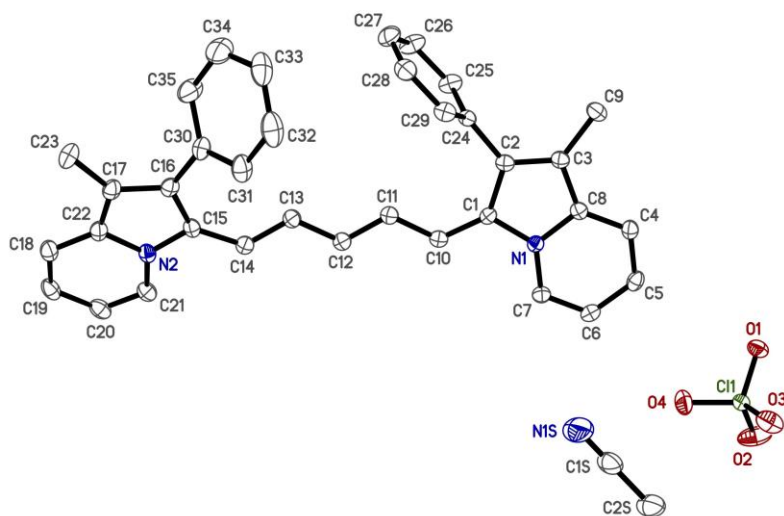
Figure 55. C5 thermal ellipsoid plot at 50% probability for a single **C5** molecule.
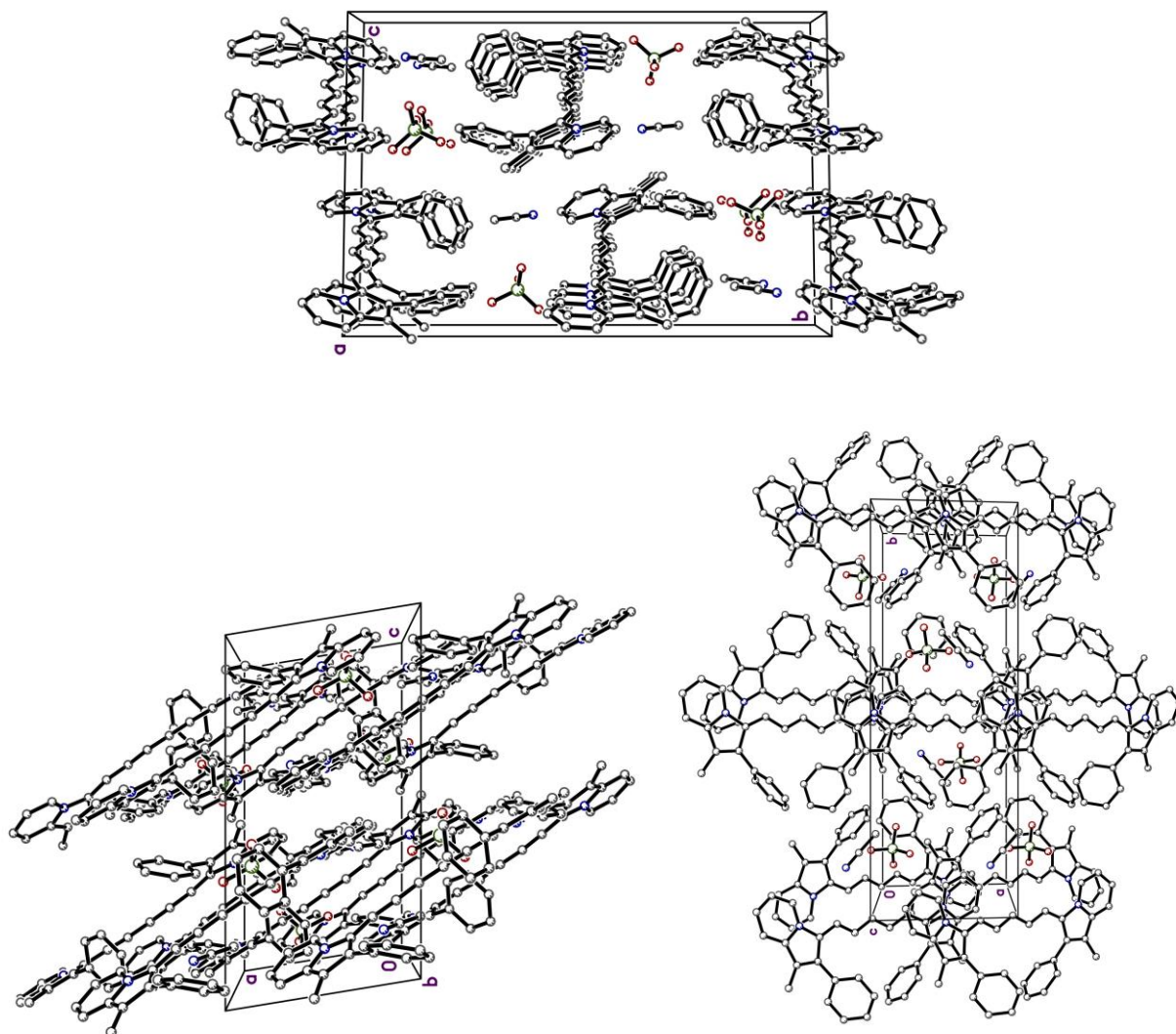
Figure 56. Crystal packing structure for **C5** from three different perspectives.

Table 39. Mulliken charges on NO_3^- atoms.

Atom Number	Atom	Charge
1	N	-0.052098
2	O	-0.315967
3	O	-0.315967
4	O	-0.315967
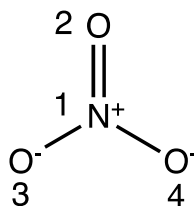
Table 40. Mulliken charges on ClO_4^- atoms.

Atom Number	Atom	Charge
1	Cl	1.351688
2	O	-0.587922
3	O	-0.587922
4	O	-0.587922
5	O	-0.587922
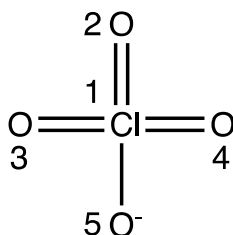
Table 41. Mulliken charges on PF_6^- atoms.

Atom Number	Atom	Charge
1	P	3.403124
2	F	-0.733854
3	F	-0.733854
4	F	-0.733854
5	F	-0.733854
6	F	-0.733854
7	F	-0.733854
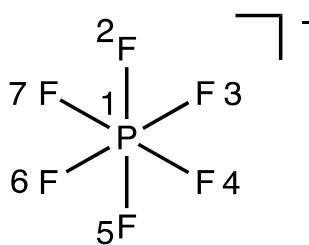
Table 42. Mulliken charges on TFSI atoms.

Atom Number	Atom	Charge
1	S	1.176786
2	C	0.742771

3	F	-0.309487
4	F	-0.294206
5	F	-0.266768
6	N	-0.878432
7	S	1.117281
8	C	0.828531
9	F	-0.315792
10	F	-0.282991
11	F	-0.274752
12	O	-0.556669
13	O	-0.568497
14	O	-0.551996
15	O	-0.565780
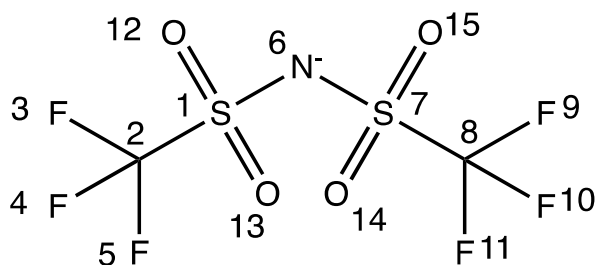
Table 43. Mulliken charges on TPB atoms.

Atom Number	Atom	Charge
1	B	-0.158270
2	C	1.128749
3	C	-0.481455
4	C	-0.418219
5	C	-0.330027
6	C	-0.418219
7	C	-0.481455
8	H	0.178060
9	H	0.145291
10	H	0.143492
11	H	0.145291
12	H	0.178060
13	C	1.128749

14	C	-0.481455
15	C	-0.418219
16	C	-0.330027
17	C	-0.418219
18	C	-0.481455
19	H	0.178060
20	H	0.145291
21	H	0.143492
22	H	0.145291
23	H	0.178060
24	C	1.128749
25	C	-0.481455
26	C	-0.418219
27	C	-0.330027
28	C	-0.418219
29	C	-0.481455
30	H	0.178060
31	H	0.145291
32	H	0.143492
33	H	0.145291
34	H	0.178060
35	C	1.128749
36	C	-0.481455
37	C	-0.418219
38	C	-0.330027
39	C	-0.418219
40	C	-0.481455
41	H	0.178060
42	H	0.145291
43	H	0.143492
44	H	0.145291
45	H	0.178060
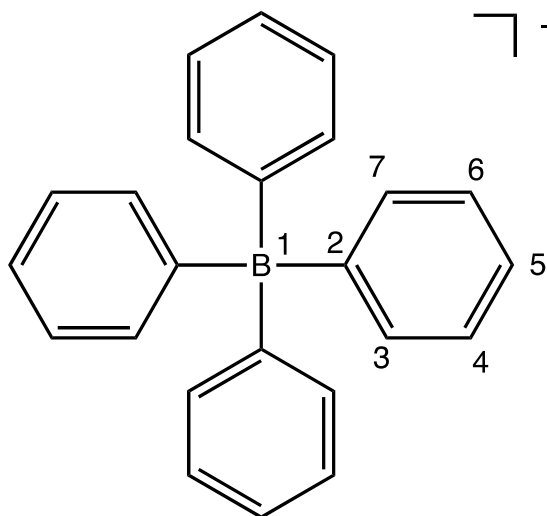
Table 44. Mulliken charges on BARF atoms.

Atom Number	Atom	Charge		Atom Number	Atom	Charge
1	B	0.246940		41	C	-0.341871
2	C	-0.467115		42	H	0.215555
3	C	0.030678		43	C	1.737881
4	C	-1.081474		44	F	-0.269514
5	C	-0.353031		45	F	-0.304927
6	C	-0.525904		46	F	-0.328041
7	C	-0.424496		47	H	0.221053
8	H	0.215602		48	C	1.828482
9	C	1.885359		49	F	-0.271783
10	F	-0.322164		50	F	-0.300031
11	F	-0.302350		51	F	-0.329847
12	F	-0.273043		52	H	0.220930
13	H	0.220926		53	C	-0.391629
14	C	1.771129		54	C	-0.316589
15	F	-0.296042		55	C	-0.740104
16	F	-0.274135		56	C	-0.283551
17	F	-0.332978		57	C	-1.233593
18	H	0.220021		58	C	0.015076
19	C	-0.337231		59	H	0.219623
20	C	0.010444		60	C	1.870671
21	C	-1.091433		61	F	-0.332687
22	C	-0.315577		62	F	-0.271987
23	C	-0.594870		63	F	-0.297009
24	C	-0.373494		64	H	0.220620
25	H	0.215116		65	C	1.887648
26	C	1.752906		66	F	-0.265933
27	F	-0.304481		67	F	-0.303000
28	F	-0.268874		68	F	-0.330092
29	F	-0.327559		69	H	0.214931
30	H	0.220899				
31	C	1.838879				
32	F	-0.272759				
33	F	-0.301823				
34	F	-0.329219				
35	H	0.221551				
36	C	-0.409728				
37	C	-0.022202				
38	C	-1.101163				
39	C	-0.314471				
40	C	-0.573120				

Figure 57. Full spectrum (300-1000 nm) of molar absorptivity and emission plot in MeCN.
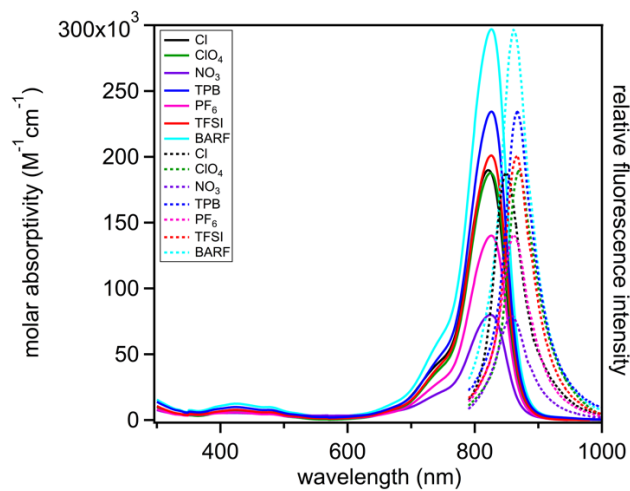
Figure 58. Full spectrum (300-1000 nm) of molar absorptivity and emission plot in DCM.
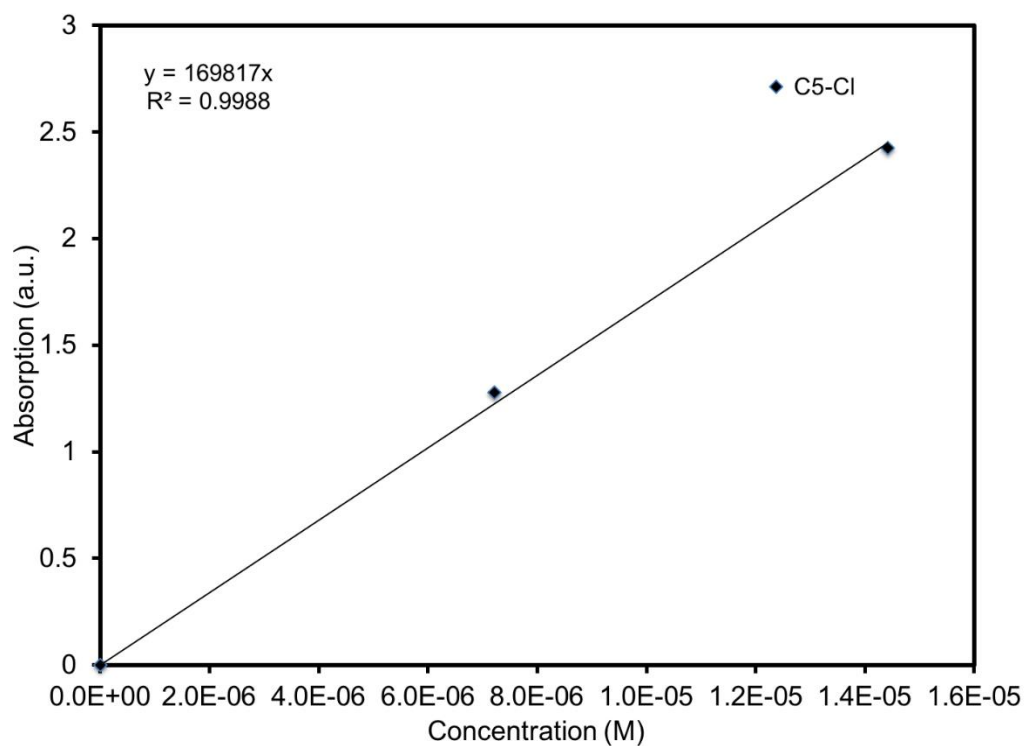
Figure 59. Concentration versus absorbance plot for **C5-Cl** in DCM.
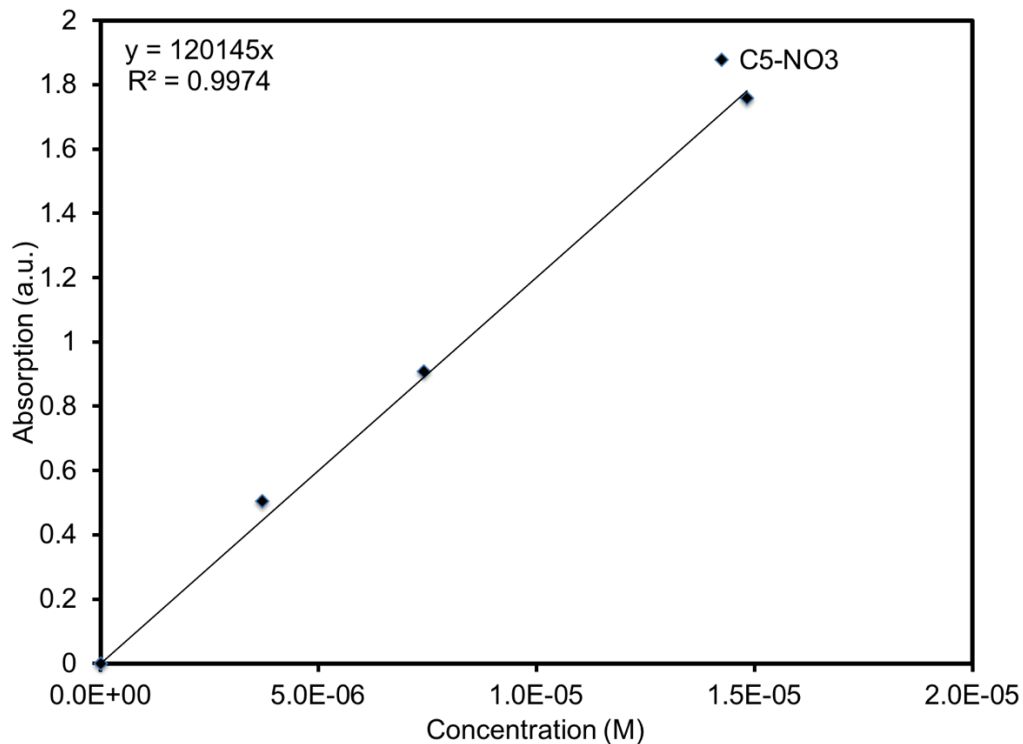
Figure 60. Concentration versus absorbance plot for **C5-NO₃** in DCM.
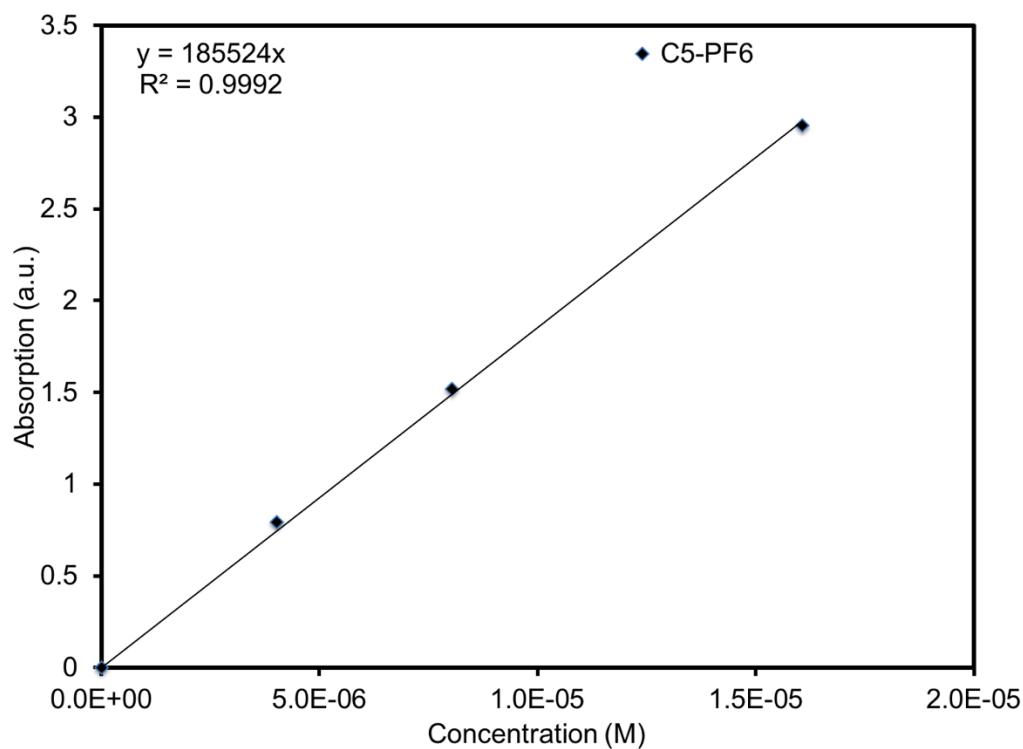
Figure 61. Concentration versus absorbance plot for **C5-PF₆** in DCM.

214
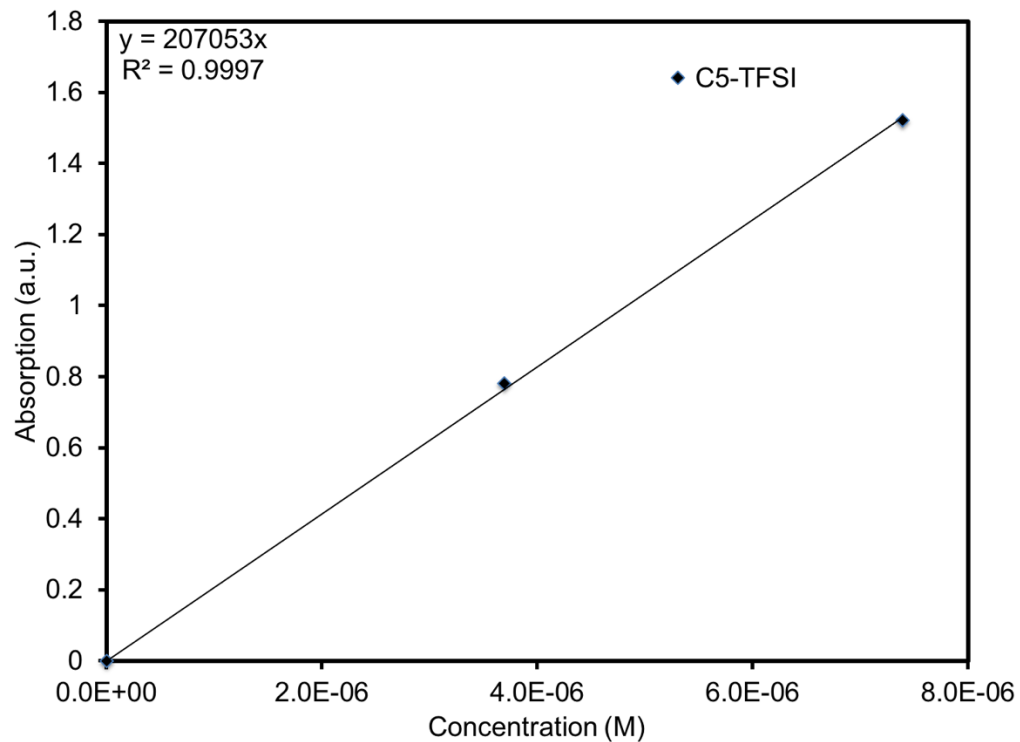
Figure 62. Concentration versus absorbance plot for **C5-TFSI** in DCM.
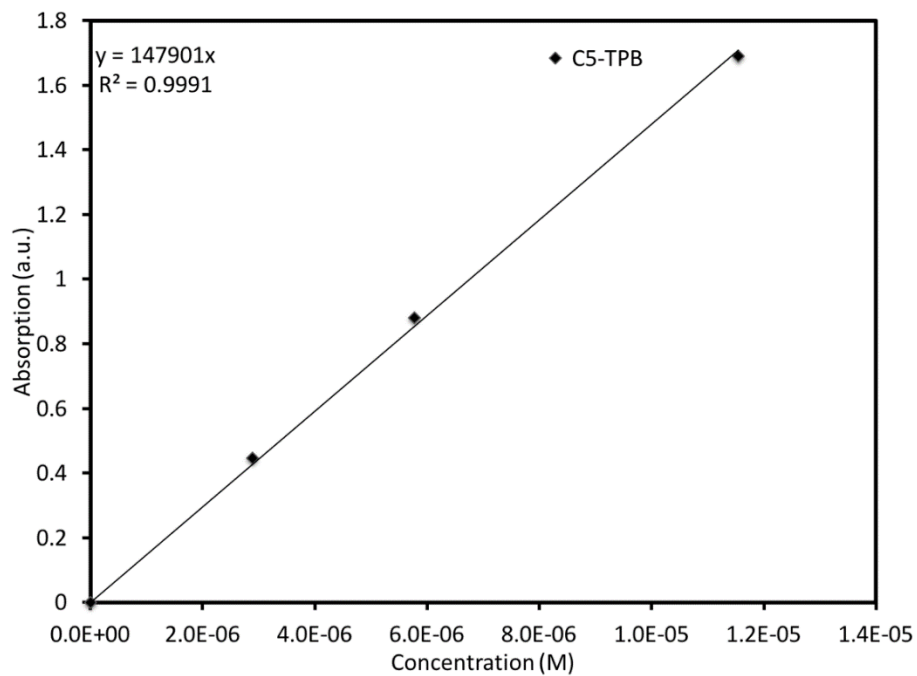
Figure 63. Concentration versus absorbance plot for **C5-TPB** in DCM.

215
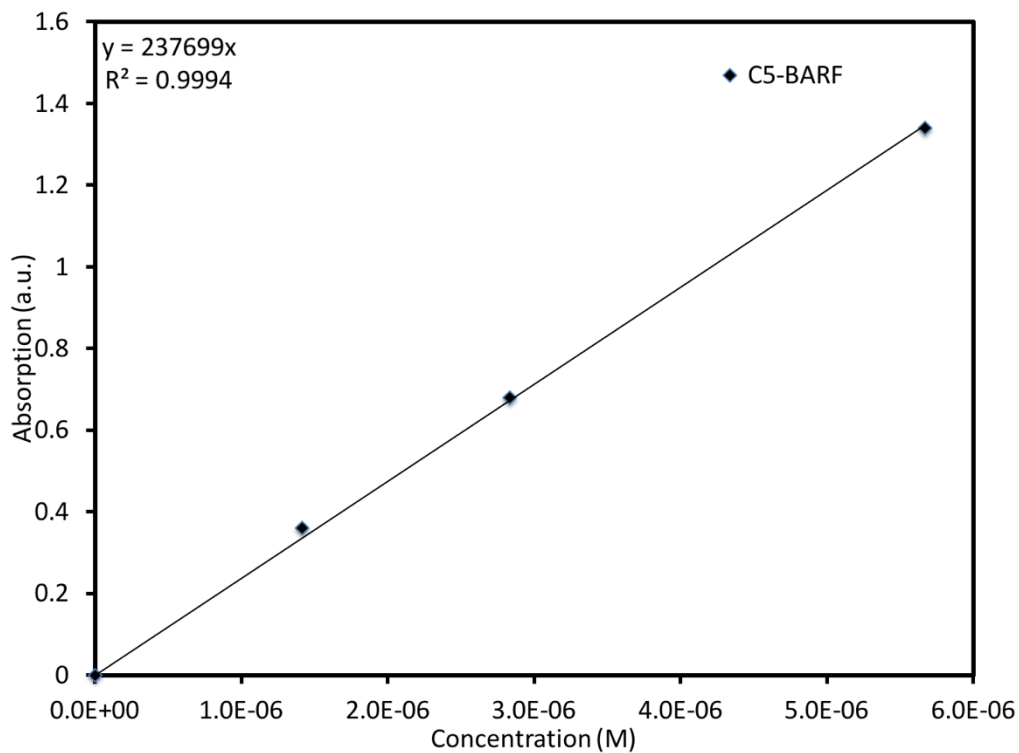
Figure 64. Concentration versus absorbance plot for **C5-BARF** in DCM.
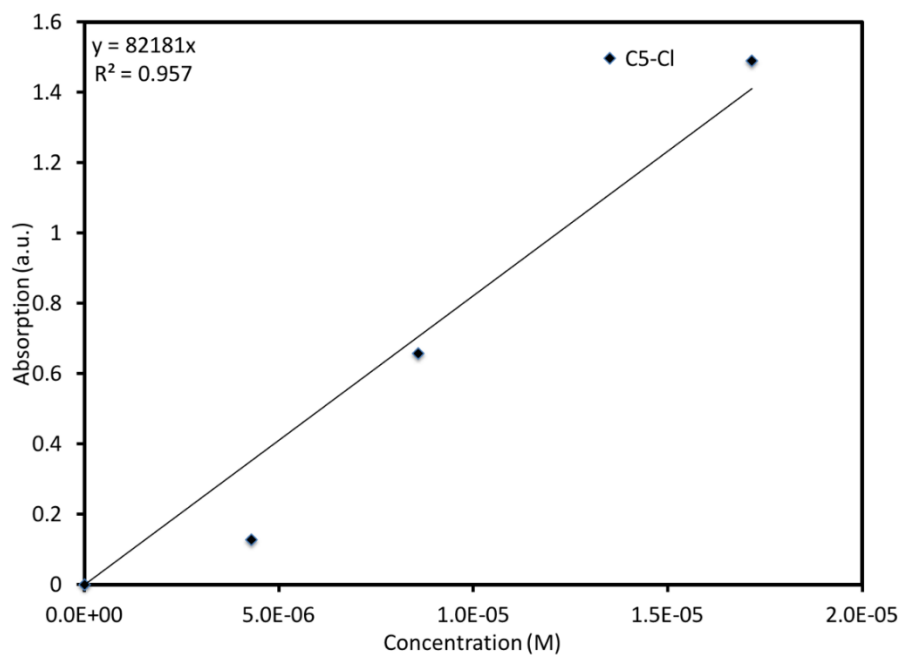
Figure 65. Concentration versus absorbance plot for **C5-Cl** in MeCN. A positive deviation from the Beer-Lambert Law is observed.
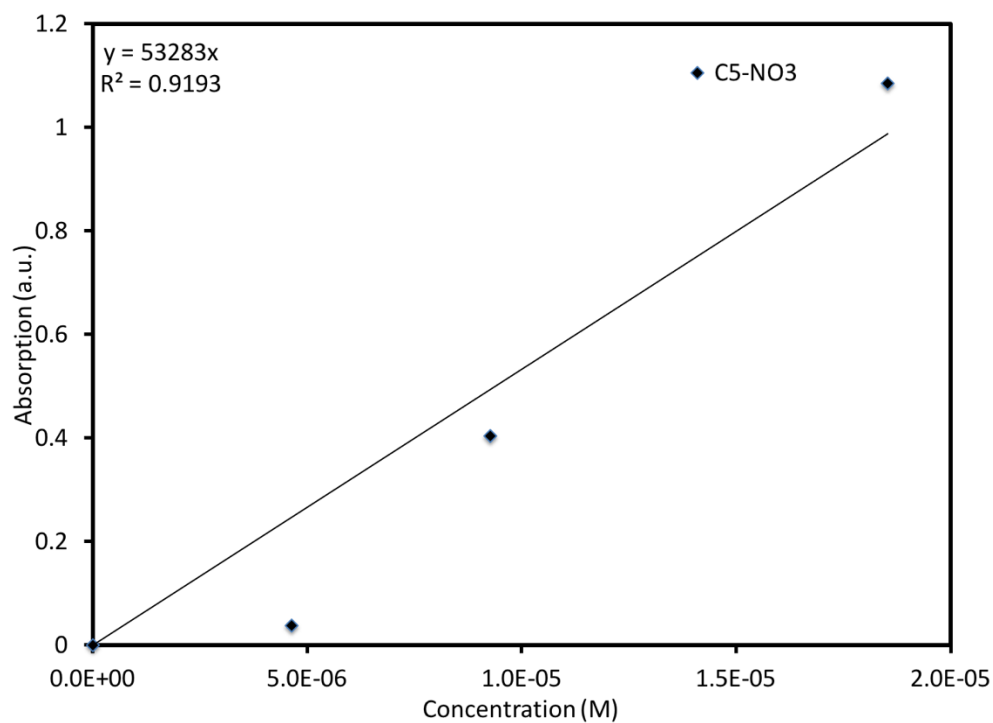
Figure 66. Concentration versus absorbance plot for **C5-NO₃** in MeCN. A positive deviation from the Beer-Lambert Law is observed.
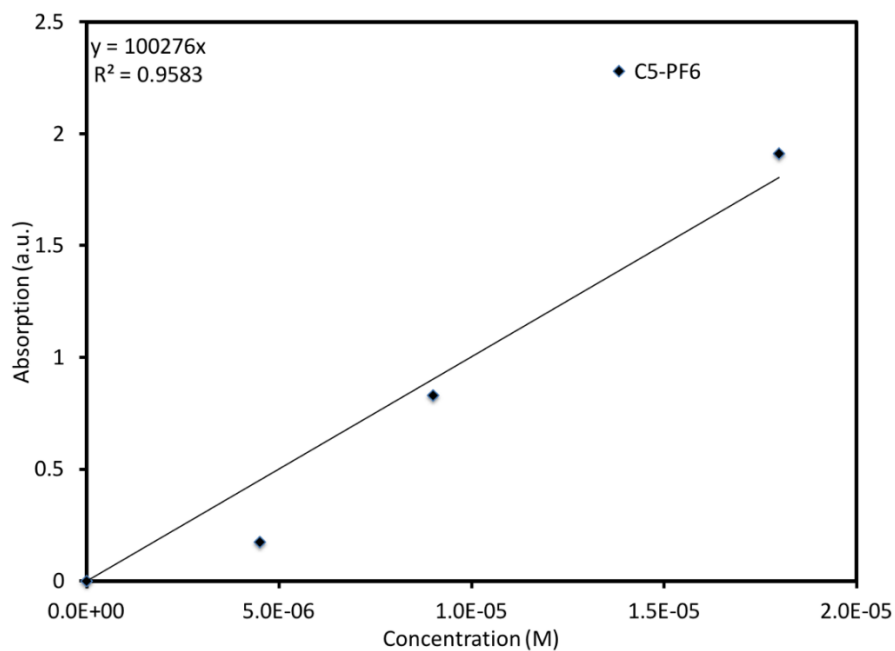
Figure 67. Concentration versus absorbance plot for **C5-PF₆** in MeCN. A positive deviation from the Beer-Lambert Law is observed.
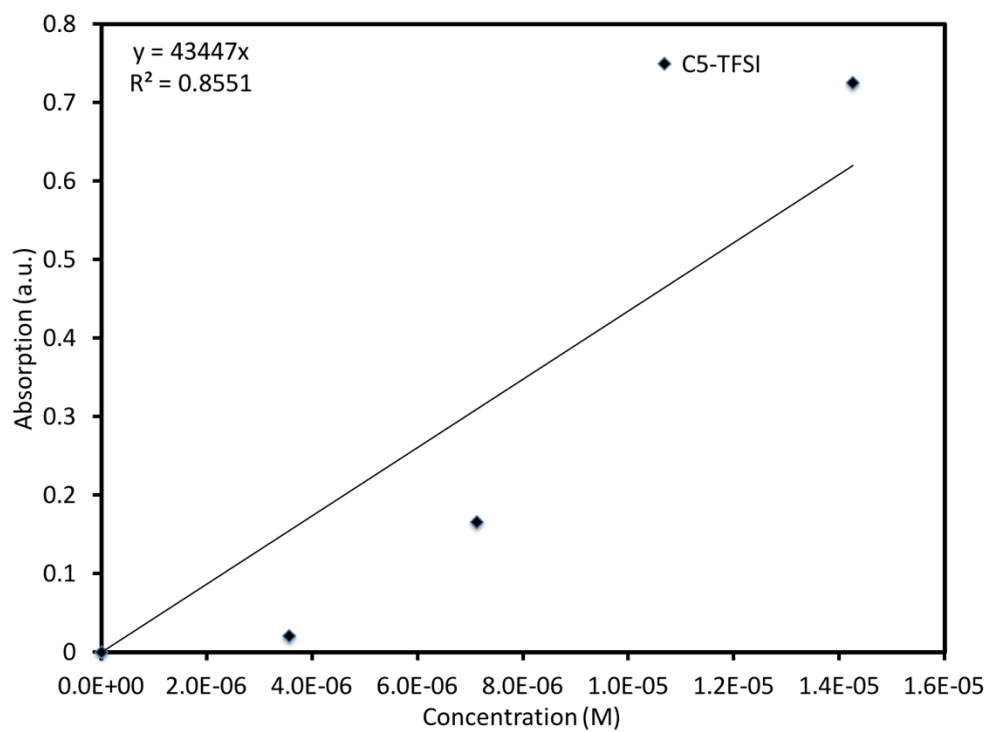
Figure 68. Concentration versus absorbance plot for **C5-TFSI** in MeCN. A positive deviation from the Beer-Lambert Law is observed.
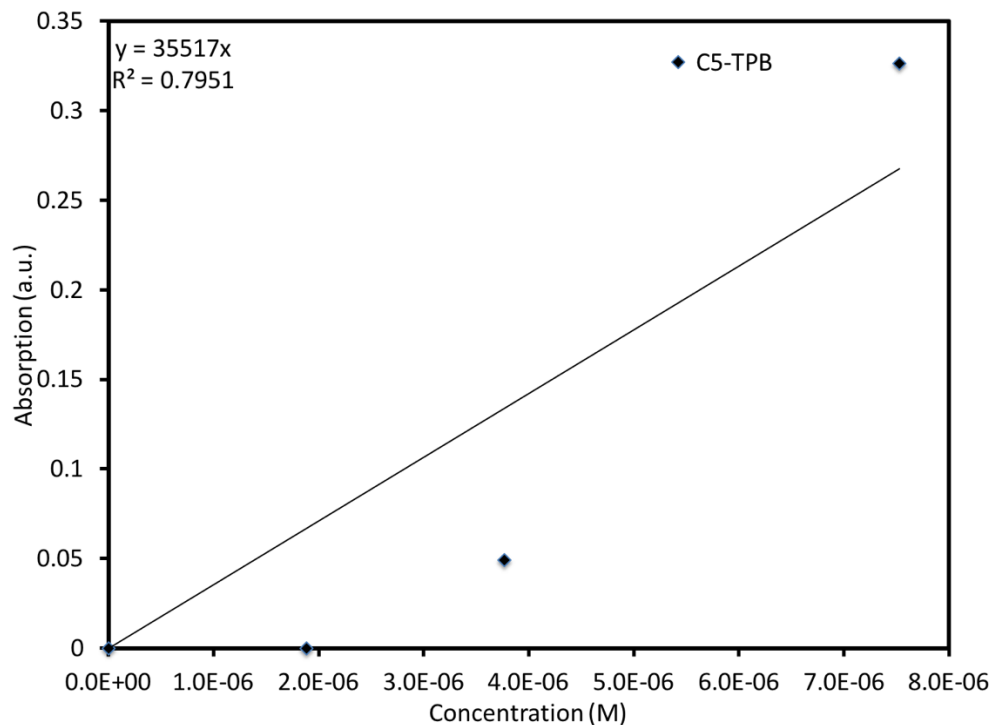
Figure 69. Concentration versus absorbance plot for **C5-TPB** in MeCN. A positive deviation from the Beer-Lambert Law is observed.
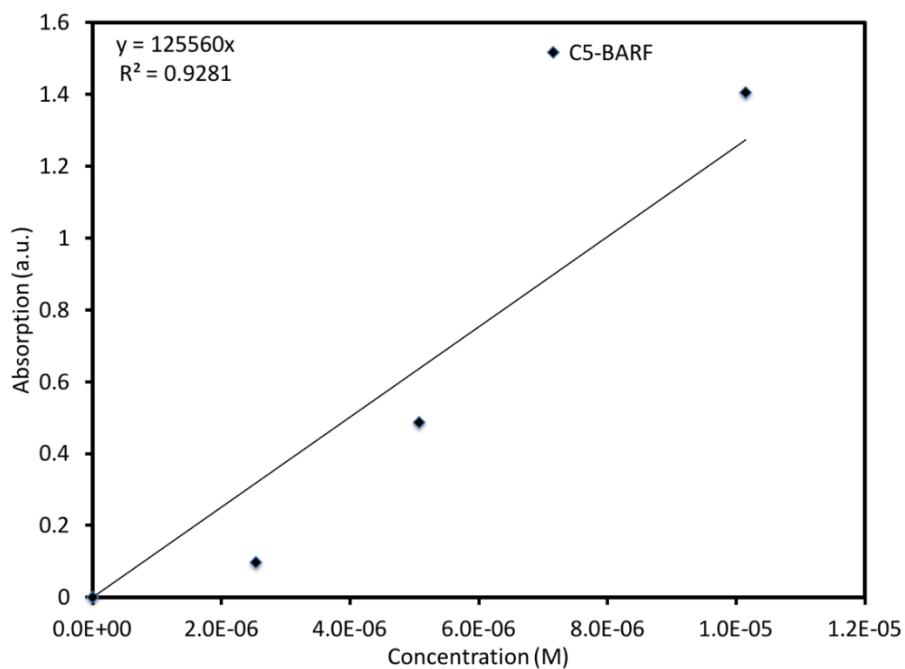
Figure 70. Concentration versus absorbance plot for **C5-BARF** in MeCN. A positive deviation from the Beer-Lambert Law is observed.
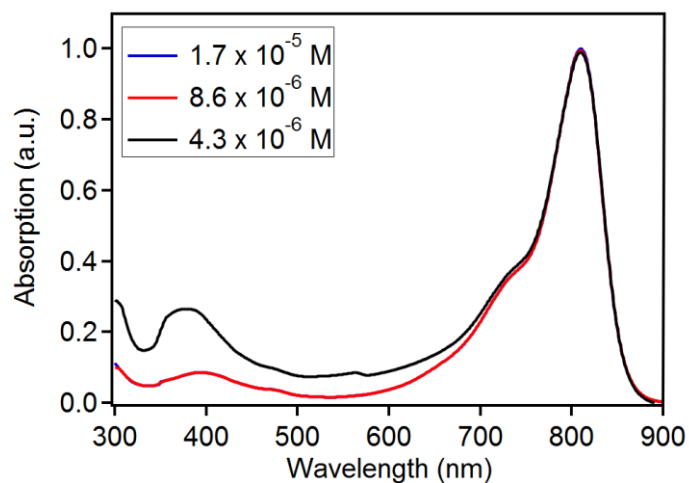
Figure 71. Absorption spectrum of varying concentrations of **C5-Cl** in MeCN showing a change in features as concentration changes.
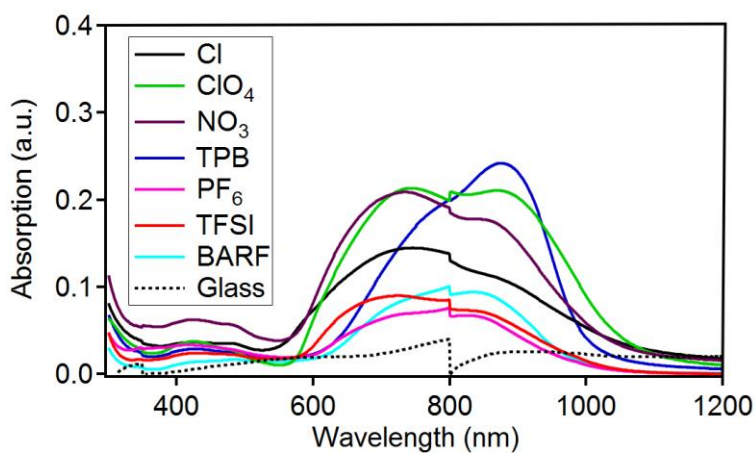
Figure 72. Raw film absorption spectrum not normalized. The blank glass absorption spectrum with no dye is shown for comparison.
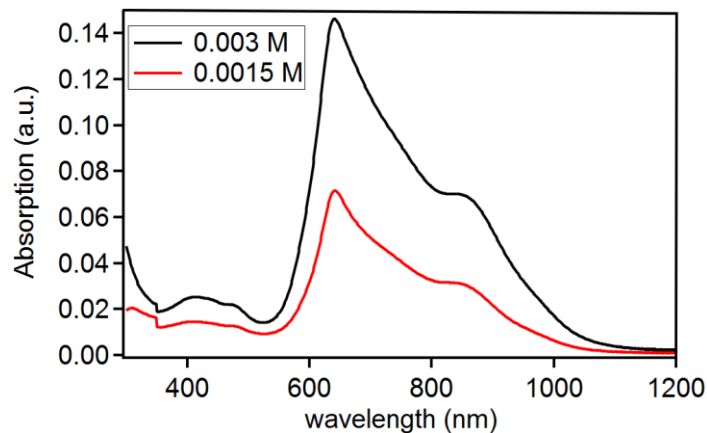
Figure 73. Film absorption with **C5-Cl** on glass prepared with varying concentrations of the dye.
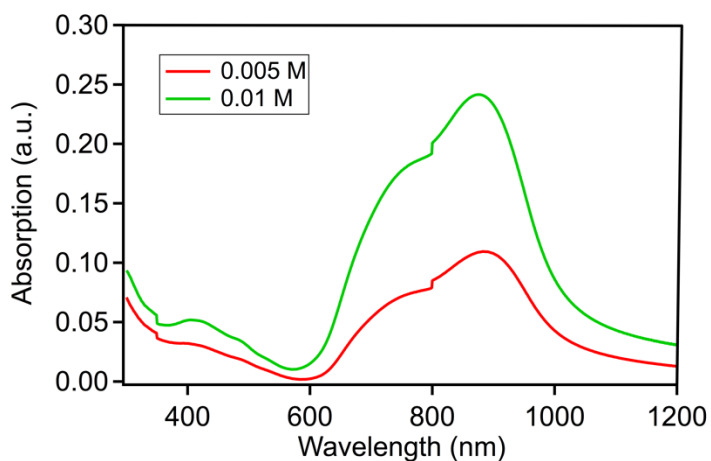
Figure 74. Film absorption with **C5-TPB** on glass prepared with varying concentrations of the dye.
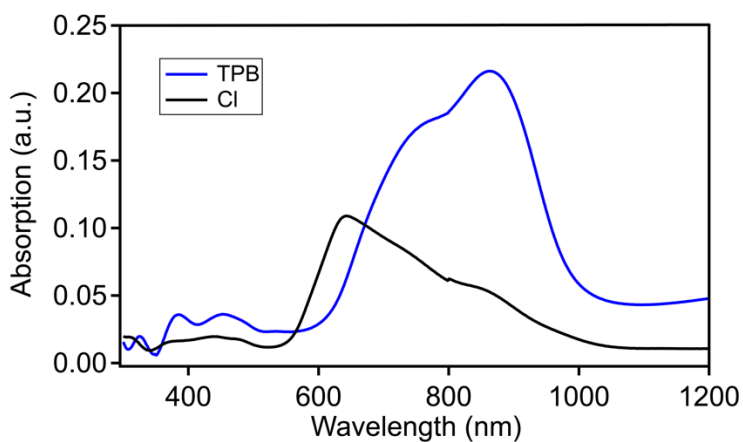
Figure 75. Film absorption with **C5-TPB** and **C5-Cl** on fluorine doped tin oxide (FTO).
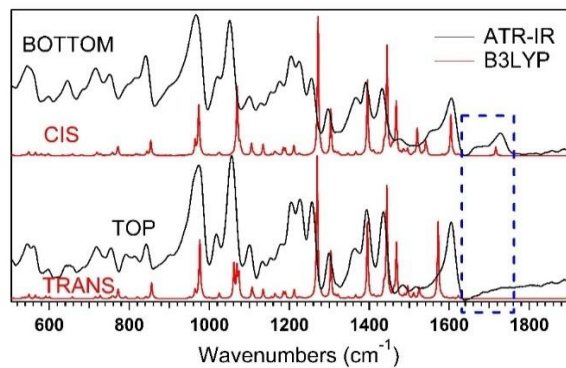
Figure 76. ATR-IR of PyIn$_2$SQ (cis) and PyIn$_2$SQ (trans) compared to computed vibrational spectrum.
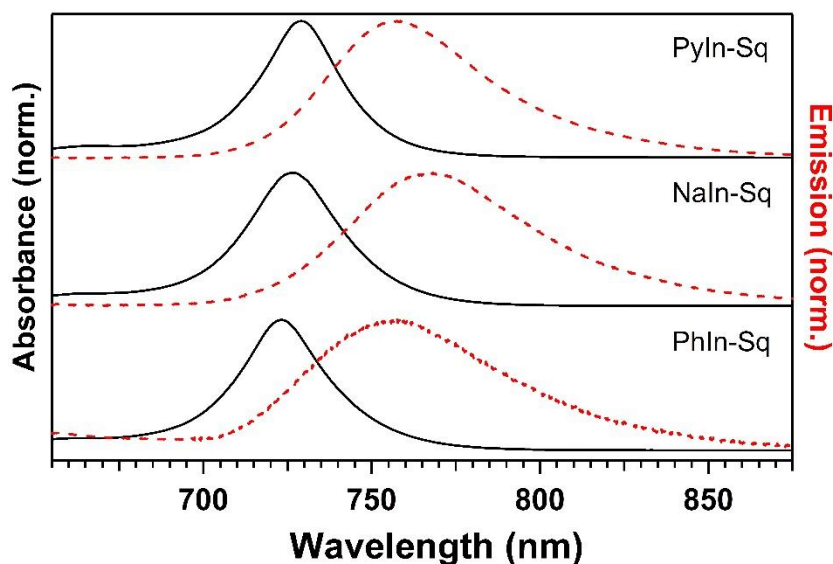
Figure 77. Comparison of NIR absorption spectra (solid black lines) and emission spectra (dashed red lines) for PhIn$_2$SQ, NaphIn$_2$SQ and PyIn$_2$SQ in toluene.
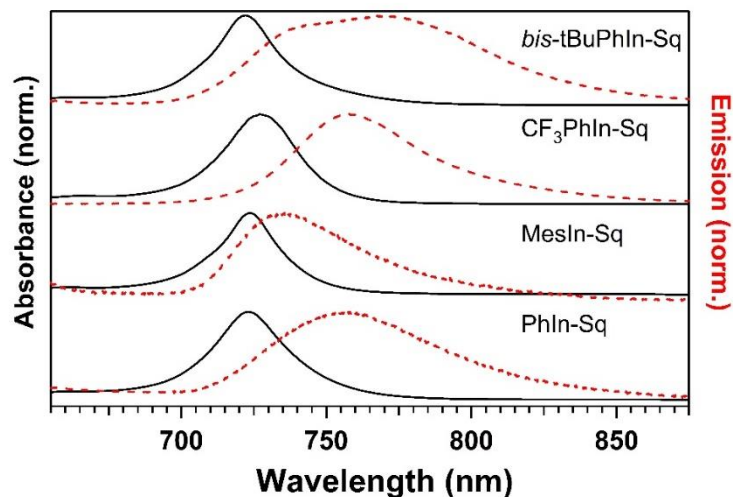
Figure 78. Comparison of NIR absorption spectra (solid lines) and emission spectra (dashed lines) for $PhIn_2SQ$, $MesIn_2SQ$, bis-CF_3In_2SQ and bis-$tBuPhIn_2SQ$ in toluene.
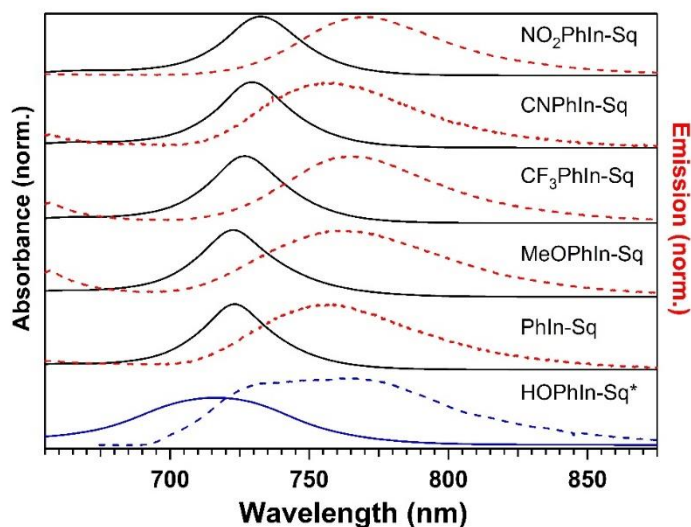
Figure 79. Comparison of NIR absorption spectra (solid black lines) and emission spectra (dashed red lines) for $PhIn_2SQ$, $MeOPhIn_2SQ$, CF_3PhIn_2SQ, $CNPhIn_2SQ$ and NO_2PhIn_2SQ in toluene. *$HOPhIn_2SQ$ spectra taken in DMSO.

223
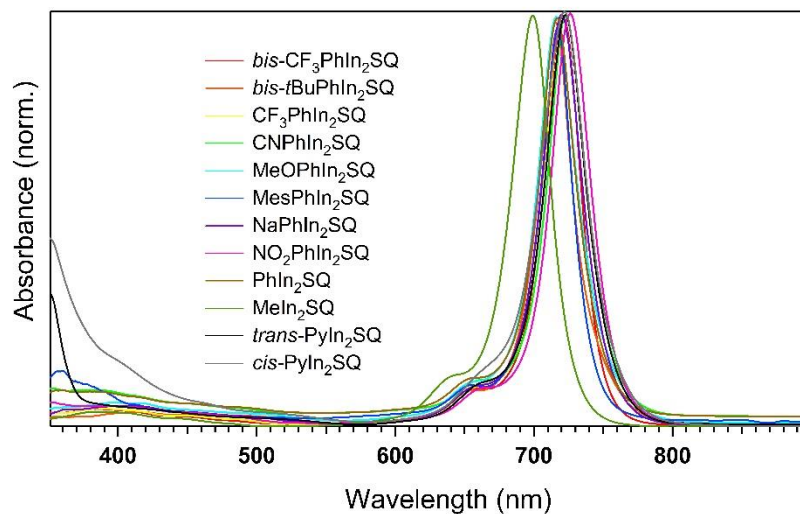
Figure 80. UV-Vis-NIR absorption spectra in dichloromethane (400-1000 nm).
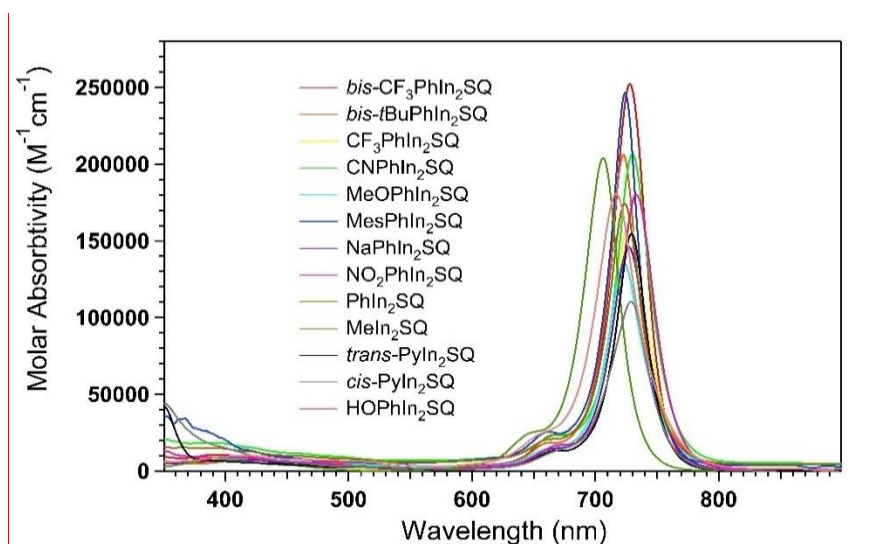
Figure 81. UV-Vis-NIR absorption spectra in toluene (400-1000 nm).

Table 45. UV-Vis-NIR absorption and emission data in DCM.

Dye	Absorption Max. (nm)	Emission Max. (nm)	Stokes Shift (nm, eV)	Φ (%)	τ (ns)
MeIn$_2$SQ	704	744	40, 0.082	1.6	0.17
PhIn$_2$SQ	716	766	50, 0.113	2.1	0.22
NaphIn$_2$SQ	719	767	48, 0.108	4.1	0.25
PyIn$_2$SQ	722	750	28, 0.064	4.8	0.70
PyIn$_2$SQ (trans)	724	749	25, 0.057	4.4	0.57
PyIn$_2$SQ (cis)	723	749	26, 0.060	6.3	0.88
MesIn$_2$SQ	717	731	14, 0.033	0.7	0.22
*Bis-t*BuPhIn$_2$SQ	716	736	20, 0.047	9.5	0.37
Bis-CF$_3$PhIn-$_2$SQ	720	749	29, 0.067	5.4	0.25
CF$_3$PhIn$_2$SQ	720	751	31, 0.071	2.5	0.20
CNPhIn$_2$SQ	723	762	38, 0.085	3.6	0.23
NO$_2$PhIn$_2$SQ	726	764	38, 0.085	3.4	0.25
MeOPhIn$_2$SQ	716	742	26, 0.061	3.0	0.27
HOPhIn$_2$SQ	N/A	N/A	N/A	N/A	N/A
1	639	657	18, 0.045	12.0	2.00
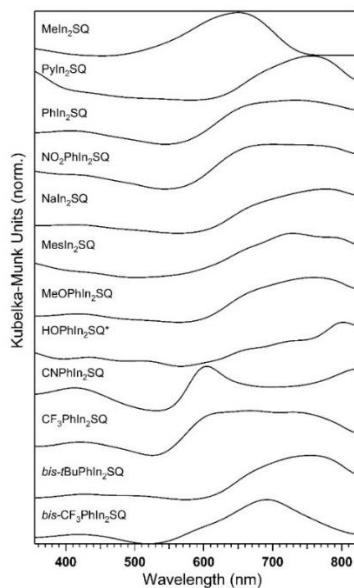
Figure 82. Diffuse reflectance of solid samples.

225
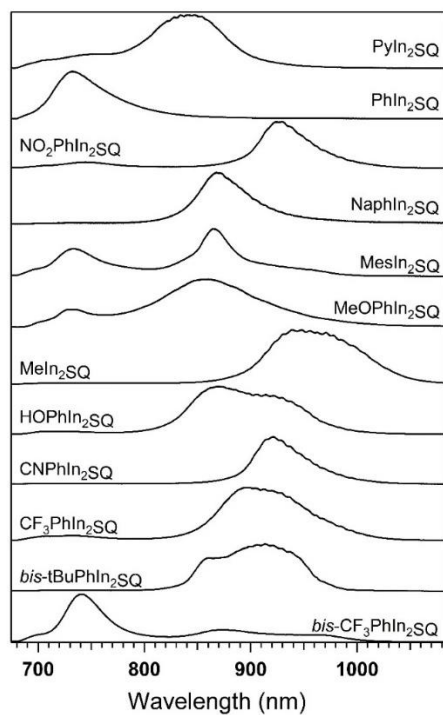
Figure 83. Emission of solid samples.
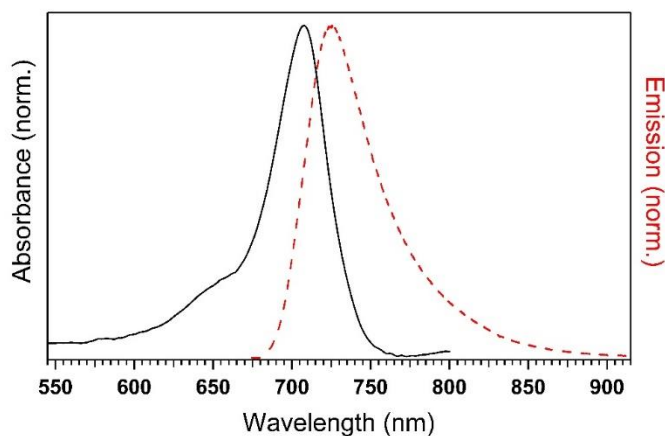
Figure 84. Absorption and Emission of MeIn$_2$SQ in water. Note: The dye was first dissolved in minimal DMSO then water was added to dilute the sample. Directly dissolving the dye in water led to very slow dye dissolving rates.

Table 46. Electrochemical properties in DCM.

Dye	E_g^{opt} (eV)	$E_{(S+/S)}$ (eV) $[E_{(S2+/S+)}]$	$E_{(S-/S)}$ (eV) $[E_{(S2-/S-)}]$	$E_{(S+/S*)}$ (V)
MeIn$_2$SQ	1.68	0.62	-1.38	-1.06
PhIn$_2$SQ	1.65	0.71	-1.54	-0.94
MesIn$_2$SQ	1.66	0.64	-1.55	-1.02
NaphIn$_2$SQ	1.64	0.62	-1.50	-1.02
PyIn$_2$SQ	1.65	0.56 [1.22]	<-2.00	-1.09
MeOPhIn$_2$SQ	1.65	0.54	-1.51	-1.11
HOPhIn$_2$SQ	1.64	0.42	-1.37	-1.22
*Bis-t*BuPhIn-$_2$SQ	1.68	0.58	-1.53	-1.10
CF$_3$PhIn$_2$SQ	1.65	0.63	-1.42	-1.02
Bis-CF$_3$PhIn-$_2$SQ	1.66	0.78	-1.33	-0.88
CNPhIn$_2$SQ	1.65	0.67	-1.49	-0.98
NO$_2$PhIn$_2$SQ	1.64	0.50 [1.21]	-1.47 [-1.79]	-1.14

E_g^{opt} values were taken at the intercept of a tangent line on the low energy side of the max absorption curve and the baseline. $E_{(S+/S)}$ and $E_{(S-/S)}$ measurements were made in dichloromethane solution using a 0.1 M Bu$_4$NPF$_6$ electrolyte and ferrocene as an internal standard. All values are reported vs. ferrocene. $E_{(S+/S*)}$ values were calculated according to the equation $E_{(S+/S*)} = E_{(S+/S)} - E_g^{opt}$.

Table 47. Dihedral angles, orbital contributions to vertical transitions, vertical transition energies and oscillator strengths computed with DFT and TD-DFT analysis at the B3LYP/6-311g(d,p) level.

dye	angle 1 (°)	angle 2 (°)	transition	contrib. (%)	vert. trans. (nm | eV)	oscillator strength	energy (Hartrees)
Ground-State, Trans Geometry							
MeIn$_2$SQ	9	-	H → L	98%	569 | 2.18	1.0118	-1186.8206365
PhIn$_2$SQ	10	62	H → L	90%	607 | 2.04	0.7524	-1570.3700726
			H^{-1} → L	8%			
PyIn$_2$SQ	8	72	H → L	58%	628 | 1.97	0.4171	-2337.5716244
			H^{-1} → L	36%			
			H^{-3} → L	5%			
Excited-State, Trans Geometry							

MeIn$_2$SQ*	25	-	H → L	83%	676 | 1.83	0.5317	-1186.8126123
			H^{-1} → L	14%			
PhIn$_2$SQ*	21	51	H → L	78%	733 | 1.69	0.3689	-1570.362595
			H^{-1} → L	19%			
PyIn$_2$SQ*	13	66	H → L	36%	757 | 1.64	0.0913	-2337.5644349
			H^{-1} → L	58%			
			H^{-3} → L	5%			
Ground-State, Cis Geometry							
MeIn$_2$SQ	0	-	H → L	98%	572 | 2.17	0.9353	-1186.8202437
PhIn$_2$SQ	13	61	H → L	98%	593 | 2.09	0.8464	-1570.369323
PyIn$_2$SQ	2	87	H → L	20%	653 | 1.90	0.1168	-2337.5697768
			H^{-1} → L	72%			
			H^{-3} → L	6%			
Excited-State, Cis Geometry							
MeIn$_2$SQ*	26	-	H → L	83%	676 | 1.83	0.5061	-1186.8128164
			H^{-1} → L	14%			
PhIn$_2$SQ*	25	54	H → L	74%	742 | 1.67	0.3280	-1570.3617374
			H^{-1} → L	23%			
PyIn$_2$SQ*	6	79	H → L	78%	869 | 1.43	0.0136	-2337.5598033
			H^{-1} → L	18%			
			H^{-3} → L	3%			

*Indicates excited-state (S$_1$) optimized geometry. [a]A slight variation in angle on each side of molecule was observed. The number reported is an average of the two angles.

PhIn₂SQ (trans, S₀, geometry optimized at B3LYP/6-311g(d,p) level).

Long Edge **Short Edge** **π-Face**
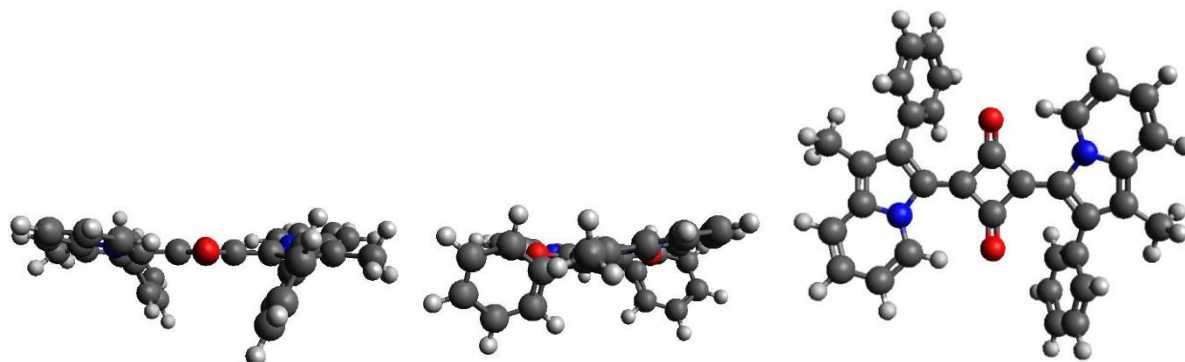
PhIn₂SQ (trans, S₁, geometry optimized at B3LYP/6-311g(d,p) level).

Long Edge **Short Edge** **π-Face**
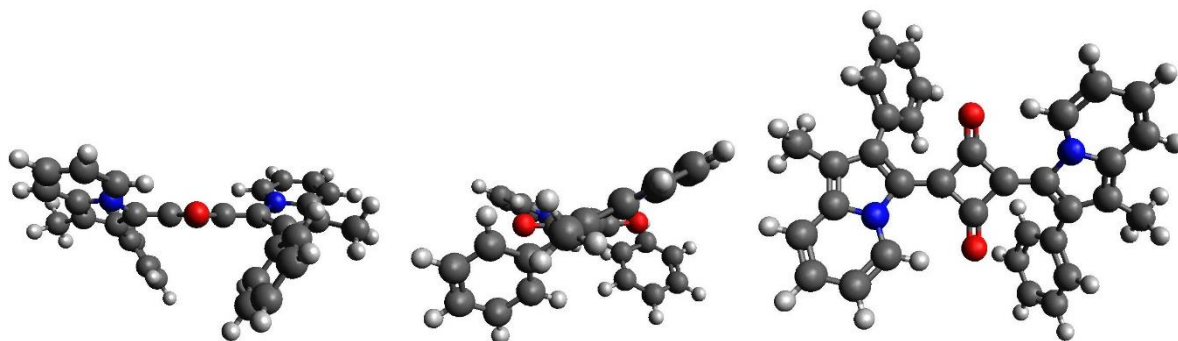
Figure 85. Geometry change perspectives upon photoexcitation.

Table 48. Further optimization of **2a** from xanthene ditriflate
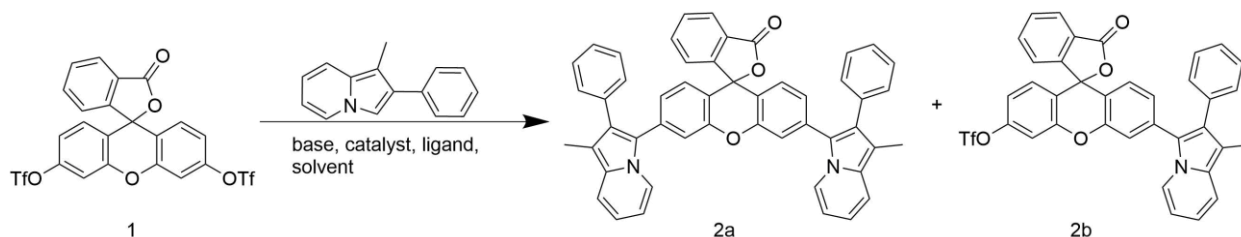
Entry	Catalyst (equiv)	Ligand (equiv)	Base (equiv)	Additive (equiv)	Solvent	Temp (°C)	Time (h)	(%) 2a:2b
1	PdCl₂(PPh₃)₂ (0.1)	None	Cs₂CO₃ (3.0)	None	NMP	80	18	<5
2	PdCl₂(PPh₃)₂ (0.1)	None	KOᵗBu (3.0)	None	NMP	80	18	0
3	PdCl₂(PPh₃)₂ (0.1)	None	NaOᵗBu (3.0)	None	NMP	80	18	0
4	Pd(OAc)₂ (0.1)	(ᵗBu)₂PMeHBF₄ (0.2)	K₂CO₃ (6.0)	PivOH (0.3)	DMA	100	20	0
5	Pd(OAc)₂ (0.1)	XPhos (0.2)	K₂CO₃ (6.0)	PivOH (0.3)	DMA	100	20	0
6	Pd(OAc)₂ (0.05)	BINAP (0.075)	Cs₂CO₃ (3.0)	None	Toluene	100	20	trace
7	Pd(OAc)₂ (0.05)	BINAP (0.075)	Cs₂CO₃ (3.0)	PivOH (0.3)	Toluene	100	20	trace
8	Pd(OAc)₂ (0.05)	BINAP (0.075)	Cs₂CO₃ (3.0)	None	THF	100	20	trace
9	Pd(OAc)₂ (0.05)	BINAP (0.075)	Cs₂CO₃ (3.0)	None	Dioxane	100	20	trace
10	Pd(dba)₃. CHCl₃ adduct (0.1)	XPhos (0.2)	Cs₂CO₃ (3.0)	PivOH (0.3)	THF	100	24	0

Unless otherwise specified, the reaction was carried out in a sealed tube under nitrogen atmosphere in the presence of **1** (0.083 mmol) and 1-methyl-2-phenylindolizine (0.167 mmol), solvent (0.34 – 2.0 mL), catalyst (5 – 10 mol %), base, and additives (pivalic acid) for 12 – 24 h at 80 – 150 °C. Isolated yields (%) were reported for **2a** and **2b**

Table 49. Further optimization of **2a** from dibromo xanthene.
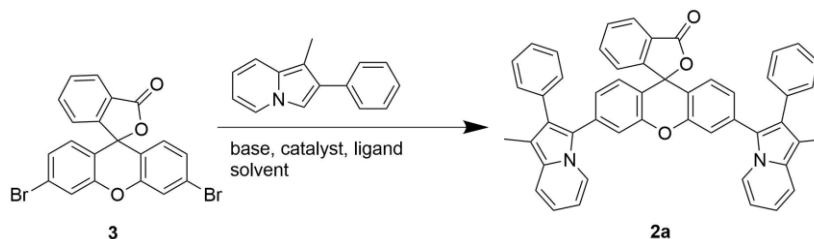
Entry	Catalyst (equiv)	Ligand (equiv)	Base (equiv)	Additive (equiv)	Solvent	Temp (°C)	Time (h)	Yield (%)
1	PdCl$_2$(PPh$_3$)$_2$ (0.1)	None	NaO^{t}Bu (5.2)	None	NMP	80	18	0
2	Pd(OAc)$_2$ (0.05)	(^{t}Bu)$_2$PMeHBF$_4$ (0.1)	K$_2$CO$_3$ (1.5)	PivOH (0.3)	DMA	100	18	0
3	Pd(OAc)$_2$ (0.1)	XPhos (0.2)	KOAc (3.0)	None	DMF	100	18	trace

Unless otherwise specified, the reaction was carried out in a sealed tube under nitrogen atmosphere in the presence of **3** (0.11 mmol) and 1-methyl-2-phenylindolizine (0.24 mmol), solvent (0.34 – 2 mL), catalyst (5 – 10 mol %), base, and additives (PivOH) for 18 – 24 h at 80 – 150 °C. Isolated yields (%) were reported for **2a**.
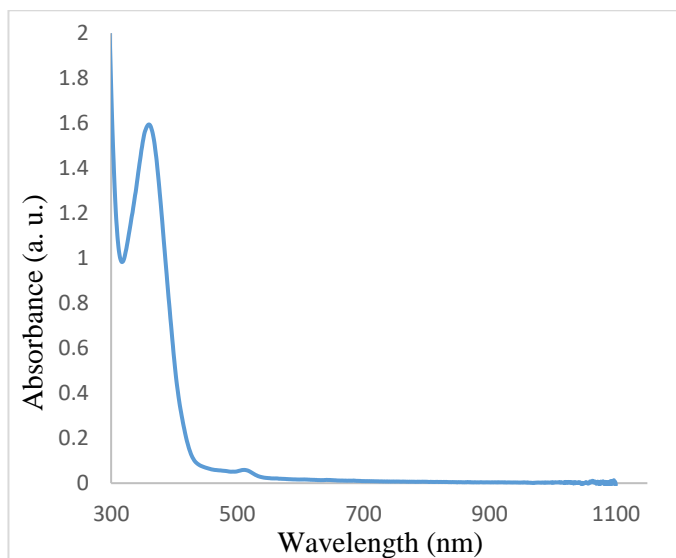
Figure 86. UV absorption of Rhodoindolizine Lactone (**2a**)
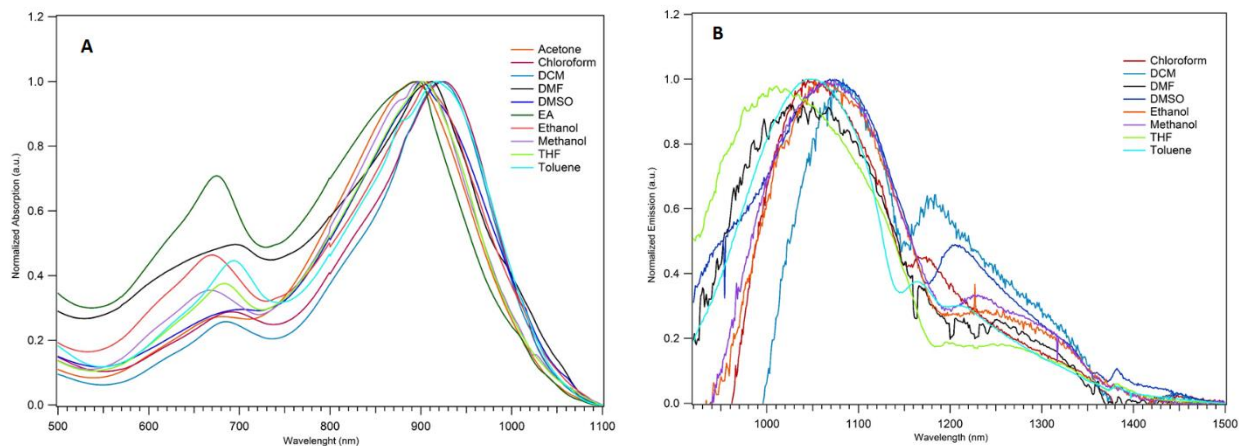
Figure 87. Absorption (A) and Emission (B) spectra for the solvatochromic effects of RhIndz ethyl ester.

Table 50. Solvent effects on the photophysical properties of RhIndz ethyl ester (**10**)

Solvent	Dielectric Constant	Dipole (D)	Abs Max (nm)	Abs Max (eV)	Emission Max (nm)	Emission Max (eV)
Acetone	21	2.88	893	1.388	***	***
Chloroform	4.8	1.04	925	1.340	1051	1.179
DCM	9.1	1.60	921	1.346	1086	1.142
DMF	38	3.82	912	1.359	1041	1.191
DMSO	46.7	3.96	901	1.376	1075	1.153
Ethyl Acetate	6.0	1.78	896	1.384	***	***
Ethanol	24.6	1.69	908	1.365	1071	1.158
Methanol	33	1.70	900	1.378	1073	1.155
THF	7.5	1.75	903	1.373	1014	1.223
Toluene	2.4	0.36	917	1.352	1057	1.173

*** no appreciable emission in these solvents
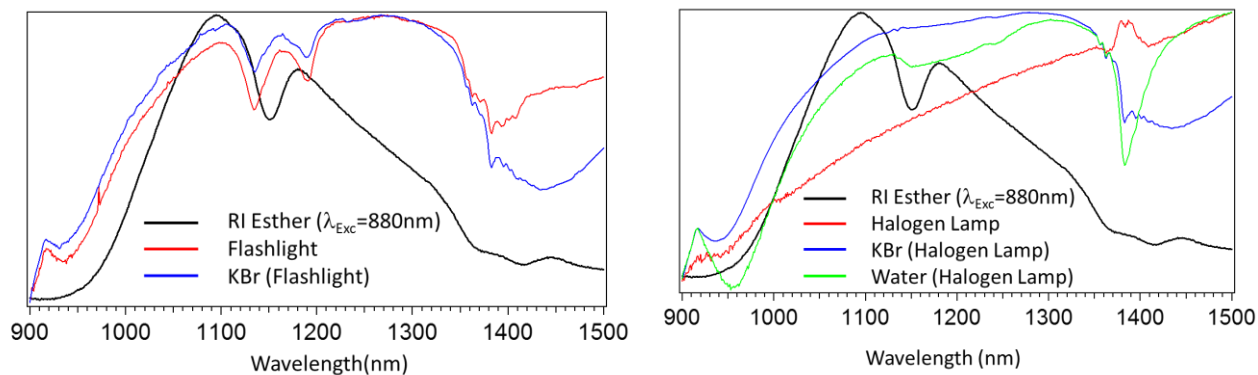
Figure 88. Spectra showing the artifact in the emission spectrum with different light sources.
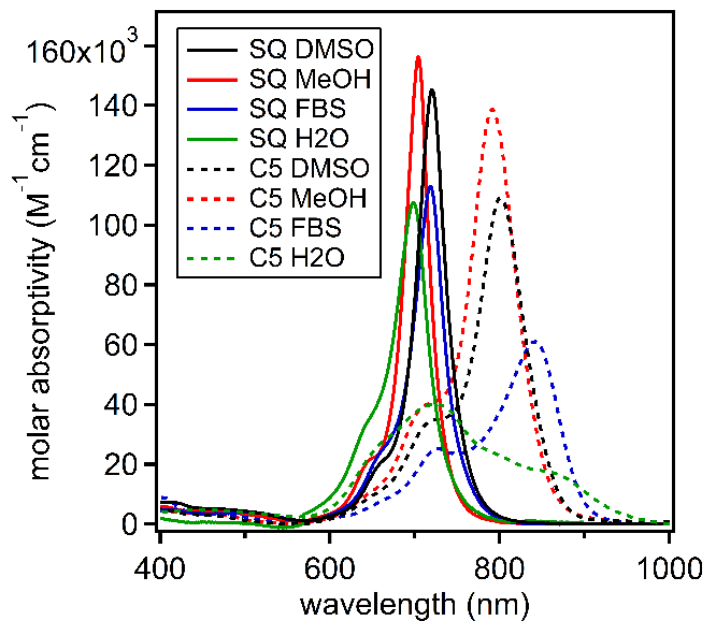
Figure 89. Vis-NIR region molar absorptivity of **SO₃SQ** and **SO₃C5** in DMSO, MeOH, H_2O, and FBS.

Table 51. Solubility of each dye in water, MeOH, and DMSO in mg/mL.

Dye	Water	MeOH	DMSO
SO₃C5	11.0	7.0	21.0
SO₃SQ	11.0	5.8	29.0
ICG	7.8	10.0	18.0
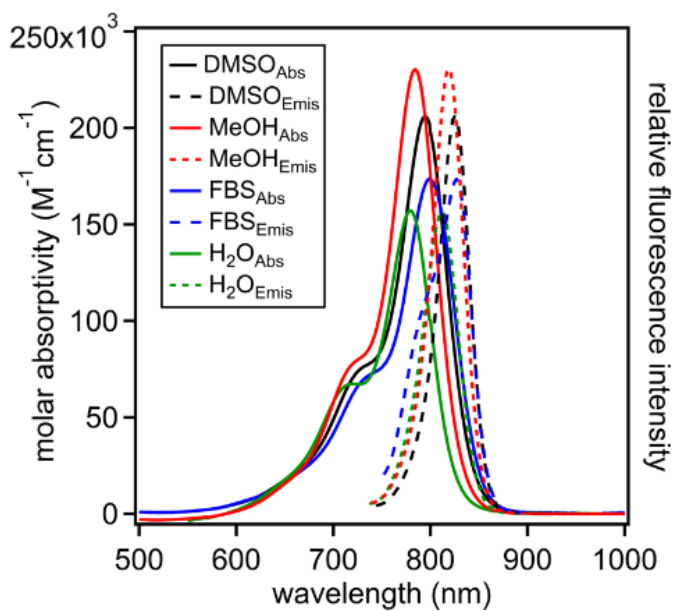
Figure 90. Vis-NIR region molar absorptivity and normalized fluorescence of **ICG** in DMSO, MeOH, H₂O, and FBS.
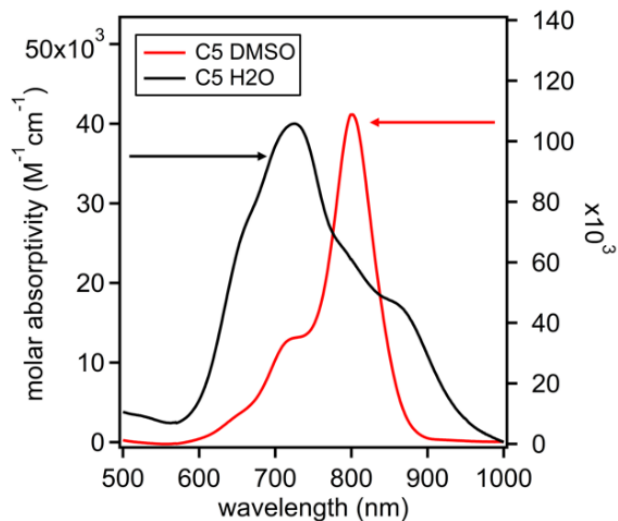
Figure 91. Vis-NIR region molar absorptivity graph of **SO₃C5** in water and DMSO demonstrating the significant aggregate absorption of **SO₃C5** in water. Two different y-axis scales are used due to large different in molar absorptivities with the two solvents.
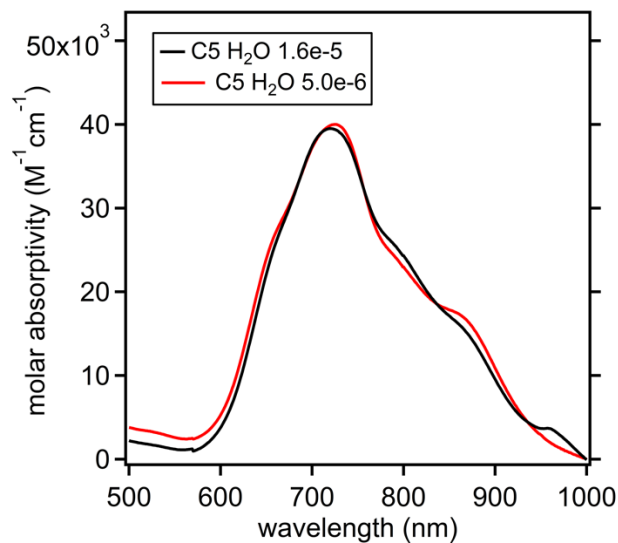
Figure 92. Vis-NIR region molar absorptivity graph of **SO₃C5** in water demonstrating no noticeable concentration dependent aggregation over a ~1 order of magnitude change in concentration.
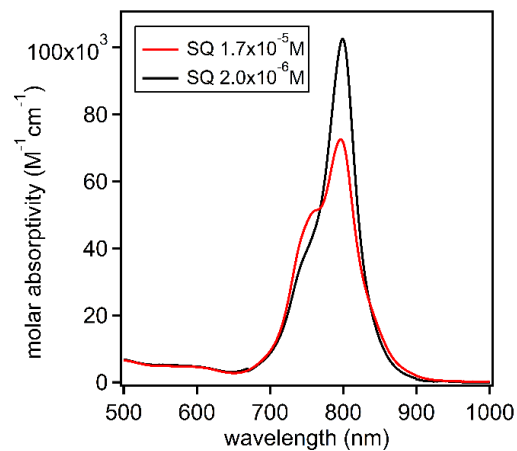
Figure 93. Vis-NIR region molar absorptivity graph of **SO₃SQ** in water demonstrating modest concentration dependent aggregation over a 1 order of magnitude change in concentration.
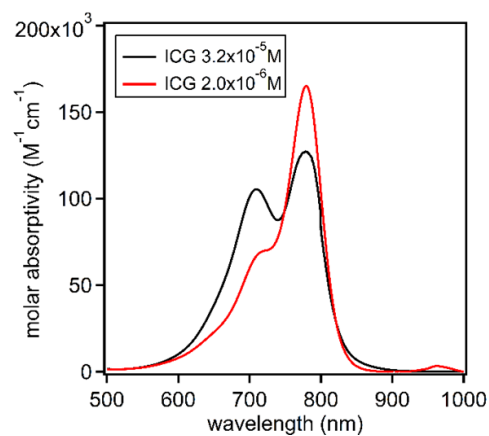
Figure 94. Vis-NIR region molar absorptivity graph of **ICG** in water demonstrating apparent concentration dependent aggregation in over a 1 order of magnitude change in concentration.
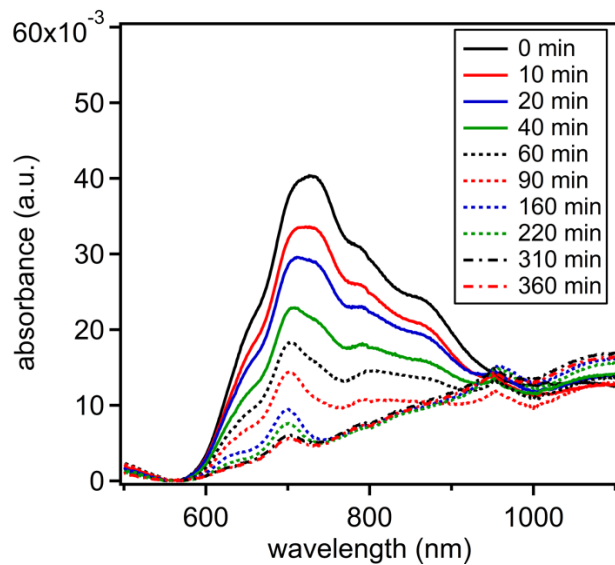
Figure 95. Photostability study with **SO₃C5** in water with continuous white light LED irradiation.
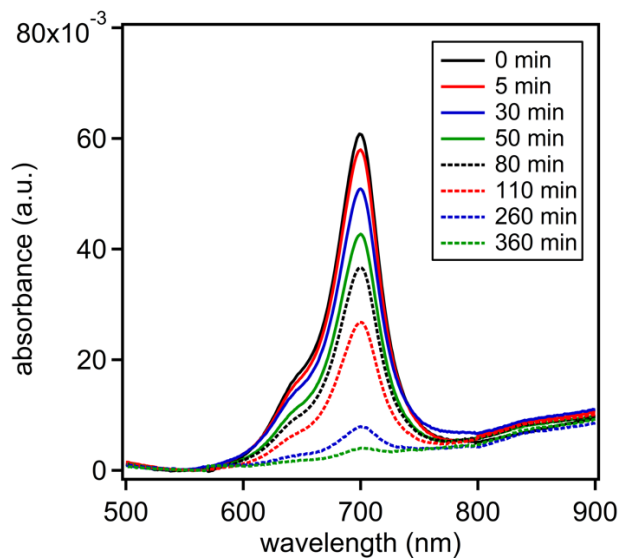
Figure 96. Photostability study with **SO₃SQ** in water with continuous white light LED irradiation.
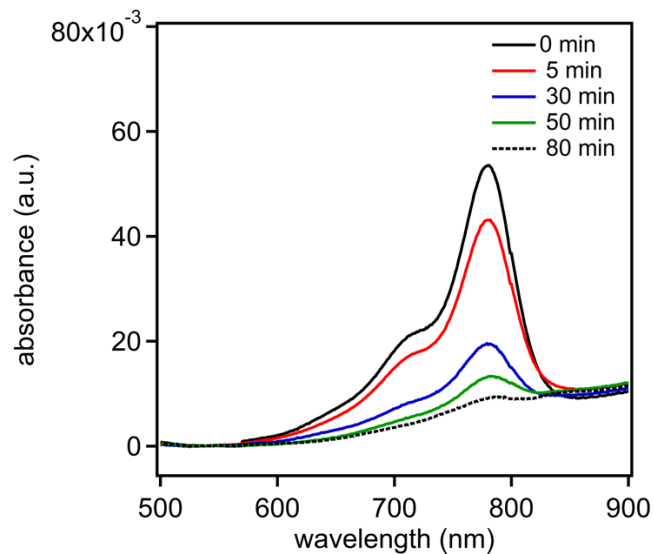
Figure 97. Photostability study with **ICG** in water with continuous white light LED irradiation.
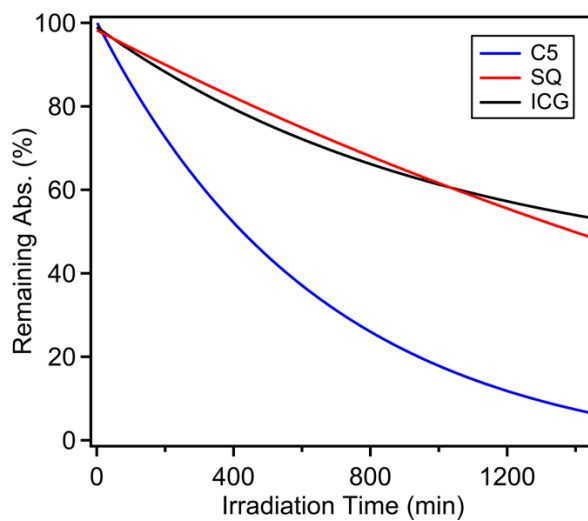
Figure 98. Photostability comparison of **SO₃C5**, **SO₃SQ**, and **ICG** in MeOH with continuous white light LED irradiation.
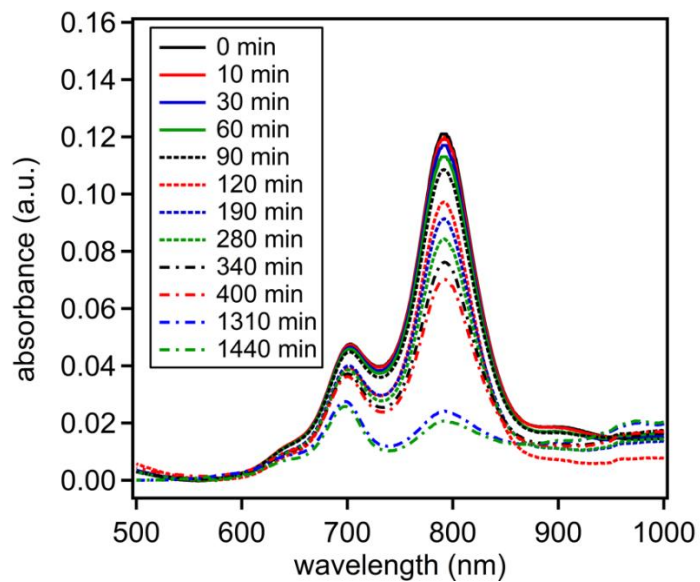
Figure 99. Photostability study with **SO₃C5** in MeOH with continuous white light LED irradiation.
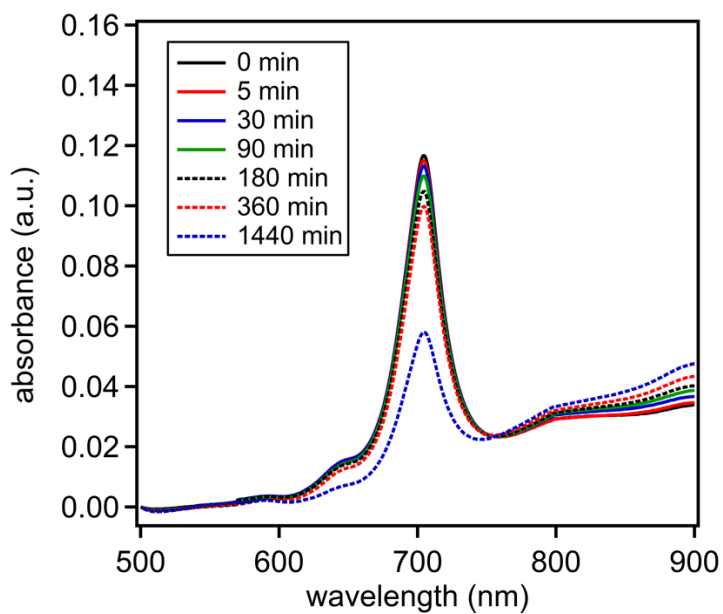
Figure 100. Photostability study with **SO₃SQ** in MeOH with continuous white light LED irradiation.
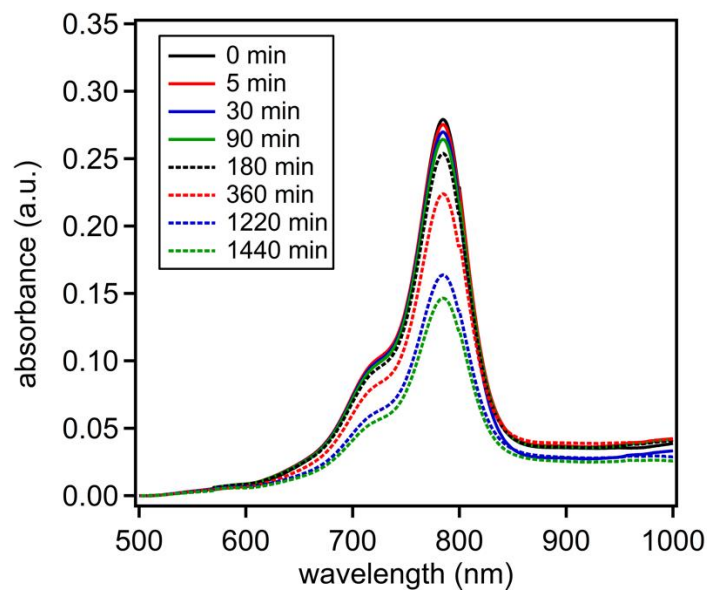
Figure 101. Photostability study of **ICG** in MeOH with continuous white light LED irradiation.

Table 52. O-alkylation condition optimization.

Entry	Base (equiv.)	Solvent	Temperature	Time	Result (SM:SP:P)
1	Na$_2$CO$_3$ (1.0)	isopropanol	Reflux (~83 °C)	16 h	1.9:1.0:0.0
2	Na$_2$CO$_3$ (1.0)	DMF	Reflux (~153 °C)	2 h	1.8:1.0:0.0
3[a]	Na$_2$CO$_3$ (2.0)	isopropanol	Reflux (~83 °C)	16 h	3.2:1.0:2.9
4[b]	CS$_2$CO$_3$ (2.5)	THF	Reflux (~66 °C)	16 h	0.0:<1.0:10.0 85% product yield

SP: This product was observed by 1H NMR and is consistent with C-alkyation at the C1 position

as evidenced by a loss of the singlet from signal C1 with a significant shift in the signals at C7 and

240

for the aryl ring doublet from the hydrogens closest to the indolizine.[a] 2.0 equivalents of 1,4-butanesultone was used.[b] 2.5 equivalents of 1,4-butanesultone was used.

Table 53. Optimization conditions for **SO₃SQ**.

Entry	Solvent	Temperature	Condition	Time	Result
1	n-BuOH:Tol (1:1)	reflux (~110 °C)	N_2	6 h	SM consumed, intractable brown precipitate formation
2	n-BuOH:Tol (1:1)	reflux (~110 °C)	O_2	6 h	SM consumed, intractable brown precipitate formation
3	n-BuOH:Tol (1:1)	pressure flask 130 °C	N_2	6 h	SM consumed, intractable brown precipitate formation
4	n-BuOH:Tol (1:1)	reflux (~110 °C)	N_2, 2-3 drops H_2O	6 h	trace product formation, SM consumed, intractable brown precipitate formation
5	n-BuOH:Tol:water (1:1:1)	slow heating to 100 °C	N_2	6 h	trace product formation, SM consumed, intractable brown precipitate formation
6	n-BuOH:Tol:water (6:6:1)	reflux (~110 °C)	N_2	2 h	trace product formation, SM consumed, intractable

					brown precipitate formation
7	n-BuOH:Tol:water (120:120:1)	reflux (~110 °C)	N_2	2 h	SM consumed, intractable brown precipitate formation, 8% product yield
8	MeOH	pressure flask (100 °C)	N_2	6 h	SM consumed, 60% yield
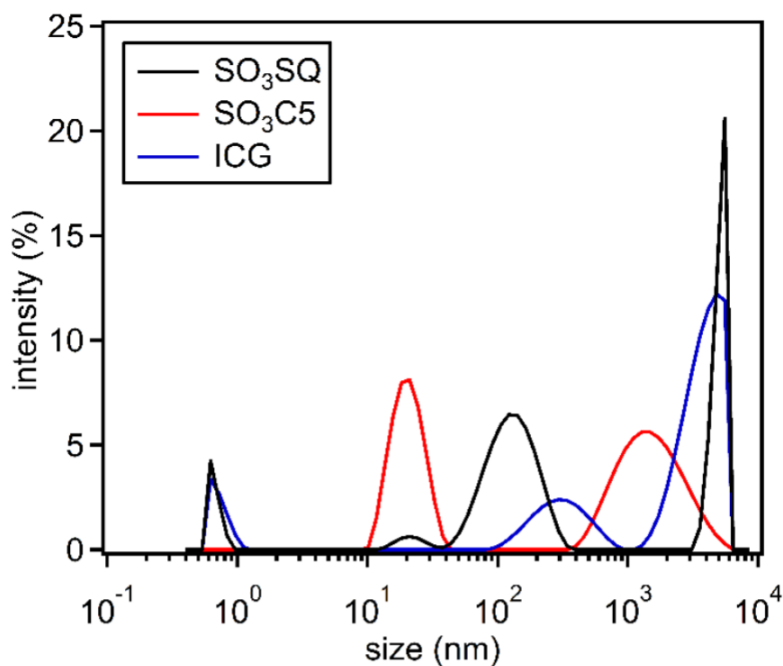
Figure 102. DLS data demonstrating aggregate size distributions for **SO₃SQ**, **SO₃C5**, and ICG in water at 5 x 10^{-6} M. DLS studies were also done for all three dyes in DMSO and demonstrated no aggregate formation.

APPENDIX B: PERMISSION FROM JOURNALS

1. Journal permission for Chapter 2.1

Rightslink® by Copyright Clearance Center

Copyright Clearance Center

RightsLink®

Home | Create Account | Help | LIVE CHAT

ACS Publications
Most Trusted. Most Cited. Most Read.

Title: Indolizine-Cyanine Dyes: Near Infrared Emissive Cyanine Dyes with Increased Stokes Shifts

Author: Jacqueline Gayton, Shane A. Autry, William Meador, et al

Publication: The Journal of Organic Chemistry

Publisher: American Chemical Society

Date: Jan 1, 2019

Copyright © 2019, American Chemical Society

LOGIN

If you're a copyright.com user, you can login to RightsLink using your copyright.com credentials.
Already a RightsLink user or want to learn more?

PERMISSION/LICENSE IS GRANTED FOR YOUR ORDER AT NO CHARGE

This type of permission/license, instead of the standard Terms & Conditions, is sent to you because no fee is being charged for your order. Please note the following:

- Permission is granted for your request in both print and electronic formats, and translations.
- If figures and/or tables were requested, they may be adapted or used in part.
- Please print this page for your records and send a copy of it to your publisher/graduate school.
- Appropriate credit for the requested material should be given as follows: "Reprinted (adapted) with permission from (COMPLETE REFERENCE CITATION). Copyright (YEAR) American Chemical Society." Insert appropriate information in place of the capitalized words.
- One-time permission is granted only for the use specified in your request. No additional uses are granted (such as derivative works or other editions). For any other uses, please submit a new request.

BACK | CLOSE WINDOW

2. Journal permission for Chapter 3.1

THE UNIVERSITY of MISSISSIPPI

Jacqueline Gayton <jgayton@go.olemiss.edu>

Re: MDPI Contact Form: Permission to use material for dissertation

1 message

support@mdpi.com <support@mdpi.com>
To: Jacqueline Gayton <jgayton@go.olemiss.edu>

Thu, Oct 10, 2019 at 3:39 AM

Dear Jacqueline,

Thank you for your email. As author of the paper and given that you are
the owner of the copyrights, you are entitled to reproduce it in other
publications.

Kind regards,
Dimity

On 2019/10/10 5:23, Jacqueline Gayton wrote:
> Hello, I would like to use our previously published work from here: https://www.mdpi.com/1420-3049/23/12/3051 in my
> dissertation. I am an
> author on the paper. Could I get permission to do this?
>
>
> Thank you, Jacqueline Gayton

3. Journal permission for Chapter 4.1

Clearance Center Inc., ("CCC's Billing and Payment terms and conditions"), at the time that you opened your RightsLink account (these are available at any time at http://myaccount.copyright.com).

Terms and Conditions

- The materials you have requested permission to reproduce or reuse (the "Wiley Materials") are protected by copyright.

- You are hereby granted a personal, non-exclusive, non-sub licensable (on a stand-alone basis), non-transferable, worldwide, limited license to reproduce the Wiley Materials for the purpose specified in the licensing process. This license, **and any CONTENT (PDF or image file) purchased as part of your order,** is for a one-time use only and limited to any maximum distribution number specified in the license. The first instance of republication or reuse granted by this license must be completed within two years of the date of the grant of this license (although copies prepared before the end date may be distributed thereafter). The Wiley Materials shall not be used in any other manner or for any other purpose, beyond what is granted in the license. Permission is granted subject to an appropriate acknowledgement given to the author, title of the material/book/journal and the publisher. You shall also duplicate the copyright notice that appears in the Wiley publication in your use of the Wiley Material. Permission is also granted on the understanding that nowhere in the text is a previously published source acknowledged for all or part of this Wiley Material. Any third party content is expressly excluded from this permission.

- With respect to the Wiley Materials, all rights are reserved. Except as expressly granted by the terms of the license, no part of the Wiley Materials may be copied, modified, adapted (except for minor reformatting required by the new Publication), translated, reproduced, transferred or distributed, in any form or by any means, and no derivative works may be made based on the Wiley Materials without the prior permission of the respective copyright owner.**For STM Signatory Publishers clearing permission under the terms of the STM Permissions Guidelines only, the terms of the license are extended to include subsequent editions and for editions in other languages, provided such editions are for the work as a whole in situ and does not involve the separate exploitation of the permitted figures or extracts,** You may not alter, remove or suppress in any manner any copyright, trademark or other notices displayed by the Wiley Materials. You may not license, rent, sell, loan, lease, pledge, offer as security, transfer or assign the Wiley Materials on a stand-alone basis, or any of the rights granted to you hereunder to any other person.

245

4. Journal permission for Chapter 5.1

Copyright Clearance Center

RightsLink®

Home   Create Account   Help   LIVE CHAT

ACS Publications
Most Trusted. Most Cited. Most Read.

Title: Donor–Acceptor–Donor NIR II Emissive Rhodindolizine Dye Synthesized by C–H Bond Functionalization

Author: Chathuranga S. L. Rathnamalala, Jacqueline N. Gayton, Austin L. Dorris, et al

Publication: The Journal of Organic Chemistry

Publisher: American Chemical Society

Date: Sep 1, 2019

Copyright © 2019, American Chemical Society

PERMISSION/LICENSE IS GRANTED FOR YOUR ORDER AT NO CHARGE

This type of permission/license, instead of the standard Terms & Conditions, is sent to you because no fee is being charged for your order. Please note the following:

- Permission is granted for your request in both print and electronic formats, and translations.
- If figures and/or tables were requested, they may be adapted or used in part.
- Please print this page for your records and send a copy of it to your publisher/graduate school.
- Appropriate credit for the requested material should be given as follows: "Reprinted (adapted) with permission from (COMPLETE REFERENCE CITATION). Copyright (YEAR) American Chemical Society." Insert appropriate information in place of the capitalized words.
- One-time permission is granted only for the use specified in your request. No additional uses are granted (such as derivative works or other editions). For any other uses, please submit a new request.

BACK   CLOSE WINDOW

5. Journal permission for Chapter 6.1

VITA

Jacqueline Gayton

University of Mississippi, Graduate Assistant, Department of Chemistry and Biochemistry

Curriculum Vitae: Updated August 2019

Contact Information:

University of Mississippi, Department of Chemistry, 481 Coulter Hall, University, MS 38677

Phone: (228) 223-7799   Email: jgayton@go.olemiss.edu Website:

www.linkedin.com/in/jacqueline-gayton-um/

EDUCATION AND TRAINING

University of South Alabama, Mobile, AL, 2010-2015, B.S. in Chemistry, 2015

Undergraduate Research Advisor: Matthew Reichert

University of Mississippi, Oxford, MS, 2015-2020, Ph.D in Chemistry, 2020

Advisor: Jared Delcamp

WORK HISTORY

University of Mississippi, Department of Chemistry and Biochem., Research and Teaching

Assistant, 2015-present

University of South Alabama, Department of Chemistry, Undergraduate Research Assistant, 2014-2015

PUBLICATIONS Total (6 published, 1 accepted, 1 submitted, 1 being submitted Summer 2020)

1) **Gayton, J.**; Autry, S. A.; Meador, W.; Parkin, S. P.; Hill, G. A.; Hammer, N. I.; Delcamp, J. H. "Indolizine-Cyanine Dyes: Near Infrared Emissive Cyanine Dyes with Increased Stokes Shifts" J. Org. Chem. **2019**, 84, 687. [link]

2) **Gayton, J. N.**; Autry, S.; Fortenberry, R. C.; Hammer, N. I.; Delcamp, J. H. "Counter Anion Effect on the Photophysical Properties of Emissive Indolizine-Cyanine Dyes in Solution and Solid State" Molecules, **2018**, 23, 3051. [link]

3) McNamara, L. E.; Rill, T. A.; Huckaba, A. J.; Ganeshraj, V.; **Gayton, J.**; Nelson, R. A.; Sharpe, E. A.; Dass, A.; Hammer, N. I.; Delcamp, J. H. "Indolizine-Squaraines: NIR Fluorescent Materials with Molecular Engineered Stokes Shifts" Chem. Eur. J. **2017**, 23, 12494. [link]

4) Rathnamalala, C.; **Gayton, J.**; Dorris, A. ; Meador, W.; Hammer, N. I.; Delcamp, J. H.; Scott, C. "Donor-Acceptor-Donor NIR II Emissive Rhodindolizine Dye Synthesized by C-H Bond Functionalization" J. Org. Chem. J. Org. Chem. **2019**, 84, 20, 13186-13193.

5) Meador, W.; Autry, S. A.; Bessetti, R.; **Gayton, J.**; Flynt, A.; Hammer, N. I.; Delcamp, J. H. "Water Soluble NIR Fluorescent Cyanine and Squaraine Dyes for Biological Imaging" J. Org. Chem. **2020**, 85, 6, 4089-4095.

6) **Gayton, J.**; Kolodziejczyk, W.; Hill, G.; Delcamp, J. H. "Phosphate and Water Sensing with Zinc Picolinate Charge Transfer Dyes" ChemistrySelect, **2020**, 5, 1945.

PRESENTATIONS

Graduate Presentations (11):

1) **July 2016.** "Perylene-Based Dyes for High Voltage Dye Sensitized Solar Cells" Feeding and Powering The World, Oxford, MS

2) **March 2017.** "Photodynamic Therapy with Organic Near-Infrared (NIR) Dyes" Departmental Seminar, Oxford, MS

3) **June 2017.** "Cyclized Perylene Diimides for Polycyclic Aromatic Hydrocarbon (PAH) Reception: Introducing the JBOX" Emergent Polymer Sensing Technologies for Gulf Coast Water Quality Monitoring, Gulfport, MS

4) **November, 2017.** "Organic Small Molecules for Phosphate and Polycyclic Aromatic Hydrocarbon (PAH) Sensing" Emergent Polymer Sensing Technologies for Gulf Coast Water Quality Monitoring, Tuscaloosa, AL

5) **February, 2018.** "Organic Small Molecules for Polycyclic Aromatic Hydrocarbon (PAH) Sensing" Emergent Polymer Sensing Technologies for Gulf Coast Water Quality Monitoring, Jackson, MS

6) **March, 2018.** "NIR Emissive Indolizine-Squaraine and Indolizine-Cyanine Dyes" ACS National Meeting, New Orleans, LA

7) **June, 2018.** "Small Organic Molecules as Phosphate Sensors and NIR Emissive Materials" Ole Miss Summer REU Program, Oxford, MS

8) **July, 2018.** "Small Organic Molecules as Phosphate Sensors and NIR Emissive Materials" Emergent Polymer Sensing Technologies for Gulf Coast Water Quality Monitoring, Hattiesburg, MS

9) **November, 2018.** "Small Organic Molecules as Phosphate Sensors and NIR Emissive Materials" Emergent Polymer Sensing Technologies for Gulf Coast Water Quality Monitoring, Starkville, MS

10) **February, 2019.** "Small Organic Molecules as Phosphate Sensors and NIR Emissive Materials" Emergent Polymer Sensing Technologies for Gulf Coast Water Quality Monitoring, Oxford, MS

11) **July, 2019.** "Small Organic Molecules as Phosphate and CO_2 Sensors" Emergent Polymer Sensing Technologies for Gulf Coast Water Quality Monitoring, Gulfport, MS

12) **November, 2019.** "Cyanines, Squaraines, and Xanthene Based NIR Emissive Materials for Biological Imaging" Defense Seminar, Oxford, MS

POSTERS

March 2015. "Hydrolysis of Fungal Chitin Utilizing Ionic Liquids as a Solvent and Catalyst" ACS National Meeting, Denver, CO.

LEADERSHIP: STUDENT MENTORING

- William Meador (Fall 2017 – present)
- Qing Li (Summer 2019 – present)